The Tectonic Evolution of the Altavista area, Southwest Virginia Piedmont

by

Alexander E. Gates II

Dissertation submitted to the Faculty of the
Virginia Polytechnic Institute and State University
in partial fulfillment of the requirements for the degree of
Doctor of Philosophy
in
Department of Geological Sciences

APPROVED:

L. Glover III, Chairman

D. A. Hewitt

C. Simpson

K. A. Eriksson

A. K. Sinha

June 1986

Blacksburg, Virginia

The Tectonic Evolution of the Altavista area,

Southwest Virginia Piedmont

by

Alexander E. Gates

L. Glover III, Chairman

Department of Geological Sciences

(ABSTRACT)

The Altavista area lies at the north end of a large area of continuous detailed mapping in the proposed westward thrusted Smith River Allochthon of the Southwest Virginia Piedmont. It also lies at the south end of an area of continuous mapping in the central Virginia Piedmont. The stratigraphy of the Smith River Allochthon has not been related to any other in the Southern Appalachians. The units defined to the north of Altavista are Late Precambrian to Early Paleozoic in age and correlated to many other areas in the Central and Southern Applalchians. At Altavista the two stratigraphies merge and are correlatable. The Bowens Creek Fault, which bounds the west side of the Smith River Allochthon, separates blocks that contain the same stratigraphy. If allochthonous at all, the Smith River Allochthon has therefore not been thrusted any great distance.

The rocks of the Smith River Allochthon have been metamorphosed to middle to upper amphibolite facies conditions during the Taconic Orogeny whereas those of Central Virginia only acheived upper greenschist conditions during this event. The Evington Group pelitic schists and gneisses in Altavista exhibit an inverted prograde metamorphism and subsequent retrogression. The Pressure-temperature path for these rocks forms the lower part of a loop from high pressure to lower pressure and higher temperature followed by a nearly isobaric retrogression. Paths of this type are characteristic of terranes that have experienced nappe emplacement. The Altavista area represents the footwall beneath a nappe that has been eroded away because the metamorphic gradient is inverted yet the stratigraphy is upright. Two phases of deformation in this event formed isoclinal folds and refolded isoclinal folds and a pervasive S_2 foliation.

The formation of large domes along the Bowens Creek Fault postdates the high grade metamorphism. The structures were formed in a three-stage dextral transpressional event. This Carboniferous dextral transcurrent event is Appalachian wide and well documented in the Brookneal zone to the east. The Bowens Creek Fault is therefore unrelated to the high grade metamorphism, further disproving the existence of the Smith River Allochthon.

ACKNOWLEDGEMENTS

Fieldwork for this project was funded through the Nuclear Regulatory Commission grant NRC 04-75-737 to Lynn Glover III and J. K. Costain. I wish to thank Lynn Glover III for originally suggesting this field area and for allowing me to continue with it through the dissertation. The discussions with Lynn both in the lab and the field provided the direction for most of the papers. I also wish to thank for many grueling hours of discussing, writing and drafting for the Brookneal Zone paper. Thanks to my committee, Lynn Glover III, Carol Simpson, Ken Eriksson, Krishra Sinha and David Hewett, for the critical reviews and helpful discussions in preparing this dissertation. Special thanks to and many graduate students including: and among others who provided much help through advice, support and discussion.

This dissertation could not have been nearly as well completed in nearly as short a time without the emotional support and efforts of Waiting at home during the late nights in the lab certainly required alot of patience and faith. I'm thankful that she believes in me. She also did most of the typing. drafted the map and many of the figures and put up with alot of moodiness. She is appreciated. has been supportive and solved innumerable problems. She is an expert in diplomacy and logistics. taught me all I know about developing film and prints - a very patient woman. Finally I wish to acknowledge the contributions, both geological and philosophical, of to my work and return to school.

TABLE OF CONTENTS

APPALACHIAN CARBONIFEROUS DEXTRAL STRIKE-SLIP FAULTS: ... 1
AN EXAMPLE FROM BROOKNEAL, VIRGINIA 1
ABSTRACT 1
INTRODUCTION 2
BROOKNEAL SHEAR ZONE 5
METAMORPHIC CONDITIONS OF DEFORMATION 15
DISPLACEMENT ESTIMATES FOR THE BROOKNEAL SHEAR ZONE . 16
AGE CONTROL ON THE STRIKE SLIP EVENT 17
COMPARISON WITH SEISMIC REFLECTION DATA 21
TECTONIC IMPLICATIONS 24
CONCLUSIONS 27
REFERENCES 28
TRANSPRESSIONAL DOME FORMATION 38
IN THE SOUTHWEST VIRGINIA PIEDMONT. 38
ABSTRACT 38
INTRODUCTION 39
PRE-DOME GEOLOGY OF THE ALTAVISTA AREA 45
DOME GEOMETRY 47
STRUCTURAL ELEMENTS 49
D_1 and D_2 Deformational Events 49
D_3 Deformation 50
D_4 Deformation 53
Mineral Lineations 58
Faults 59
STRUCTURAL DEVELOPMENT 62
TECTONIC IMPLICATIONS 69
CONCLUSIONS 70
REFERENCES 71
PROGRADE METAMORPHISM AND HYDROTHERMAL
RETROGRESSION 79
DURING NAPPE EMPLACEMENT, SOUTHWEST VIRGINIA PIEDMONT 79
ABSTRACT 79
INTRODUCTION 80

GEOLOGIC SETTING 81
PETROGRAPHY 86
Prograde Assemblages Southeast of the Sil-Isograd 87
Prograde Assemblages Northwest of the Sil-Isograd 88
St-Bearing Retrograde Rocks 88
Cld-Bearing Retrograde Assemblages 91
Rocks with Extreme Composition 93
MINERAL CHEMISTRY 93
Muscovite 94
Plagioclase 94
Biotite 97
Garnets 97
Staurolite 101
Chlorite 107
Chloritoid 107
Other Minerals 108
PETROLOGIC EVOLUTION 108
Prograde Assemblages 109
St-Retrograde Reactions 115
Cld-Retrograde Reactions 119
Conditions of Metamorphism 121
Location P-T Reaction Space 121
Thermobarometry 124
P-T Path 127
DISCUSSION 129
Retrogression and Fluids 129
TECTONIC IMPLICATIONS 131
REFERENCES 135
THE SMITH RIVER ALLOCHTHON: GEOLOGY AND REGIONAL CONTEXT 142
ABSTRACT 142
INTRODUCTION 143
STRATIGRAPHY 147
LYNCHBURG GROUP 152
Interpretation 156

CATOCTIN FORMATION 156
Interpretation 157
EVINGTON GROUP 158
Basal Graywacke. 158
Quartzite 159
Lower Pelite. 159
Lower Calc-silicate/sandy pelite. 160
Middle pelite. 161
Upper Calcsilicate/Quartzite Sequence. 161
Upper Pelite. 162
Interpretation 162
STRUCTURE AND METAMORPHISM. 166
D_1 167
D_2 168
M_1 170
Interpretation 172
D_3, D_4 and M_2 173
Interpretation 173
REGIONAL CORRELATION OF MAJOR STRUCTURES 174
TECTONIC EVOLUTION 175
CONCLUSIONS 177
REFERENCES 178
APPENDIX A 184
FIELD LOCATIONS 184
APPENDIX B 188
APPENDIX C 202

Vita 256

LIST OF ILLUSTRATIONS

Figure 1. Tectonic-Fault trace map of the Appalachians 3
Figure 2. Geologic Map of the Southwest Virginia Piedmont 6
Figure 3. Geologic Map of the Brookneal Area 7
Figure 4. C and S Bands in Melrose Granite 10
Figure 5. Photomicrograph of Mylonite 10
Figure 6. Shear Bands in Arvonia Schist 13
Figure 7. Stereographic Projection of Poles to Shear Bands 14
Figure 8. Graph of Strain Versus Distance 18
Figure 9. Block Diagram of Reactivation 23
Figure 10. Plate Tectonic Model 26
Figure 11. Tectonic map of the Southern Appalachians 40
Figure 12. Domes and Anticlines in the Smith River Allochthon 41
Figure 13. Geologic Map of the Altavista Area 44
Figure 14. Stereographic Projections of Poles to S_2 48
Figure 15. Crenulation Cleavages in Lynchburg Schist 52
Figure 16. Stereographic Projections of L_3 and Poles to S_3 54
Figure 17. Stereographic Projections of L_4 and Poles to S_4 56
Figure 18. Altavista Cross-Section 57
Figure 19. Photomicrograph of Shear Bands 52
Figure 20. Detailed Structural Map 60
Figure 21. Stereographic Projection of Mineral Lineations 61
Figure 22. Structural Development Diagrams 64
Figure 23. Schematic block diagram of Altavista. 68
Figure 24. Tectonic Map of the Southern Appalachians 82
Figure 25. Geologic/Metamorphic Map of Altavista 85
Figure 26. Mineral Textures 90

Figure 27. Muscovite and Plagioclase Chemistry 95
Figure 28. Biotite Chemistry 100
Figure 29. Garnet Composition Profiles 105
Figure 30. Prograde Pseudobinary 114
Figure 31. St- and Cld-Retrograde Pseudobinary 115
Figure 32. Cld+Grt-Retrograde Pseudobinary 122
Figure 33. KFMASH Schreinemakers Diagram 123
Figure 34. P-T Path with Control Points 128
Figure 35. Idealized P-T Loop for Altavista Area 133
Figure 36. Tectonic Model for Altavista 134
Figure 37. Tectonic Map of the Southern Appalachians 144
Figure 38. Geologic Map of the Smith River Allochthon 146
Figure 39. Geologic Map of the Altavista Area 151
Figure 40. Stratigraphic Column for the Altavista Area 153
Figure 41. Lynchburg Channel Deposit 155
Figure 42. Cross-Beds in Lower Evington Group 155
Figure 43. Disharmonic Folds in Calc-silicate 163
Figure 44. F_2 Folds in Lynchburg Formation 164
Figure 45. Stereographic Projection of Poles to S_2 169
Figure 46. P-T Path for the Taconic M_1 Metamorphism 171

LIST OF TABLES

Table 1. Rb/Sr Data for Melrose Granite 19

Table 2. Age Control on Southern Appalachian Faults 22

Table 3. Plagioclase Analyses 96

Table 4. Biotite Analyses 98

Table 5. Garnet Analyses 102

Table 6. Mass Balance Coefficients 110

Table 7. Mass Balance Analyses 111

Table 8. Pressure-Temperature Data 126

Table 9. Correlation and Timing of Events 149

APPALACHIAN CARBONIFEROUS DEXTRAL STRIKE-SLIP FAULTS:

AN EXAMPLE FROM BROOKNEAL, VIRGINIA

A.E. Gates , C. Simpson and L. Glover III

ABSTRACT

The northern Appalachian, dextral fault system of late Paleozoic age is also present in the central and southern Appalachians. An example of a dextral strike-slip fault is the 4 km wide Brookneal shear zone in the southwest Virginia Piedmont. The shear zone is, in part, superimposed on the Melrose Granite where an S-C mylonite was produced by dynamic recrystallization of all constituent minerals. The Arvonia metasedimentary and Charlotte belt metavolcanic rocks contain spaced dextral shear bands at a consistent $+24° \pm 3°$ to the shear zone boundary. A minimum displacement estimate of 17 km was obtained from rotated foliation measurements in the Melrose Granite. The age of movement on the Brookneal shear zone has been constrained by isotopic dating to between 324 and 300 Ma. Other faults in the southern Appalachians, including the Nutbush Creek and Modoc zones show similar ages and relative offsets. Possible plate tectonic models that could account for the late Paleozoic dextral fault system throughout the Appalachians include: (1) tectonic escape resulting from the collision of a plate with North America to the north of the Canadian Appalachians, (2) postcollision interplate readjustments involving counterclockwise rotation of Africa relative to North America, and (3) oblique convergence of eastern North America with an oceanic plate moving west.

INTRODUCTION

The geologic provinces that lie to the east of the Blue Ridge, Green and Long Mountains of the Appalachians (Figure 1) are generally considered to have been produced by compressional tectonics [Bird and Dewey, 1970; Hatcher, 1972 and 1978; Rankin, 1975; Rodgers, 1970]. Interpretations of recent seismic sections across the Appalachians show that the thrust faulting and associated folding, which are characteristic of the western part of the orogen, continue eastward to the Atlantic Coast [Cook et al., 1979; Harris and Bayer, 1979]. Evidence for a late Paleozoic transcurrent or transpressional episode in the northern Appalachians however, has been steadily growing over the past few years [Bradley, 1982; Webb, 1969; McCabe et al., 1980; Anderson, 1972; Johnson and Wones, 1984]. In this paper, we discuss new evidence for late Paleozoic transcurrent faults in the southern Appalachians, and suggest that a transcurrent fault system of orogenic proportions existed during that time.

Dextral strike-slip faults in the northern Appalachians were first recognized by Webb [1969]. Several researchers reached similar conclusions over the next few years but results were not compiled until the work of Bradley [1982]. This compilation summarized all documented faults and associated pull-apart basins in the northern and maritime Appalachians. Ages of sediments in the pull-apart basins indicate that fault activity in the northern Appalachians occurred from the late Devonian to early Permian, with peak activity between 340 and 285 Ma [Bradley, 1982]. Although the Cobequid-Chedabucto fault of Nova Scotia (Figure 1) is estimated to have had as much as 225 km of dextral offset [McCabe et al., 1980] most of the faults have dextral offsets of 50 km or less.

The strike-slip faults have been incorporated into several tectonic models in recent years. Arthaud and Matte [1977] considered several of the known dextral faults in the northern and maritime Appalachians to be part of a late Variscan, right-lateral Riedel

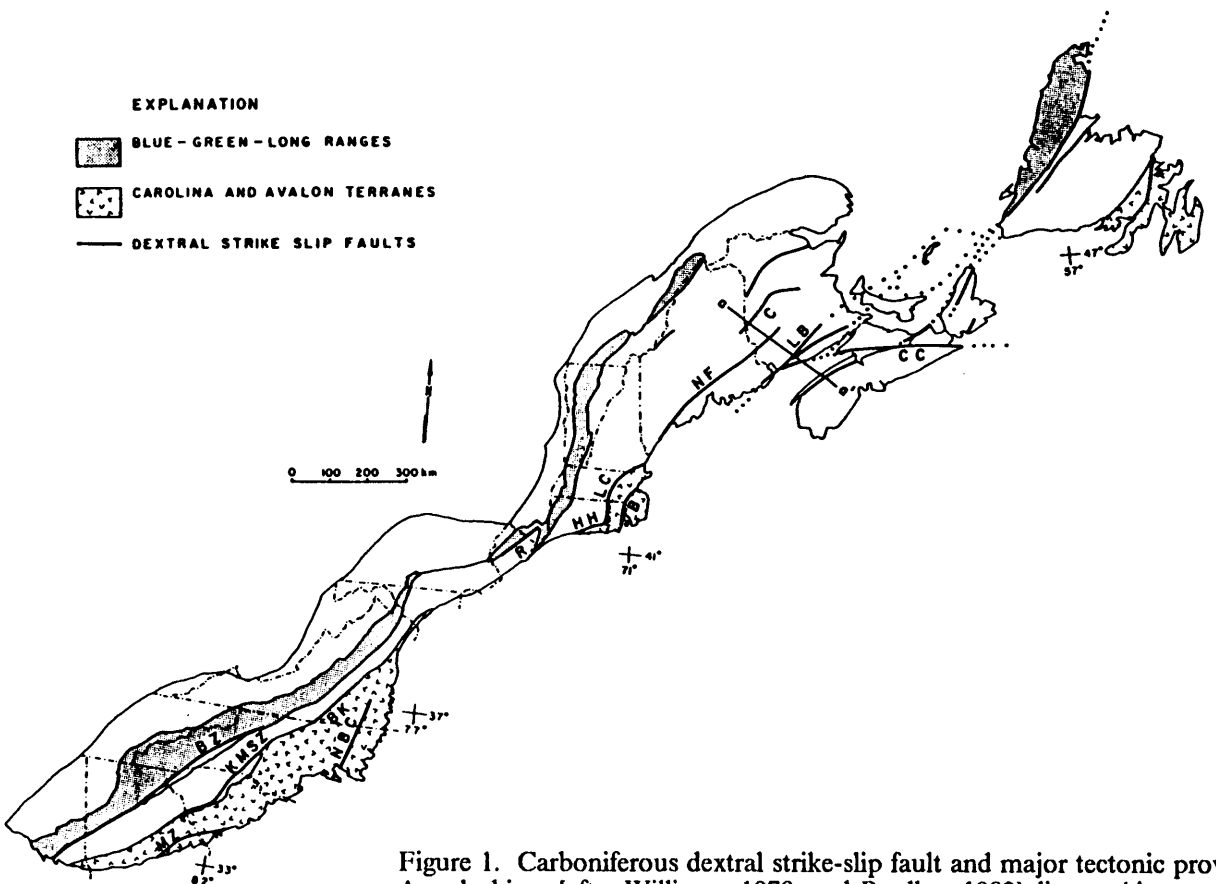

Figure 1. Carboniferous dextral strike-slip fault and major tectonic province map of the Appalachians [after Williams, 1978, and Bradley, 1982]; line a-a′ intersects faults with offset estimates that are used to calculate a cumulative dextral movement. BZ = Brevard zone, MZ = Modoc zone, KMSZ = Kings Mountain shear zone, NBC = Nutbush Creek fault, BK = Brookneal shear zone, R = Ramapo fault, HH = Honey Hill fault, LC = Lake Char fault, B = Beaverhead shear zone, NF = Norumbega-Fredrickton fault, C = Catamaran fault, LB = Lubec-Belleisle fault, CC = Cobequid-Chedabucto fault; Long Range includes the Sutton Mountains and Notre Dame province.

shear system between the Euro-American and African plates. Lefort and Van der Voo [1981] examined the middle to late Carboniferous strike-slip faults of the Appalachian chain and found a distinctive geometric pattern: an east-west set of dominantly dextral faults, and a southwest-northeast set of both sinistral and dextral faults. These authors applied the models of Tapponnier and Molnar [1976, 1977] and Molnar and Tapponnier [1977], wherein a rigid indenter into a rigid-plastic plate causes lateral escape of material along strike-slip faults on either side of the compression zone. According to Lefort and Van der Voo [1981], in the case of the Appalachians, the rigid indenter was the Reguibat Uplift on the West African Shield, and the position of indentation was somewhere in the central Appalachians. This model was used to explain both dextral and sinistral faults in the northern Appalachians, but in the central and southern Appalachians, a sinistral strike-slip fault (the New York-Alabama lineament) as well as northwest-directed thrust faults were predicted [Lefort and Van der Voo, 1981].

Dextral movement within the Eastern Piedmont fault system of Hatcher et al. [1977] was predicted by Bobyarchick [1981] on the basis of analogy with the Eocene-Miocene collision of Arabia and Eurasia. A promontory of the African plate in collision with North America at an unspecified position "north of Virginia" was postulated to have caused rocks in the Suwanee basin of Florida to escape to the south [Bobyarchick, 1981].

This paper documents the continuation of the late Paleozoic dextral strike-slip system through the central and southern Appalachians, based on new data from the Central Piedmont Suture at Brookneal, Virginia, and compilation of published work on other faults (Figure 1). Some of the faults shown in Figure 1 have complex kinematic histories that include a component of dextral movement, for example: the Beaverhead shear zone of the Narragansett Basin [McMaster et al., 1980; Mosher, 1983], the Lake Char fault [Goldstein and Hutton, 1984], the Brevard zone [Sinha and Glover, 1978; Bobyarchick, 1984],and the Kings Mountain shear zone [Horton, 1982] (Figure 1).

BROOKNEAL SHEAR ZONE

A particularly clear example of a dextral ductile fault zone occurs in the Brookneal area of the southwestern Virginia Piedmont (Figures 1, 2 and 3). The Brookneal area contains the Central Piedmont Suture between a dominantly metavolcanic terrane to the east and a dominantly metasedimentary terrane of North American affinity to the west [Glover and Sinha, 1973; Hatcher, 1978; Williams, 1978; Gates, 1981] (Figures 2 and 3). The suture zone contains the late Cambrian to Ordovician, 512 ± 5 Ma (by zircons), 470 Ma (by Rb/Sr whole rock) [A.K. Sinha, personal communication, 1984] Melrose Granite, which was subsequently cut by a 4-km-wide dextral shear zone (the Brookneal shear zone) during the late Paleozoic (Figure 3). The Brookneal shear zone, therefore, is a simple dextral shear zone because it represents a single phase of deformation in the Melrose Granite.

The Melrose Granite is undeformed along its western edge where the coarse, seriate, biotite-titanite granodioritic to quartz dioritic rocks contain well preserved igneous textures. In the western, least deformed portion of the Brookneal shear zone, the Melrose Granite is foliated and grainsize is slightly reduced. Quartz is flattened and exhibits undulose extinction, subgrain formation and recrystallization. One to two centimeter microcline phenocrysts and sausseritized plagioclase exhibit brittle fractures and recrystallized grain boundaries. Green, retrograde biotite grains are bent around more rigid grains and commonly contain kink bands. Half centimeter titanite grains appear to "float" undisturbed through the deforming matrix at low strain but are severely fractured and far less abundant in the higher strain regions of the shear zone. Thin, widely spaced zones of intense shearing cut the mildly deformed granite. The microstructures within these zones resemble those of the main shear zone. Metamorphic grade is indicated to be in the albite-epidote, lower amphibolite facies by the stable albite-epidote-biotite assemblage.

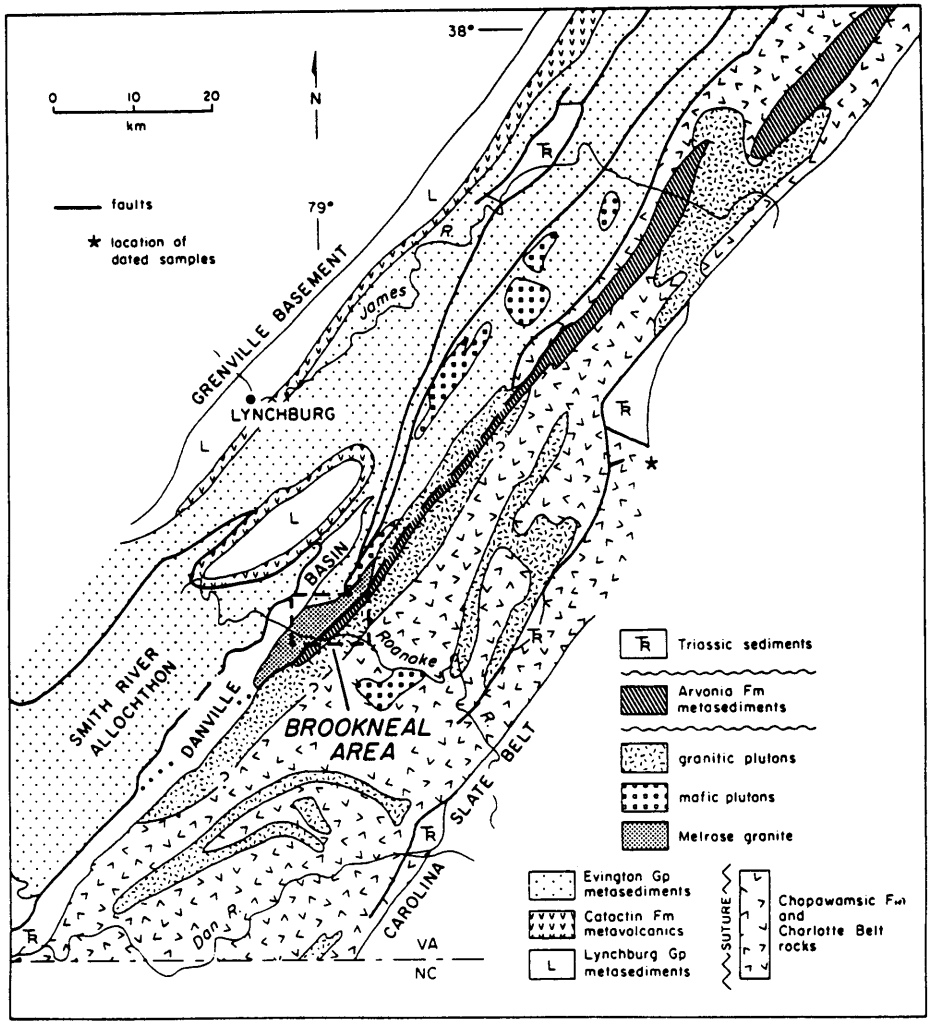

Figure 2. Geologic map of the central and southwestern Virginia Piedmont. Detailed mapping area corresponds to Figure 3. (Map after Smith et al. [1964]; Ern [1968]; Brown [1969]; Marr [1980a and b]; Gates [1981]; Conley and Henika [1973]; Henika and Thayer [1977]; Tobish and Glover [1971]; and unpublished data from Orogenic Studies Lab [1985]).

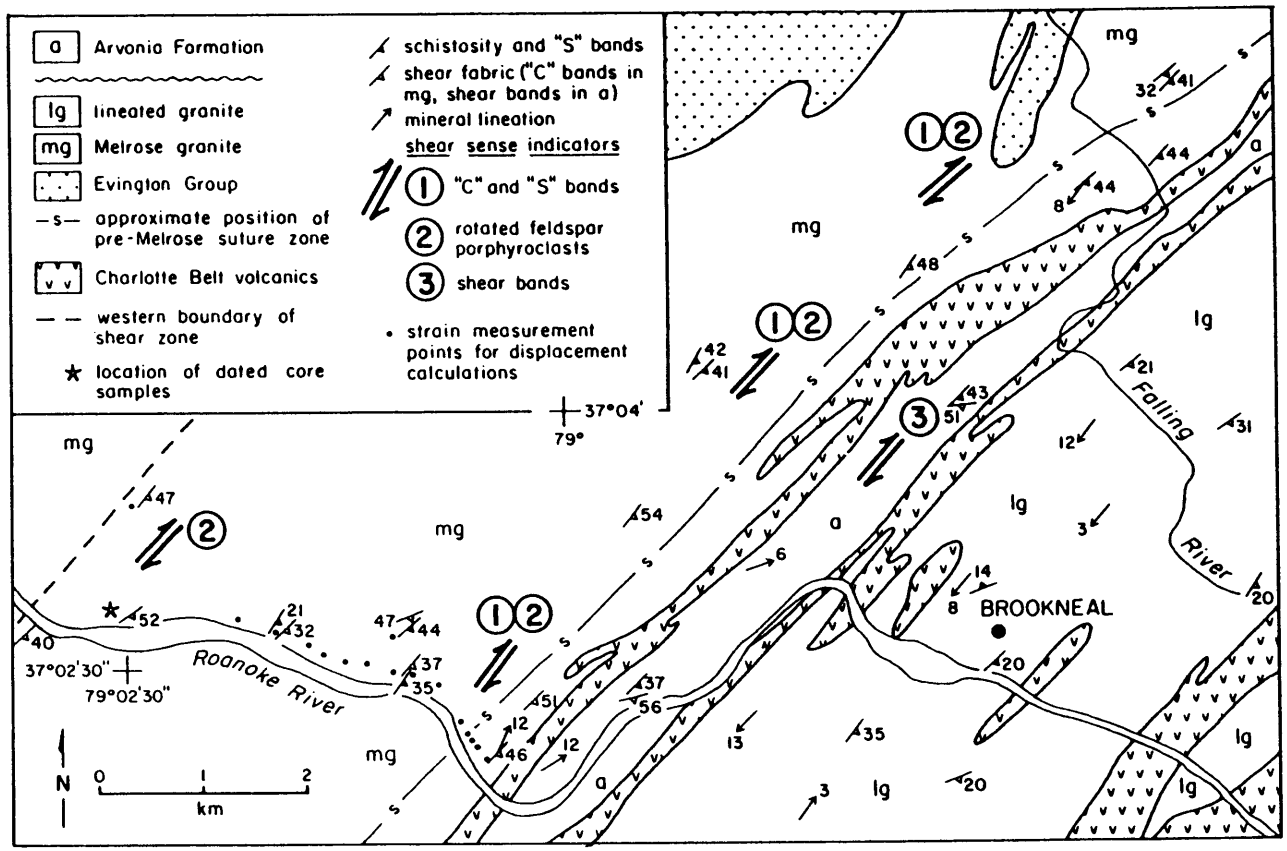

Figure 3. Detailed geologic map of the Brookneal Area (location on Figure 2.)

Within the main portion of the Brookneal shear zone, the rocks have undergone a reduction in grain size dominantly by ductile deformation mechanisms and have acquired two mylonitic foliations. Earlier S foliations, defined by quartz ribbons (Type 2B of Boullier and Bouchez [1978]) and aligned chlorite, green biotite and white mica grains, curve into C planes (Figure 4), (where C stands for "cisaillement" or shear) [Berthe et al., 1979; Simpson, 1984; Lister and Snoke, 1984]. Plagioclase and K feldspar porphyroclasts show evidence for brittle fracturing followed by dynamic recrystallization along grain margins and fracture planes. The resulting structure (Figure 5) is that of a Type I, S-C mylonite, using the terminology of Lister and Snoke [1984]. The C planes strike 040° and dip 50°SE, subparallel to the mapped boundary of the Brookneal shear zone. Mineral elongation lineations vary in plunge from ca. 12° toward 230°, through horizontal, to 8° toward 050°. Narrow (centimeter scale) ultramylonite zones occur throughout the Brookneal shear zone and increase in concentration eastward. All minerals are dynamically recrystallized into 5 to 20 μm grains within these ultramylonites. The easternmost 0.3 km of the exposed zone is almost entirely composed of ultramylonitic granite. Foliations and lineations within the ultramylonite are very similar in orientation to those within the C planes farther to the west. Sense of movement determinations using such features as S-C planes [Berthe et al., 1979], fractured and recrystallized feldspar grains, elongate, dynamically recrystallized quartz grains [Simpson and Schmid, 1983] and mica "fish" [Lister and Snoke, 1984] all give consistent results: movement on the Brookneal shear zone was dominantly dextral strike-slip. Minor components of normal and less common reverse movement are indicated by the gently SW and NE plunging elongation lineations, respectively. The plunge of the lineations however could have been produced by later deformation.

The effects of the dextral Brookneal shear zone continue to the east of the Melrose Granite into the lineated granite, metavolcanic-volcaniclastic Charlotte belt rocks and the metasedimentary Arvonia Formation (Figure 3). Dextral shear features in these

Figure 4. Melrose Granite deformed in the Brookneal Shear Zone displays S (schistosity) that curves into C ("cisaillement" or shear) planes. Movement sense is right lateral. Scale bar = 1 cm.

Figure 5. Photomicrograph of Melrose Granite deformed in the right lateral Brookneal shear zone. S = schistosity, C = shear planes, M = muscovite-biotite intergrowth, F = potassium feldspar porphyroclasts, rxf = dynamically recrystallized feldspar. Scale bar = 1 mm, plane polarized light.

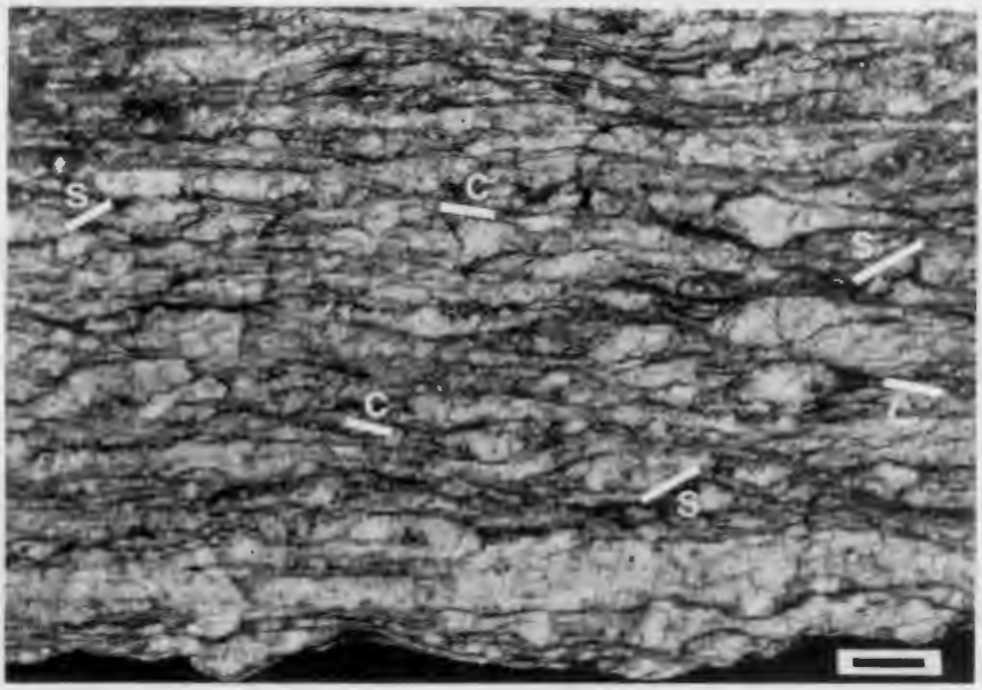
S
C
S
C
S

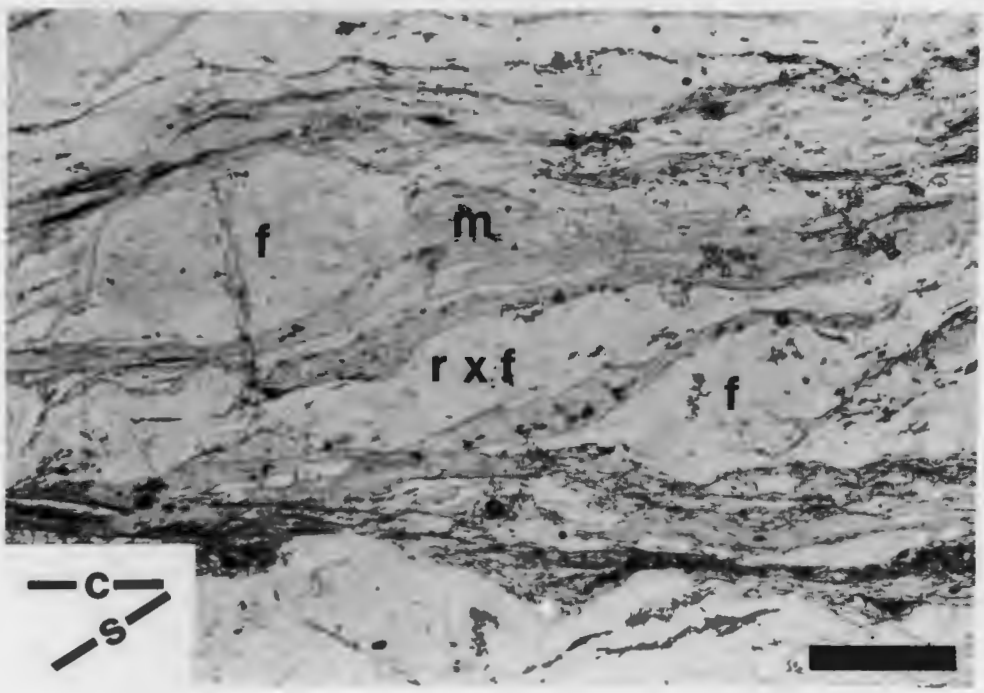
f
m
r x f
f
C
S

rocks, unlike in the Melrose Granite, occur in discrete, spaced zones that diminish in intensity and regularity to the east. The lineations in the strongly deformed, lineated granite are very similar in orientation to those in the Melrose Granite, indicating that the dextral deformation episode affected both bodies. The lineated granite however, contains no movement indicators.

The metasedimentary Arvonia Formation contains a thick section of graphite schist with good dextral movement indicators. The main foliation, defined by muscovite, graphite and quartz ribbons, is cut by a centimeter scale, spaced extensional crenulation cleavage or shear banding [Platt and Vissers, 1980] with a consistent dextral movement sense (Figure 6). The shear bands, defined by fine-grained muscovite and graphite, deflect the main foliation into sigmoidal shaped lozenges (Figure 6).

The shear bands in the Arvonia Formation are neither parallel to the Brookneal shear zone boundary nor to the "C" bands in the Melrose Granite (Figure 3). Stereographic projections of poles to the shear bands yield a tight concentration of points at $+24° \pm 3°$ from the pole to the main shear zone orientation (Figure 7). In their analysis of a dextral shear zone from central Spain, Weijermans and Rondeel [1984] showed that shear bands in anisotropic rocks were oriented consistently at 18 to 25° to the shear zone boundary. They developed a method to determine shear strain if initial orientations of anisotropies are known. In the case of the Arvonia Formation however, the entire belt of rock has been sheared, precluding this method of strain calculation.

Shear bands also occur sporadically in the hornblende-andesine, metabasalts of the Charlotte belt (Figures 2 and 3). Broadly spaced (1-2 cm) dextral shear bands in the eastern map area (Figure 3) cut the medium- to coarse-grained schists. The shear bands are defined by fine spindles of pale green amphibole, chlorite, magnetite and epidote and deflect the earlier foliation defined by aligned hornblende. Closer to the main shear zone,

Figure 6. Arvonia graphitic schist with dextral shear bands cutting the main foliation. S = main foliation. SB = shear bands. Scale bar = 1cm.


SB
S

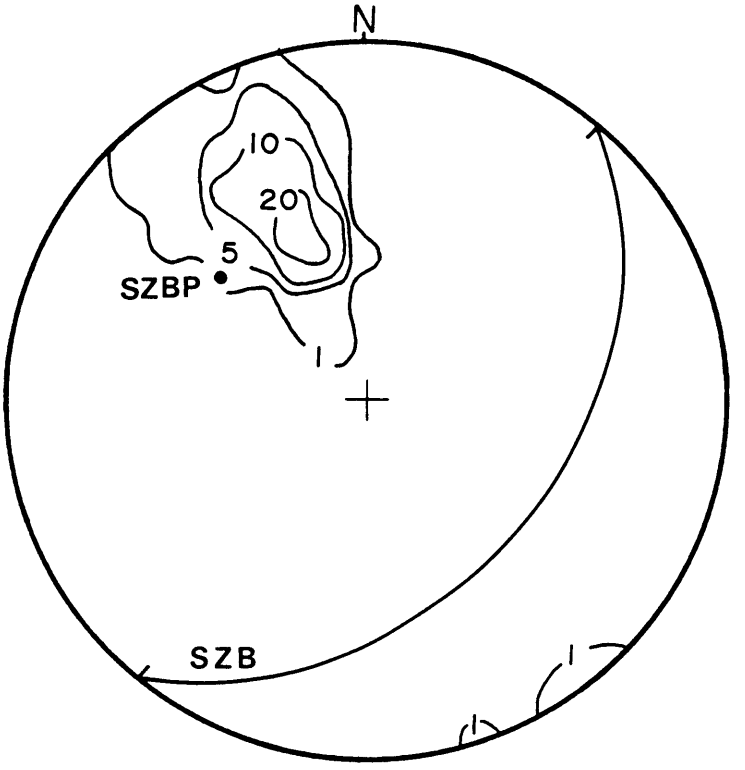

Figure 7. Contoured stereographic projection of poles to shear bands with great circle of C planes and shear zone boundary. SZBP = pole to shear zone boundary. 175 points.

andesine is albitized and hornblende is patchy and partially or totally replaced by epidote, fine amphibole and chlorite masses.

METAMORPHIC CONDITIONS OF DEFORMATION

The Brookneal shear zone in the Melrose Granite is defined by a stable assemblage of epidote, albite, green biotite, muscovite, calcite and chlorite. Thin, 3 to 4 m mafic dikes in the granite are composed of pale green amphibole, albite, minor amounts of chlorite and opaques. These assemblages indicate an albite-epidote, lower amphibolite facies metamorphic condition during deformation. Recrystallization of feldspar along grain boundaries indicates temperatures greater than 450°C [Voll, 1976; Tullis, 1983] but probably not much greater because recrystallization is not ubiquitous and is almost absent in low strain areas. In the Arvonia Formation, metamorphic conditions of deformation cannot be constrained because the composition is inappropriate for the formation of index minerals. The Charlotte belt metavolcanic rocks contain a primary hornblende-andesine assemblage, indicative of middle to upper amphibolite facies conditions. Where sheared however, the rock contains pale green amphibole, albite, epidote and chlorite, which indicate albite-epidote amphibolite facies.

Metamorphic conditions of deformation in the Brookneal shear zone were therefore laterally consistent and of albite-epidote facies (approximately 450°C). The temperature estimate is probably imprecise because the ductile response of feldspar is governed by strain rate, fluid pressure, fluid composition and confining pressure as well as temperature.

DISPLACEMENT ESTIMATES FOR THE BROOKNEAL SHEAR ZONE

Several features support the assumption that the C and S planes in the Melrose Granite formed during the same deformational event in the Brookneal zone. The western margin of the Melrose Granite is undeformed and yet both S and C planes occur in even the lowest strain portions of the zone (Figure 3). There is also a general parallelism of ultramylonite foliation, C planes and the Brookneal shear zone margin. Using the models of Berthe et al. [1979] and Simpson [1984] the S planes are considered to have first formed at 45° to the shear zone boundary in response to initial compression across the Brookneal shear zone. The C planes are considered to have initiated and remained subparallel to the shear zone boundary. With increasing shear strain, the S planes rotated toward parallelism with C planes. Thus, to a first approximation, the S planes can be considered to track the trajectory of the long axis of the finite strain ellipsoid between the C, or shear planes. Angular relationships (θ') between S and C planes vary across the Brookneal zone and have been used to compute approximate values for shear strain (γ) and displacement using Ramsay and Graham's [1970] equations:

$$\gamma = \frac{2}{\tan 2\theta'} \qquad \text{displacement (S)} = \int_0^x \gamma \, dx$$

Sixteen points were measured in a linear traverse across the shear zone (Figure 3), and like values were averaged to yield the twelve graphed points for the integration (Figure 8). A minimum displacement estimate of 17 km dextral offset is obtained by these methods. Regions of discontinuous outcrop within ultramylonite zones on the easternmost margin of the Brookneal shear zone were not included in the displacement estimate calculations. The well-developed shear bands with dextral offset that continue far to the east of the Melrose Granite in the Arvonia Formation and volcanic units

(Figure 3), cannot be used for additional displacement calculation because the orientation of the initial anisotropy is not known. Thus, actual displacement values may be well in excess of 20 km.

AGE CONTROL ON THE STRIKE SLIP EVENT

An exact date for movement on the Brookneal shear zone is difficult to determine due to the problems inherent in dating mylonites. Isotopic equilibration may be precluded during mylonitization, resulting in a partial reset of the system and therefore erroneous ages [Hickman and Glassley, 1984; Sinha et al., 1984]. Two samples of deformed Melrose Granite for age determination were taken from a drill core (Figure 3) to ensure fresh rock from an otherwise deeply weathered terrane. The samples were prepared using standard separation and columnation techniques. Dating was performed by S. Becker on the Orogenic Studies Laboratory thermoionic sourced mass spectrometer. Results were standardized using SRM 987. Rb/Sr biotite-whole rock dating of the two samples yields a metamorphic cooling age of 300 ± 5 Ma (Table 1). This age appears to postdate most of the movement on the shear zone because the closure temperature of ^{87}Sr in biotite is 300°C [Dodson, 1973]. Under these conditions, feldspar grains would be expected to deform by brittle failure. Grain size reduction of feldspar in the Brookneal shear zone however, is accomplished mainly through dynamic recrystallization, which suggests temperatures in the range of 450°C during deformation [Voll, 1976; Tullis, 1983].

Constraining the older age limit on the shear zone is a little more difficult because of the complex nature of the metamorphism in the Brookneal area. Gates [1981] and Glover et al. [1983], identified an abrupt western termination of the regional "Acadian" metamorphism at the Brookneal zone, possibly as a result of faulting. "Acadian" mineral

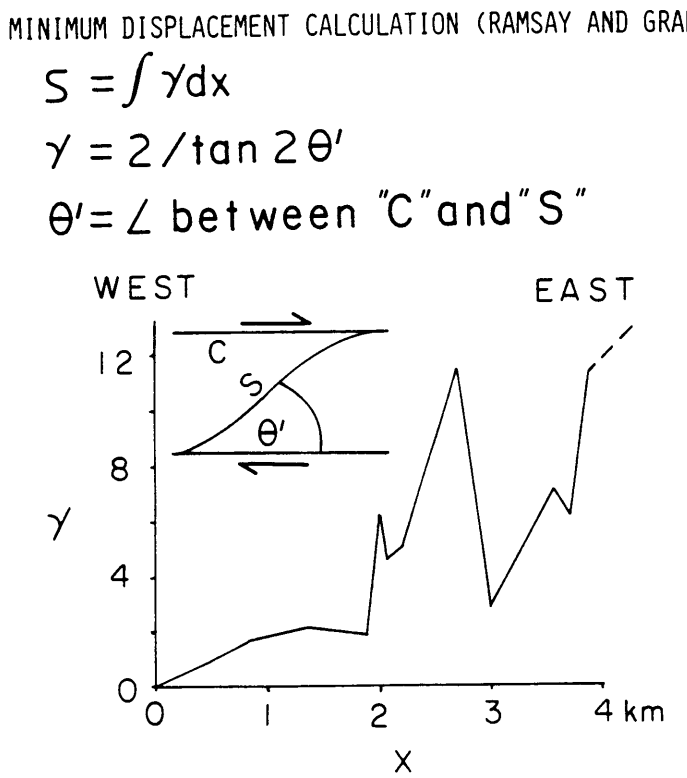

Figure 8. Graph of shear strain (γ) versus distance across the Brookneal shear zone. Integration of area under the curve yields a minimum displacement estimate of 17 km dextral offset. Inset: angular relationships used to determine γ.

TABLE 1. Isotopic Data For Melrose Samples

Sample	$^{87}Rb/^{86}Sr$	$^{87}Sr/^{86}Sr$	Sr ppm	Rb ppm
ML3-37	0.472	0.70837	468	76
ML3-37(bt)	21.656	0.80021	43	318
ML3-44	0.405	0.70804	574	80
ML3-44(bt)	26.239	0.81783	37	329
ML3-50	0.444	0.70838	498	22

Biotite-whole rock age determinations on samples from core of deformed Melrose Granite. Based on replicate analyses, the precision of the isochron ages is ± 5 Ma ($1\ \sigma$).

cooling ages can be obtained from the consistent upper amphibolite grade, metavolcanic rocks of the Charlotte belt [Glover et al., 1983]. The belt has been extended into southern and central Virginia through field mapping [Tobisch and Glover, 1971; Henika and Thayer, 1977] without major lithologic or metamorphic changes. An $^{40}Ar/^{39}Ar$ hornblende cooling age of 324 ± 3 Ma was obtained from typical Charlotte belt rocks in central Virginia (Figure 2), which agrees well with ages from southern Virginia [Glover, et al., 1983]. This age is interpreted to represent cooling through a 500 ± 50°C blocking temperature [Hanson and Gast, 1971; Harrison and McDougall, 1980].

The Charlotte belt hornblende-andesine amphibolites in the Brookneal area (Figure 3) are cut by dextral shear bands defined by a lower grade epidote-amphibole-albite-chlorite assemblage. The dextral shear foliation postdates the regional "Acadian" metamorphism and exhibits the same metamorphic assemblage as the Melrose Granite in the adjacent main shear zone. Movement on the Brookneal shear zone is therefore reasonably constrained to between 300 ± 5 Ma and 324 ± 3 Ma. This movement age is supported by the following stratigraphic constraints: (1) the late Ordovician to early Silurian(?) [Tillman, 1970], sheared, metasedimentary Arvonia Formation, unconformably overlies the Melrose Granite [Gates, 1981]; and (2) undeformed Triassic sediments of the Danville Basin overlie the Melrose Granite (Figure 2) and postdate the dextral shear zone [Gates, 1981].

To the east of Brookneal, the dextral Nutbush Creek shear zone (Figure 1) is constrained in age by the synkinematic, 312 Ma Buggs Island Granite and the postkinematic 285 Ma Wilton Granite [Druhan and Rollins, 1984], both of which lie within the shear zone (Table 2). Dextral offset in the Nutbush Creek zone is indicated by S-C mylonites, shear bands, and vergence of small scale folds [Bartley et al., 1984]. This zone has been suggested on the basis of gravity and magnetic data to continue farther south as the Modoc zone (Figure 1) [Hatcher and Zietz, 1980]. The dextral Modoc zone is constrained in age by the synkinematic 313 Ma Lake Murray and 292 Ma Lexington

plutons and the postkinematic 285 Ma Columbia pluton [Kimbrill et al., 1984; Snoke and Secor, 1983] (Table 2). However, Secor et al. [1984], suggest that the Lake Murray pluton is prekinematic and that the 25 km dextral offset across the Modoc zone, determined by offset structures, is confined to the interval 292 to 285 Ma (Table 2).

The approximate 324 to 300 Ma age of cooling and deformation for the Melrose Granite agrees with the 313 to 285 Ma activity range for the other dextral faults in the central and southern Appalachians [Snoke and Secor, 1982] (Table 2) and falls within the 340 to 285 Ma peak activity range for those of the northern Appalachians [Bradley, 1982]. These faults have relatively minor offset (generally less than 50 km), however the extent and consistency in age and movement sense attest to the distributed nature of this Appalachian-wide dextral strike-slip event.

COMPARISON WITH SEISMIC REFLECTION DATA

Recent seismic traverses across the Blue Ridge and Piedmont terranes by COCORP [Cook et al., 1979], USGS [Harris et al., 1980], and Virginia Tech [L. Glover et al., unpublished manuscript, 1984] show extensive thrust faulting. The lines show the listric nature of these faults but show no high angle, strike-slip faults. Their absence may either indicate that the thrust surfaces were largely reactivated as strike-slip faults during the dextral event (Figure 9) or that near-vertical offsets with real or apparent minor displacement caused by the dextral transcurrent faulting are not easily resolved by seismic reflection methods.

TABLE 2. Age Control on Southern Appalachian Faults

Fault Zone	Granites	Age Ma	Tectonics
Brookneal	Melrose	512 ± 5 (U/Pb)[1]	prekinematic
		300 ± 5 (Rb/Sr)*[2]	synkinematic
Nutbush Creek	Buggs Island	313 ± 15 (Rb/Sr)[3,6]	synkinematic
	Wilton	285 ± 10 (Rb/Sr)[4,6]	postkinematic
Modoc	Lake Murray	313 ± 24 (Rb/Sr)[5]	synkinematic
	Lexington	292 ± 15 (Rb/Sr)[3,5]	synkinematic
	Columbia	285 ± 7 (Rb/Sr)[4,5]	postkinematic

U/Pb ages on zircons, Rb/Sr ages on whole rock samples.
*Rb/Sr biotite-whole rock metamorphic cooling age.
[1]A. K. Sinha, personal communication, 1984.
[2]Becker, unpublished manuscript, 1983.
[3]Kish, 1983.
[4]Fullagar and Butler, 1979.
[5]Snoke et al., 1980.
[6]Druhan and Rollins, 1984.

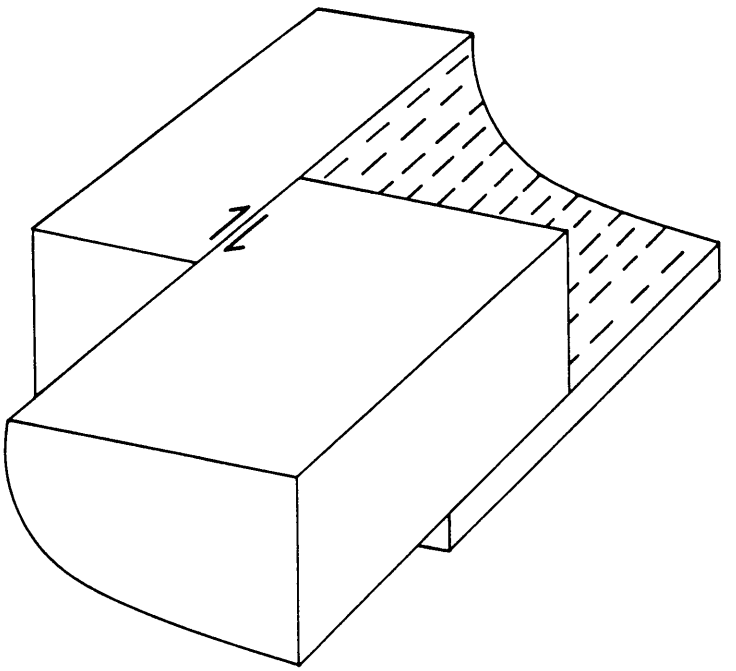

Figure 9. Block diagram illustrating one mechanism by which an earlier thrust fault may be reactivted into a dextral strike-slip fault. Thrust hanging wall lies to the east.

TECTONIC IMPLICATIONS

The continuation of the northern Appalachian, Carboniferous dextral strike-slip system of Bradley [1982] through the central and southern Appalachians modifies some of the previously proposed tectonic models. Many of the models employ the escape tectonics mechanisms proposed by Tapponnier and Molnar [1976, 1977] and Tapponnier et al. [1982] in which a rigid indenter impinges upon another more passive lithospheric plate. Blocks on the colliding face of the indented plate are forced away from the collision zone in opposite directions along large strike-slip faults. Lefort and Van der Voo [1981] proposed an escape model for the Appalachians that explains the northern dextral faults but requires coeval thrust faults as well as a sinistral strike-slip fault in the southern Appalachians. Similarly, Bobyarchick [1981] predicted the southern Appalachian dextral faulting event with an escape tectonics model that requires an indenter just north of Virginia and therefore, coeval sinistral faulting in the northern Appalachians. A viable model that employs these mechanisms to explain the Appalachian-wide event, is that proposed by Burke and Sengor [1985] in which the rigid indenter impinged the North American plate to the north of the maritime Canadian provinces. The southward escape of an eastern block (Africa?) would require a dextral strike-slip fault zone throughout the entire Appalachian orogen. This model requires concomitant sinistral strike-slip faults throughout the North Atlantic Caledonides. Arthaud and Matte [1977] and Dewey [1982] ascribed the northern Appalachian dextral faults to minor plate readjustments subsequent to the Acadian Orogeny or during the Alleghanian Orogeny.

Although only a small number of dextral faults have been identified in the central and southern Appalachians, many known fault zones of apparently similar age have unclear or unstudied movement histories. In the central Appalachians, where proven strike-slip faults are almost conspicuously absent, Ratcliffe [1971] documented the reac-

tivation of the dextral Ramapo fault into a Triassic graben-bounding normal fault (Figure 1). Bobyarchick and Glover [1979] demonstrated the Triassic reactivation of large, late Paleozoic faults of undetermined movement sense into basin-bounding normal faults in the eastern Virginia Piedmont. The extensive Triassic normal and oblique fault system, especially well developed in the central Appalachians, may therefore coincide with, and partially obscure, many faults displaying Carboniferous dextral movement. The Modoc-Nutbush Creek fault (Figure 1) is partially covered by Atlantic coastal plain sediments. Other dextral faults may be completely covered by the coastal plain units or may lie offshore.

Cumulative dextral offset was calculated for those faults along the line a-a′ on Figure 1 for which displacement estimates could be found. A total of 341 km dextral offset was obtained: 225 km for the Cobequid-Chedabucto [McCabe et al., 1980], 65 km for the Lubeck-Belleisle [Webb, 1969], 35 km for the Norumbega [Johnson and Wones, 1984] and 16 km for the Catamaran [Anderson, 1972]. The line a-a′ also intersects faults for which no displacement estimates are published, and the cumulative displacement does not include covered and offshore faults, nor strain absorbed by rocks outside of the shear zones.

McKerrow and Ziegler [1972] proposed large-scale rotation of a South American-African plate relative to North America during the late Paleozoic. Their model requires approximately 2000 km of dextral offset in the Appalachians, nearly an order of magnitude greater than the cumulative displacement estimates suggest. McKerrow and Ziegler's [1972] model does, however, suggest an alternate solution, that of a major transform system similar to the San Andreas fault system in California.

The models of Arthaud and Matte [1977] and Dewey [1982] each call for minor plate readjustments, but the total extent and cumulative displacement of the Carboniferous dextral fault system, while in agreement with their basic models, suggests that the readjustment event was in fact fairly major (Figure 10).

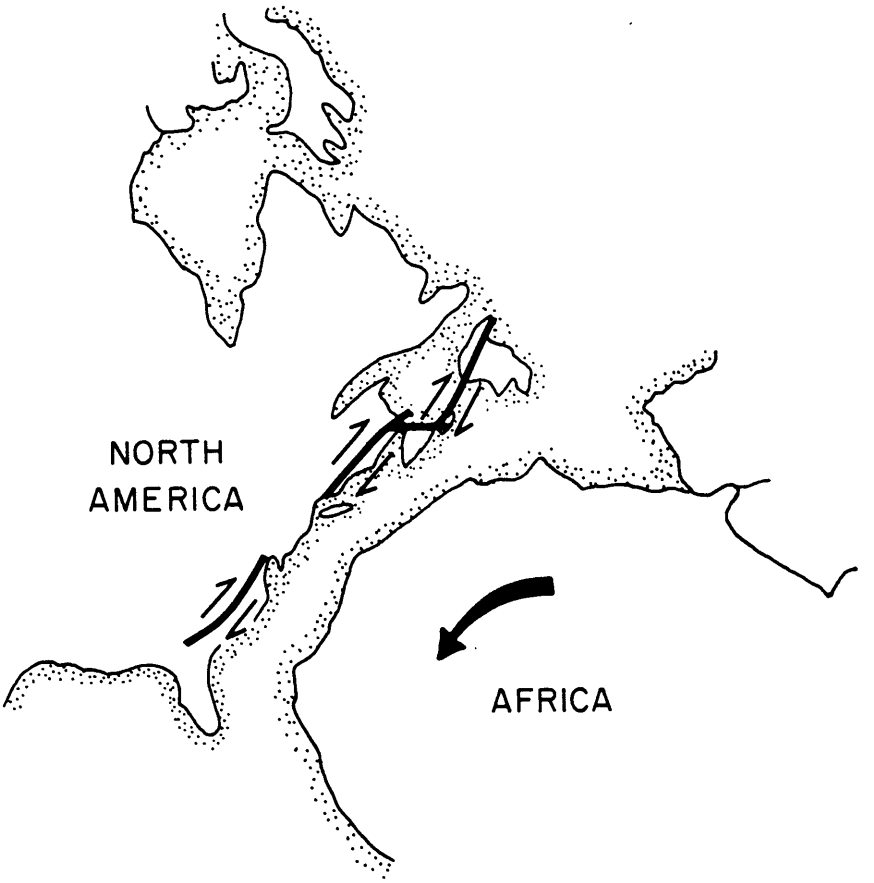

Figure 10. Suggested Carboniferous rotational readjustment of the African plate relative to North America and the resultant dextral transcurrent fault system in the Appalachians.

An alternative model for the late Paleozoic Appalachian transcurrent system is that of oblique convergence of North America with an oceanic plate that was subducted to the west-southwest [Snoke and Secor, 1982]. Sinha and Zietz [1982] in an attempt to explain late Paleozoic plutonism in the central and southern Appalachians, suggested that a subduction zone along the eastern margin of the Avalon terrane initiated at about 330 Ma, followed by an Alleghanian continental collision at 270 to 240 Ma. The 324 to 300 Ma transcurrent movement on the Brookneal shear zone could coincide with such a subduction event. An oblique convergence model to explain the strike-slip faults within the Sunda arc of the western Pacific was proposed by Fitch [1972]. Oblique convergence of an oceanic portion of the India plate with the southern margin of the China plate along the Sunda island arc has resulted in dextral transcurrent movement along Semangko fault on Java and Sumatra. The faulting is accompanied by thermal bulging and magmatism [Fitch, 1972]. A similar model for oblique convergence between North America and an oceanic plate could have resulted in movement along the Brookneal and other Appalachian dextral shear zones during the late Paleozoic.

CONCLUSIONS

The late Paleozoic dextral transcurrent system extends from the Canadian maritimes through the southern Appalachians. A clear example of the fault system is the Brookneal shear zone which has a minimum of 17 km dextral offset. At least three valid models may explain the transcurrent system: (1) escape tectonics due to an indenter north of Canada [Burke and Sengor, 1985], (2) plate readjustments subsequent to major orogeny [Arthaud and Matte, 1977; Dewey, 1982], and (3) oblique continent-ocean collision [Snoke and Secor, 1982]. The available evidence is insufficient to constrain these models at the present time.

REFERENCES

Anderson, F. D., The Catamaran fault, north-central New Brunswick, *Can. J. Earth Sci.*, *9*, 1278-1286, 1972.

Arthaud, F., and P. H. Matte, Late Paleozoic strike-slip in southern Europe and northern Africa: Results of a right lateral shear zone between the Appalachians and the Urals, *Geol. Soc. Am. Bull.*, *88*, 1305-1320, 1977.

Bartley, J. M., R. D. Turner, J. Mies, R. Druhan, and J. R. Butler, Kinematic analysis of the Nutbush Creek mylonite zone at Satterwhite Point, Kerr Lake, North Carolina, *Geol. Soc. Am. Abstr. Programs, SE sect.*, *15*, (2), 124, 1984.

Berthe, D., P. Choukroune, and P. Jegouzo, Orthogneiss, mylonite and non-coaxial deformation of granites: The example of the South Amorican shear zone, *J. Struct. Geol.*, *1*, 31-42, 1979.

Bird, J. M., and J. F. Dewey, Lithosphere plate-continental margin tectonics and the evolution of the Appalachian Orogen, *Geol. Soc. Am. Bull.*, *81*, 1031-1060, 1970.

Bobyarchick, A. R., The eastern Piedmont fault system and its relationship to Alleghanian tectonics in the southern Appalachians, *J. Geol.*, *89*(5), 335-347, 1981.

Bobyarchick, A. R., A late Paleozoic component of strike-slip in the Brevard Zone, southern Appalachians, *Geol. Soc. Am. Abstr. Programs SE Sect.* , *15*(2), 126, 1984.

Bobyarchick, A. R., and L. Glover III, Deformation and metamorphism in the Hylas zone and adjacent parts of the eastern Piedmont in Virginia, *Geol. Soc. Am. Bull., 90,* 739-752, 1979.

Boullier, A. M., and J. L. Bouchez, Le quartz en rubans dans les mylonites, *Bull. Soc. Geol. Fr., 20,* 253-262, 1978.

Bradley, D. C., Subsidence in late Paleozoic basins in the northern Appalachians, *Tectonics, 1*(1), 107-123, 1982.

Brown, W. R., Geology of the Dillwyn Quadrangle, Virginia, *Rep. Invest. Va. Div. Miner. Resour., 10,* 77 pp., 1969.

Burke, K., and C. Sengor, Tectonic escape in the evolution of the continental crust, in *Deep Structure of the Earth's Crust, Geophys. Monogr. Ser.*, edited by L. Brown and M. Barazangi, AGU, Washington, D. C., in press, 1985.

Conley, J. F., and W. S. Henika, Geology of the Snow Creek, Martinsville East, Price and Spray Quadrangles, Virginia, *Rep. Invest. Va. Div. Miner. Resour. , 33,* 71 pp., 1973.

Cook, F. A., D. S. Albaugh, L. D. Brown, S. Kaufman, J. E. Oliver, and R. D. Hatcher, Jr., Thin-skinned tectonics in the crystalline southern Appalachians; COCORP seismic reflection profiling of the Blue Ridge and Piedmont, *Geology, 7,* 563-567, 1979.

Dewey, J. F., Plate tectonics and the evolution of the British Isles, *J. Geol. Soc., 139,* Part 4, 371-412, 1982.

Dodson, M. H., Closure temperature in cooling geochronological and petrological systems, *Contrib. Mineral. Petrol., 40*, 259-274, 1973.

Druhan, R. M., and F. O. Rollins, The Nutbush Creek Fault Zone in the Eastern Piedmont of North Carolina, *Geol. Soc. Am. Abstr. Programs , 16*(6), 135, 1984.

Ern, E. H., Geology of the Buckingham Quadrangle, Virginia, *Rep. Invest. Va. Div. Mineral. Resour., 15*, 45 pp., 1968.

Fitch, T. J., Plate convergence, transcurrent faults and internal deformation adjacent to southeast Asia and the western Pacific, *J. Geophys. Res.,77*, 4432-4461, 1972.

Fullagar, P. D., and J. R. Butler, 325 to 265 M.Y. old granite plutons in the Piedmont of the southeastern Appalachians, *Am. Jour. Sci.,279*, 161-185, 1979.

Gates, A. E., Geology of the western boundary of the Charlotte belt at Brookneal, Va., M. S. thesis, Va. Polytech. Inst. Blacksburg, 1981.

Glover, L., III, and A. K. Sinha, The Virgilina deformation, a late Precambrian to early Cambrian (?) orogenic event in the central Piedmont of Virginia and North Carolina, *Am. J. Sci., 273-A*, 234-251,, 1973.

Glover, L., III, J. A. Speer, G. S. Russell, and S. S. Farrar, Ages of regional metamorphism and ductile deformation in the central and southern Appalachians, *Lithos, 16*, 223-245, 1983.

Goldstein, A.G., and J. J. Hutton, Kinematic indicators in Lake Char mylonites, *Geol. Soc. Am. Abstr. Programs NE sect.*, *16*(1), 18, 1984.

Hanson, G. N., and P. W. Gast, Kinetic studies in contact metamorphic zones, *Geochim. Cosmochim. Acta*, *35*, 101-107, 1971.

Harris, L. D., and K. C. Bayer, Sequential development of the Appalachian orogen above a master decollement- A hypothesis, *Geology*, *7*, 568-572, 1979.

Harris, L. D., A. G. Harris, W. deWitt Jr., and K. C. Bayer, Evaluation of southern eastern overthrust belt beneath Blue Ridge-Piedmont thrust, *Am. Assoc. Pet. Geol. Bull.*, *65*(12), 2497-2505, 1980.

Harrison, T. M., and I. McDougall, Investigations of an intrusive contact, northwest Nelson, New Zealand: II. Diffusion of radiogenic and excess ^{40}Ar in hornblende revealed by $^{40}Ar/^{39}Ar$ age spectrum analysis, *Geochim. Cosmochim. Acta*, *44*, 2005-2020, 1980.

Hatcher, R. D., Jr., Developmental model for the southern Appalachians, *Geol. Soc. Am. Bull.*, *81*, 933-940, 1972.

Hatcher, R. D., Jr., Tectonics of the western Piedmont and Blue Ridge, southern Appalachians: review and speculation, *Am. Jour. Sci.*, *278*, 276-304, 1978.

Hatcher, R. D., Jr., and I. Zietz, Tectonic implications of regional aeromagnetic and gravity data from the southern Appalachians, Proceedings, Caledonides in the U.S.A., edited by D. R. Wones, *Mem. Va. Polytech. Inst. State Univ., Dep. Geol. Sci., 2*, 235-245, 1980.

Hatcher, R. D., Jr., D. E. Howell, and P. Talwani, Eastern Piedmont fault system; speculation on its extent, *Geology, 5*, 636-640, 1977.

Henika, W. S., and P. A. Thayer, Geologic maps of the Blairs, Mount Herman Danville and Ringgold Quadrangles, Virginia, *Va. Div. Miner. Resour. Publ., 2*, 45pp., 1977.

Hickman, M. H., and W. E. Glassley, The role of metamorphic fluid transport in the Rb-Sr isotopic resetting of shear zones: Evidence from Nordre Stromfjord, West Greenland, *Contrib. Mineral. Petrol., 87*, 265-281, 1984.

Horton, J. W., Jr., Shear zone between the inner Piedmont and Kings Mountain belts in the Carolinas, *Geology, 9*, 28-33, 1982.

Johnson, T. D. and D. R. Wones, Sense and mode of shearing along the Norumbega fault zone, Eastern Maine, *Geol. Soc. Am. Abstr. Programs, NE Sect., 16*, 27, 1984.

Kimbrill, O., D. T. Secor Jr., and A. W. Snoke, Evidence for Late Paleozoic folding of the Modoc Zone, *Geol. Soc. of Am. Abstr. Programs, 16*, no. 6, 658, 1984.

Kish, S. A., A geochronological study of deformation and metamorphism in the Blue Ridge and Piedmont of the Carolinas, Ph. D. dissertation, 220 pp., Univ. of N. C., Chapel Hill, 1983.

Lefort, J. P., and R. Van der Voo, A kinetic model for the collision and complete suturing between Gondwana and Laurussia in the Carboniferous, *J. Geol.*, *84*(5), 537-550, 1981.

Lister, G. S., and A. W. Snoke, S-C mylonites, *J. Struct. Geol.*, *6*(6), 617-638, 1984.

Marr, J. D., Jr., Geology of the Willis Mountain Quadrangle, Virginia, *Va. Div. Miner. Resour. Publ.*, *25*, 1 p., 1980a.

Marr, J. D., Jr., Geology of the Andersonville Quadrangle, Virginia, *Va. Div. Miner. Resour. Publ.*, *26*, 1 p., 1980b.

McCabe, P. J., K. L. McCarty, and S. B. Pluim, Terrestrial sedimentation associated with strike-slip fault movement in middle Carboniferous of Nova Scotia, Canada, *Am. Assoc. Pet. Geol. Annu. Conv. Abstr.*, *89*, 747, 1980.

McKerrow, W. S., and A. M. Ziegler, Paleozoic oceans, *Nat. Phys. Sci.*, *240*, 92-94, 1972.

McMaster, R. L., J. de Boer, and B. P. Collins, Tectonic development of the southern Narragansett Bay and offshore Rhode Island, *Geology*, *8*, 496-500, 1980.

Molnar, P., and P. Tapponnier, The collision between India and Eurasia, *Sci. Am.*, *236*(4), 30-41, 1977.

Mosher, S., Kinematic history of the Narragansett Basin, Massachusetts and Rhode Island: Constraints on Late Paleozoic plate reconstructions, *Tectonics*, *2*(4), 327-344, 1983.

Platt, J. P., and R. L. M. Vissers, Extensional structures in anisotropic rocks, *J. Struct. Geol.*, *2*, 397-410, 1980.

Ramsay, J. G. and R. H. Graham, Strain variation in shear belts, *Can. J. Earth Sci.*, *7*, 786-813, 1970.

Rankin, D. W., The continental margin of eastern North America in the southern Appalachians: The opening and closing of the proto Atlantic Ocean, *Am. J. Sci.*, *275A*, 298-336, 1975.

Ratcliffe, N. M., The Ramapo fault system in New York and adjacent northern New Jersey: A case of tectonic heredity, *Geol. Soc. Am. Bull.*, *82*, 125-142, 1971.

Rodgers, J., The tectonics of the Appalachians, New York, *Interscience Publ.*, 271, 1970.

Secor, D. T., Jr., A. W. Snoke, and R. D. Dallmeyer, Character of Alleghanian deformation in the southern Appalachians, *Geol. Soc. Am. Abstr. Programs*, *16*(6), 646, 1984.

Simpson, C., Borrego Springs-Santa Rosa mylonite zone: A late Cretaceous west directed thrust in southern California, *Geology*, *12*, 8-11, 1984.

Simpson, C., and S. M. Schmid, An evaluation of criteria to deduce the sense of movement in sheared rocks, *Geol. Soc. Am. Bull.*, *94*, 1281-1288, 1983.

Sinha, A. K., and L. Glover III, U/Pb systematics of zircons during dynamic metamorphism: A study from the Brevard Fault Zone, *Contrib. Mineral. Petrol.*, *66*, 305-316, 1978.

Sinha, A. K., and I. Zietz, Geophysical and geochemical evidence for a Hercynian magmatic arc, Maryland to Georgia, *Geology*, *10*, 593-596, 1982.

Sinha, A. K., D. A. Hewitt, J. D. Rimstidt, and B. Partin, Distribution of strain and chemical domains in mylonite: Correlation with isotopic ages, *Geol. Soc. Am. Abstr. Programs*, *16*(6), 657, 1984.

Smith, J. W., R. C. Milici, and S. S. Greenberg, Geology and mineral resources of Fluvanna County, Virginia, *Va. Div. Miner. Resour. Bull.*, *79*, 62 pp., 1964.

Snoke, A. W., and D. T. Secor, Jr., The eastern Piedmont fault system and its relationship to Alleghanian tectonics in the southern Appalachians: A discussion; *J. Geol.*, *90*, 209-211, 1982.

Snoke, A. W., and D. T. Secor, Jr., The sense of shear in the Modoc Zone, South Carolina Piedmont-Implications for late Paleozoic geodynamic scenario, *Geol. Soc. Am. Abstr. Programs SE Sect.*, *15*(2), 1983.

Snoke, A. W., S. A. Kish, and D. T. Secor, Jr., Deformed Hercynian granitic rocks from the Piedmont of South Carolina, *Am. J. Sci.*, *280*, 1018-1034, 1980.

Tapponnier, P., and P. Molnar, Slip-line field theory and large scale continental tectonics, *Nature*, *264*, 319-324, 1976.

Tapponnier, P., and P. Molnar, Active faulting and cenozoic tectonics of China, *J. Geophys. Res.*, *82*, 2905-2930, 1977.

Tapponnier, P., G. Peltzer, A. Y. Le Dain, R. Armigo, and P. Cobbold, Propagating extrusion tectonics in Asia: New insights from simple experiments with plasticine, *Geology*, *10*, 611-616, 1982.

Tillman, C. G., Metamorphosed trilobites from Arvonia, Virginia, *Geol. Soc. Am. Bull.*, *81*(4), 1189-1200, 1970.

Tobisch, O. T. and L. Glover, III, Nappe formation in part of the southern Appalachian Piedmont, *Geol. Soc. Am. Bull.*, *82*, 2209-2230, 1971.

Tullis, J. A., Deformation of feldspars, in *Feldspar Mineralogy* edited by P. H. Ribbe, *Short Course Notes Mineral. Soc. Am.*, *2*, 2nd ed., 297-323, 1983.

Voll, G., Recrystallization of quartz, biotite and feldspars from Erstfeld to the Leventinia Nappe, Swiss Alps, and its geological significance, *Schweiz. Mineral. Petrogr. Mitt.*, *56*, 641-647, 1976.

Webb, G. W., Paleozoic wrench faults in the Canadian Appalachians, in North Atlantic geology and continental drift, *Mem. Am. Assoc. Pet. Geol.*, *12*, 754-786, 1969.

Weijermans, R., and H. E. Rondeel, Shear band foliation as an indicator of sense of shear: Field observations in central Spain, *Geology*, *12*, 603-606, 1984.

Williams, H., Tectonic lithofacies map of the Appalachian orogen, *Map 1*, Mem. Univ. of Newfoundland, St. Johns, 1978.

TRANSPRESSIONAL DOME FORMATION

IN THE SOUTHWEST VIRGINIA PIEDMONT.

A. E. Gates

ABSTRACT

A series of domes lie along the Bowens Creek Fault which bounds the west side of the Smith River Allochthon terrane in the Southwestern Virginia Piedmont. Several well developed domes at Altavista are characterized by multiple crenulation cleavages, reverse faults and dextral transcurrent shear bands. Detailed structural analysis indicates that the domes were formed in a three stage deformational event that resulted from transpression in a major shear zone.

The foliation, structures and stratigraphy were sub-horizontal prior to the transpressional event. The first stage of the event was characterized by the formation of north-south oriented, en-echelon folds and crenulation cleavage. The structures were then rotated in a northeast trending dextral transcurrent shearing. The final stage of deformation is characterized by northeast trending folds and crenulation cleavage.

The interference pattern of the early north-south folds on the late southwest trending folds form the domes and saddled antiforms. The domal structures are bounded by reverse faults that were active concurrently with the transcurrent faults. The domes are therefore proposed to be "positive flower" or "keystone" structures generated through compression across the transcurrent fault zone. The Altavista area

forms an external zone to the major Carboniferous dextral transcurrent Brookneal zone, 10 km to the east.

INTRODUCTION

The Bowens Creek Fault bounds the western edge of the Smith River Allochthon in the southwest Virginia Piedmont (Figures 11 and 12). The Bowens Creek along with the Ridgeway-Chatham Fault on the eastern side of the Smith River allochthon (Figure 12) were proposed to be the surface expression of the decollement upon which the allochthon was transported (Conley and Henika, 1970; 1973; Conley, 1978). The primary basis for the proposal of an allochthonous Smith River terrane was an erroneous Grenville age on the Leatherwood Granite which intruded the amphibolite grade rocks subsequent to the peak of metamorphism (Conley and Henika, 1973). The Blue Ridge rocks upon which the allochthon was to have been thrusted, are Late Precambrian to Early Paleozoic in age (Conley and Henika, 1970; 1973; Conley, 1978). The Bowens Creek Fault also fortuitously coincides with amphibolite facies isograd in the Taconic metamorphism that decrease in grade progressively to the west (Gates and Speer, in prep.). The fault therefore appears to have thrusted higher grade rocks over those of lower grade.

The Bowens Creek fault has been correlated by detailed mapping with the Brevard Zone (Figure 11) (Rankin et al., 1972; Espenschade et al., 1975; Rankin, 1975; Conley, 1979). Reed and Bryant (1964) and Bobyarchick (1984) have proposed a dextral transcurrent origin for late movement on the Brevard zone in North Carolina. Lemmon (1980) noted consistant northeast trending, horizontal mineral stretching lineations of post 440 Ma age near the transition of the Brevard into the Bowens Creek Fault, further supporting a strike-slip origin of the faults. Although a strike-slip origin

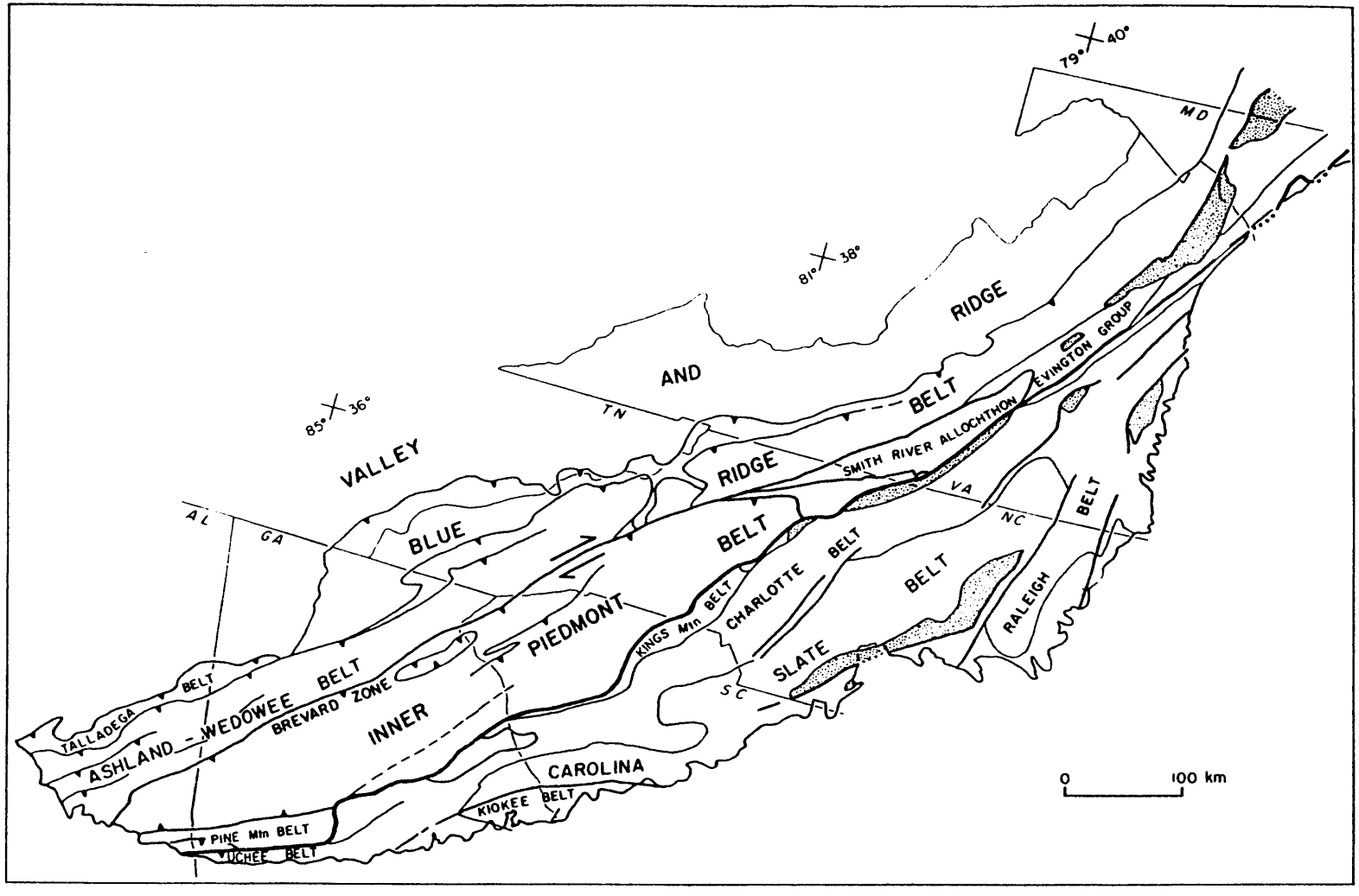

Figure 11. Tectonic map of the Southern Appalachians with Brevard Fault Zone and Triassic sedimentary basins (stippled).

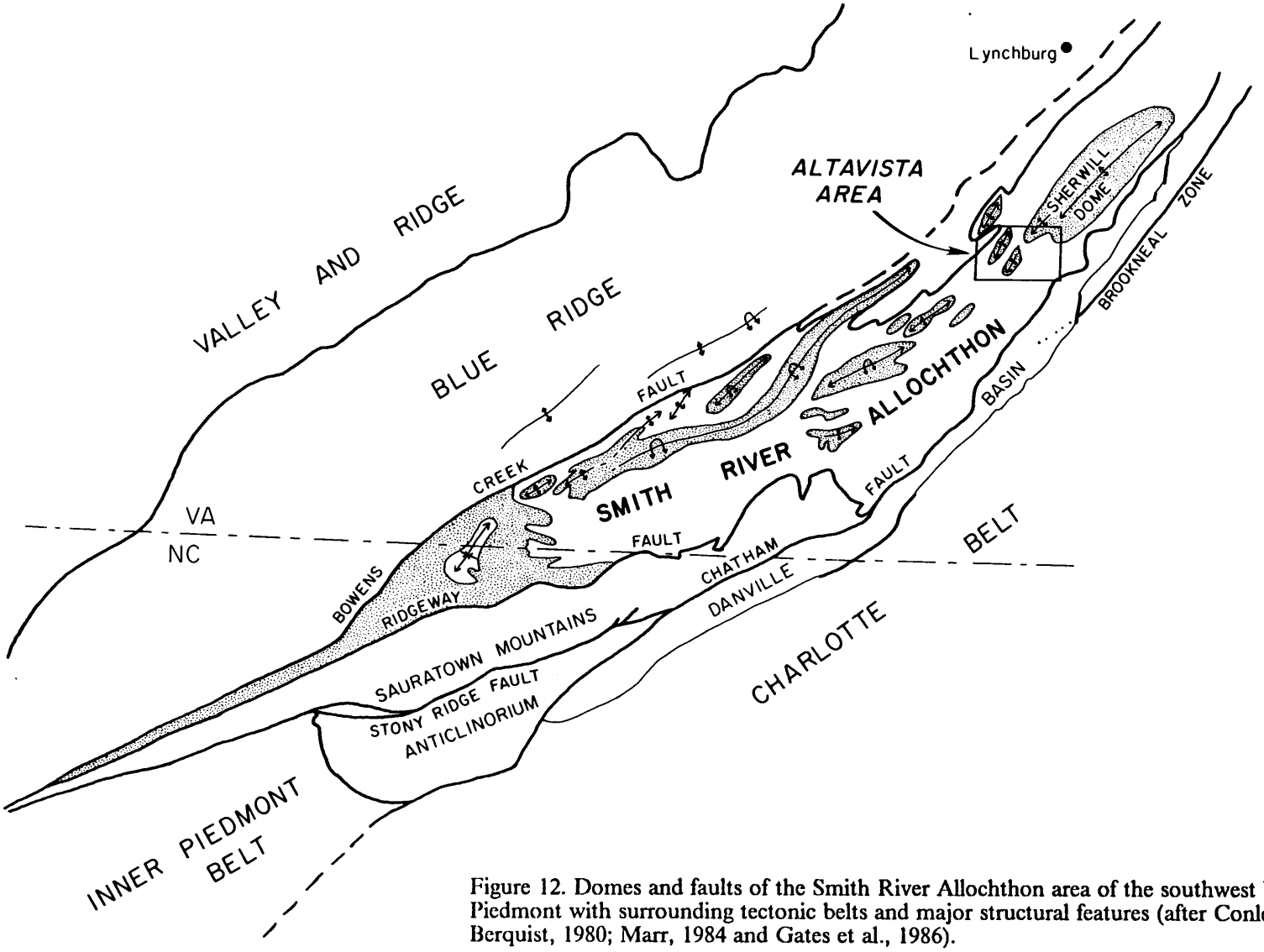

Figure 12. Domes and faults of the Smith River Allochthon area of the southwest Virginia Piedmont with surrounding tectonic belts and major structural features (after Conley, 1978; Berquist, 1980; Marr, 1984 and Gates et al., 1986).

for the Bowens Creek Fault has not previously been proposed, Scheible (1980) questioned the proposed thrust origin on the basis of steepness of dip and continuity in orientation of the fault zone.

The movement on the northern Brevard zone and Bowens Creek Fault is proposed to have occurred between 356 and 300 Ma (Conley, 1978) through a compilation of available K/Ar and Rb/Sr mineral age data. Fullagar and Dietrick (1976) and Mose (personal communication, 1986) also found a predominance of Rb/Sr mineral ages within this range along the Bowens Creek Fault. A late Devonian to Carboniferous age of uplift and cooling is therefore suggested.

A series of north to northeast trending domes and antiforms with saddled crests occur along the Bowens Creek Fault (Espenshade, 1954; Brown, 1958; Redden, 1963; Conley and Henika, 1970; 1973; Price et al., 1980; Marr, 1984) (Figure 12). Transpressional dome and anticline formation is well documented in transcurrent fault zones (Wilcox et al., 1973; Sylvester and Smith, 1976; Harding and Lowell, 1979; DeSmet, 1984). The structures are formed through compression across an otherwise transcurrent zone. The antiformal structures are produced by both reverse faulting and folding concurrent with the strike-slip movement, or transpression (Harland, 1971). This paper presents a detailed analysis of the northeast trending domes in the Altavista area which include the Hundley dome, the Reed Creek dome, and the southern part of the large Sherwill dome (Figure 13). Through analysis of stratigraphy, metamorphism, multiple creulation cleavages and meso-megascopic structures, the continuation of transcurrent deformation into the Bowens Creek Fault is tested.

Figure 13. Geologic map of the Altavista area.

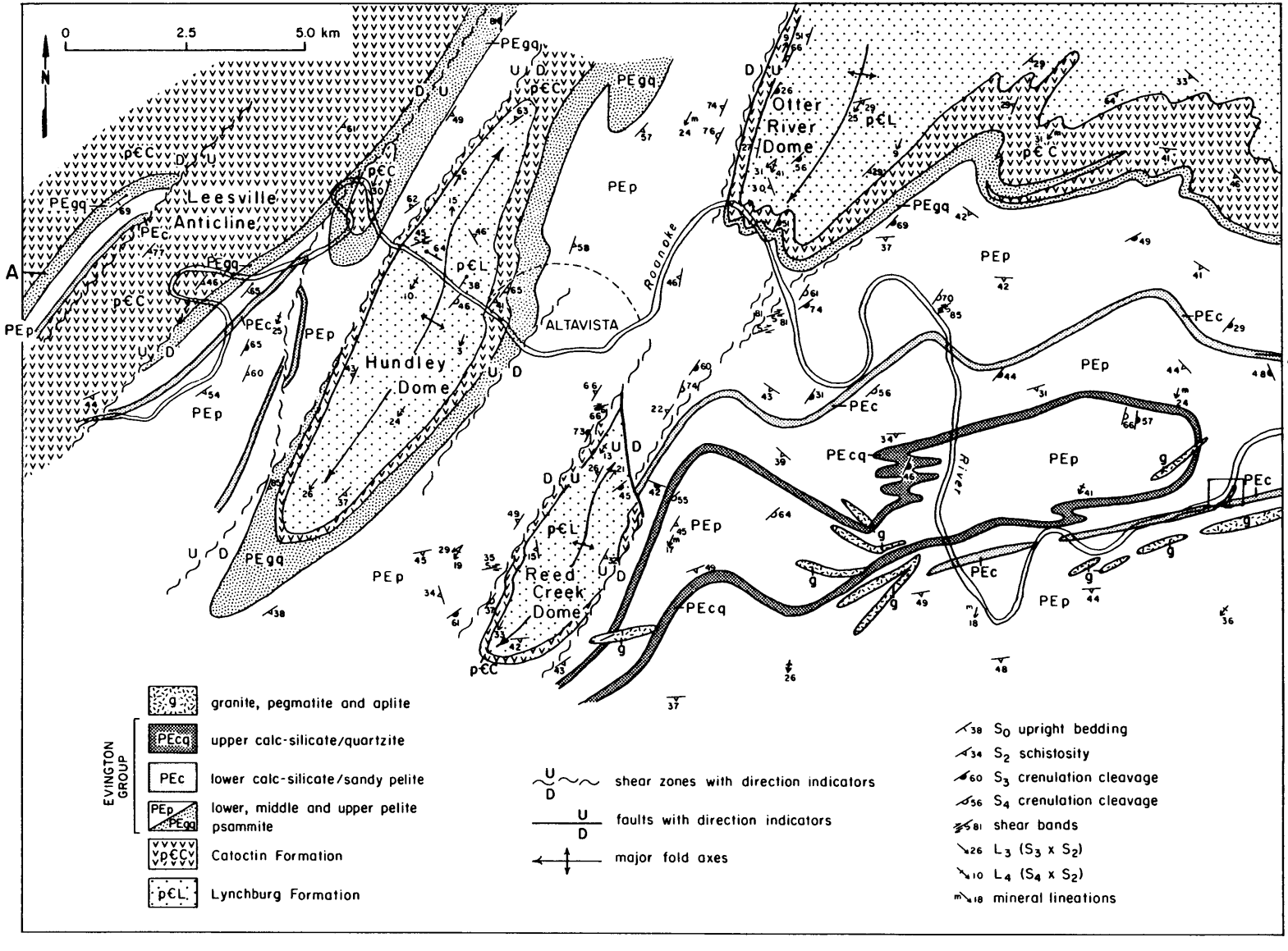
0
2.5
5.0 km
N
Leesville Anticline
Hundley Dome
Reed Creek Dome
Otter River Dome
ALTAVISTA
Roanoke River
A
A'
granite, pegmatite and aplite
upper calc-silicate/quartzite
lower calc-silicate/sandy pelite
lower, middle and upper pelite psammite
EVINGTON GROUP
Catoctin Formation
Lynchburg Formation
shear zones with direction indicators
faults with direction indicators
major fold axes
S0 upright bedding
S2 schistosity
S3 crenulation cleavage
S4 crenulation cleavage
shear bands
L3 (S3 x S2)
L4 (S4 x S2)
mineral lineations

PRE-DOME GEOLOGY OF THE ALTAVISTA AREA

The oldest unit in the Altavista area is the Late Precambrian, Lynchburg Formation (Brown, 1958; Espenshade, 1954; Wehr and Glover, 1985) which is exposed in the cores of the domes (Figure 13). The Lynchburg in Altavista is composed of metamorphosed arkosic to lithic conglomerate that grades upward into medium grained, feldspathic sandstone to graywacke with thin micaceous laminations (Gates and Glover, in prep.). The sandstones are locally intruded by muscovite-biotite-garnet pegmatite and granite dikes. Overlying the Lynchburg Formation is the Late Precambrian, metavolcanic Catoctin Formation (Brown, 1958). The medium to coarse-grained, Catoctin hornblende-andesine schists include 5 to 60 m thick discontinuous layers of quartzite, local tonalitic pegmatites or metamorphic segregations and epidote-quartz layers and boudins.

Conformably overlying and in gradational contact with the Catoctin Formation is the metasedimentary Evington Group of latest Precambrian to Cambro-Ordovician(?) age (Espenshade, 1954; Brown, 1958; Evans, 1984). The Evington Group consists of a basal metagraywacke with cross-beds, that coarsens upward into a massive quartzite (Gates and Glover, in prep.). The upper Evington Group consists of a thick pelitic sequence with sporadic, thin calc-silicate/siltstone to sandstone layers. The pelitic rocks are sillimanite-staurolite-garnet schists to gneisses that are retrograded to chloritoid-chlorite schists in discrete zones that contain hydrothermal kyanite and tourmaline deposits (Gates and Speer, in prep.). The pelites are locally migmatitic and intruded by garnet-tourmaline pegmatite, aplite and granite dikes. The middle and upper portions of the pelitic unit contain two 5 to 50 m thick, thinly layered calc-silicate units that are composed of diopside-amphibole-garnet-epidote schist with pelitic laminations. Associated with the upper calc-silicate unit is a massive, coarse grained, calc-silicate bearing quartzite.

The Lynchburg through Catoctin units have been interpreted as a rift basin sequence capped by rift generated basalts (Brown, 1958; 1970; Rankin, 1975; Wehr and Glover, 1985). The overlying Evington Group has been interpreted as a drift sequence (Wehr and Glover, 1985) and the deeper water equivalent of the Valley and Ridge shelf (Brown, 1970; Evans, 1984).

Glover et al. (1983) have proposed that the regional metamorphism of the Smith River Allochthon terrane is attributable to the Taconic Orogeny. The Leatherwood Granite intrudes the Smith River area subsequent to the peak of metamorphism (Conley and Henika, 1973; Conley, 1978) and has been dated at 462 ± 20 Ma using Rb/Sr whole rock methods (Odom and Russell, 1975). Rb/Sr biotite-whole rock ages of 440 ± 22 Ma (Odom and Russell, 1975) were obtained from pelitic, sillimanite-staurolite gneisses in the center of the allochthon. These ages indicate that the amphibolite grade M_1 metamorphism is Ordovician or Taconic in age.

The Taconic deformation which is concurrent with M_1 is characterized by two phases of deformation, D_1 and D_2. The associated F_1 and F_2 fold generations are recumbent isoclinal and coaxial. S_1 and S_2 foliations were also developed during the D_1 and D_2 deformational events respectively. S_1 was transposed into the pervasive S_2 foliation and is preserved as intrafolial folds in pelitic gneisses and aligned inclusions in porphyroblasts that are oblique to the enclosing S_2 foliation. S_2 is defined by prismatic and platy minerals that were produced during the M_1 metamorphism (Gates and Speer, in prep.). A late M_1 retrogression produced slightly foliated to randomly oriented minerals that were apparently formed late in D_2. Because the M_1 metamorphism is Taconic in age and defines S_1 and S_2, both D_1 and D_2 are Taconic or older. Stereographic projections of poles to S_2 foliation in the eastern and least deformed portion of the area (Figure 14A), yield a tight cluster of points. These data were measured on the south flank of the Sherwill dome and appear to have undergone passive rotation from the sub-horizontal orientation they exhibited as a result of

Taconic deformation. The dip of the foliation flattens to the south of Altavista (away from the Sherwill dome) (Marr, 1984) and is sub-horizontal in the center of the Smith River area farther to the south (Conley and Henika, 1973).

DOME GEOMETRY

Three of the domes in the Altavista area were mapped in detail: the Hundley dome, the Reed Creek dome and a flank dome on the composite Sherwill dome, herein named the Otter River dome (Figure 13). Each dome exhibits the same stratigraphic sequence of Lynchburg Formation in the core and Catoctin Formation through lower Evington Group comprising the rim. The westernmost Hundley dome is lozenge-shaped with a general sigmoidal geometry. The northwest side of the western limb and southeast side of the eastern limb of the dome are straight, nearly parallel and strike 045° The Catoctin Formation and lower Evington Group units are thinner along these sides than the others and locally have been reverse faulted. The other sides of the dome exhibit a more northerly strike and the northeast side exhibits parasitic folds. The dome is generally divisible into three subareas on the basis of the major fold axis and the orientation of intersection lineations. Stereographic projections of these sub-areas (Figure 14B) show that the β-axes derived from poles to S_2, plunge 19/033 in the northern section, approximately 21/195 in the central, and 17/221 in the southern section. The axis therefore reverses plunge direction in the northern section of the dome and is generally sigmoidal in shape.

The southern half of the Otter River dome was mapped in detail (Figure 13). The geometry is generally similar to the Hundley dome but the southern terminus contains many mesoscopic folds, and the southeast limb is more curved. The dome fold axis of

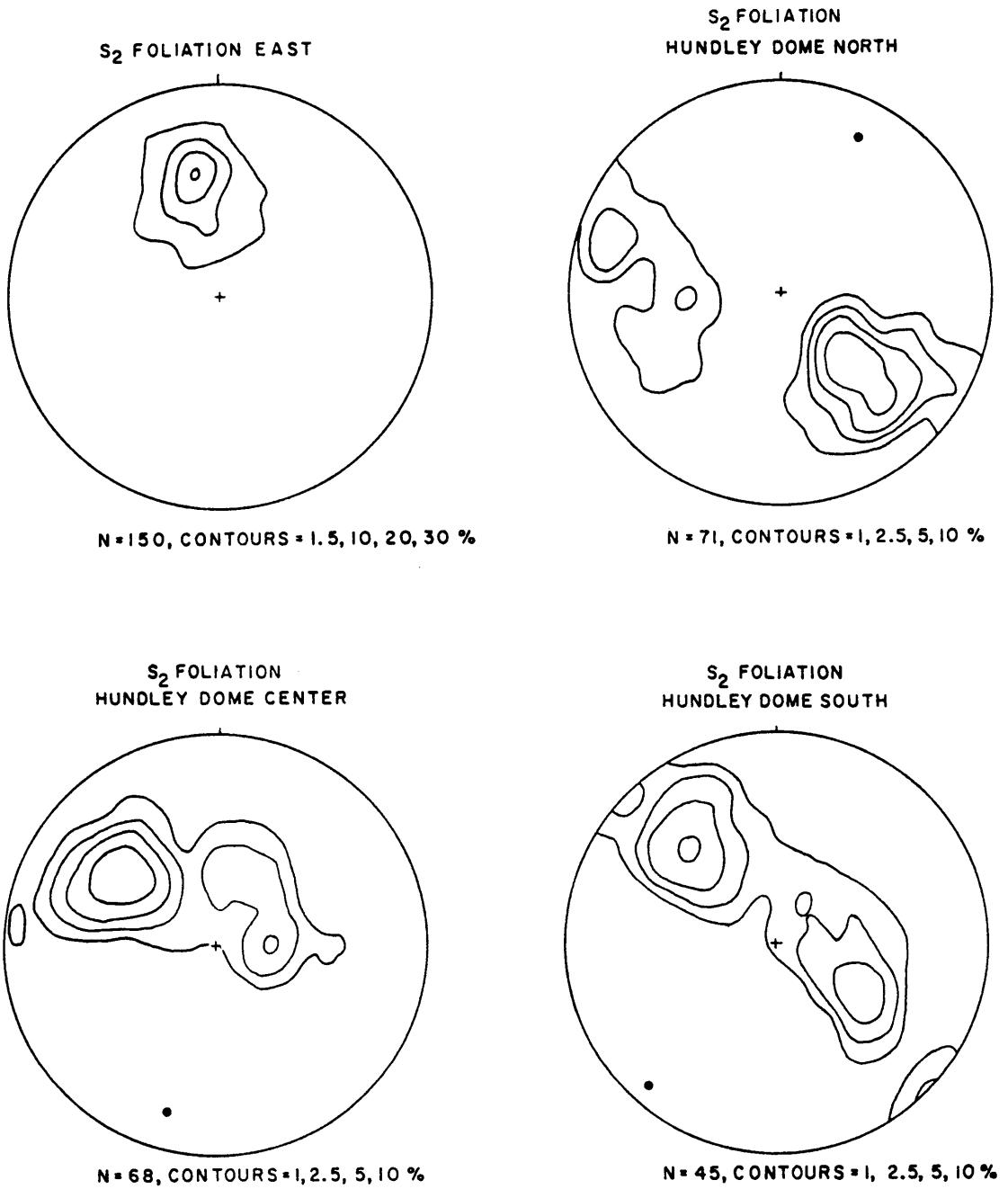

Figure 14. Stereographic projections of poles to S_2 foliation. A) From the eastern Altavista map area. B) Northern, central and southern Hundley dome as indicated.

the southern portion plunges 18/230 and the central 6/209, similar to the Hundley dome but trending more towards the west.

The Reed Creek dome (Figure 13) is the smallest and farthest south of those studied. The northwest side exhibits thinned units, is generally straight and is oriented at about 038° but the southeast limb is strongly curved to the west. The southwest and northeast sides are folded on both the outcrop and map scale. The northwest and southeast sides are cut by east and west dipping reverse faults respectively that locally remove the Catoctin and lower Evington Group units. The plunge of the fold axis in the southern area is 22/234, the central 15/212 and the northern 8/226. The northern terminus of the dome is removed by a west dipping reverse fault that strikes 356 (Figure 13).

STRUCTURAL ELEMENTS

D_1 and D_2 Deformational Events

Early deformational events D_1 and D_2 are associated with the Taconic high grade metamorphism (Gates and Glover, in prep). F_1 and F_2 mesoscopic isoclinal folds and rootless isoclines are preserved in the pelitic gneisses and calc-silicate units. Map scale isoclinal folds occur in the southeastern map area (Figure 13) with axial planes of F_2 subparallel to those of F_1. The pervasive foliation in the Altavista area is S_2 which is defined by all platy and elongate minerals. S_1 is poorly developed or almost thoroughly transposed into S_2. It is preserved only locally in isoclinal hinges and rootless isoclines in the S_2 schistosity and as obliquely aligned inclusions in the cores of porphyroblasts.

D_3 Deformation

The D_3 and D_4 deformational events formed the domes in the Altavista area (Figure 13). Structural features produced in these events appear intimately related in space and are best developed in discrete zones. Greenschist grade platy mineral growth that characterizes the M_2 metamorphism, defines the cleavages developed in these deformational events. The maximum intensity of deformation occurs around the domes and occupies a belt approximately 15 km in width. Crenulation cleavages formed in these events however, occur far outside of the high strain area.

Mesoscopic F_3 folds are locally preserved in the Altavista area. They are upright, open to gentle and symmetric to slightly asymmetric in most areas. Wavelength of the mesoscopic folds varies from 3 to 10 cm and amplitude is 1 to 4 cm. In most cases however, F_3 folds have undergone rotation, and have been tightened and overturned during D_4. They are preserved in the Lynchburg Formation, Catoctin Formation and calc-silicate rocks of the Evington Group.

An S_3 crenulation cleavage formed during the D_3 event. S_3 (Figure 15) is tightly (3 to 5 mm) spaced and forms symmetric to slightly asymmetric, zonal microfolds (Gray, 1977) in the S_2 foliation. S_3 appears approximately axial planar to the F_3 structures but both have been tightened and rotated during the D_4 deformation. S_3 is well developed in micaceous units and overprints the slightly to randomly oriented minerals of the M_1 retrogression, including the hydrothermal kyanite deposits. Aligned fine grained muscovite and chlorite replace the M_1 minerals along S_3 cleavage planes.

In the southeast corner of the study area (Figure 13), outside of the the 15 km wide intensely deformed area, weakly developed intersection lineations (S_3 X S_2 or L_3) in pelitic schists form a tight concentration of points on a stereographic projection (Figure 16A). The orientation is 24/197 and the tight clustering indicates that subsequent deformation was minor or involved only passive rotation. Plots of S_2 from the

Figure 15. Sample of mica schist from the upper Lynchburg Formation showing S_3 and S_4 crenulation cleavage intersections with the S_2 surface. Scale bar = 5 cm.

Figure 19. Photomicrograph of shear bands in chloritoid-chlorite, Evington Group pelitic schist. c = chloritoid, m = mica, q = quartz ribbon and SB = shear bands with movement directions shown by arrows. Scale bar = 1 mm.

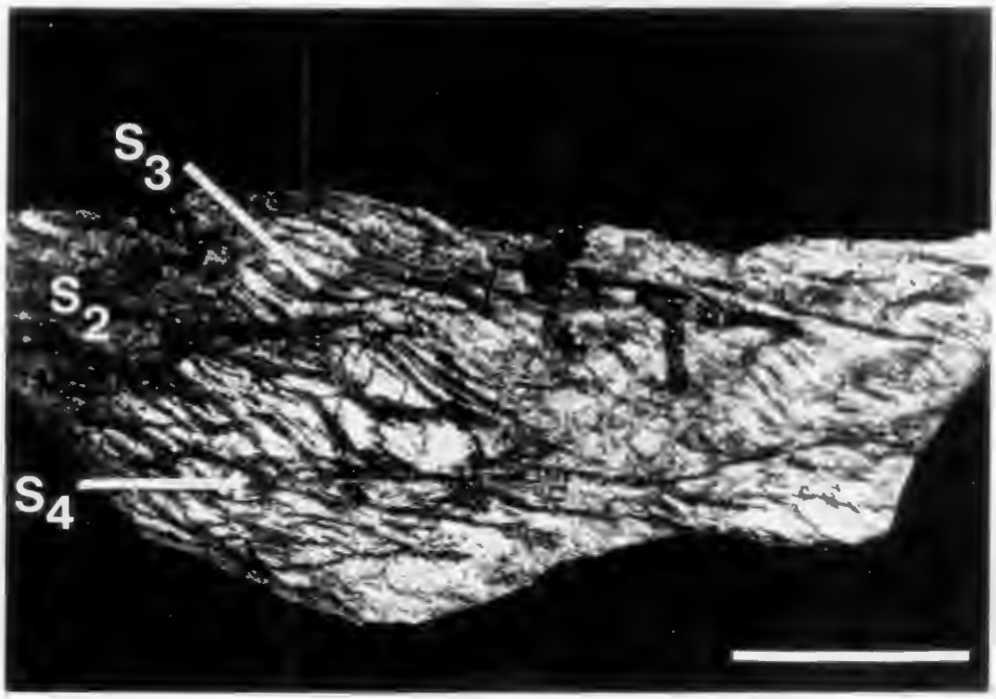
S3
S2
S4

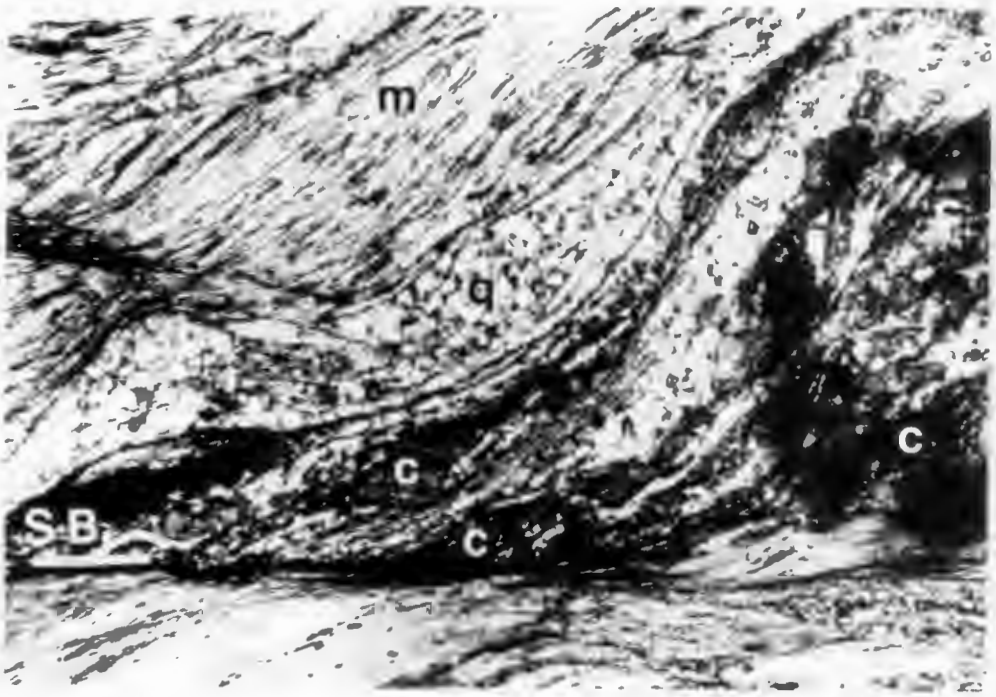
m
q
c
c
c
S-B

same area (Figure 14A) also yield a tight clustering. Around the domes however, the L_3 lineations form a diffuse concentration of points with trends ranging from that of the eastern area (197) to approximately 255, with the major concentration at 220 (Figure 16B). In the Hundley dome, L_3 lineations form a sigmoidal pattern that follows the major dome axis (Figure 13). Poles to S_3 form a girdle that defines a fold axis of 16/219 (Figure 16C). The early crenulation cleavage was therefore folded during a later event. The axis and distribution of poles to S_3 in Figure 16C is comparable to the plot of poles to S_2 in the southern Hundley dome (Figure 14B).

Map scale F_3 structures are identifyable in and between the domes (Figure 13). F_3 folds produce the northeast and southwest closures of the domes in otherwise northeast trending anticlines (Figure 13). The original orientation of F_3 structures is difficult to determine because of subsequent deformation. The trend of the F_3 fold axes ranges from 188 to 240 and plunge varies from 40S to 15N. Mesoscopic folds in the core of the Hundley dome and map scale structures there and between the Reed Creek and Otter River domes (Figure 13) suggest that the initial orientation of F_3 axes were approximately horizontal and trended nearly north-south. Because the north-south oriented structures are only present along the northeast trending Bowens Creek Fault, they were probably originally en-echelon as some still are (Figure 12).

D_4 Deformation

The F_4 folds are northeast trending and well developed on the outcrop and map scale (Figure 13). Mesoscopic folds are tight and asymmetric with axial planes inclined to the northwest. The F_4 folds contain well developed parasitic folds on the limbs and are best displayed in the Evington Group pelites. These folds occur on most commonly the southwest and northeast parallel sides of the domes and comprise the

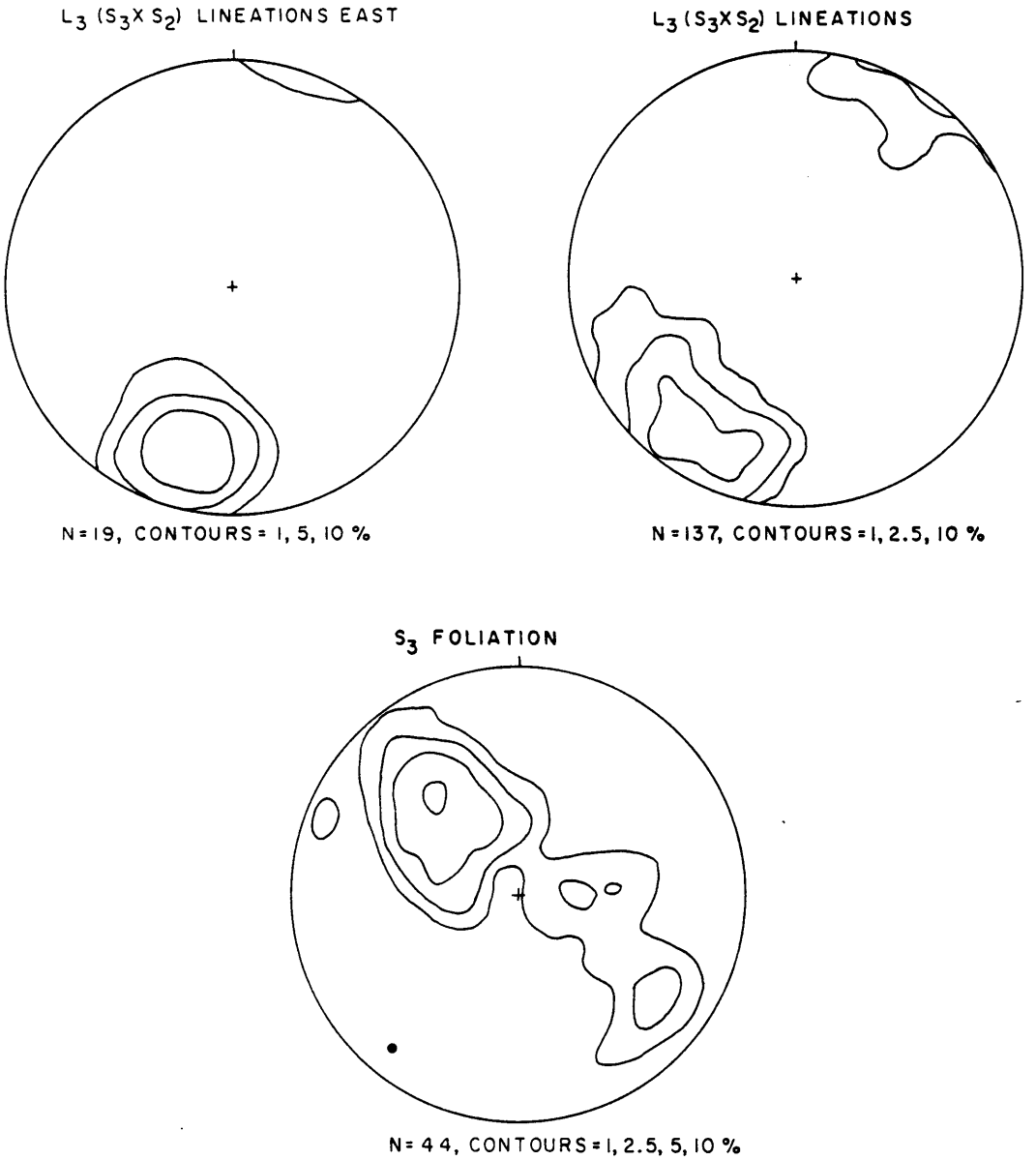

Figure 16. Stereographic projections of: A) L_3 lineations (S_3 X S_2) from the eastern map area (minor D_4 deformation), B) L_3 lineations from within the domed area and C) poles to S_3 from within the domed area.

parasitic folds on the terminations (Figure 13). Fold axes trend 225 and plunge ranges from 30 SW to 10 NE depending upon the position on the F_3 structure.

The S_4 crenulation cleavage overprints the S_2 and S_3 cleavages (Figure 15). S_4 is upright to asymmetric to the northwest and narrowly (3 - 4 mm) to widely (1 - 2 cm) spaced with irregular to sinuous axes. The cleavage is a spaced, zonal type (Gray, 1977) forming microfolds in the S_2 pervasive foliation. Where S_4 crosses S_3, the resultant interference pattern displays S_3 crenulations that wind sinuously across the S_4 crenulation axes (Figure 15). A stereographic projection of poles to S_4 yields a cluster of points that defines an approximate plane of 036 64 SE (Figure 17A) indicating that S_4 is not axial planar to the F_4 folds. The angle between S_4 and S_3 crenulation cleavages is highly variable. S_4 usually lies in a counterclockwise direction (negative rotation) from S_3 as in Figure 15, but is also found with a clockwise (positive) angle. L_4 (S_4 X S_2) intersection lineations form a similar cluster trending approximately 22/214 (Figure 17B) and indicating that S_4 underwent only minor rotation. This axial orientation is nearly identical to that defined by the poles to S_3 and poles to S_2 in the southern Hundley dome. S_2 and S_3 were therefore folded about an F_4 fold axis.

The map scale F_4 folds produce the major northeast trend of the domes. The folds are more asymmetric and inclined to overturned in the western portion of the map area than in the east (Figures 13 and 18). The en-echelon, north-south oriented F_3 structures form saddles on the F_4 northeast trending anticlines. The domes therefore represent a type 1, 0-90° (Ramsay, 1967) interference pattern.

Also intersecting the S_2 and S_3 cleavages are shear bands (extensional crenulation cleavage of Platt and Vissers, 1980) with consistant dextral offset. The shear bands are narrowly (3 mm) to widely (2 cm) spaced and best developed in the pelitic Evington Group schists. M_2 chlorite and muscovite grains are bent into "fish" (Eisbacher, 1970; Lister and Snoke, 1984) and M_1 chloritoid forms sigmoidal porphyroclasts with tails trailing into the shear bands (Figure 19). Sigmoidal quartz ribbons (type 2B and 4B

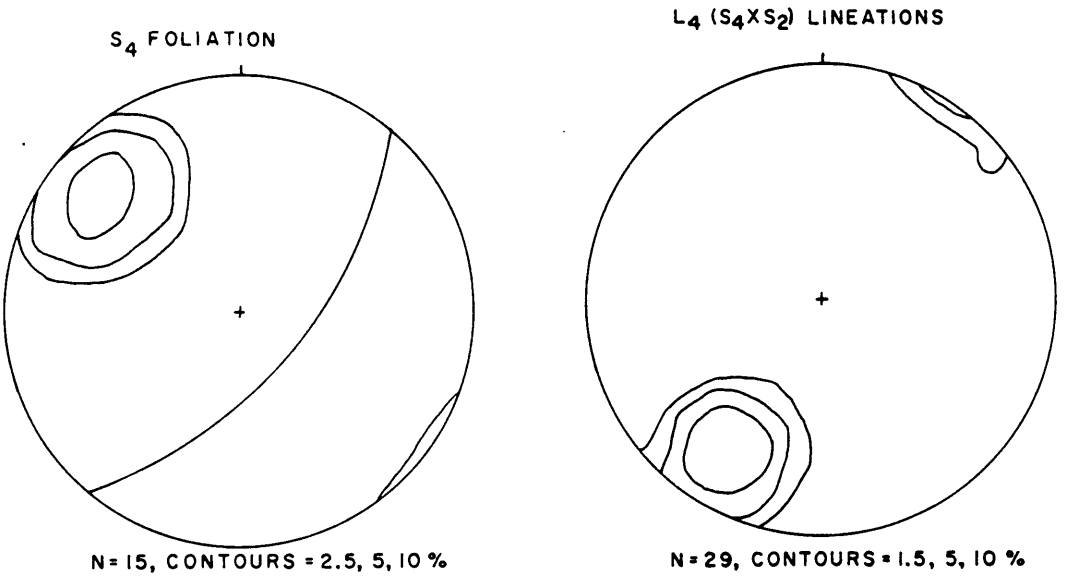

Figure 17. Stereographic projections of A) poles to S_4 crenulation cleavage and B) F_4 fold axes and L_4 (S_4 X S_2) intersection lineations.

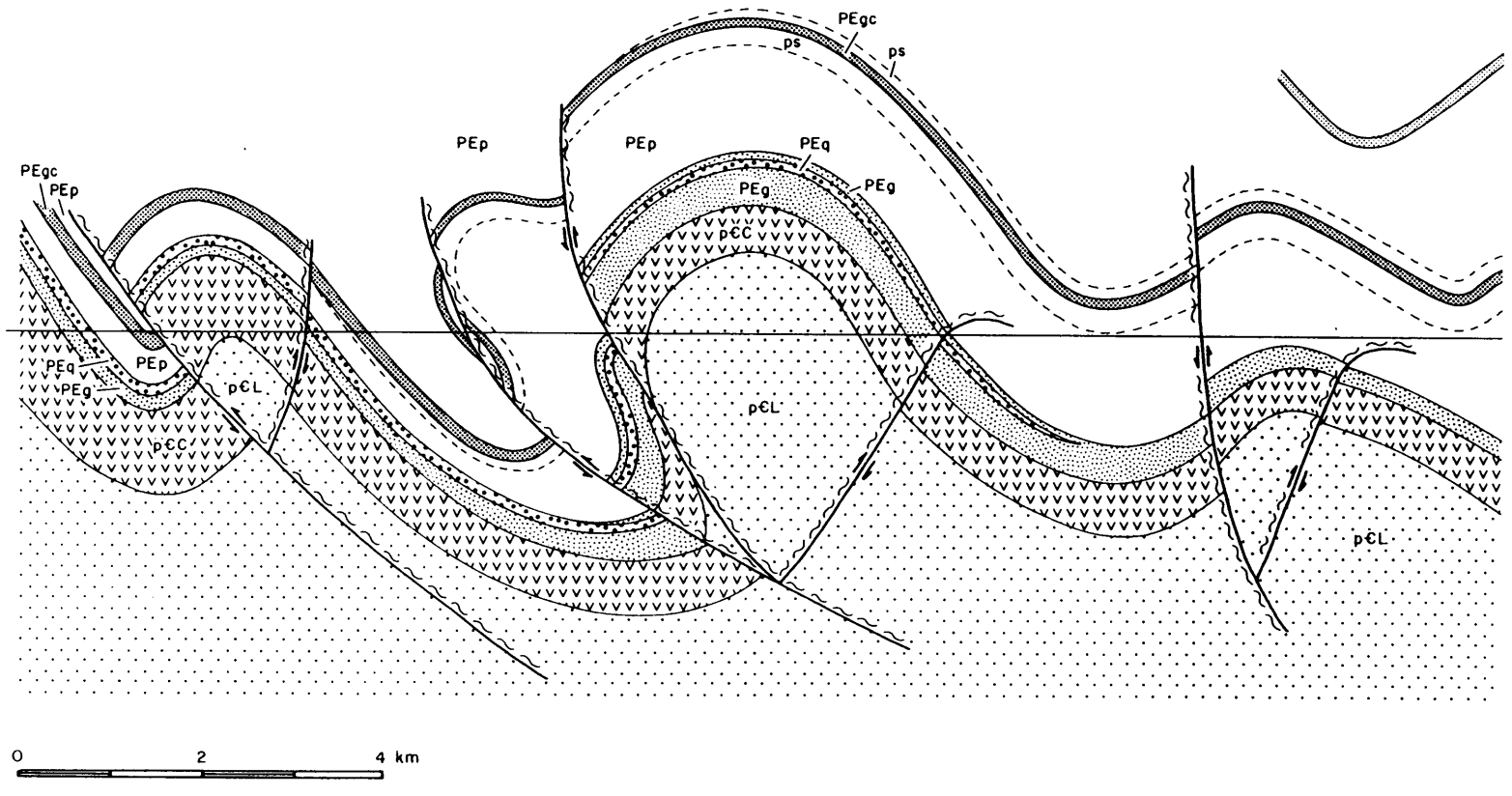

Figure 18. Cross-section of the Altavista Area.

of Boullier and Bouchez, 1978) are layered with the mica, chlorite and chloritoid. The shear bands are defined by fine recrystallized chlorite and muscovite and offset the earlier foliations. Kyanite is also kinked and bent into the shear bands. Thin granite and pegmatite dikes in the Lynchburg Formation are offset in a dextral sense by spaced extensional step faults. The shear bands however, are rare in the Lynchburg and Catoctin formations. Poles to shear bands from the entire field area define a rather diffuse partial girdle. In areas where F_4 structures are poorly developed (between the Otter River and Reed Creek domes and in the central Hundley dome), the shear bands generally trend 071 65 SE to vertical. The shear bands were therefore reoriented during D_4.

In the small granite dikes of the southeastern map area (Figures 13 and 20) C and S bands (Berthé et al., 1979) are also developed. Early formed S planes (schistosity) defined by quartz ribbons (type 2B of Boullier and Bouchez, 1978) and aligned mica curve into C planes (cisaillement or shear planes) in a consistant dextral sense. Feldspar porphyroclasts show evidence of brittle fracturing followed by dynamic recrystallization along the grain margins. The resulting structure is a type I S-C mylonite of Lister and Snoke (1984).

Mineral Lineations

Mineral stretching lineations are also common in the Altavista area. Biotite, muscovite, chlorite and less commonly hornblende, tourmaline, staurolite and rods of quartz are aligned on the S_2 surface. The stereographic projection of the lineations is nearly indistinguishable from that of F_3 fold axes and L_3 intersection lineations. In hand sample, the mineral lineations are parallel to L_3 lineations, L_4 lineations, lie somewhere between the two or show no apparent angular relationship. The variability

of the orientations suggest that several sets of mineral lineations of varying age and degree of reorientation may exist. The main concentration of data lies at 19/223 (Figure 21) or approximately at the F_4 fold axis.

Faults

There are many large and small scale ductile and locally brittle faults. Offsets range from several centimeters to several meters for small scale faults and tens to hundreds of meters for large scale faults. Movement directions were determined by offset units, missing or tectonically "thinned" units and "dragged" foliation against the fault plane but in some cases, they were indeterminate. Three distinct groups of faults are apparent.

Group one minor faults are reverse faults that exhibit consistent strikes of 015 and steep dip angles to both east and west (Figure 20). The large scale fault of group one trends 356 and has faulted out the north end of the Reed Creek dome (Figure 13). Offset for this fault appears large (approximately 250 m to 1 km) but cannot be accurately estimated. The orientation of the group one faults suggests that they were active during D_3.

Group two reverse faults are the most common and strike 045 to 059 with dips of 45 to 60 to both northwest and southeast. Large scale faults of group two include reverse faults that bound the northwestern Hundley dome, both sides of the Leesville Anticline and the northeast side of the Reed Creek dome (Figure 13). Many of the other northeast trending, straight limbs of the domes exhibit intense cleavage devel-

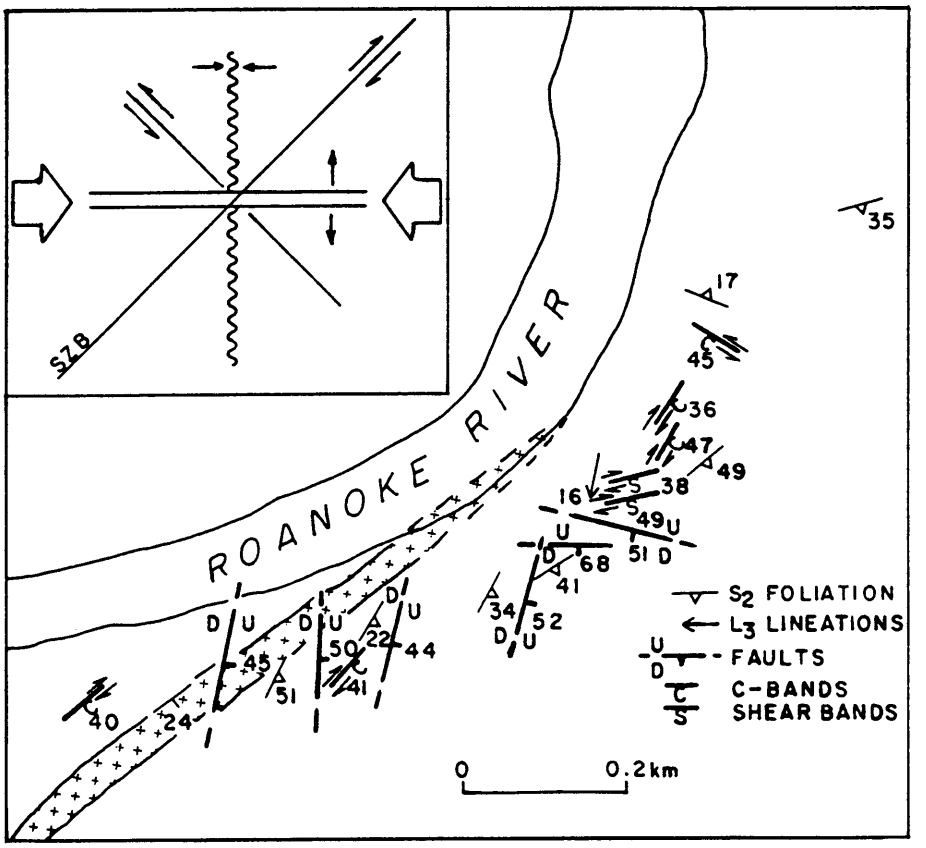

Figure 20. Detailed geologic map of the eastern Altavista map area. Inset: simple shear model of principle stress with resulting dextral and sinistral shears and compression and extension directions.

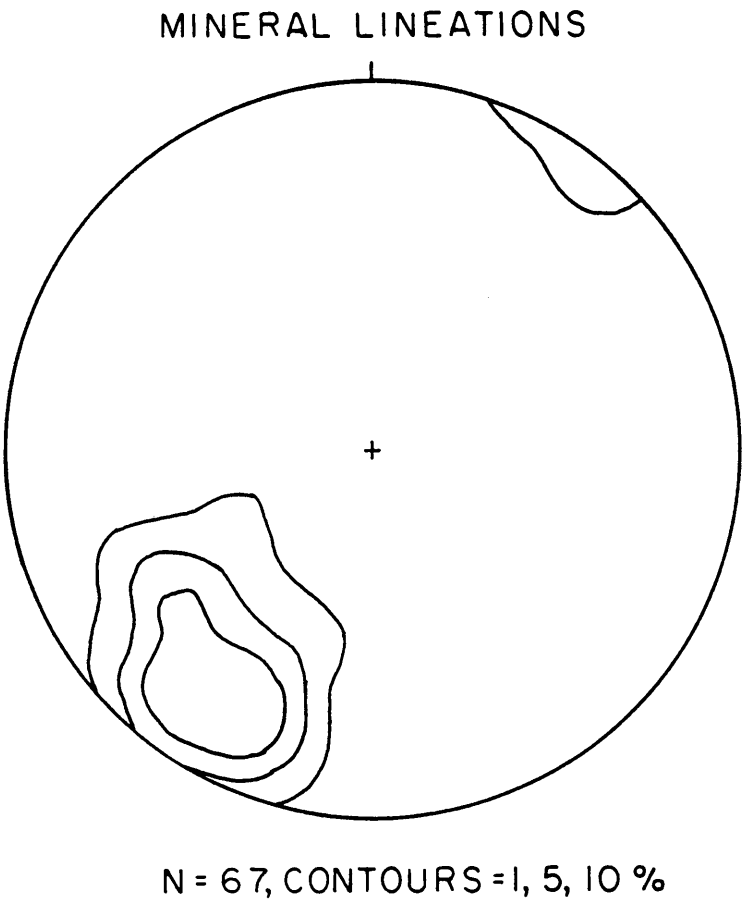

Figure 21. Stereographic projection of mineral lineations.

opment, thinned units and near vertical, northwest or southeast oriented (pure dip-slip) mineral lineations locally. These sides appear to be sheared in a reverse sense which suggests that the domes emerged along faults as well as by folding (Figure 18). Because of the orientation and well developed S_4 crenulation cleavage, group two faults appear to have been active during the D_4 deformation.

The final group (three) is represented only by four documented examples of normal faults oriented at approximately 100 with variable dips to both north and south (Figure 20). The deformation episode that these faults are associated with is questionable but because they mainly occur in areas that experienced only mild D_4 deformation, they are attributed to the D_3 event.

There are many other minor faults in the area the orientations of which are appropriate for these groups, but for which movement directions could not be determined. Similarly, there are several minor faults in the area which cannot be classified into the three groups. Most of these faults are in another orientation or are strike-slip faults and represented by too few examples.

STRUCTURAL DEVELOPMENT

The structures in the Altavista area indicate a complex kinematic history. The domes, reverse faults and multiple crenulation cleavages support a history of compressional tectonics but many other structural elements require deformation associated with transcurrent movement.

The consistent and widespread dextral shear bands which form in initially anisotropic rocks (Platt and Vissers, 1980), indicate that dextral transcurrent movement occurred throughout the Altavista area. C and S bands (Berthé et al., 1979) in small granite bodies in the eastern map area also show consistant dextral movement.

C planes, which are formed in initially isotropic rocks, are assumed to parallel the shear zone boundary (Berthé et al., 1979) which in this case is 045 - 050. The shallow plunge of the majority of the mineral lineations, if associated with shear movement, also supports a dominantly transcurrent shear zone. The dominant trend of the mineral lineations is 223, which defines the stretching direction, agrees with the orientation of the C planes. The shear bands are therefore oriented at $+21°$ to $+28°$ from the shear zone boundary. Gates et al. (1986) found that shear bands in the nearby transcurrent Brookneal zone (Figure 12) similarly formed at $+24 \pm 3°$ to the shear zone boundary. The Brookneal zone is also dextral and oriented at 040.

Employing the dextral shear model, the first post-Taconic (D_1, D_2 and M_1) structures formed in the Altavista area were the large and small scale F_3 folds and S_3 crenulation cleavage. The initial orientation of the structures cannot be absolutely determined but the weakly overprinted center of the Hundley dome and nearly undeformed S_3 crenulation cleavage of the eastern map area indicate a trend of approximately 195 to 200. If the structures were produced in a simple shear system, they would have been formed with axial surfaces parallel to the X-Y plane of the finite strain ellipsoid (Ramsay and Graham, 1970; Ramsay, 1980). The D_3 structures (Figure 22A) would then be analogous to the early S bands formed in isotropic rocks (Berthé et al., 1979; Simpson, 1984). In simple shear with a horizontal initial orientation (in the X-Y plane), the folds would have formed at -45° to the shear zone boundary (Ramsay and Graham, 1970). According to field and experimental observations however, compressive structures in a transcurrent system actually form at approximately 25 to 45° from the shear zone boundary (for actual estimates see Ghosh, 1966; Tchalenko, 1970; Wilcox et al., 1973; Dubey, 1980; DeSmet, 1984; Ingles, 1985). This angle is dependent on the rheology of the rock (Tchalenko, 1970), the initial orientation of the anisotropies (Ramsay et al., 1983) and the amount of pure shear or transpression in the system (Harland, 1971; Sanderson and Marchini, 1984).

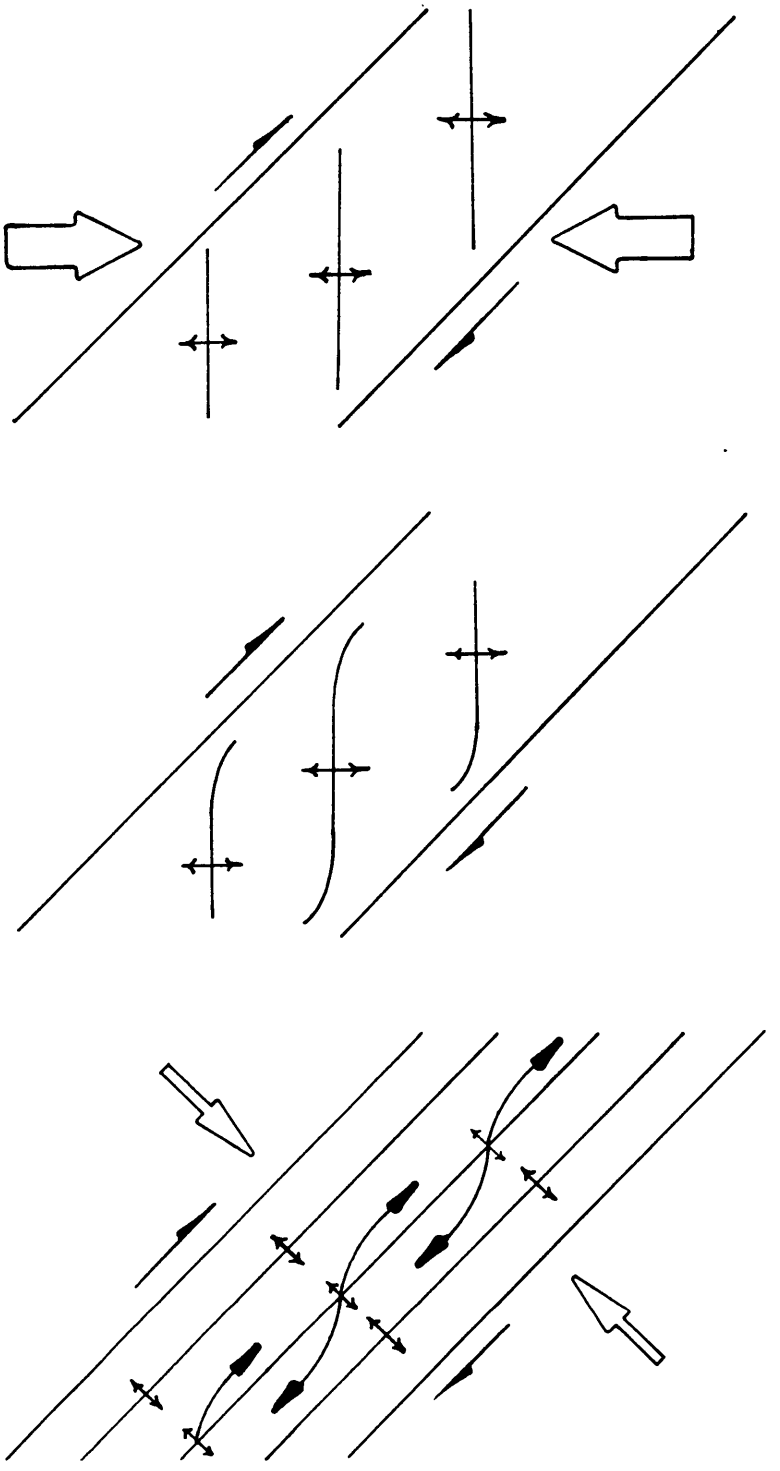

Figure 22. Schematic diagrams of: A) D_3 deformation with F_3 structures, shear zone boundary and principle stress directions, B) dextral shear and partial reorientation of structures, and C) D_4 deformation with F_4 structures and reverse faults.

The Bowens Creek Fault has an approximate strike of 045 to 050. If associated with the fault, the F_3 structures were en-echelon and formed with an initial orientation of 000 to 015 (180 to 195) or the approximate orientation of the least deformed structures. These structures may also have undergone minor clockwise rotation during the subsequent dextral shearing or F_4 folding event. In the eastern map area where relatively little D_4 deformation took place (Figure 20), group one reverse faults are oriented at 35 to 45° from the strike of the C planes in the granite (approximate shear zone boundary). In this area, normal faults are oriented approximately 90° from the reverse faults and an apparent conjugate left lateral fault is oriented 75° from the C planes (Figure 21). This configuration of compressional, extensional and conjugate faults is essentially that predicted by the simple shear model.

After formation of the D_3 structures which include the F_3 folds, S_3 crenulation cleavage, group one reverse faults and group three normal faults, rotation of the structures through dextral shearing apparently took place (Figure 22B). Evidence for this phase is only well documented in the dextral shear bands. The F_3 crenulation axes (L_3 lineations) are deformed and offset by the shear bands which are in turn locally folded in F_4 folds. There is also a great variability (both positive and negative rotation) in the acute angle between S_3 and S_4 foliations. The variability in the angle cannot purely reflect the degree of reorientation of S_3 during D_4 deformation or the angle would vary inversely with S_4 intensity. This relation was not observed and does not explain the rotation of S_3 to S_4 in both positive and negative senses.

Mineral lineations intersect, are parallel to and are folded by F_3 crenulation axes. This variability indicates that they probably formed continuously throughout the D_3 deformation and possibly also in the D_2 and D_4 events. If the majority of the lineations are associated with dextral shear zone movement then they approximate the shear orientation (223).

The D_4 deformation (Figure 22C) produced the northeast-trending F_4 map scale and mesoscopic folds, S_4 asymmetric crenulation cleavage, group two reverse faults and apparent reverse shear zones on the northeast trending sides of the domes. Reorientation and transposition of many of the early structures occurred during the D_4 event. The D_4 structures appear to reflect northwest-southeast oriented compression and can be explained by two possible processes. The first is that of transpression as proposed by Harland (1971), Sylvester and Smith (1976), Harding and Lowell (1979), DeSmet (1984) and Sanderson and Marchini (1984) for many other fault systems. According to Sanderson and Marchini (1984), the angle of the compressional structures to that of the transcurrent zone is a function of the amount of pure shear or compression across the zone. Compressional features that parallel the transcurrent zone would require a system of pure compression with no simple shear.

Sylvester and Smith (1976), Wilcox et al. (1973) and Harding and Lowell (1979) found that reverse faults could be active concurrently with strike-slip faults. Low to high angle reverse faults that dip in opposite directions are synchronously active with nearby parallel strike-slip faults on portions of the San Andreas fault and in the Ardmore Basin, Oklahoma. The reverse faults emerged from basement, cut the cover rocks and produced asymmetric structures that verge in opposite senses. The fault movement caused emergence of antiformal, fault bounded basement blocks in "keystone structures" (Sylvester and Smith, 1976) or "positive flower structures" (Harding and Lowell, 1979). The compression appears late in the developement of the shear zone but synchronous with strike-slip movement (Figure 22). Sylvester and Smith (1976) attribute the two strain directions to tectonic transpression (Harland, 1971) but where zones of pure compression and zones of simple shear are simultaneously operative. Woodcock and Robertson (1982) found a similar strike-slip/reverse fault combination in the Antalya complex of southwestern Turkey. They could not resolve whether the two movement directions were synchronously formed but con-

strained them to have both been active over a relatively short period of time. They proposed that the oblique strain may have been resolved into concurrent compressional and transcurrent forces.

In Altavista, D_3 formed the en-echelon structures that were subsequently variably rotated. The D_4 event involved folding, cleavage development, continued formation of subhorizontal stretching lineations and zones of intense deformation that parallel the shear zone boundary. The stratigraphically documented reverse faults occur on the straight limbs of the southeast Reed Creek dome, the northwest Hundley dome and both limbs of the Leesville anticline. The unfaulted straight limbs of the domes exhibit intense S_4 cleavage development and are tectonically thinned. Locally developed near vertical mineral lineations have been found in the intense cleavage zones suggesting that they were sheared. The antiformal cores of the Altavista domes have therefore emerged through the cover rocks (Figure 18) as "keystone structures" described in the San Andreas system (Sylvester and Smith, 1976) or "positive flower structures" described in the Ardmore Basin (Harding and Lowell, 1979) and the Betic Cordilleras (DeSmet, 1984).

If the Rb/Sr and K/Ar mineral ages on the northern Brevard zone (Conley, 1978) and Bowens Creek Fault (Fullagar and Dietrich, 1976; D. Mose, pers. comm., 1986) reflect the uplift and dextral transcurrent movement, then the fault was active at approximately 350 to 275 Ma. The dextral Brookneal zone which lies 10 km to the east of Altavista was active from 324 to 300 Ma (Gates et al., 1986). The geometry of this central major transcurrent zone and the concurrently active transpressional to compressional area with structural vergence away from the center (Figure 23) is analogous to the Crevillente zone (DeSmet, 1984) in the Betic Cordilleras. The geometry of the domes of the two areas is also similar as are the sequence of events.

DeSmet (1984) found that domal "positive flower" structures formed in the external zone of a major strike-slip fault in the Betic Cordilleras of southern Spain. The

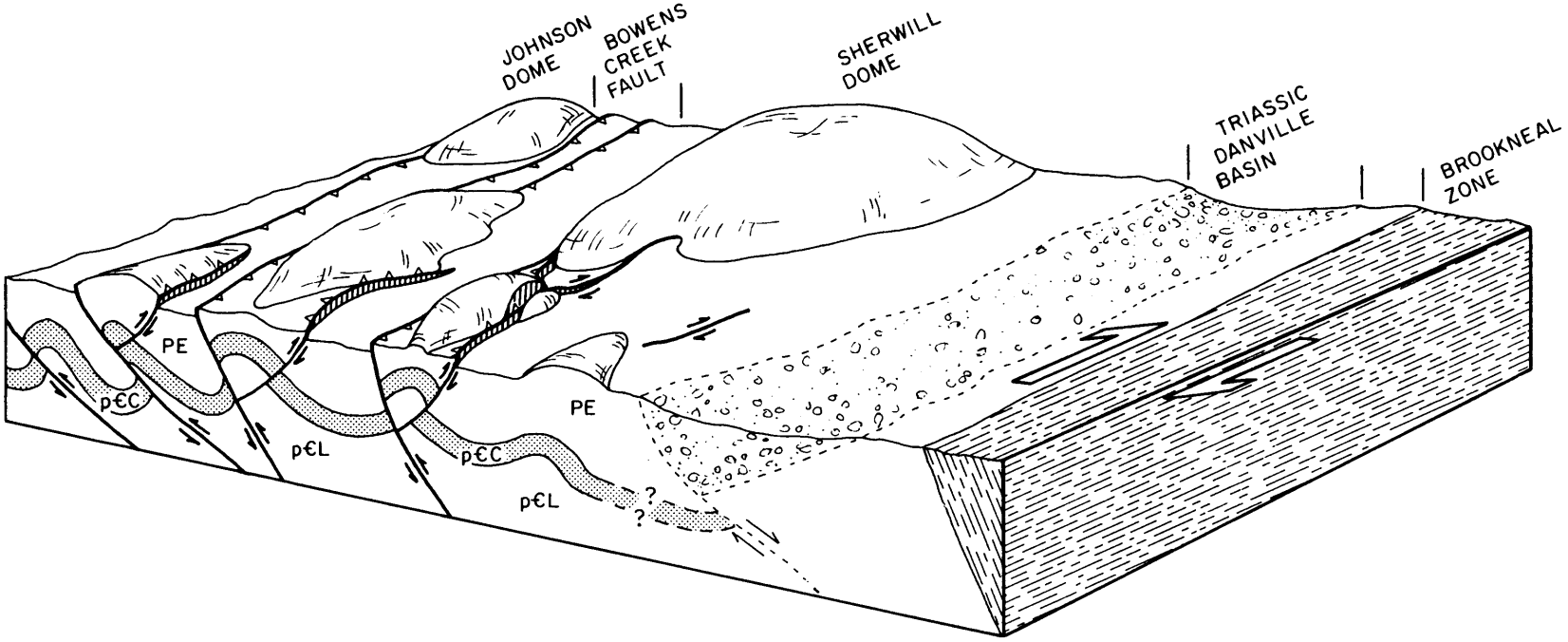

Figure 23. Schematic structural topography block diagram of the Altavista to Brookneal area. Map units correspond to Figure 13 (Catoctin Fm. shaded). Block surface in the Evington Group.

Crevillente strike-slip fault is flanked by inversely symmetrical zones of compressional structures that verge away from the central fault. The progression from center to edge of the zone is: a purely transcurrent zone; an area of sigmoidal, slightly asymmetric, dominantly fault bounded domes and an area of thrust faults and highly asymmetic structures. De Smet (1984) proposed a three stage formation for the domes. A series of en-echelon structrues were formed at 25° from the main shear zone boundary in the early stage. In the middle stage, structures were rotated in some cases and faulted in others depending on local conditions. In the final stage, compression across the zone occurred, producing thrust faults and asymmetric structures as in Altavista.

A second possibility for Altavista is that the D_4 deformation may have occurred in a subsequent compressional event that was unrelated to D_3 and the dextral shearing. Both the D_3 and D_4 events were ductile however, and took place under the same M_2 metamorphic conditions (middle to upper greenschist) suggesting a short time span between the two because mineral ages indicate uplift during this deformation.

TECTONIC IMPLICATIONS

The domes and Bowens Creek Fault formed through the interaction of two deformational events (D_3 and D_4). If both the D_3 and D_4 events were produced as two phases in a single transpressional event, then only one compression direction is required. According to the simple shear model (Ramsay and Graham, 1970), the major compression direction lies 45° from the shear zone and perpendicular to the major structural trend. In both Altavista and Brookneal the compression would have been oriented approximately east-west.

If the D_3 and D_4 events are unrelated, then two compression directions are required. The D_3 compression is that described above (east-west). The D_4 compression

direction would have been oriented approximately southeast-northwest or perpendicular to the F_4 structural trend. This model does not require strict transpression.

The main drawback in applying the formation of the Altavista domes to tectonic models is the lack of solid age constraints on each phase of deformation (D_3 and D_4). The deformations overprint rocks with Taconic deformational features which constrains the age to approximately post Ordovician. Deformation predates the Jurassic age diabase dikes and Triassic age brittle deformation associated with the formation of the Danville Basin (Figure 12). Fullagar and Dietrick (1984) and Mose (personal communication) the Rb/Sr whole rock and mineral ages of 350 to 275 Ma from rocks along several portions of the Bowens Creek Fault falls within that range and agrees with the activity range of the nearby, dextral Brookneal zone (Figure 12). The Brookneal zone exemplifies the Appalachian dextral shear system that extends from Maritime Canada to Georgia. Bradley (1980) summarized the transcurrent faults of the Northern Appalachians and found the peak activity to have occurred between 345 and 285 Ma. The age, metamorphic grade of deformation and orientation of the Bowens Creek deformation zone in Altavista is nearly the same as the Brookneal zone. The Bowens Creek-Brevard zone deformation apparently formed during this Carboniferous Appalachian dextral transcurrent event (Gates, et al., 1986).

CONCLUSIONS

The domes in the Altavista area of the western Virginia Piedmont were imposed on a terrane that was previously deformed and metamorphosed during the Taconic Orogeny. The terrane contained horizontal foliation and structures of D_1 and D_2 deformational events prior to the development of the domes. The D_3 deformation produced en-echelon north-south oriented symmetric map scale and mesoscopic F_3

folds, S_3 crenulation cleavage and group one small and large scale reverse faults. It also formed the group three east-west oriented normal faults and the northeast trending horizontal mineral lineations, dextral shear bands and dextral C - S mylonites in small granite bodies. These D_3 structures were partially rotated by continued dextral shear across the area.

The subsequent D_4 deformation is similar to D_3 in location and metamorphic grade. D_4 structures include northeast trending asymmetric F_4 map scale and mesoscopic folds, S_4 crenulation cleavage and group two reverse faults and shear zones on the limbs of the domes. The D_4 deformation produced "keystone" or "positive flower" structures represented by the northeast trending anticlines that are separated into domes by F_3 synclines.

The transpressional event is constrained to have occurred between Ordovician and Jurassic. It may be related to the Carboniferous Appalachian dextral transcurrent event as suggested by nearby K/Ar and Rb/Sr age determinations. The Altavista area forms an external zone to the nearby dextral transcurrent Brookneal zone that exhibits a similar age of activity metamorphic grade of deformation to Altavista.

REFERENCES

Berthe, D., Choukroune, P. and Jegouzo, P., 1979, Orthogneiss, mylonite and non-coaxial deformation of granites: The example of the South Amorican shear zone; J. Struct. Geol., vol. 1, p. 31-42.

Berquist, C. R., 1980, Sandy Level Quadrangle: Its Geology and Regional Interpretation, in Price, V. Jr., Thayer, P. A., and Ronson, W. A., eds., Geol. Inv. of the Pied.

and Triassic Rocks, Cent. N. Ca. and Va.; Carolina Geol. Soc. Field Trip Guide-book, P. I-1 - I-10.

Bobyarchick, A. R., 1984, A late Paleozoic component of strike-slip in the Brevard Zone, southern Appalachians; Geol. Soc. Am. Abstr. w. Programs, vol. 15, no. 2, p. 126.

Boullier, A. M. and Bouchez, J. L., 1978, Le quartz en rubans dans les mylonites; Bull. Soc. Geol. Fr., vol. 20, p. 253-262.

Bradley, D. C., 1982, Subsidence in late Paleozoic basins in the northern Appalachians; Tectonics, vol. 1, no. 1, p. 107-123.

Brown, W. R., 1958, Geology and mineral resources of the Lynchburg quadrangle, Virginia; Va. Div. of Min. Res. Bull. 74, 99p.

Brown, W. R. 1970, Investigations of the sedimentary record in the Piedmont and Blue Ridge of Virginia; in Fisher,G. W., Pettijohn, F.J., Reed, J. C., and Weaver, K. N. eds. Studies of Appalachian geology; Central and Southern: New York, Wiley Interscience, p. 335-349.

Conley, J. F., and Henika, W. S., 1970, Geology of the Philpott Reservoir quadrangle, Virginia; Vir. Div. Min. Res. Rept. Inv. 22, 46pp.

Conley, J. F. and Henika, W. S., 1973, Geology of the Snow Creek, Martinsville East, Price and Spray Quadrangles, Virginia, Rept. Invest. Va. Div. Miner. Resour., no. 33, 71 pp..

Conley, J. F. , 1978, Geology of the Piedmont of Virginia, Interpretations and Problems; in contributions to Virginia Geology, Va. Div. of Min. Res., Publication 7, p. 115-149.

Conley, J. F., Marr, J. D., Jr. and Berquist, C. R., Jr., 1981, Stratigraphic relationships between rocks of the Blue Ridge Anticlinorium and the Smith River Allochthon in the Southwestern Virginia Piedmont; Vir. Div. Min. Res., 13 ann. Vir. Geol. Field Conf., 34pp.

DeSmet, M. E. M., 1984, Wrenching in the external zone of the Betic Cordilleras, southern Spain; Tectonophysics, Vol. 107, p. 57-79.

Dubey, A. K., 1980, Model Experiments showing Simultaneous development of Folds and transcurrent faults., Tectonophysics, v. 65, p. 69-84.

Eisbacher, G. H., 1970, Deformation mechanisms of mylonite rocks and fractured granulites in Cobequid Mountains, Nova Scotia, Canada; Geol. Soc. Am. Bull., v. 81, p. 2009-2020.

Espenshade, G. H., 1954, Geology and mineral Deposits of the James River-Roanoke River Manganese District, Virginia, U. S. Geol. Surv. Bull. 1008, 155p.

Espenshade, G. H., Rankin, D. W., Shaw, K. W. and Neuman, R. B., 1975, Geologic map of the east half of the Winston-Salem quadrangle, North Carolina-Virginia; U. S. Geol. Surv. Misc. Inv. Series Map I-709-B.

Evans, N. H., 1984, Latest Precambrian to Ordovician metamorphism and orogenesis in the Blue Ridge and western Piedmont, Virginia Appalachians; unpub. PhD dissertation, Virginia Polytechnic Institute and State University; p. 324.

Fullagar, P. D. and Dietrich, R. V., 1976, Rb-Sr isotopic study of the Lynchburg and probable correlative formations of the Blue Ridge and western Piedmont of Virginia and North Carolina; Am. J. Sci., V. 276, p. 347-365.

Gates, A. E., C. Simpson, and L. Glover III, 1986, Appalachian Carboniferous dextral strike-slip faults: an example from Brookneal, Virginia; Tectonics, vol. 5, no. 1, p. 119-133.

Gates, A. E. and Glover, L., III, in prep., The Smith River Allochthon: Geology and Regional Context.

Gates, A. E. and Speer, J. A., in prep., Prograde Metamorphism and Hydrothermal Retrogression during Nappe Emplacement, southwest Virginia Piedmont.

Ghosh, S. K., 1966, Experimental tests of buckling folds in relation to strain ellipsoid in simple shear deformations; Tectonophysics, vol. 3, no. 3, p. 169-185.

Glover, L., III, Speer, J. A., Russell, G. S. and Farrar, S.S., 1983, Ages of regional metamorphism and ductile deformation in the central and southern Appalachians; Lithos, vol. 16, p. 223-245.

Gray, D. R., 1977, Morphologic Classification of crenulation cleavages; Jour. Geol., v. 85, p.763-780.

Harding, T. P., and J. D. Lowell, 1979, Structural styles, their plate tectonic habitats, and hydrocarbon traps in petroleum provinces; Am. Assoc. Pet. Geol. Bull., vol. 63, no. 7, p. 1016-1058.

Harland, W. B., 1971, Tectonic transpression in Caledonian Spitzbergen, Geol. Mag. 108 (1), p. 27-42.

Henika, W. S. and Thayer,P. A., 1977, Geologic maps of the Blairs, Mount Herman Danville and Ringgold Quadrangles, Virginia; Va. Div. Miner. Resour. Publ., no. 2, 45pp.

Ingles, J., 1985, Theoretical and natural strain patterns in ductile simple shear zones; Tectonophysics, vol. 115, p. 315-334.

Kaldy, W. J., 1977, Geology and Geophysics of the Sherwill dome of southwestern Piedmont of Virginia; Univ of Ken., M. S. unpublished.

Lemmon, R. E., 1980, Geologic history of the Henderson gneiss, western North Carolina; *in* Price, V. Jr., Thayer, P. A., and Ronson, W. A., eds., Geol. Inv. of the Pied. and Triassic Rocks, Cent. N. Ca. and Va.; Carolina Geol. Soc. Field Trip Guidebook, P. VII - 1-16. Lister, G. S. and Snoke, A. W., 1984, S-C mylonites, J. Struct. Geol., vol. 6, no. 6, p. 617-638.

Marr, J. D., Jr., 1984, Geologic Map of the Pittsville and Chatham quadrangles, Virginia; Vir. Div. Min. Res., Pub. 49.

Odom, A. L., and G. S. Russell, 1975, The time of regional metamorphism of the Inner Piedmont, North Carolina and Smith River Allochthon: Inferences from whole-rock ages; Geol. Soc. Am. Abstrs. w. Progs., vol. 7, no. 4, p. 522.

Platt, J. P. and Vissers, R. L. M., 1980, Extensional structures in anisotropic rocks, J. Struct. Geol., vol. 2, p. 397-410.

Price, V., Conley, J. F., Piepul, R. G., Robinson, G. R., Thayer, P A. and Henika, W. S., 1980, Geology of the Whitmell and Brosville quadrangles, Virginia; Vir. Div Min. Res., pub. 21.

Ramsay, J. G., 1967, Folding and Fracturing of Rocks; New York, McGraw-Hill Book Co. (International Series of Earth and Planetary Science), p. 568.

Ramsay, J. G., 1980, Shear zone geometry: a review, J. Struct, Geol., v. 2, no. 1/2, p. 83-99.

Ramsay, J. G., Casey, M. and Kligfield, R., 1983, Role of shear in development of the Helvetic fold-thrust belt of Switzerland; Geology, vol. 11, no. 8, p. 439-442.
Ramsay, J. G. and Graham, R. H., 1970, Strain variation in shear belts, Can. J. Earth Sci., vol. 7, p. 786-813.

Rankin, D. W., 1975, The continental margin of eastern North America in the Southern Appalachians, the opening and closing of the Proto-Atlantic Ocean; *in* Tectonics and Mountain Ranges; Am. Jour. Sci., Vol. 273-A, p. 298-336.

Rankin, D. W., Espenshade, G. H. and Neuman, R. B., 1972, Geologic map of the west half of the Winston-Salem quadrangle, North Carolina-Virginia; U. S. Geol. Surv. Misc. Inv. Series Map I-709-A.

Redden, J. A. 1963, Stratigraphy and metamorphism of the Altavista Area; in Geological Excursions in Southwestern Virginia; Eds. R. V. Dietrich; Vir. Polytech. Inst. Eng. Ext. Ser., Geol. Guidebook No. 2, p77-99.

Reed, J. C., Jr. and Bryant, B., 1964, Evidence for strike-slip faulting along the Brevard Zone in North Carolina; Geol. Soc. Am. Bull., Vol. 75, p. 1177-1195.

Sanderson, D. J. and Marchini, W. R. D., 1984, Transpression; J. Struct. Geol., V. 6, NO. 5, p. 449-458.

Scheible, P., 1980, Geologic problems in the crystalline rocks of the Martinsville, Rocky Mount, Virginia area, *in* Price, V. Jr., Thayer, P. A., and Ronson, W. A., eds., Geol. Inv. of the Pied. and Triassic Rocks, Cent. N. Ca. and Va.; Carolina Geol. Soc. Field Trip Guidebook, P. I-1 - I-10.

Simpson, C., 1984, Borrego Springs-Santa Rosa mylonite zone: A late Cretaceous west directed thrust in southern California; Geology, vol. 12, p. 8-11.

Simpson, C. and Schmid, S. M., 1983, An evaluation of criteria to deduce the sense of movement in sheared rocks; Geol. Soc. Am. Bull., vol. 94, p. 1281-1288.

Sylvester, A. G. and Smith, R. R. 1976, Tectonic Transpression and basin controlled deformation in San Andreus Fault Zone, Salton Trough, California; Am. Assoc. Pet. Geol. Bull, V. 60, no. 12, p. 2081-2102.

Tchalenko, J. S., 1970, Similarities between shear zones of different magnitudes; Geol. Soc. Am. Bull., vol. 81, 1625-1640.

Wehr, F. and Glover, L. III, 1985, Stratigraphy and Tectonics of the Virginia-North Carolina Blue Ridge: Evolution of a late Proterozoic- early Paleozoic hinge zone; Geol. Soc. of Am. Bull., v. 96, p. 285-295.

Wilcox, R. E., Harding, T. P. and Seely, D. R., 1973, Basic wrench tectonics; Am. Assoc. Pet. Geol. Bull., vol. 57, no. 1, p. 74-96.

Williams, H., 1978, Tectonic lithofacies map of the Appalachian orogen, Map 1, Mem. Univ. of Newfoundland, St. Johns.

Woodcock, N. H. and Robertson A. H. F., 1982, Wrench and Thrust tectonics along a Mesozoic-Cenozoic Continental margin: Antalya Complex, SW Turkey; J. Geol. Soc. of London, v. 139, pt 2, p. 147-163.

PROGRADE METAMORPHISM AND HYDROTHERMAL RETROGRESSION DURING NAPPE EMPLACEMENT, SOUTHWEST VIRGINIA PIEDMONT

A. E. Gates and J. A. Speer

ABSTRACT

The northern terminus of a broad belt of Taconic age amphibolite grade metamorphic rocks that includes the Inner Piedmont Belt of the southen Appalachians occurs in the southwest Virginia Piedmont. The prograde metamorphism in Altavista is inverted in an upright stratigraphy. A sil-in, st-out isograd across the northern and western map area represents the reaction: mus + st → grt + bt + als. Ten kilometers to the south or the high temperature side of the isograd there are migmatites and small granite, aplite and pegmatite dikes. On the low temperature side, metamafic rocks define the isograd between amphibolite and greenschist facies conditions.

The prograde metamorphic rocks later underwent retrogression in continuous but incomplete reequilibration. The sil-bearing rocks (bt + grt + sil) underwent the reaction : grt + bt + als + H_2O → mus + st. The st armored the grt and the assemblage was bt + st + sil (st-retrograde rocks). Although some rocks retain this assemblage, many continued to receive fluid and underwent cld-production reactions: st + grt + bt + H20 → cld + mus and st + bt + H20 → cld + chl. Several other assemblages are included in these cld-retrograde rocks such as spessartine rich grt + cld + chl from the reaction st + grt + chl → cld and ky + cld + chl from st + chl → cld + als. These zones of retrogression are approximately parallel to structural trend. At the center of several

zones are deposits of pure kyanite and deposits of pure tourmaline, both of which indicate extreme hydrothermal activity that was apparently confined to structurally controlled fluid conduits.

Pressure-temperature calculations both on rims and in mineral profiles indicate that peak temperature conditions followed higher pressure lower temperature conditions. Peak temperature ranged from 650° C in sil-bearing rocks to 570° C in st-bearing prograde rocks. Application of the retrograde rocks to an experimentally calibrated petrogenetic grid indicates nearly isobaric cooling through 120° C. The P-T path therefore represents the late stage of a P-T loop that characterizes nappe emplacement. Early thrusting of the nappe caused a rapid pressure increase in the footwall which had previously undergone regional metamorphism. Thermal equilibration and decompression caused an increase in temperature and decrease in pressure in these rocks. The thermal equilibration produced the inverted prograde metamorphism and drove dehydration reactions which liberated fluids. The fluids then flushed back up through the pile along the conduits. The fluids drove retrograde reactions and produced the hydrothermal deposits.

INTRODUCTION

This study documents the processes of Taconic metamorphism and relates them to the structural and tectonic development of the western Virginia Piedmont in the Altavista area. The metamorphism records the history of nappe emplacement which includes a prograde and retrograde sequence. The retrograde portion of the P-T path was accompanied by extreme hydrothermal activity along structurally controlled fluid conduits.

The Altavista area lies in the northern part of the Smith River Allochthon terrane (Conley and Henika, 1970; 1973) (Figure 24), a large area composed of amphibolite

grade metamorphic rocks. The terrane is bounded to the east by the Ridgeway fault and to the west by the Bowens Creek Fault (Conley and Henika, 1970; 1973) which separates it from an area of greenschist facies rocks to the west. Glover et al. (1983) suggested that this area records metamorphism that resulted from the Taconic Orogeny. Rb/Sr biotite-whole rock cooling ages of 440 ± 22 Ma (Odom and Russell, 1976) from pelitic gneisses and Rb/Sr whole rock ages of 462 ± 20 Ma (Odom and Russell, 1976) and 450 Ma (Rankin, 1975) from the Leatherwood Granite which intruded the Smith River area subsequent to the peak of metamorphism support the Ordovician Taconic age of metamorphism. Amphibolite grade Taconic metamorphism continues further south into the Inner Piedmont belt of the Carolinas and Georgia (Glover et al.., 1983).

To the north of Altavista, the rocks are of lower grade. In central and northern Virginia, the western Piedmont rocks are of upper greenschist to lowermost amphibolite facies (Espenshade, 1954; Brown, 1958; Evans, 1984). The Altavista area therefore represents the northernmost portion of this large amphibolite grade metamorphic belt.

GEOLOGIC SETTING

The oldest unit in the Altavista area is the Late Precambrian Lynchburg Formation (Brown, 1958; Espenshade, 1954) and is exposed in the cores of the domal structures that characterize the area (Figure 25). The Lynchburg Formation in Altavista is composed of mica-poor, metamorphosed feldspathic to arkosic, conglomerate that grades upward into medium grained, feldspathic sandstone to graywacke with thin micaceous laminations. The sandstones are sparsely intruded by muscovite-biotite-garnet pegmatite dikes within the Hundley Dome (Figure 25). Conformably overlying the Lynchburg Formation is the Late Precambrian, metavolcanic Catoctin Formation (Brown, 1958). The medium to coarse-grained, hornblende-andesine amphibolite schists include 5 to 60

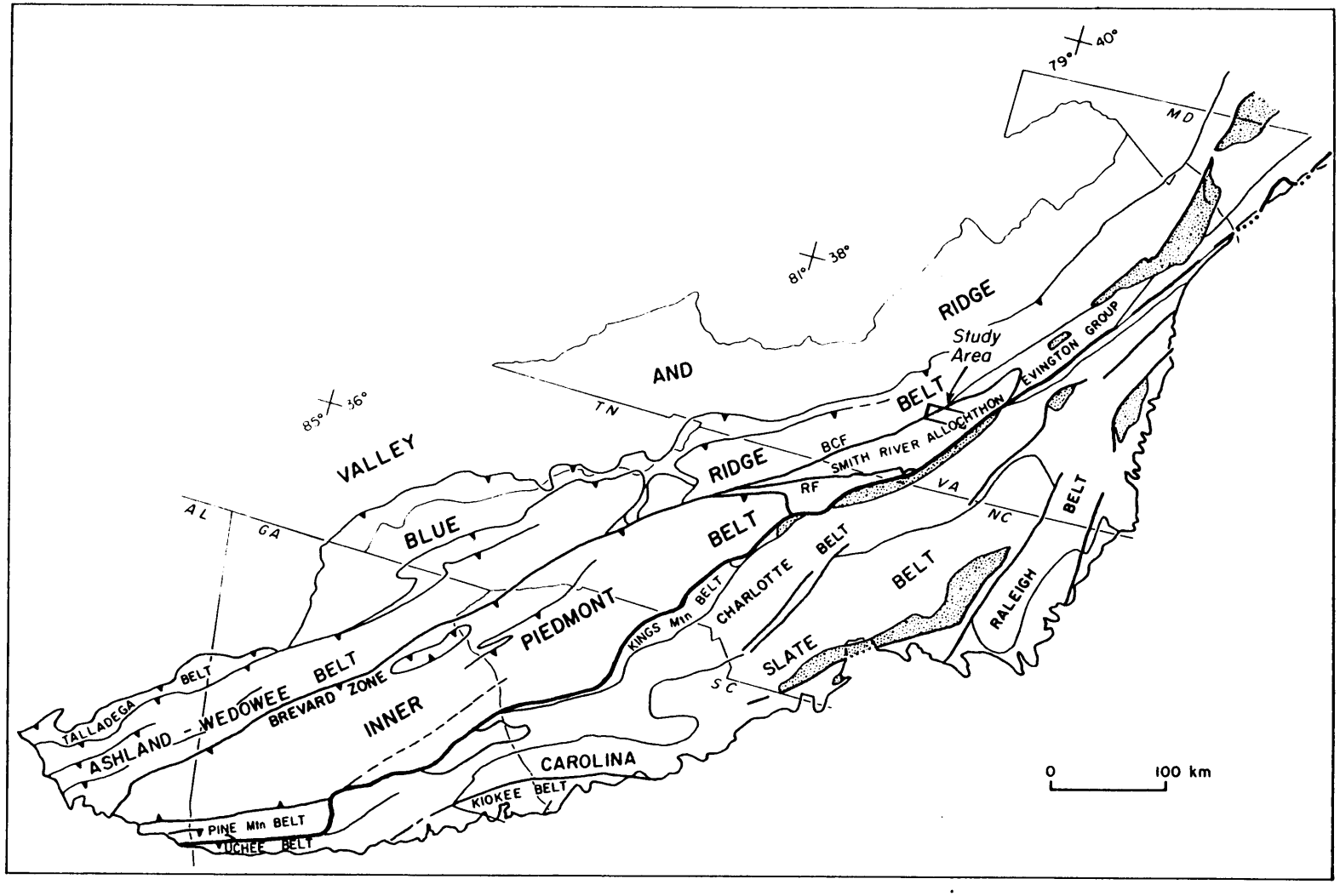

Figure 24. Regional tectonic map of the Southern Appalachians showing major belts, Smith River Allochthon and study area. BCF = Bowens Creek Fault, RF = Ridgeway Fault.

m thick discontinuous layers of metasandstone and epidote-quartz layers and boudins. Conformably overlying the Catoctin Formation is the metasedimentary Evington Group of latest Precambrian to Cambro-Ordovician(?) age (Espenshade, 1954; Brown, 1958; Redden, 1963; Brown, 1970). The Evington Group consists of metagraywacke and quartzite succeeded by a thick pelitic sequence. The pelitic rocks range from sillimanite-staurolite-garnet schist/gneiss to chloritoid-chlorite schist. The unit is intruded by garnet-tourmaline pegmatite, aplite and granite dikes along the southern boundary of the map area (Figure 25). The upper portion of the pelitic unit contains two 5 to 50 m thick, thinly layered calc-silicate units with marble and diopside-amphibole-garnet-epidote schist with pelitic laminations and separated by a pelitic section. The upper calc-silicate is interlayered with a massive, coarse grained, calc-silicate bearing quartzite.

In the westernmost map area, the deformation is less intense and younging direction is determined through graded and cross-beds (Gates and Glover, in prep.). The Catoctin metabasalt is a greenstone in this area indicating that greenschist facies conditions prevailed in contrast to the amphibolite facies that prevailed in the rest of the Altavista area.

The Altavista area has undergone four deformational events (Gates, in prep.; Gates and Glover, in prep.). The first two deformational events D_1 and D_2 are related in time and space to the M_1 metamorphism and occured during the Taconic Orogeny. D_1 structures are difficult to identify in outcrop, but the large isoclinal fold in the southwestern map area (Figure 25) may be an F_1 fold. S_1 has generally been transposed into S_2 but rootless isoclines and isoclinal fold hinges in the S_2 foliation record the earlier foliation which was folded by F_2. Porphyroblasts in the pelitic schists and gneisses contain cores with aligned inclusions (S_1) that are oblique to the pervasive S_2 foliation. The F_2 folding event is isoclinal and recumbent and reoriented or modified the F_1 folds. The metamorphic assemblages studied in this report were mainly formed during and after the D_2 event but the M_1 metamorphism spans both deformational events.

Figure 25. Geologic/metamorphic map of the Altavista area with assemblages and isograds.

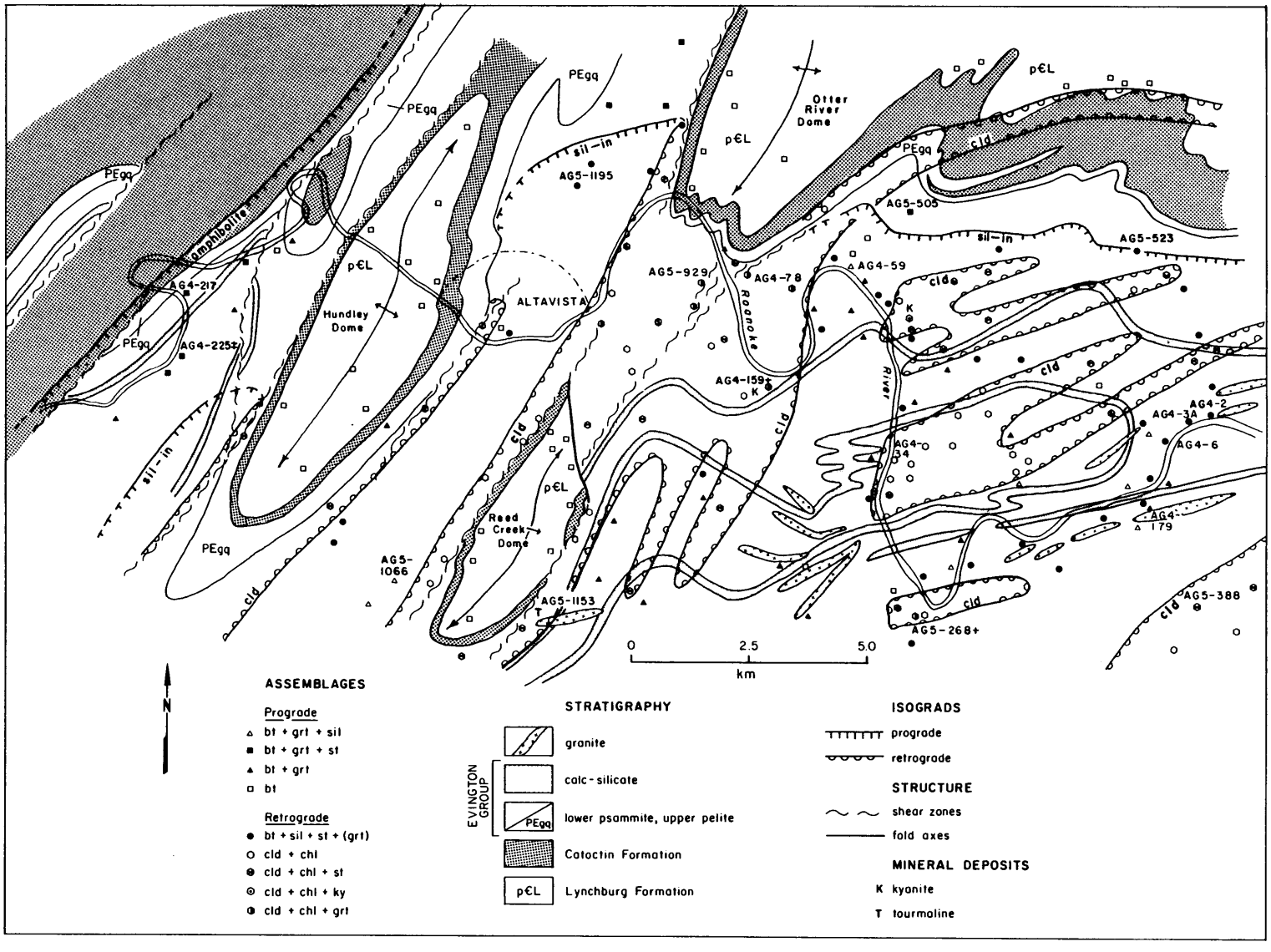
PEgq
sil-in
AG5-1195
Otter River Dome
p€L
cld
AG5-505
AG5-523
AG4-59
AG4-78
AG5-929
Roanoke River
Hundley Dome
ALTAVISTA
AG4-217
AG4-225+
AG4-159+
AG4-34
AG4-3A
AG4-2
AG4-6
AG4-179
Reed Creek Dome
AG5-1066
AG5-1153
AG5-268+
AG5-388
0
2.5
5.0
km
N
ASSEMBLAGES
Prograde
bt + grt + sil
bt + grt + st
bt + grt
bt
Retrograde
bt + sil + st + (grt)
cld + chl
cld + chl + st
cld + chl + ky
cld + chl + grt
STRATIGRAPHY
granite
EVINGTON GROUP
calc-silicate
PEgq
lower psammite, upper pelite
Catoctin Formation
p€L
Lynchburg Formation
ISOGRADS
prograde
retrograde
STRUCTURE
shear zones
fold axes
MINERAL DEPOSITS
K kyanite
T tourmaline

The eastern half map area exhibits structures and foliation with an east-west strike and south directed dip. The D_1 and D_2 events produced a horizontal foliation and recumbent isoclinal folds. This area was later passively rotated to the south during the formation of the Sherwill Dome (Figure 25) (Gates, in prep). D3 and D4 were the two latest events and unrelated to the early Taconic events. The D3 and D4 events formed the folds and domes in the western map area in late transpressive deformational events (Gates, in prep) but imposed minimal deformation on the eastern map area. The trend of the F3 and F4 structures is northeast, in sharp contrast with the east-west trending structures to the east (Figure 25). Multiple crenulation cleavages are well developed in the areas that exhibit F3 and F4 folds. The M_2 metamorphism is related to the late event and produced muscovite and chlorite overgrowths on the M_1 minerals.

PETROGRAPHY

The conditions of Taconic (M_1) metamorphism in the Altavista area are best determined by the assemblages and textures in the pelitic schists and gneisses of the Evington Group. There are early prograde assemblages and a series of late retrograde assemblages that reflect the changing metamorphic conditions. The prograde, amphibolite grade metamorphism defines a sil-in, st-out isograd between sillimanite bearing rocks (bt + grt + sil) to the south and east and staurolite bearing rocks (bt + grt + st) to the north and west (Figure 25). The sillimanite bearing rocks are therefore stratigraphically higher in the section than the staurolite assemblages. The decrease in temperature to the west is also indicated by the metamafic rocks of the Catoctin Formation. The Catoctin is an amphibolite in all parts of the field area except the westernmost band (Figure 25) where it ranges from an amphibole bearing greenstone at

the eastern contact to a greenstone. Amphibolite facies conditions therefore prevailed in the central and eastern areas but greenschist facies prevailed in the west.

Mineral abbreviations in the following discussion are from Kretz (1983).

Prograde Assemblages Southeast of the Sil-Isograd

Unretrograded bt + grt + sil rocks occur in small patches across the southern and eastern part of the map area (Figure 25). The three phase bt + grt + sil assemblage is characteristic of this zone. Sandy sections of the Evington Group exhibit grt + bt and bt assemblages. These assemblages also contain ms + pl + qtz and accessory tourmaline, magnetite, apatite, ilmenite and zircon. Fine fibrolitic to locally granular sillimanite defines the S_2 foliation with ms + bt or is randomly oriented. Sillimanite occurs throughout the rock, in biotite, muscovite quartz and as porphyroblastic aggregates. Garnet poikiloblasts are subhedral to anhedral and are embayed by the sillimanite and biotite intergrowths (Figure 29A). The garnet contains quartz inclusions that in some samples define S_1 foliation oblique to the enclosing S_2 Small anhedral shards of garnet occur in intergrowths of sillimanite and biotite and appears to have been consumed in this assemblage. Reversely zoned plagioclase of An38-51 forms subhedral poikiloblasts that contain quartz and euhedral muscovite inclusions. The biotite and muscovite in the matrix is subhedral to anhedral and contains inclusions of sillimanite and ilmenite.

Migmatites occur in the pelites in the southeast field area (Figure 25). Associated with the migmatites are small two mica, garnet-tourmaline granite, pegmatite and aplite dikes that are concordant to the D_2 trend. The granites are fine grained monzogranites (Streckheisen,1973) with a granitic texture. The mafic phases include garnet, tourmaline,

epidote, biotite and muscovite and are early in the crystallization sequence. The feldspars and quartz are late and appear to have crystallized at the same time.

Prograde Assemblages Northwest of the Sil-Isograd

The northern and western area is characterized by the bt + grt + st, st + bt and bt assemblages. Other phases in these rocks include ms, qtz, pl, mag, ap and possible ilmenite. The bt + grt + st rocks exhibit a slightly stronger S_2 foliation than the sil-bearing assemblage and porphyroblasts as much as thirty times as large as the enclosing matrix grains. The staurolite porphyroblasts are up to 3 cm and exhibit inclusion free rims on quartz included cores (Figure 26A). The aligned inclusions are oblique to the enclosing S_2 foliation. Subhedral garnet is 2 to 4 mm, and inclusion free. Aligned biotite forms subhedral porphyroblasts and is generally subhedral to rounded. Plagioclase forms 5 mm poikiloblasts that are normally zoned, twinned and generally sericitized. These rocks are also relatively muscovite rich and quartz poor. In sample AG5-505 (Figure 25), the garnet is 1 to 3 cm, and includes euhedral unzoned staurolite that composes as much as 60% of the porphyroblast. These garnets also enclose bt, pl and accessory fluor-apatite. The rock however contains no quartz.

St-Bearing Retrograde Rocks

The st-bearing retrograde rocks are distinguished from the prograde rocks by the coexistence of sil + st and the isolation of grt from sil. The rocks at the prograde isograd also contain bt + grt + st + sil but with all phases in apparent equilibrium and occurring over a very restricted area. The st-retrograde rocks occur to the southeast of

Figure 26. Textures A) Staurolite from AG4-217 displaying seive texture. Scale bar = 5mm. B) Pseudomorph of cld, ms and chl after st from AG4-388. Scale bar = 2mm. C) Bt in reaction with st to cld and chl from AG5-268+. Scale bar = 2mm. D) Cld containing st inside and ky near rims AG4-159+. Scale bar = 2mm.

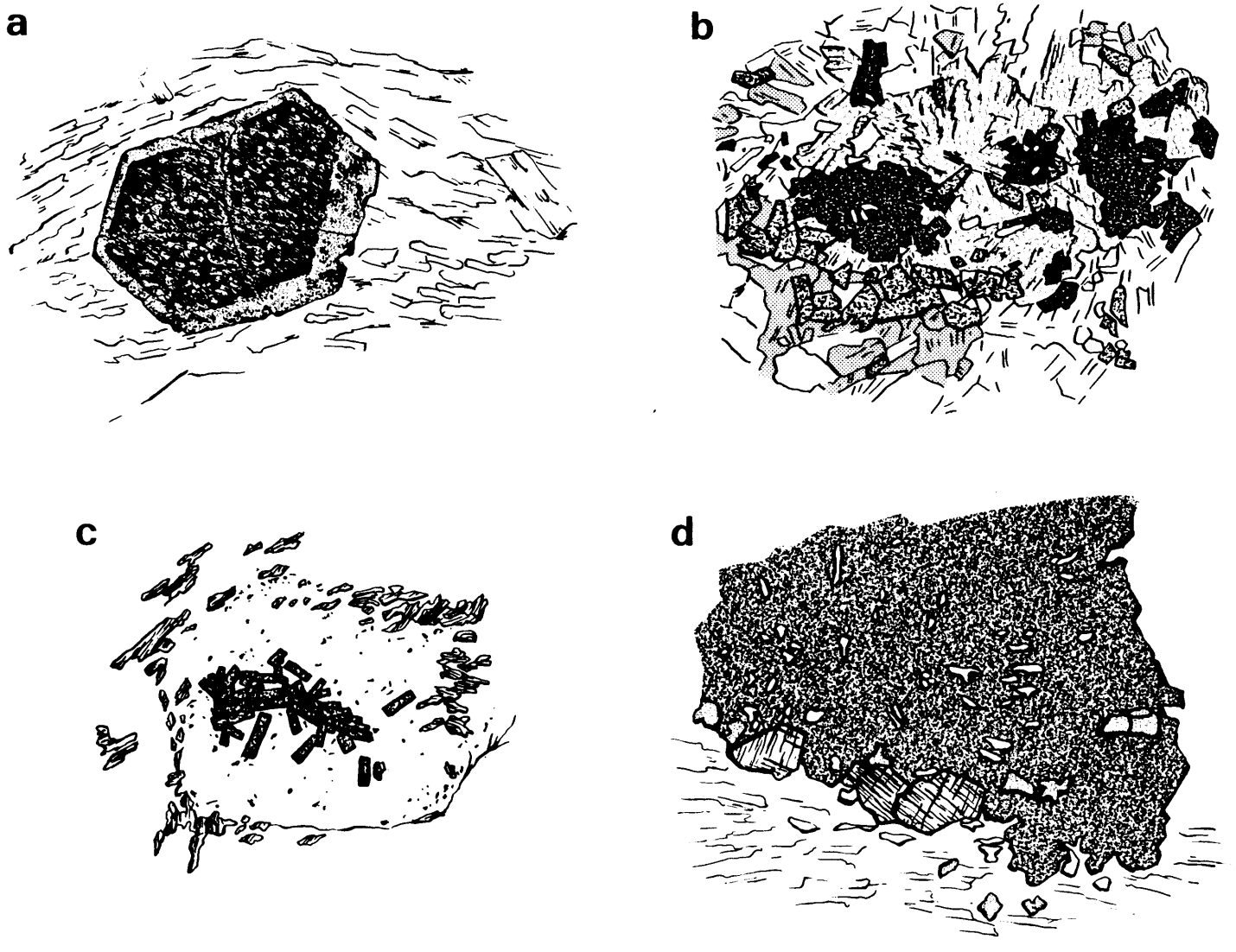
a
b
c
d

the prograde sil-in isograd in all areas between those with rocks that exhibit the bt + grt + sil assemblage and the cld-bearing retrograde assemblages. The rocks also contain ms + pl + qtz ± ky ± chl ± cld and accessory tourmaline, apatite, ilmenite, magnetite and zircon. These rocks exhibit varying degrees of continual but incomplete re-equilibration. Prior to the retrogression, the rocks contained the prograde bt + grt + sil assemblage. Euhedral garnet forms 2 to 6 mm porphyroblasts with muscovite and biotite pressure shadows and locally show rotatation. The garnets exhibit a sharp core-rim boundary defined by aligned to randomly oriented sillimanite fibers that wrap the cores (Figure 29D). The garnets are otherwise clearly isolated from sillimanite in all but a few rocks and are armored by staurolite and biotite. The rounded garnet cores contain aligned quartz inclusions that are oblique to S_2 whereas the rims are inclusion free (Figure 29D). Small to medium sized (1 - 5 mm), euhedral staurolite grains occur in aligned fibrolitic sillimanite masses and rim or are included in garnet with biotite laths. The staurolite is generally clear but larger grains are slightly poikiloblastic with quartz inclusions. Euhedral kyanite laths have replaced the fibrolite masses in some samples. Muscovite and quartz contain sillimanite fibers but biotite does not. Normally zoned and sericitized plagioclase is poikiloblastic with quartz, small poorly developed mica, magnetite and ilmenite.

Cld-Bearing Retrograde Assemblages

The later retrogression is characterized by cld + chl assemblages that contain ms, mag and, depending on the rock, qtz, st, ky, grt and/or sil as stable or relict phases. The cld + chl rocks occur in east-west oriented bands that parallel the S_2 foliation and F_2 structural trend (Figure 25) in the eastern map area. The bands are evident on aeromagnetic maps of the area as weak magnetic highs. In the west, near the domes, the

bands have been reoriented in the later D3 and D4 deformational events. The assemblages of the late phase retrogression are:

cld + chl + st

cld + chl + grt

cld + chl + ky.

Cld + chl most commonly occurs as either a two phase assemblage or with staurolite. Chloritoid forms small subhedral to euhedral grains with muscovite and minor chlorite in fractured and disaggregated staurolite porphyroblasts with biotite at the margins of the retrograde zones (Figure 26B). Within the areas of cld-retrograde assemblages (Figure 25), randomly oriented chloritoid in muscovite and minor chlorite form pseudomorphs after staurolite (Figure 26C). Chloritoid porphyroblasts in fine chlorite and muscovite, generally contain small staurolite grains and bundles of sillimanite fibers as relicts of the earlier assemblages. Chlorite occurs as oriented plates with zircon and rutile inclusions and remnant biotite along cleavage planes or as small fibrous rosettes. In contrast to the prograde and st-retrograde rocks, muscovite constitutes the most abundant phase, composing 65 to 95% of the cld + chl rocks.

In sample AG5-929 (Figure 25), garnet occurs with the cld + chl + ms assemblage (cld + chl + grt). The garnets occur as euhedral to subhedral, 3 to 5 mm porphyroblasts and inclusions within chloritoid porphyroblasts (Figure 29D). Unlike many other chloritoid bearing rocks, the garnet-chloritoid rocks contain no staurolite in the matrix nor within the chloritoid.

In sample AG4-159+ (Figure 25), kyanite occurs as a stable phase with chloritoid and chlorite (cld + chl + ky) (Figure 26D). 1 to 2 mm euhedral prisms are both included in chloritoid and in the fine chlorite-muscovite matrix. Small, euhedral to subhedral staurolite grains are included in chloritoid and subhedral to anhedral grains occur in the matrix. Sillimanite is also enclosed within chloritoid. This sample contains one small quartz vein but no quartz in the matrix.

Rocks with Extreme Composition

In some areas, kyanite forms deposits of intergrown laths with 1 to 5% interstitial muscovite. These deposits which range from several centimeters to two to three meters in thickness, occur within chloritoid-muscovite schists. The chloritoid is stable with kyanite near the deposits. These deposits are rimmed by tourmaline-magnetite-muscovite intergrowns. In other parts of cld + chl areas, deposits of 90% fine randomly oriented tourmaline with interstitial quartz exhibit the same intergrowth on the rims. Tourmaline is a common accessory to all of the pelitic rocks but occurs in higher concentrations in the chlorite-chloritoid schists.

MINERAL CHEMISTRY

Polished sections of eighteen samples were analyzed for mineral chemistries with an automated , nine spectrometer ARL-EMX electron microprobe. The analytical schemes used in standardization and analysis are those of Solberg and Speer (1982). Data was converted to oxide weight percentages using techniques of Bence and Albee (1968). Oxide weight percents were recalculated into mineral formulae using the SUPERRECAL computer program (Rucklidge, 1971). In recalculating hydrous phases, the OH + F + Cl molecular total was summed to the assumed correct stoichiometry (4 for biotite). Boron was iteratively entered in weight percent for tourmaline analyses to yield a molecular total of 3.

Muscovite

The white micas from the Altavista area (Appendix C) are K and Na bearing with trace amounts of margaritic component. Na/(Na + Ca + Ba) ranges from 0.106 to 0.291 and is generally lower for bt + grt + sil rocks than the other assemblages (Figure 27A). Paragonitic content is similarly lower for these rocks than rocks containing the other assemblages. Si occupancy ranges from 3.03 to 3.12 atoms/12 anions and is independant of assemblage. Ba ranges from 0.01 to 0.047 atoms/24 anions and is generally higher for sil-bearing rocks than st- and cld-bearing rocks. Total interlayer occupancy is $1.66 \leq (K + Na + Ca + Ba) \geq 1.911$ and is higher in sil rocks than in the other assemblages. F content is from 0.0 to 0.064 /24 anions and is independent of assemblage.

Plagioclase

Plagioclase (Appendix C, Table 3) is sericitized in many samples and albitized in most st-bearing prograde and retrograde rocks. Plagioclase is represented by sericite pseudomorphs in cld-bearing rocks. An content ranges from 6 to 51 % for rim analyses and exhibits a general decreasing trend from sil-bearing rocks through st-bearing prograde and retrograde rocks (Figure 27B). Michel-Levy optical compositional methods indicate the same trend but yield slightly higher An components. Individual plagioclase grains are reversely zoned from An 38 at the core to An 51 at the rim in bt + grt + sil and normally zoned from An 43 at the core to An 15 at the rim for some grains in st-retrograde samples. All st-prograde and many st-retrograde plagioclase grains are unzoned.

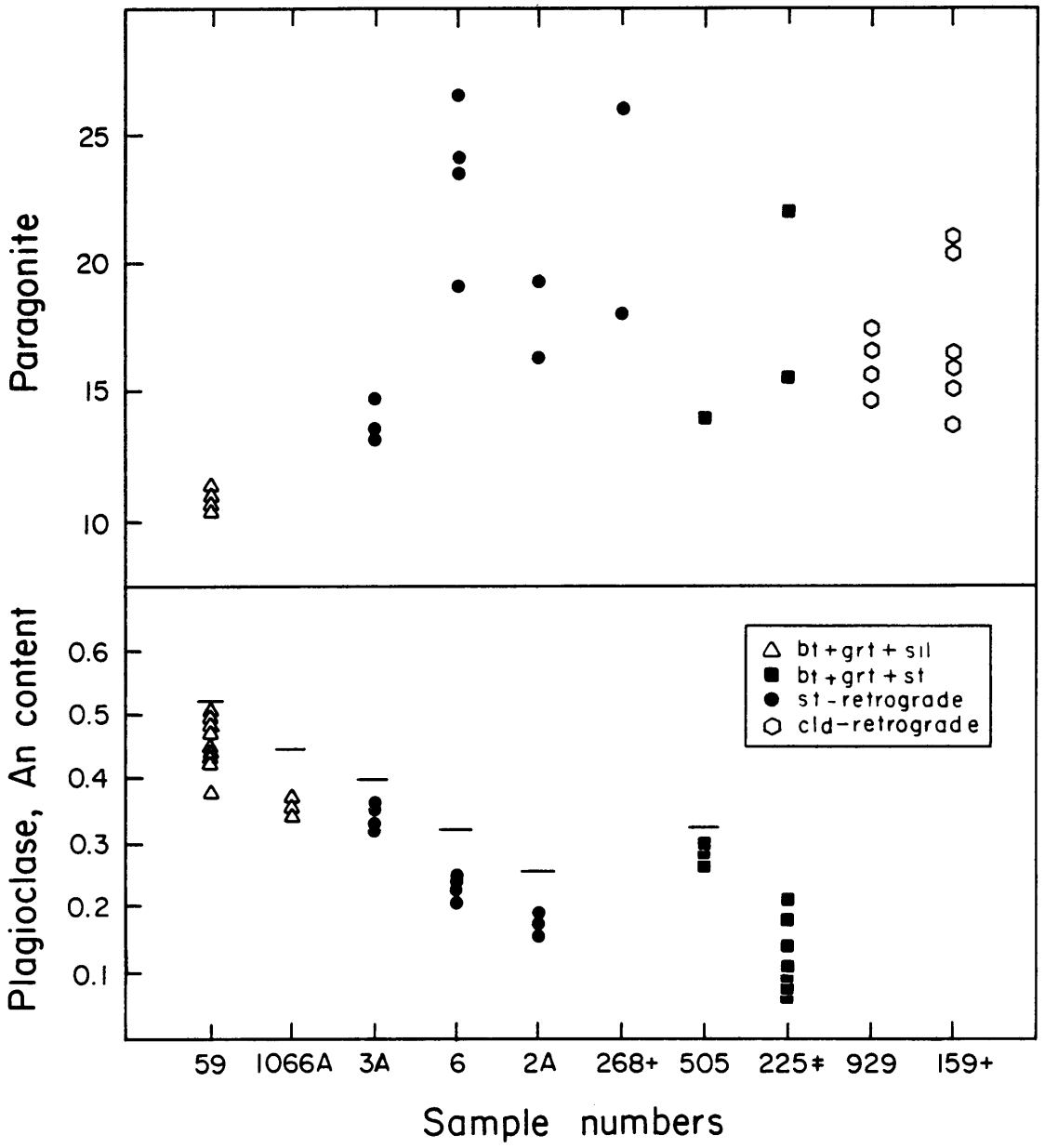

Figure 27. Composition discrimination graphs of: A) Paragonite component in muscovite, B) An content in plagioclase.

Table 3: Average Plagioclase Analyses used in Thermo-barometry

Sample:	4-59R	5-1066	4-59C
SiO_2	55.40	60.25	58.53
TiO_2	0.02	0.00	0.00
Al_2O_3	29.94	25.74	27.77
FeO	0.09	0.10	0.03
MgO	0.02	0.02	-0.03
CaO	10.49	7.28	7.85
BaO	0.00	0.00	0.00
Na_2O	5.43	6.89	7.04
K_2O	0.05	0.06	0.05
Total	101.48	100.34	101.26
Number of ions with 8 O			
Si	2.456	2.668	2.581
Al	1.564	1.343	1.443
Ti	0.001	0.000	0.000
	4.021	4.012	4.024
Fe	0.003	0.004	0.001
Mg	0.001	0.002	-0.002
Ca	0.498	0.345	0.371
Na	0.467	0.592	0.602
K	0.003	0.003	0.003
Ba	0.000	0.000	0.000
	0.974	0.945	0.975

Biotite

Fe/(Fe + Mg) for biotite (Appendix C, Table 4) ranges from 0.35 to 0.67 and varies systematically in each of the assemblages. The composition of the biotite in the sil- and st-bearing prograde and st-retrograde rocks can be distinguished on the basis of Fe/(Fe + Mg), Al, AlIV, F, and Ti (Figures 28A - 28C). Fe/(Fe + Mg) ranges from 0.37 to 0.55 for biotite in bt + grt + sil rocks, 0.35 to 0.45 in bt + grt + st rocks and 0.55 to 0.67 in st-retrograde rocks. AlIV varies from 2.42 to 2.85 /24 anions and forms concentrations for the st-retrograde rocks at 2.44 to 2.54, bt + grt + st at 2.56 to 2.68 and bt + grt + sil at 2.65 to 2.8 (Figure 28A). AlVI varies from 0.77 to 1.02 /24 anions with the major concentration between 0.85 and 0.95 regardless of assemblage. Interlayer occupancy ranges from 1.72 to 1.83 (K + Na + Ca) atoms/24 anions for the sil assemblage, 1.64 to 1.80 (K + Na + Ca + Ba) atoms/24 anions for st-retrograde and 1.62 to 1.77 (K + Na + Ca + Ba) atoms/24 anions for st-prograde rocks. Ba is from 0 to 0.04 atoms/24 anions with higher values in st-retrograde than bt + grt + st rocks. Fluorine contents concentrate between 0.07 to 0.20 atoms/ 24 anions for bt + grt + st rocks and approximately 0.15 to 0.32 for st-retrograde rocks (Figure 28B). Total titanium also forms three distinct groups: 0.170 to 0.220 atoms/24 anions for st rocks, 0.210 to 0.170 for sil rocks and 0.125 to 0.175 for st-retrograde rocks (Figure 28C).

Garnets

The garnets in the Altavista area are almandine-rich, containing between 49 and 84 mol % almandine, 7.9 to 14.7 mol % pyrope, 1.5 to 34.5 % spessartine , and 2.1 to 13.3 mol % grossular (Appendix C, Table 5). They show a compositional zoning that is different for each assemblage. The garnets coexisting with bt + sil exhibit profiles

Table 4: Average Biotite Analyses used in Thermo-barometry

Sample:	4-59	5-1066	5-523	4-225+	4-217	5-505
SiO_2	35.19	38.93	34.83	34.84	36.04	35.51
TiO_2	1.68	1.86	1.71	1.66	1.60	1.47
Al_2O_3	20.37	19.88	19.28	19.00	19.42	20.01
FeO	18.49	22.75	21.09	20.97	21.10	23.38
MnO	0.19	0.09	0.08	-0.01	-0.02	0.08
MgO	11.04	7.82	8.77	8.60	8.34	7.57
CaO	0.05	0.06	0.01	0.00	0.00	0.06
BaO	0.00	0.00	0.31	0.02	-0.12	0.20
Na_2O	0.30	0.27	0.22	0.12	0.16	0.29
K_2O	9.01	8.85	8.37	8.47	8.53	8.65
F	0.00	0.00	0.24	0.32	0.30	0.16
Cl	0.00	0.00	0.00	0.00	0.00	0.02
H_2O	3.85	3.95	3.88	3.84	3.86	3.88
Total	101.17	100.73	98.80	97.84	97.20	101.24
Number of ions with 24 O + OH + F + Cl						
Si	5.363	5.338	5.355	5.396	5.482	5.370
Al	2.637	2.662	2.645	2.604	2.518	2.630
	8.000	8.000	8.000	8.000	8.000	8.000
Al	0.921	0.890	0.847	0.863	0.964	0.937
Ti	0.187	0.193	0.198	0.193	0.183	0.167
Fe	2.292	2.885	2.712	2.716	2.684	2.957
Mn	0.024	0.011	0.010	-0.001	-0.003	0.011
Mg	2.439	1.769	2.010	1.986	1.891	1.707
	5.864	5.767	5.777	5.757	5.719	5.779
Ca	0.007	0.010	0.002	0.000	-0.001	0.011
Na	0.086	0.080	0.065	0.036	0.048	0.085
K	1.704	1.713	1.641	1.672	1.655	1.669
Ba	0.000	0.000	0.019	0.001	-0.007	0.012
	1.797	1.803	1.726	1.709	1.695	1.777
Cl	0.000	0.000	0.000	0.000	0.000	0.004
F	0.000	0.000	0.117	0.155	0.144	0.079
H	3.804	3.996	3.979	3.972	3.913	3.914

Table 4. Biotite Analyses Continued

Sample:	5-268	4-179	4-2A	4-6	4-3A
SiO_2	37.03	35.50	37.18	37.72	37.58
TiO_2	1.31	1.56	1.45	1.31	1.72
Al_2O_3	18.84	19.89	19.07	19.32	19.13
FeO	14.03	21.10	13.14	16.94	16.17
MnO	0.09	0.06	0.09	0.07	0.13
MgO	14.07	9.43	14.01	12.87	11.99
CaO	-0.02	0.04	0.00	0.02	0.04
BaO	0.28	0.00	0.21	0.18	0.21
Na_2O	0.23	0.24	0.26	0.33	0.25
K_2O	8.71	8.81	8.61	8.49	8.85
F	0.57	0.00	0.27	0.86	0.76
Cl	0.00	0.00	0.00	0.07	0.07
H_2O	3.73	3.97	3.88	3.69	3.68
Total	98.63	100.59	98.17	101.87	100.60
Number of ions with 24 O + OH + F + Cl					
Si	5.508	5.346	5.530	5.502	5.545
Al	2.492	2.654	2.470	2.498	2.455
	8.000	8.000	8.000	8.000	8.000
Al	0.811	0.876	0.870	0.823	0.872
Ti	0.146	0.176	0.162	0.144	0.191
Fe	1.745	2.658	1.635	2.066	1.995
Mn	0.011	0.008	0.011	0.009	0.016
Mg	3.120	2.115	3.106	2.798	2.637
	5.823	5.833	5.785	5.840	5.710
Ca	-0.003	0.006	-0.001	0.003	0.007
Na	0.067	0.069	0.076	0.093	0.070
K	1.653	1.691	1.633	1.580	1.666
Ba	0.016	0.000	0.012	0.010	0.012
	1.733	1.766	1.720	1.686	1.756
Cl	0.000	0.000	0.000	0.017	0.020
F	0.270	0.000	0.126	0.397	0.357
H	3.701	3.984	3.844	3.591	3.627

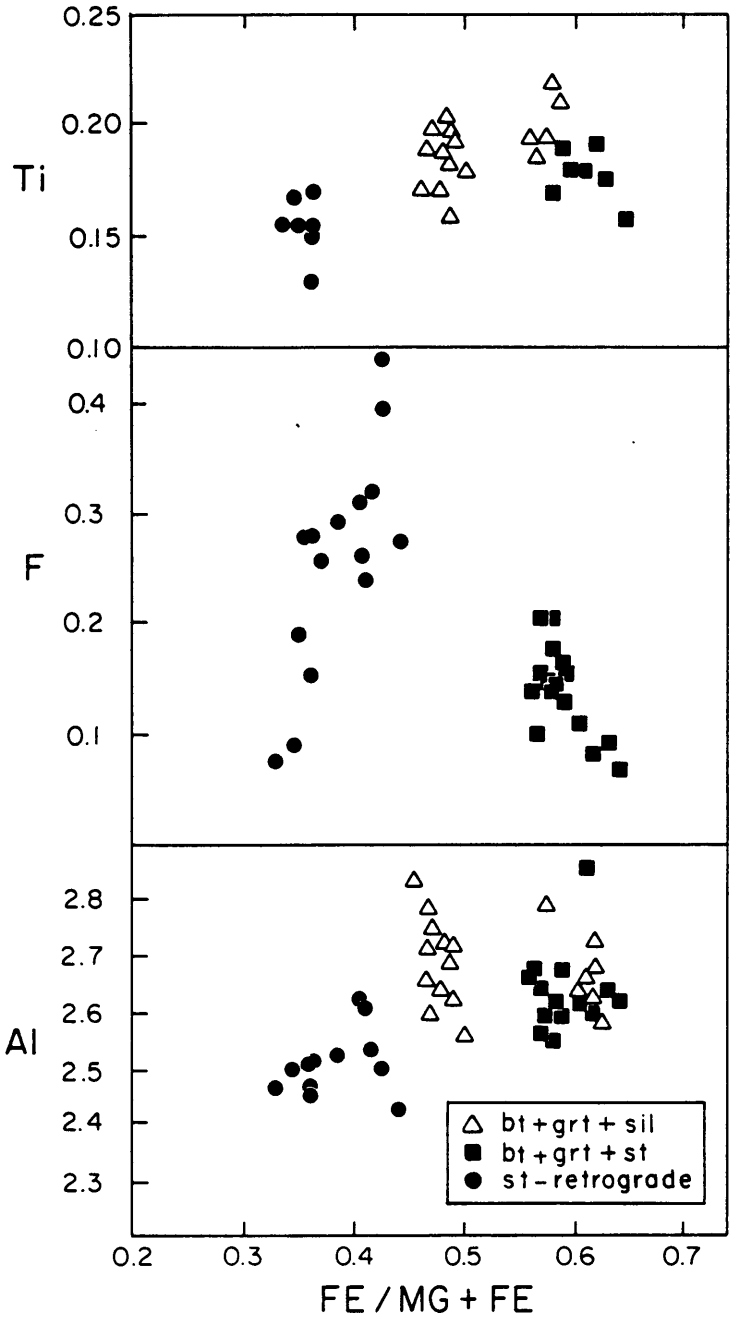

Figure 28. A) AlIV vs. Fe/(Fe + Mg) in biotite, B) F vs. Fe/(Fe + Mg) in biotite, C) Ti vs. Fe/(Fe + Mg) in biotite.

that suggest a two stage history. They contain quartz inclusions and embayments of sil + bt intergrowths. The cores (Z1) are high Fe and Ca and low Mn and Mg relative to the rims (Z2) (Figure 29A). The transition between the variable cores and relatively flat rims is abrupt. At the rim edge Fe increases and Mg decreases causing an inflection in the Fe/(Fe + Mg) profile.

Garnets coexisting with bt + st generally do not exhibit the Z1 and Z2 core growth profiles (Figure 29B). They contain a Z3 profile, which is relatively flat with no sharp core to rim transitions and moderate spessartine and grossular components. Garnets in the cld + chl retrograde assemblage exhibit a profile unrelated to Z1, Z2 and Z3. They are unzoned to slightly zoned and contain almandine of 49 to 54 mol %, pyrope of 12.4 to 14.6 mol %, spessartine of 27.2 to 34 mol % and grossular of 2.7 to 3.5 mol %. These garnets define a Z4 growth phase (Figure 29C).

The garnets from the st-bearing retrograde rocks contain included cores that are separated from the rims by a layer of sillimanite fibers (Figure 29D). The core profiles are very similar to those of the garnets from the bt + grt + st assemblage (Figure 29A). The rims however exhibit flat profiles with high Fe, Mg and Ca contents and low Mn contents relative to the core. Garnets with compositions similar to those in the cld + chl rocks also occur in AG4-2A of the st-retrograde rocks where they are more variable in composition. This low almandine (48.9 to 55.3mol %) garnet represents the Z4 garnet phase which is associated with kyanite unlike the others in the st-retrograde rocks which are associated with sillimanite.

Staurolite

The Fe/(Fe + Mg) ratio for staurolites (Appendix C) ranges from 0.865 to 0.74. Staurolites from the bt + grt + st assemblage range from 0.865 to 0.84 and retrograde

Table 5: Average Garnet Analyses used in Thermo-barometry

Sample:	4-59R	4-59C	5-1066	4-225+	4-217	5-505
SiO_2	38.08	38.93	38.24	37.54	38.04	37.73
TiO_2	0.15	0.14	0.10	0.13	0.12	0.15
Al_2O_3	20.78	21.43	20.90	21.42	21.00	21.19
FeO	28.60	30.46	33.90	35.55	36.14	34.49
MnO	8.62	5.55	4.87	2.84	0.22	2.67
MgO	3.00	3.01	2.16	2.51	2.29	2.71
CaO	2.90	3.79	1.97	0.80	3.21	2.40
Total	102.18	103.38	102.24	100.79	101.01	101.41
Number of ions with 12 O						
Si	3.007	3.019	3.029	3.005	3.028	3.000
Ti	0.009	0.009	0.006	0.008	0.007	0.009
Al	0.000	0.000	0.000	0.000	0.000	0.000
	3.016	3.027	3.035	3.013	3.035	3.009
Al	1.934	1.958	1.951	2.020	1.970	1.985
Fe	0.066	0.042	0.049	0.000	0.030	0.015
	2.000	2.000	2.000	2.020	2.000	2.000
Fe	1.823	1.934	2.197	2.380	2.376	2.279
Mg	0.353	0.348	0.256	0.300	0.272	0.321
Mn	0.577	0.365	0.327	0.193	0.015	0.180
Ca	0.245	0.315	0.167	0.069	0.274	0.204
	2.997	2.962	2.946	2.941	2.936	2.984

Table 5. Garnet Analyses Continued

Sample:	5-523	5-268	4-179	4-2A	4-6	4-3
SiO_2	37.53	37.99	38.06	38.61	37.99	37.13
TiO_2	0.13	0.14	0.15	0.13	0.15	0.19
Al_2O_3	21.19	21.02	21.02	21.12	21.21	
	21.14					
FeO	32.79	22.45	36.63	25.25	33.17	33.75
MnO	6.25	14.83	0.66	9.67	2.01	0.95
MgO	2.23	2.91	2.33	3.63	3.27	2.96
CaO	1.40	1.18	3.21	2.04	3.45	4.88
Total	101.48	100.50	102.14	100.42	101.31	101.14
Number of ions with 12 O						
Si	2.997	3.031	3.011	3.054	3.004	2.956
Ti	0.008	0.009	0.009	0.007	0.009	0.011
Al	0.000	0.000	0.000	0.000	0.000	0.032
	3.004	3.040	3.020	3.062	3.013	3.000
Al	1.994	1.976	1.960	1.969	1.976	1.951
Fe	0.006	0.024	0.040	0.031	0.024	0.049
	2.000	2.000	2.000	2.000	2.000	2.000
Fe	2.183	1.474	2.383	1.639	2.169	2.199
Mg	0.266	0.346	0.274	0.427	0.385	0.351
Mn	0.423	1.002	0.044	0.648	0.135	0.064
Ca	0.120	0.101	0.272	0.173	0.292	0.416
	2.991	2.923	2.974	2.888	2.981	3.031

Figure 29. Textures in garnets with corresponding compostition profiles A) For AG4 - 59 (bt + grt + sil), B) For AG4 - 225 (bt + grt + st), C) For AG5 - 929 (cld + chl + grt), D) For AG4 - 3A (st-retrograde).

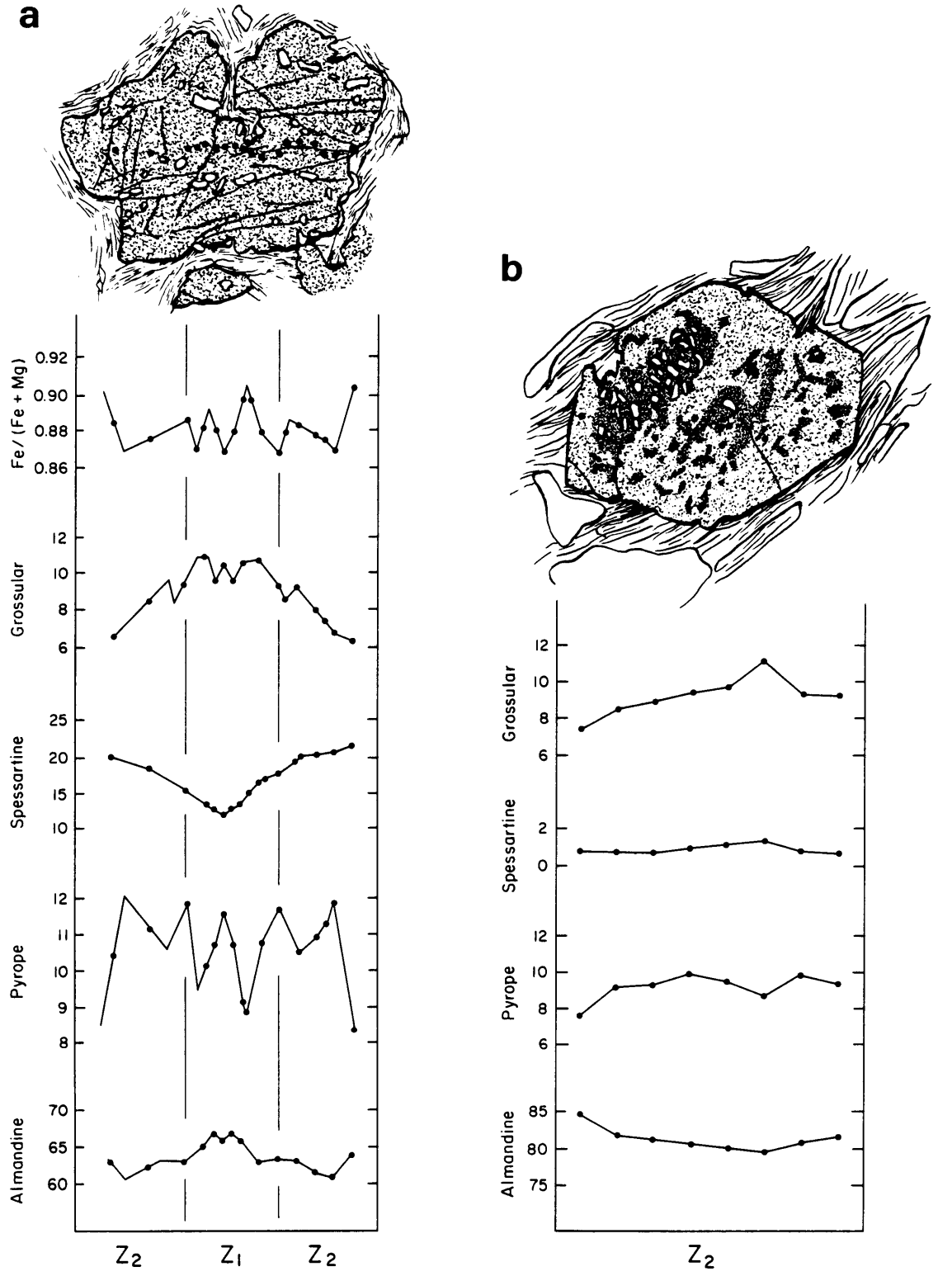
a
b
Fe / (Fe + Mg)
0.92
0.90
0.88
0.86
Grossular
12
10
8
6
Spessartine
25
20
15
10
Pyrope
12
11
10
9
8
Almandine
70
65
60
Z2
Z1
Z2
Grossular
12
10
8
6
Spessartine
2
0
Pyrope
12
10
8
6
Almandine
85
80
75
Z2

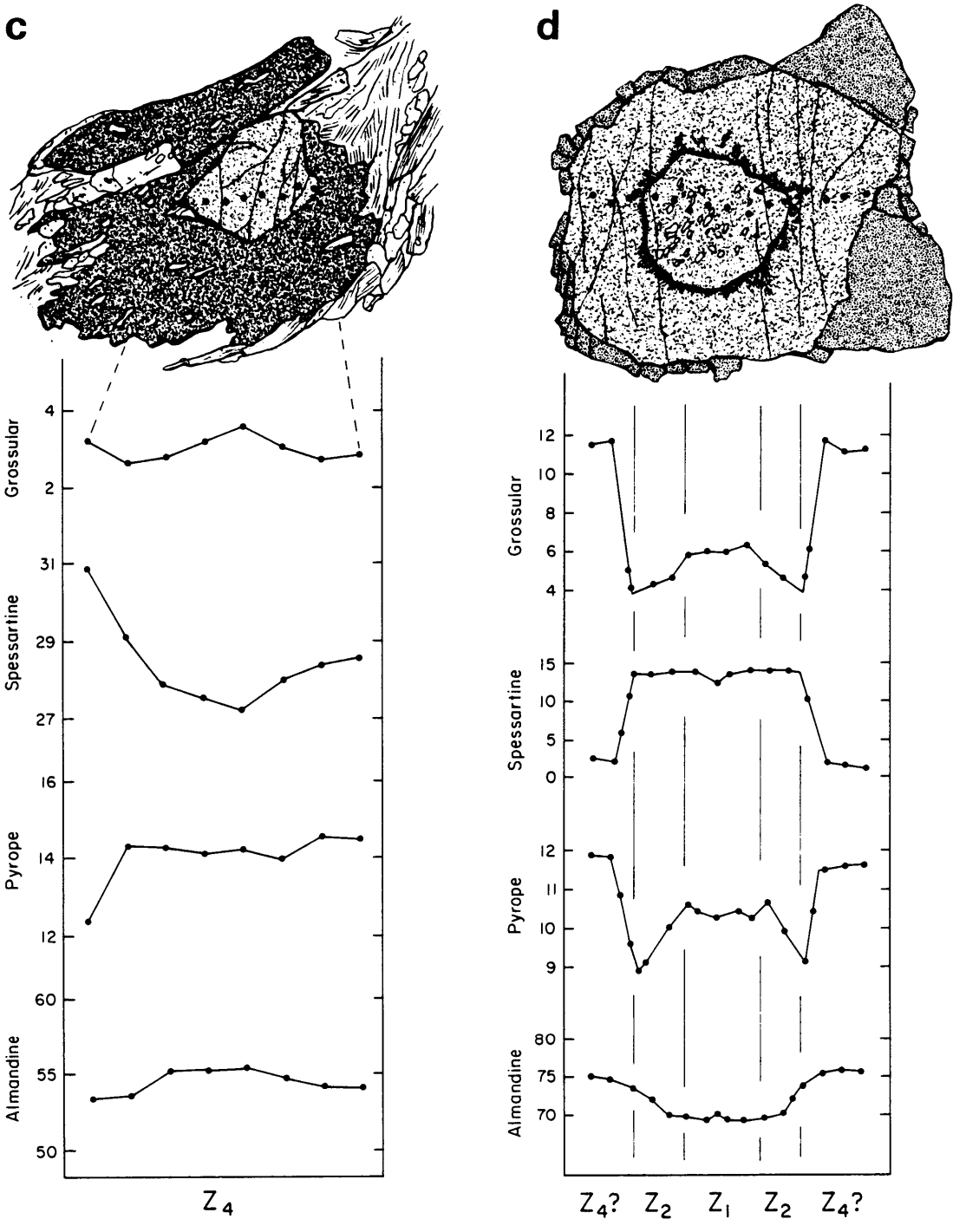
c
d
Grossular
Spessartine
Pyrope
Almandine
4
2
31
29
27
16
14
12
60
55
50
12
10
8
6
4
15
10
5
0
12
11
10
9
80
75
70
Z4
Z4?
Z2
Z1
Z2
Z4?

staurolite from 0.79 to 0.74. Zinc component is minor from 0.011 to 0.065 atoms/44 anions. Mn content is generally low (0.01 to 0.03 atoms/44 anions) for all but those in the cld + chl assemblage where it is 0.12 to 0.16.

Chlorite

The Fe/(Fe + Mg) ratio for chlorite (Appendix C) ranges from 0.40 to 0.56. Chlorite only occurs in the retrograde rocks and is usually a replacement of biotite. The lowest Fe/(Fe + Mg) ratio occurs where cld + chl replace st + bt, and high ratios occur in garnet and kyanite bearing rocks. Mn content ranges from 0.02 to 0.04 atoms/18 anions for most samples but 0.0 to 0.01 for garnet bearing assemblages. Fluorine content is variable from 0.02 to 0.06 atoms/18 anions.

Chloritoid

The Fe/(Fe + Mg) ratio for chloritoid (Appendix C) ranges from 0.89 to 0.78, the lower values in replacements of st + bt and the high values with gt or ky. Mn content is from 1.95 to 6.82 mol %, the highest values (6.82 to 4.5) are in ky bearing rocks, moderate values (4.3 to 3.0) in the garnet assemblage and low values (4.0 to 1.95) in st + chl rocks.

Other Minerals

Tourmaline is a common accessory mineral in the Evington Group metapelites and occurs in vein deposits in the cld + chl schists. Fe/(Fe + Mg) ratios range from 0.36 to 0.45 and are generally lower for tourmaline in the vein deposits. They are relatively sodic with values from 0.48 to 0.69 atoms/31 anions and calcium values from 0.1 to 0.17. Fluorine content varies from 0.04 to 0.18 atoms/31 anions and generally higher for grains in vein deposits and at the non-vein grain rims. Apatite is also a common accessory mineral and occurs as small inclusions in plagioclase and 0.5mm inclusions in garnet porphyroblasts of AG5-505. The grains are fluoro-apatite and contain 84 to 95 mol % F/(F + Cl + OH). Opaque phases include ilmenite, which dominates in the bt + grt + sil rocks and magnetite, which dominates in the bt + grt + st prograde and cld- and st-retrograde rocks. Aluminosilicates, including kyanite and sillimanite porphyroblasts contain between 0.3 and 0.4 weight percent Fe +3.

PETROLOGIC EVOLUTION

Metamorphic reactions are based on petrographic observations (Figures 26A-D and 29A-D). Many of the reactions were constrained using the least squares, mass balance methods of LeMaitre (1981) (Table 6) with weight percent oxide analyses from appropriate samples (Table 7). In some cases, analyses of a mineral were unacceptable and substituted with those from nearby samples with the same mineralogy and chemistry (Table 6). In other cases, phases were exhausted in reaction and therefore were not present in the sample. Analyses were substituted for the missing phases from samples at a similar stage of retrogression. The prograde and retrograde pseudo binary diagrams

(Figures 30, 31, and 32) were used to select samples from which analyses could be substituted.

Prograde Assemblages

The prograde assemblages formed earliest and reflect a regional high temperature event. To represent this prograde metamorphism, a T-X(Fe + Mg) pseudobinary diagram (Thompson, 1976) (Figure 30) was constructed based on assemblages and chemical analyses. The unretrograded assemblages and retrograde rocks that contain relicts of the high temperature event define an isograd of sil-in, st-out (Figure 25). The bt + grt + sil rocks lie to the southeast and represent the high temperature three phase assemblage. The isograd between these and the bt + grt + st assemblage rocks to the northwest represents the discontinuous terminal reaction:

$$qtz + pl + st + ms \rightarrow grt + bt + sil + H_2O \quad I$$

(Figure 30) in the KFMASH model system. The sil-bearing assemblage is on the high temperature side of the reaction and to the southeast in the map area.

The bt + grt + st assemblages represent conditions of the continuous reaction:

$$mag + pl + qtz + st + bt \rightarrow gt + ilm + ms + H_2O \quad II$$

(Figure 30). Fe/Fe+Mg ratios of the bt + grt + st indicate lower temperatures to the north and especially to the west using the methods of Thompson (1976) (Figures 25 and 30).

The continuous reaction displayed by the bt + grt + sil assemblages is:

$$grt + ms \rightarrow bt + als + qtz + pl + ilm + mag + H_2O \quad III$$

(Figure 30). Unfortunately most rocks displaying the high temperature assemblages have been retrograded and are st-bearing. The high Mn content of the high temperature assemblage garnets, especially in AG4-59, causes non-ternary (AKFM projection) be-

Table 6: Mass Balance Reactions and Coefficients (Wt. %)

Reaction	Minerals														Residual
	Qtz	Grt	Bt	Sil	Ky	St	Pl	Ms	Mag	Ilm	Chl	Cld	Tur	H_2O	B_2O_3	
I																
RE	5.25					70.21	3.71	20.82								
PR		19.95	16.56	61.77										1.72		2.768
II																
RE	17.84		22.09			36.63	5.96		17.48							
PR		70.38						28.15		0.96				0.51		4.610
III																
RE		41.00						59.00								
PR	10.86		38.27	27.29			14.57		6.89	0.56				1.56		1.981
V																
RE			16.79	72.81					8.02					2.38		
PR						72.81					3.87					0.1613
VIII																
RE	3.57		19.46			65.28			7.06					4.63		
PR								18.43			2.93	78.64				0.6250
IX																
RE	5.11					94.34								0.57		
PR					57.39			2.72	1.48		0.92	37.50				0.1725
XII																
RE	3.22	2.34				65.71			8.02		15.95			3.34	1.43	
PR												85.73	14.27			0.2006

Analyses for Reaction I from AG5-523 (Pl from AG4-6); Reaction II from AG4-225++; Reaction III from AG4-59; Reaction V from AG5-268+ (Mt from AG4-159+, Sil from AG5-523); Reaction VIII from AG5-1195 (Mus from AG4-159+, Bt from AG5-505); Reaction IX from AG4-159+; Reaction XII from AG5-929 (St from AG5-1195). RE = Reactants, PR = Products.

Table 7: Analyses used in Mass Balance Calculations

AG5-523 Mineral:	Grt	St	Ms	Bt	Sil	Pl
SiO_2	37.53	28.73	44.99	34.83	38.27	63.04
TiO_2	0.13	0.23	0.57	1.71	-0.01	0.02
Al_2O_3	21.19	52.42	33.97	19.28	60.20	25.00
FeO	32.79	14.57	2.70	21.09	0.39	0.05
MnO	6.25	0.19	-0.03	0.08	0.05	0.03
MgO	2.23	1.55	0.62	8.77	0.09	-0.01
CaO	1.40	-0.01	-0.02	0.01	0.00	4.53
BaO	0.15	0.12	0.34	0.31	0.07	0.00
Na_2O	-0.02	-0.02	1.11	0.22	0.00	8.60
K_2O	-0.02	-0.03	9.00	8.37	0.07	0.04
F	0.04	0.01	0.03	0.24	-0.04	0.00
H_2O	0.00	2.35	4.45	3.88	0.00	0.00
Total	101.48	100.11	97.73	98.80	99.10	101.30

AG4-225+ + Mineral:	Grt	St	Ms	Bt	Pl	Ilm
SiO_2	37.54	28.14	46.74	34.84	62.04	0.42
TiO_2	0.13	0.54	0.22	1.66	-0.01	53.39
Al_2O_3	21.42	53.97	36.58	19.00	22.74	0.13
FeO	35.55	13.63	1.71	20.97	-0.07	45.16
MnO	2.84	0.09	-0.07	-0.01	-0.07	0.72
MgO	2.51	1.36	0.41	8.60	0.00	0.11
CaO	0.80	-0.02	-0.01	0.00	4.18	0.02
BaO	-0.03	-0.08	0.00	0.02	-0.08	0.29
Na_2O	0.01	-0.03	1.60	0.12	8.81	-0.01
K_2O	-0.02	-0.03	8.66	8.47	0.00	0.03
F	0.01	0.01	-0.04	0.32	-0.02	0.05
H_2O	0.00	2.36	4.58	3.84	0.00	0.00
Total	100.79	99.93	100.38	97.84	97.54	100.30

Table 7. Mass Balance Analyses Continued

AG4-59 Mineral:	Bt	Pl	Grt	Ms	Sil	Mt	Ilm
SiO_2	36.18	55.40	38.08	46.08	38.16	0.45	0.15
TiO_2	1.68	0.02	0.15	0.70	-0.01	0.33	49.91
Al_2O_3	20.37	29.94	20.78	34.49	62.63	3.87	0.03
FeO	18.49	0.09	28.60	2.94	0.37	93.09	49.15
MnO	0.19	0.02	8.62	0.01	0.03	0.21	1.46
MgO	11.04	0.02	3.00	0.72	0.04	0.05	0.34
CaO	0.05	10.49	2.90	0.01	0.03	0.08	0.05
Na_2O	0.30	5.43	0.02	0.83	0.00	0.13	0.04
K_2O	9.01	0.05	0.03	9.78	0.00	0.07	0.06
H_2O	3.85	0.00	0.00	4.49	0.00	0.00	0.00
Total	101.17	101.48	102.18	100.05	101.25	97.83	101.21

AG5-268+ Mineral:	Chl	Ms	St	Bt	Pl
SiO_2	25.71	45.88	28.34	37.03	63.92
TiO_2	0.06	0.33	0.32	1.31	0.01
Al_2O_3	23.89	35.74	53.61	18.84	22.65
FeO	16.29	1.90	12.61	14.03	-0.07
MnO	0.11	-0.02	0.27	0.09	-0.04
MgO	19.99	0.43	2.28	14.07	0.00
CaO	-0.02	-0.01	-0.02	-0.02	2.78
BaO	0.06	0.36	0.03	0.28	0.29
Na_2O	-0.03	1.71	-0.02	0.23	7.98
K_2O	0.01	7.65	-0.05	8.71	0.00
F	0.08	-0.02	-0.07	0.57	-0.02
H_2O	11.71	4.48	2.40	3.73	0.00
Total	97.97	98.43	99.73	98.87	97.54

Table 7. Mass Balance Analyses Continued

AG5-1195 Mineral:	Bt	St	Chl	Cld	Ms
SiO_2	35.51	28.19	25.18	25.05	45.36
TiO_2	1.47	0.65	0.20	0.12	0.39
Al_2O_3	20.01	53.68	23.02	40.09	36.10
FeO	23.38	12.98	26.77	23.36	1.93
MnO	0.08	0.60	0.36	1.11	-0.04
MgO	7.57	1.22	13.46	2.24	0.47
CaO	0.06	0.05	0.05	0.34	-0.01
BaO	0.20	0.00	0.00	0.00	0.33
Na_2O	0.29	0.06	0.01	0.00	1.43
K_2O	8.65	0.01	0.13	0.19	8.12
F	0.16	0.00	0.00	0.07	0.02
H_2O	3.88	2.36	11.49	7.23	4.46
Total	101.24	99.80	100.70	99.80	98.56

AG4-159+ Mineral:	Chl	Cld	Ms	Ky	Mt	St
SiO_2	24.86	25.09	45.36	37.90	0.14	29.01
TiO_2	0.11	0.06	0.39	-0.01	0.25	0.36
Al_2O_3	23.63	40.67	36.10	62.08	0.36	55.05
FeO	21.21	22.11	1.93	0.30	93.09	10.52
MnO	0.39	1.84	-0.04	-0.08	0.13	0.72
MgO	15.99	2.99	0.47	0.02	0.02	1.18
CaO	0.00	-0.01	-0.01	-0.02	0.04	-0.01
BaO	0.00	0.00	0.33	-0.03	0.38	-0.01
Na_2O	0.00	-0.01	1.43	-0.03	0.01	0.02
K_2O	-0.02	0.03	8.12	-0.05	0.03	-0.04
F	0.15	0.07	0.02	0.00	0.09	0.02
H_2O	11.36	7.29	4.46	0.00	0.00	2.37
Total	97.69	100.13	98.56	100.01	94.44	99.17

AG5-929 Mineral:	Chl	Cld	Grt	Ms	Mt	Tur
SiO_2	25.06	25.10	37.91	46.14	0.18	36.35
TiO_2	0.08	0.08	0.16	0.65	0.25	0.43
Al_2O_3	22.91	40.73	21.21	34.65	0.58	32.11
FeO	21.04	22.05	24.65	2.96	94.03	7.72
MnO	0.19	0.80	12.81	-0.06	0.20	-0.03
MgO	16.71	3.21	3.72	0.72	0.02	6.15
CaO	-0.01	0.15	1.02	-0.02	0.03	0.58
BaO	-0.02	0.00	0.07	0.39	0.14	0.03
Na_2O	-0.03	0.00	0.00	1.26	0.00	1.69
K_2O	-0.03	0.04	-0.01	9.07	0.02	-0.02
F	0.09	0.00	0.01	0.06	0.12	0.14
B_2O_3	0.00	0.00	0.00	0.00	0.00	10.51
H_2O	11.37	7.31	0.00	4.47	0.00	3.55
Total	97.36	99.57	101.47	100.29	95.57	99.18

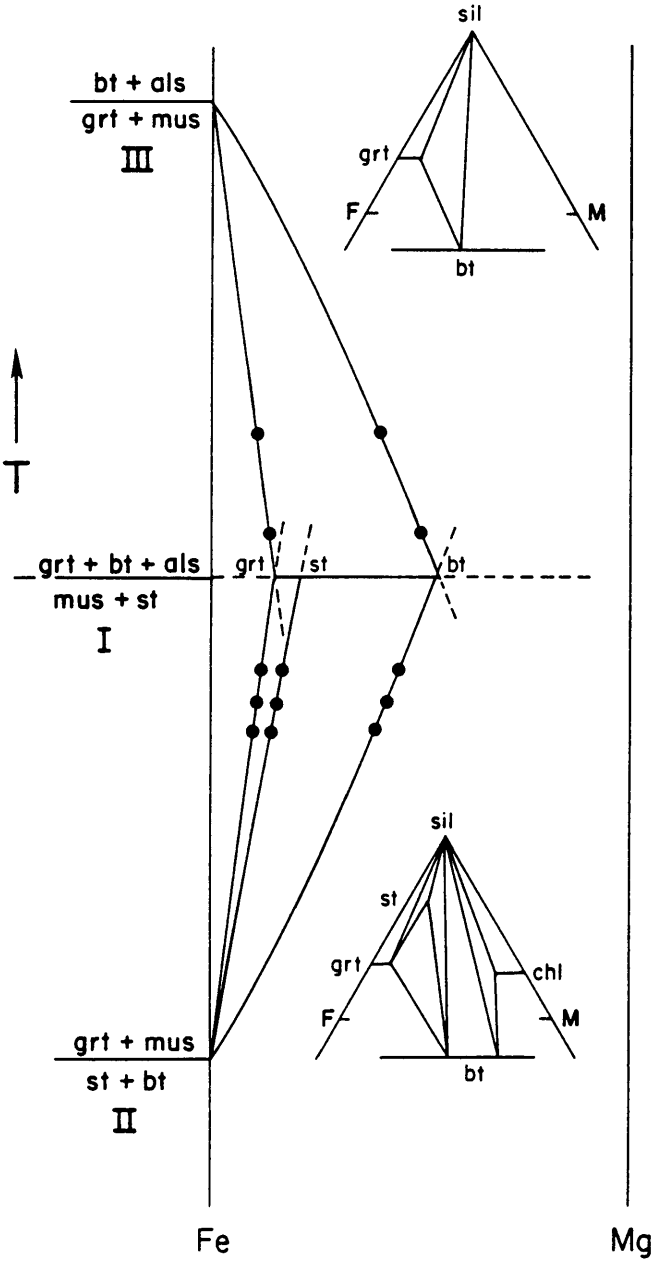

Figure 30. Pseudobinary diagram for prograde assemblages and reactions using methods of Thompson (1976).

havior of the rocks and the discontineous reaction (I) to actually be continuous causing occurrence over an area.

Garnet profiles from the high temperature assemblage indicate a two stage growth history, Z1 and Z2 (Figure 29A). The low temperature assemblage profiles show only a single stage history, Z3 (Figure 29B). If the prograde event is synchronous across the area then Z2 and Z3 represent the same growth phase under different conditions.

The one problem in construction of the loop is sample AG5-505 (Figure 29). The bt + grt + st assemblage has a low Fe/(Fe + Mg) ratio in biotite indicating that it should be the lowest grade sample of that assemblage. The high Fe/(Fe + Mg) ratio in garnet however, is inconsistent. The sample also contains fluoro-apatite, sillimanite fibers in muscovite and no quartz. The high fluorine activity and lack of quartz may have allowed the bt + grt + st assemblage to persist to much higher temperatures. The Fe/(Fe + Mg) ratios of grt + bt fit the higher temperature portion of the T-X(Fe - Mg) loop (Figure 30). This high temperature positon is supported by geothermometry (see thermobarometry section). The assemblage however cannot be used in AKFM (Thompson, 1957) construction because quartz is absent and is not considered further.

St-Retrograde Reactions

The st-bearing retrograde assemblages are confined to rocks that were originally bt + grt + sil bearing. The st-retrograde rocks contain garnets with core profiles that replicate the full garnet growth profiles Z1 and Z2 of the high temperature assemblage (Figures 29A and 29D). The garnet cores are also stable with sillimanite which characterizes garnet assemblages at temperatures above reaction I. The production of staurolite in these rocks occurred through a decrease in temperature and introduction of fluid as the bt + grt + sil rocks moved to the low temperature side of the reaction

grt + bt + sil → st + ms (I) (Figure 31). Textural evidence for the st-retrograde reaction is the replacement of bt + grt + sil by fine-grained intergrowths of bt + grt + st. The reaction however did not go to completion because of either a lack of energy or fluid, or armoring of phases. Staurolite formed around the garnet and armored it from the bt + sil matrix, isolating the reactants. The stable three phase assemblage then became bt + st + sil. As temperature further decreased, the bt + st + sil assemblage underwent the continuous retrograde reaction:

$$mag + H_2O + bt + als \rightarrow st + ms + qtz \quad IV$$

(Figure 31) depending on the availability of fluid. The staurolite that formed through this reaction is not associated with garnet. It occurs mostly as smaller euhedral grains in mats of sillimanite or with biotite. The Fe/(Fe + Mg) ratio in staurolite and biotite decreased in the reaction (IV) making them chemically distinct from the prograde bt + st which underwent reaction II (grt + ms → st + bt) and became Fe-rich.

The st-retrograde rocks that contain chlorite received a continuous fluid input during the retrogression and underwent the non-terminal discontinuous retrograde reaction:

$$H_2O + mag + bt + als \rightarrow st + chl \quad V$$

(Figure 31). This retrogression of the prograde st-bearing rocks did not include this reaction because sillimanite was not stable in that assemblage. Some rocks continued to receive fluid and energy and proceded along the continuous retrograde reaction:

$$qtz + H_2O + st + bt \rightarrow chl + ms + mag \quad VI$$

(Figure 31). The only other reaction expressed in these rocks is the polymorphic phase transition from sil to ky which probably occurred approximately at reaction V (bt + als → st + chl) (Figure 31). Many of the st-retrograde rocks contain euhedral kyanite overgrowths on the fibrolitic sillimanite.

The st-retrograde rocks exhibit varying degrees of continual but incomplete re-equilibration. Either the fluid or the energy input into these rocks was insufficient to

Figure 31. Pseudobinary diagram for st-retrograde and cld-retrograde assemblages and reactions (method of Thompson, 1976).

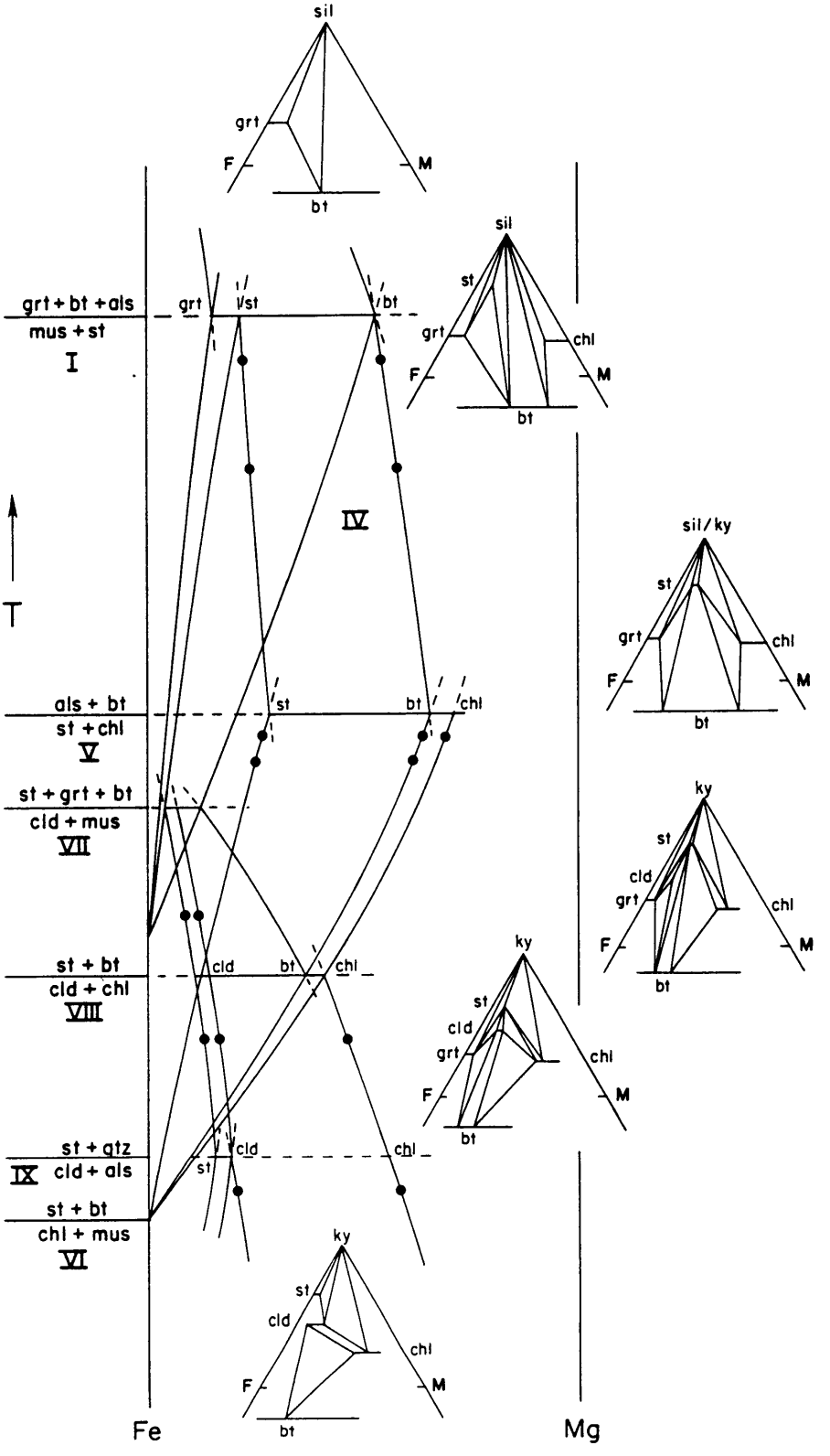
sil
grt
F
M
bt
grt + bt + als
mus + st
I
grt
st
bt
sil
st
grt
chl
F
M
bt
IV
T
sil/ky
st
grt
chl
F
M
bt
als + bt
st + chl
V
st
bt
chl
st + grt + bt
cld + mus
VII
ky
st
cld
grt
chl
F
M
bt
st + bt
cld + chl
VIII
cld
bt
chl
ky
st
cld
grt
chl
F
M
bt
st + qtz
IX cld + als
st + bt
chl + mus
VI
cld
chl
st
ky
st
cld
chl
F
M
bt
Fe
Mg

drive the reactions to completion, leaving relicts of each reaction. The effect of armoring and patchy equilibrium is not only to preserve relicts of early reactions but also to locally change the bulk chemistry. Therefore rocks of a single bulk chemistry can show reactions that would normally only be observable in multiple samples of differing compositon.

Cld-Retrograde Reactions

Those rocks that continued to receive fluid proceeded to the cld-producing, st-consuming retrograde reactions. There are several cld-bearing assemblages, cld + chl + st, cld + chl + grt and cld + chl + ky, all of which postdate both the early prograde and later st-retrograde reactions. Evidence for the succession of cld-assemblages is both textural and by mineral chemistry. The formation of cld from st occurs through several different reactions because there is both high Fe prograde and high Mg retrograde staurolite (Figure 31). The high temperature cld-producing retrograde terminal discontinuous reaction is:

$$H_2O + st + grt + bt \rightarrow cld + mu + mag \quad VII$$

(Figure 31) which is restricted to the prograde st-assemblage because the reactants st + grt + bt were present and the st inclusions in cld from that assemblage are high in Fe. Retrogression of the prograde st-assemblage is only documented in one sample.

Most of the cld was produced in the retrograde non-terminal discontinuous reaction:

$$H_2O + qtz + mag + st + bt \rightarrow cld + chl \quad VIII$$

(Figure 31). Textures showing this reaction include euhedral cld which occurs in and around anhedral and disaggregated staurolite and forms pseudomorphs with chlorite after st. Because garnet appears to have been the limiting reactant in reaction VII, and biotite was later chloritized, the products of both reactions VII and VIII are the same.

St from the retrograde assemblage however is identifiable by its higher Mg content (Figure 31).

The third st to cld retrograde reaction is non-terminal, discontinuous and affected both prograde and retrograde staurolites. The reaction is:

$$qtz + st + H_2O \rightarrow cld + als + ms + mag + chl \quad IX$$

(Figure 31). Rocks displaying this reaction texture occur around the kyanite deposits. Both kyanite and staurolite occur as euhedral inclusions in the chloritoid but only kyanite is euhedral in the matrix. Another, higher temperature kyanite-chloritoid reaction that may have occurred around the kyanite deposits is st + chl → cld + ky. The evidence for this reaction is not conclusive because the products are the same as reaction IX. In some samples however, chlorite appears stable and quartz is absent. The mass balance calculations (Table 6) indicate that reaction IX was operative in those cld + ky samples analyzed.

The grt + cld assemblages exhibit a different series of reactions. Garnet occurs not only as porphyroblasts but also as cores in chloritoid indicating that it formed prior to the chloritoid. In sample AG5-268+ (Figure 25) the garnet exists in a reaction texture with chlorite and is surrounded by staurolite and biotite. The suggested reaction for this assemblage is the retrograde, non-terminal, discontinuous reaction:

$$qtz + H_2O + st + bt \rightarrow grt + chl + ms \quad X$$

(Figure 32). Reactants may have been consumed or the reaction was incomplete. Staurolite remained to lower temperatures and the product assemblage underwent the continuous reaction:

$$qtz + H_2O + grt \rightarrow chl + st \quad XI$$

(Figure 32). The rocks finally underwent the terminal discontinuous reaction:

$$qtz + mag + H_2O + B_2O_3 + st + grt + chl \rightarrow cld + tur \quad XII$$

The staurolite was consumed and remnant garnet was included in the chloritoid. These reactions however, cannot be represented on the main T-X(Fe-Mg) pseudo binary (Fig-

ure 31) because the garnets contain between 30 and 35 % spessartine and therefore do not exhibit the ternary behavior modeled by the AKFM system. They overlap the other cld-producing reactions.

Some of the st-retrograde rocks also contain phases formed during partial re-equilibration with the cld + chl assemblages. AG5-268+ is the only sample that contains chloritoid but other associated products are present in other samples. AG4-2 contains the high spessartine garnets enclosed by staurolite aggregates. Where garnet has not developed, staurolite is intergrown with biotite in aggregates. The rock apparently underwent reaction X (st + bt → grt + chl). In AG4-6 high Fe garnet is rimmed by euhedral to subhedral chlorite. The garnets from all other st-retrograde samples exhibit aggregate rims of staurolite and biotite.

Conditions of Metamorphism

Location P-T Reaction Space

The conditions of metamorphism in the rocks from Altavista is observable in P-T space in the KFMASH system (KFASH and KMASH also) at constant μH_2O (Figure 33) (Albee, 1965; Harte and Hudson, 1979). The highest temperature discontinuous reaction is als + bt + grt → st + ms (I) which characterizes the prograde metamorphism and the initial retrogression of the bt + grt + sil rocks. The reaction has a negative slope and is pressure sensitive over a wide range of temperatures (Figure 33). The next observed retrograde reaction is als + bt → st + chl (V), which only occurred in the st-retrograde rocks. The reaction is isothermal and constrains the first reaction in that the two meet at the chloritoid cordierite absent invariant point (Figure 33).

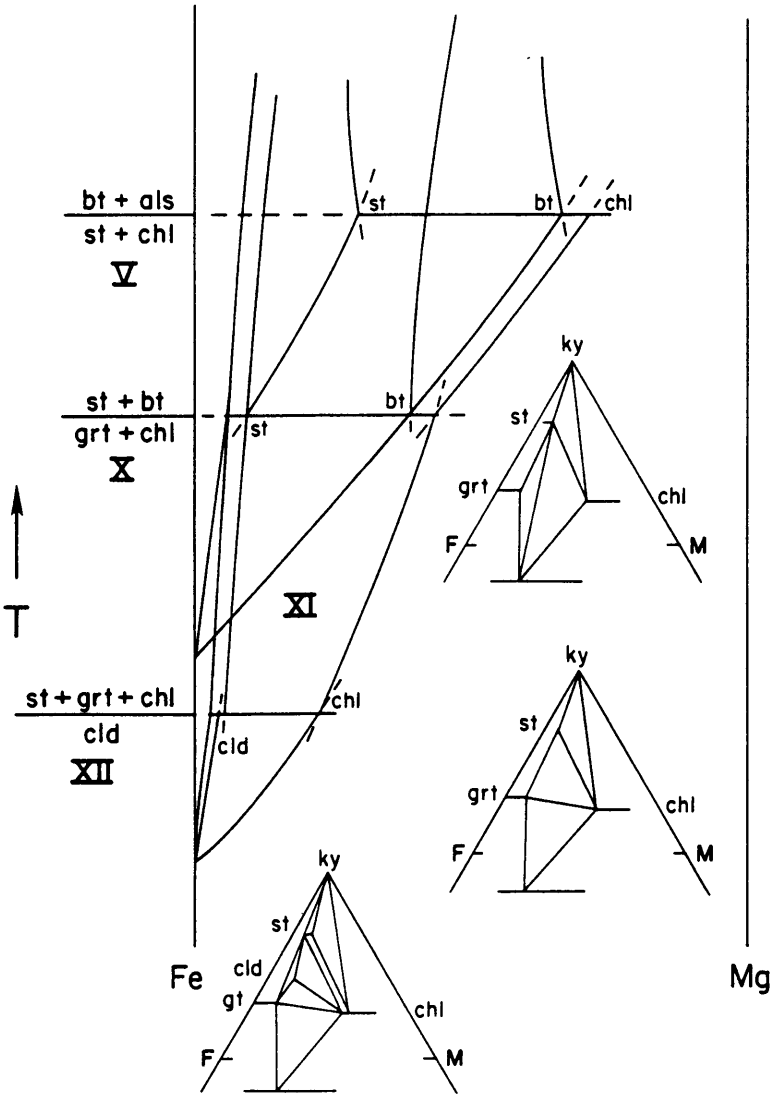

Figure 32. Pseudobinary diagram for cld-grt retrograde assemblages and reactions (method of Thompson, 1976).

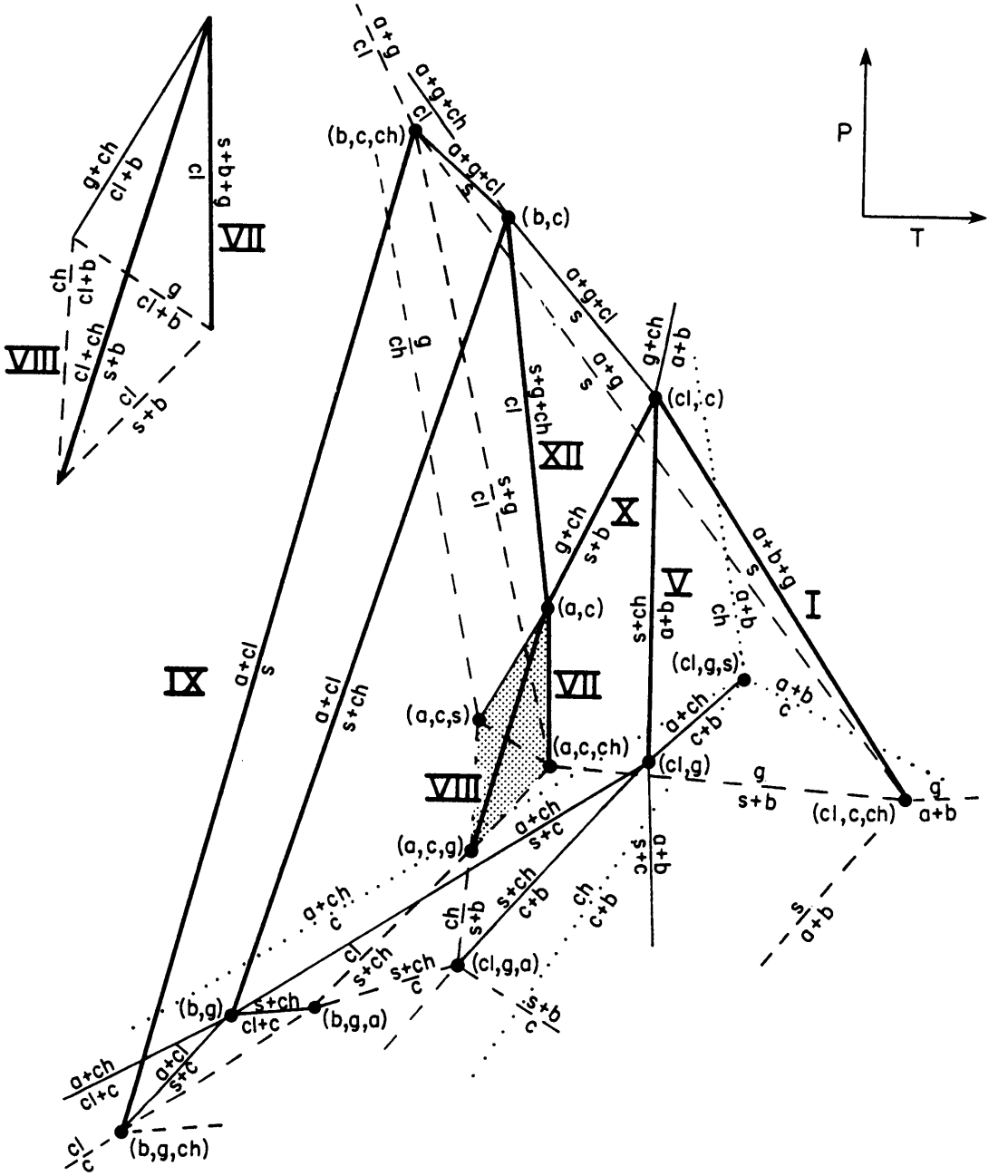

Figure 33. Projection showing positions of reactions in P-T space. Reaction labels correspond to Figures 29, 30, and 31. Diagram from Harte and Hudson (1979).

The best constraints on the P-T path are those reactions that define the aluminosilicate-cordierite absent invariant point. On the low pressure side of the point, the reaction st + bt + grt → cld (VII) is the first encountered in retrogression. The reaction is isothermal but occurs over a limited pressure range (Harte and Hudson, 1979). The second chloritoid reaction, st + bt → cld + chl (VIII) occurs at slightly lower temperatures than the first (Figure 33). This reaction is relatively pressure insensitive but also occurs under limited pressure conditions. The two reaction lines that extend to the high pressure side of the invariant point are documented in the garnet-chloritoid assemblages. These reactions, st + bt → gar + chl (X) and st + grt + chl → cld (XII) are also pressure insensitive but occur over a wider range of temperatures (Figure 33). The garnets produced in this reaction are spessartine rich and therefore are not part of the KFMASH system.

The reaction cld + bt → chl in the KFASH system may have occurred but is not provable. The grt → chl reaction on the opposite or high pressure side of the als, cd, st absent invariant point is only well restricted in temperature for the pure Fe system. The final observed reaction is st + qtz → als + cld (IX) which apparently produced kyanite in the Altavista area. The reaction occurs over a large range of P-T space. Another possible kyanite producing reaction that would have occurred prior to reactio IX, is st + qtz → ky + cld.

Thermobarometry

Several geothermometers and one geobarometer were applied to the rocks in the Altavista area. Although none of the assemblages or compositions of assemblages are ideal for use with these systems, results are fairly consistent. Combining these data with application of reaction textures to the petrogenetic grid of Koons and Thompson (1985),

the P-T conditions of the various reactions can be reasonably constrained. The grt-bt geothemometer (Ferry and Spear, 1978) with Mn and Ca corrections (Pigage and Greenwood, 1982; Ganguly and Saxena, 1984) was applied to the data. Generally, the bt + grt + sil assemblage yielded the highest temperatures (avg. 620-640°C), the bt + grt + st moderate (avg. 570-590° C) and the st-retrograde moderate to low temperatures (avg. 500-520° C) (Table 8).

The temperatures for the st-retrograde rocks are questionable because bt + grt may not be in equilibrium, or may record lower temperature reactions or re-equilibration. Sample AG5-505 with bt + grt + st assemblage yielded temperatures of 695 to 779° C indicating that it is the highest temperature sample but with an assemblage indicative of moderate temperatures.

The Ferry and Spear (1978) calibration yields the lowest temperatures but does not take Mn or Ca into account. The method of Pigage and Greenwood (1982) yield the highest temperatures, unreasonably high according to Graham and Harte (1985). The corrections of Ganguly and Saxena (1984) for Ca and Mn yield temperatures that are similar to, but slightly higher than Ferry and Spear (1978). The Pigage and Greenwood (1982) method changes the temperature order of the samples. The others appear to generally support the order indicated by the T-X (Fe-Mg) diagram (Figure 30).

The geobarometer pl + grt + alsil + bt (Newton and Haselton, 1981) was applied to the bt + grt + sil assemblage. Unfortunately most of the bt + grt + pl + sil assemblages contain st, for which no geobarometer exists. Garnets with Mn > 0.33Mg are suggested to be inappropriate for this geobarometer (Newton and Haselton, 1981), which is exhibited by all of the samples. In an attempt to evaluate and correct for the effect of Mn, two pressure determinations were performed for each sample. For the first, the Fe, Mg, and Ca components were used as measured in the pressure calculation. For the second, ideal mixing of the components with 0 spessartine was assumed. The calculation for an ideal mixing without Mn yields the higher pressures. Pressures are 5.75

Table 8: Temperatures from Garnet/Biotite Geothermometry

SAMPLE	*ASSEMBLAGE*	TEMPERATURES (°C) *F. & S.*	*G. & S.*	*P. & G.*
AG5-1066A	bt + grt + sil	617	655	715
AG4-59	bt + grt + sil	588	616	731
AG4-59C		567	585	
AG5-523	bt + grt + sil + st	558	591	652
AG4-225	bt + grt + st	570	581	619
AG4-217	bt + grt + st	551	571	610
AG5-268	st-retrograde	488	538	667
AG4-179	st-retrograde	514	533	571
AG4-2A	st-retrograde	503	517	643
AG4-6	st-retrograde	488	487	564
AG4-3	st-retrograde	473	484	559

F. & S. = Ferry and Spear (1978), G. & S. = Ganguly and Saxena (1984), P. & G. = Pigage and Greenwood (1983); AG4-59C from garnet core, assemblage unknown.

and 6.28Kb without Mn and 4.5 and 5.57Kb with Mn (Figure 34). The lower the Mn component, the closer the results of the two methods.

This calibration was also used for calculating conditions of formation for the core of the garnets from AG4-59, assuming that the core was stable with the same assemblage as the rim, that the biotite which is ubiquitously present, had composition comparable to present and that the growth period and that the zones in plagioclase directly correspond to the zones in the garnet. The results are 585° C and 6.59 kb (rim 615° C, 5.75 kb) suggesting a down pressure, up temperature trajectory from core to rim (Figure 31). Use of Figure 2 of Spear and Selverstone (1983) for the same assemblage yields a similar trajectory.

P-T Path

The temperature-pressure determinations and reactions observed can reasonably constrain a path in P-T space (Figure 34). Koons and Thompson (1985) have compiled all experimental data on the KFMASH system and combined them with the phase relations demonstrated by Harte and Hudson (1979) and Albee (1965) to construct a petrogenetic grid. The observed reaction of highest temperature is bt + grt + sil → st + ms (I). Experimental data indicate that this reaction takes place at 670 to 680° C in the high pressure portion of the sillimanite field of Holdoway (1971) and throughout the sillimanite field of Richardson et al.. (1969). The garnet in samples from Altavista contain Mn and Ca and biotite contains Ti which is not modelled in the KFMASH system. Geothermometry and indicates that the reaction occurred at 595 - 615° C. Re-equilibration of the grt + bt may have reset the ratios to yield lower temperatures. The next reaction (sil + bt → st + chl + ms, V) is experimentally calibrated and projected to occur at 625 to 640° C (Schreyer and Seifert, 1969; Schreyer and Baller, 1971; Koons

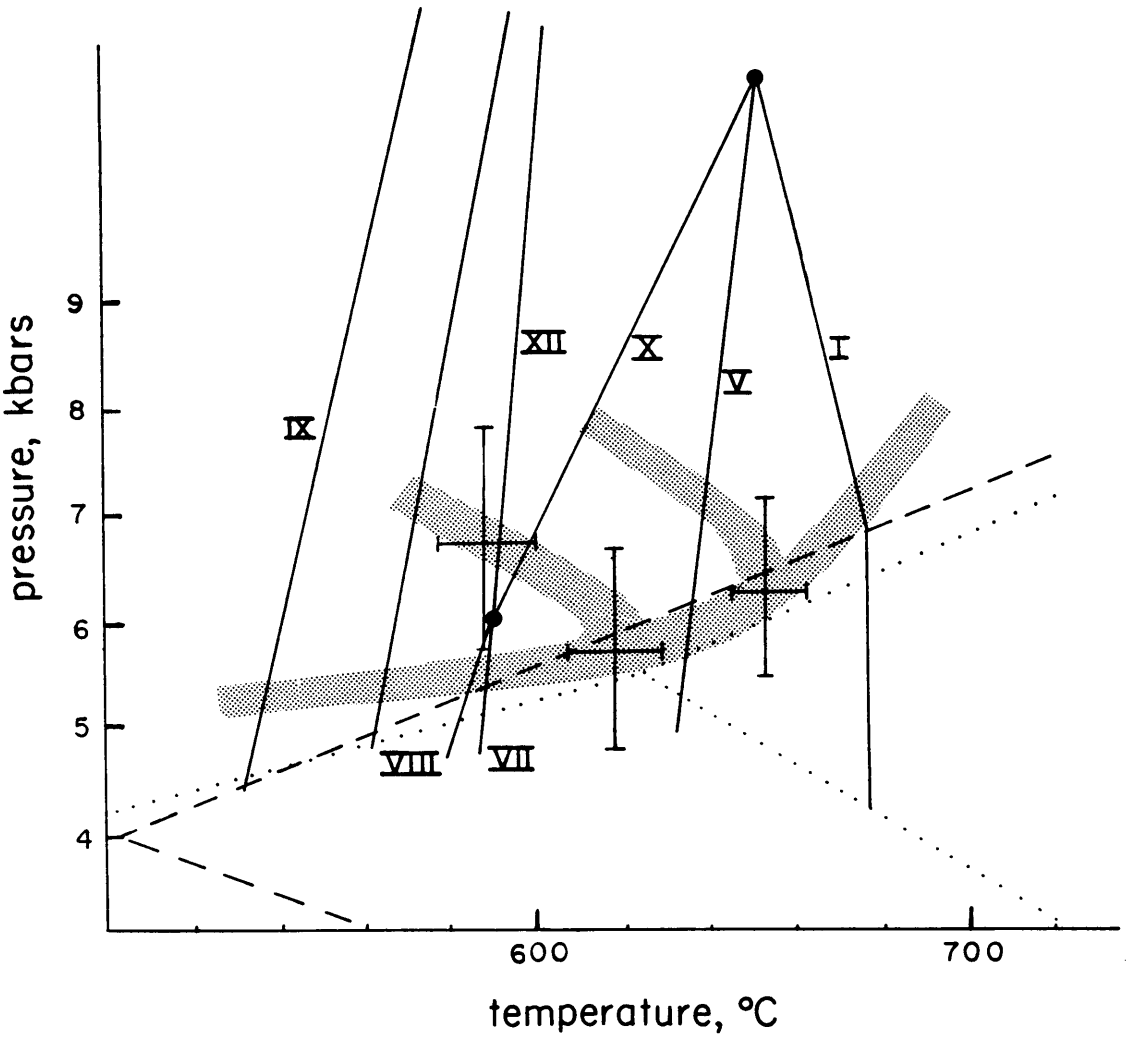

Figure 34. P-T loop for rocks in Altavista area using thermobarometry and reactions for constraint. Petrogenetic grid from Koons and Thompson (1985).

and Thompson, 1985). Geothermometry suggests that the temperature was actually between 570 and 540° C though constraints are partially imposed by the st-retrograde rocks in which grt + bt have likely reequilibrated. The rocks indicative of lower temperatures than this reaction show the polymorphic transition of sillimanite to kyanite.

The position of the phase transition constrains the pressure to between 5.0 and 6.1 Kb considering the cld + chl retrograde reactions (VII and VIII). The cld + chl reactions occur at 570 to 590° C and between 4.9 and 6.0 Kb in the KFMASH system (Koons and Thompson, 1985). The Mn content is relatively small in the minerals of these assemblages as is Zn in the staurolite. The system therefore should behave nearly ideally. The kyanite producing reaction, st + qtz → ky + cld (IX) is experimentally calibrated (Ganguly, 1972) to 520 to 530° C over the pressure range. The possible, early ky producing reaction (st + chl → ky + cld) is proposed to occur at 550 to 560° C and at pressures above 4.9 Kb (Koons and Thompson, 1985).

The retrogression appears relatively isobaric through 120 to 150° C of cooling. Geothermometers indicate this cooling trend but generally yield lower temperatures of reaction than the experimental and projection curves. The presence of Mn, Ca, Na and Ti however is not modelled by the KFMASH system and subsequent re-equilibration of the phases may have occurred. The curves also assume end members or arbitrary mineral compositions in reactions which causes uncertainty in the position in P-T space.

DISCUSSION

Retrogression and Fluids

The zones containing the cld + chl assemblages form parallel bands across the eastern map area (Figure 25) that exhibit weak positive magnetic signatures. In the

central and western map area, the rocks were folded by F_3 and F_4 folding events into a series of domes. The trend of the retrograde zones is also parallel to these structures. The retrograde zones were therefore conformable to the horizontal structures and stratigraphy when they were formed, during the D_2 deformational event.

The apparent metamorphic gradient appears to increase away from the centers of the cld + chl retrograde zones. Although irregular in distribution, the assemblages indicative of lowest temperature tend to lie well within the cld + chl zones. These ky-bearing assemblages also lie near the rocks of the most extreme composition. The 1 to 2 m thick kyanite segregations with tourmaline and magnetite rims and 0.5 to 1.5 m thick tourmaline segregations lie immediately within schists of 90 to 95% muscovite.

The areas around the cld + chl, severely retrograded zones are characterized by partially retrograded rocks. They contain st + bt bearing retrograde assemblages (from bt + grt + sil) in which the hydration reactions (I and V) have not gone to completion. The two main cld-producing reactions (VII and VIII) have in most cases, gone to completion. Reaction VII (st + grt + bt → cld + mus) requires 3 H_2O for every 2 cld produced and reaction VIII (st + bt → cld + chl) requires 11.3 H_2O for every 4 cld produced. Other hydration reactions that occur in this zone are replacement of plagioclase by muscovite and biotite by chlorite. The ky-producing reaction (IX) which occurs closer to the center of the zone also consumes H_2O. The kyanite deposits at the center of the hydrated zones, on the other hand, are anhydrous.

The change in mineralogy and bulk composition directly reflects the conditions and composition of the infiltrating fluid. Wintsch (1975) has shown that fluids with high αH^+ or αHCl (low pH) relative to αKCl and $\alpha NaCl$ will cause muscovite to react to kyanite by dissolution. Kerrick et al.. (1985) and Mohr (1986) however suggest that such aluminosilicate segregations actually result from deposition of Al, transported as Al complexes in fluid. Both processes require high quantities of fluid. Outside of the kyanite deposits, tourmaline deposits occur with interstitial quartz and magnetite. The

sodic tourmaline occurs as small intergrown needles that are oriented perpendicular to the walls of the enclosing schist and randomly oriented within the deposit. The enclosing muscovite schist contains 5-20% tourmaline adjacent to the deposit and lesser amounts farther away. Unlike the kyanite deposits, the tourmaline veins are commonly oblique to the S_2 foliation. They appear to define fracture fillings that in some cases were folded during the F_3 event.

The tourmaline deposits occur near rocks that display reaction XII which produced tur. The deposits were formed by a B_2O_3 rich fluid that removed K^+ (removal of ms) and or deposited Na^+. Orville (1963) has shown that relatively cool fluids will exchange Na for K as they move through hot rocks. This suggests that the source for fluids could have been from lower levels in the pile where temperatures were lower. Away from the deposits, plagioclase is replaced by muscovite, suggesting hotter fluids. Yardley and Baltatzis (1985) have studied a similar situation in the Dalradian schists of Scotland and Ireland. By calculating fluid compositions for different source rock types they estimated fluid to rock ratios of between 625:1 for a metamorphic fluid source and 7:1 for a granite fluid fluid. Source conditions of the fluid in the Altavista area cannot be determined without isotopic study.

TECTONIC IMPLICATIONS

There are several stages in the evolution of nappe emplacement. The path of P-T in response to the movement history is documented in many examples (Spear and Selverstone, 1983; Selverstone, 1984; Spear et al.., 1984). In general, the rocks of the footwall of a nappe undergo regional metamorphism followed by a rapid pressure rise as the nappe is thrust over them (P max) (Figure 35). The slow downward conduction or convection of heat from the high temperature rocks in the hanging wall causes a

slower thermal response in the footwall. The temperature therefore increases (T max) as pressure decreases through erosion of the overlying strata. The final phase involves cooling through equilibration which is the retrograde path (Figure 35) (Spear et al.., 1984).

The Altavista metamorphic sequence records the final or retrograde phase in the nappe evolution. The position of most of the study area is on the footwall of a nappe because the stratigraphy is upright, yet the prograde metamorphic gradient is inverted. Garnet/plagioclase core compositions suggest that early pressures were higher and temperatures were lower, recording part of the progression from P max to T max (Figures 35 and 36A) (Spear et al.., 1984). The peak metamorphism was the thermal equilibration of the upper footwall or the thermal maximum (Figure 36B). The peak prograde conditions (T max) are represented by the bt + grt + sil and bt + grt + st assemblages and migmatization and granite intrusion in the southern map area (Figure 25). The hot nappe overlying these rocks caused heat to slowly convect or conduct down to lower levels in the footwall. The additional heat drove prograde, dehydration reactions in the rocks (Figure 36B). The liberated fluid from these reactions was then forced up through the strata along fluid conduits (Figure 36C). The driving force for the fluids was pressure, temperature or chemical gradient and the conduits were structural discontinuites. This process is summarized by Ethridge et al.. (1983). Derivation of retrograding fluids from moderately deeper levels in a metamorphic pile was suggested by Mohr (1986) in possible correlative rocks in North Carolina. The fluid drove retrograde reactions in rocks adjacent to conduits and partial retrograde reactions in rocks farther away. Rocks close to the conduits reacted longer and to lower temperatures producing the apparent decrease in grade into the most intensely hydrated areas and K/Na exchange reactions in the tourmaline and kyanite deposits.

The retrogression appears to have taken place under nearly isobaric conditions. The process therefore may not have started until much of overlying orogen and moun-

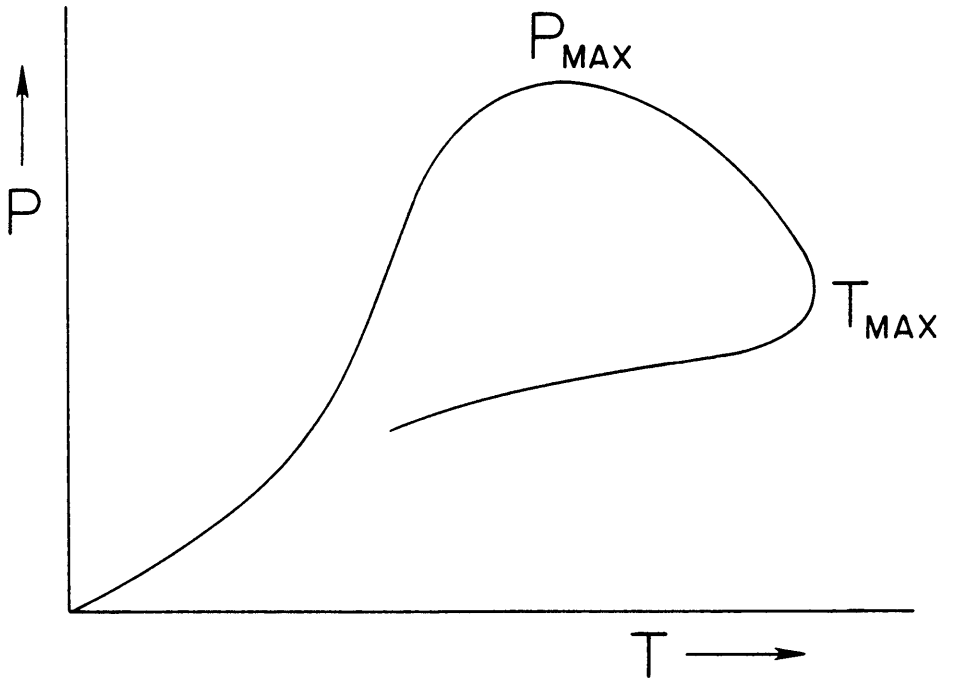

Figure 35. Inferred and calculated P-T loop for the Altavista area using terminology of Spear et al (1984).

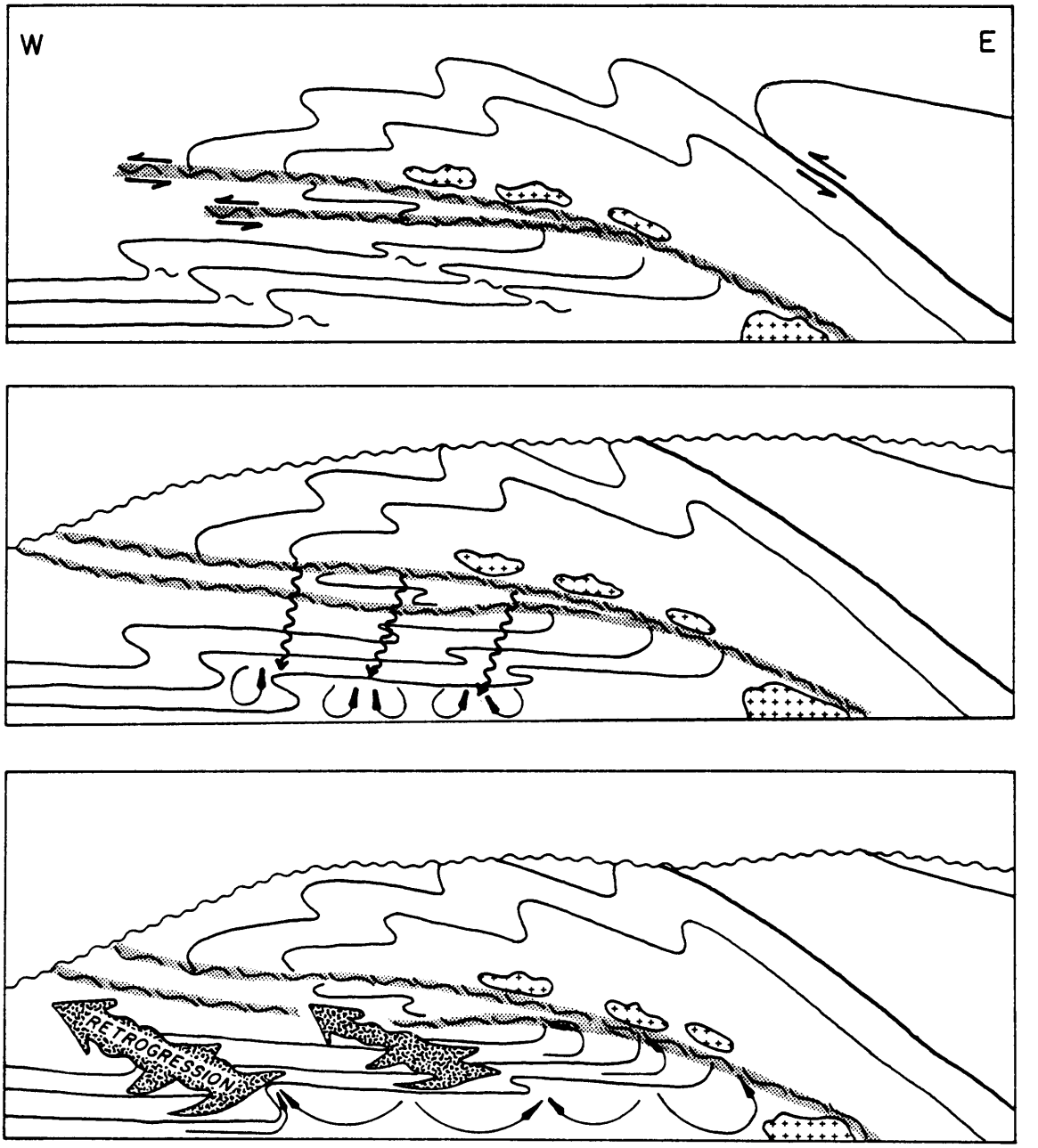

Figure 36. Tectonometamorphic model for the Altavista area with the corresponding positions of P-T loop (Figure 34). A) Nappe emplacement, increase in pressure to P max. B) Conduction or Convection to T max. C) The retrograde path and hydration of the pile.

tain system was eroded away. Otherwise, the fluid may have been quite a bit cooler than the rocks and the process may have taken place relatively quickly. The retrograde portion of the "ideal" P-T loop is proposed to have been relatively isobaric (Spear et al., 1984).

REFERENCES

Albee, A.L., 1965, A petrogenetic grid for the Fe-Mg silicates of Pelitic schists; American Journal of Science, V. 263, p. 512-536.

Bence, A. E. and Albee, A. L., 1968, Empirical correction factors for the electron microanalysis of silicates and oxides; Journal of Geology, v. 76, p. 382-403.

Brown, W. R., 1958, Geology and mineral resources of the Lynchburg quadrangle, Virginia; Virginia Division of Mineral Resources Bulletin 74, 99p.

Brown, W. R. 1970, Investigations of the sedimentary record in the Piedmont and Blue Ridge of Virginia; in Fisher,G. W., Pettijohn, F.J., Reed, J. C., and Weaver, K. N. eds. Studies of Appalachian geology; Central and Southern: New York, Wiley Interscience, p. 335-349.

Conley, J. F., and W. S. Henika, 1973, Geology of the Snow Creek, Martinsville East, Price and Spray Quadrangles, Virginia, Report of Investigations Virginia Division Mineral Resources, no. 33, 71 pp.

Conley, J. F. , 1978, Geology of the Piedmont of Virginia, Interpretations and Problems; in contributions to Virginia Geology, Virginia Division of Mineral Resources, Publication 7, p. 115-149.

Espenshade, G. H., 1954, Geology and mineral Deposits of the James River-Roanoke River Manganese District, Virginia, U. S. Geological Survey Bulletin 1008, 155p.

Etheridge, A., Wall, V. J. and Vernon, R. H., 1983, The role of the fluid phase during regional metamorphism and deformation; Journal of Metamorphic Geology, v. 1, p. 205-226.

Evans, N. H., 1984, Latest Precambrian to Ordovician metamorphism and orogenesis in the Blue Ridge and western Piedmont, Virginia Appalachians; unpub. PhD dissertation, Virginia Polytechnic Institute and State University; p. 324.

Ferry, J. M., and Spear, F. S., 1978, Experimental Calibration of partitioning of Fe and Mg between biotite and garnet; Contributions of Mineralogy and Petrology, v. 66, p. 113-117.

Ganguly, J., 1972, Staurolite stability and related parageneses: theory, experiments and application; Journal of Petrology, V. 13, P. 335-365.

Ganguly, J. and Saxena, S. K., 1984, Mixing properties of aluminosilicate garnets: constraints from natural and experimental data, and applications to geothermobarometry; American Mineralogist, v. 69, p. 88-97.

Gates, A. E., 1981, Geology of the Western Boundary of the Charlotte Beolt at Brookneal, Virginia; M.S. thesis, Virginia Polytechnic Institute and State University, 88pp.

Gates, A. E., in prep, Transpressional Dome Formation in the Southwestern Virginia Piedmont;

Gates, A. E., Simpson C., and Glover L., III, 1986, Appalachian Carboniferous dextral strike-slip faults: an example from Brookneal, Virginia; Tectonics, vol. 5, no. 1, p. 119-133.

Glover, L., III, Speer, J. A., Russell, G. S. and Farrar, S. S., 1983, Ages of regional metamorphism and ductile deformation in the Central and Southern Appalachians; Lithos, V. 16, P. 223-245.

Graham, C. M. and Harte, B., 1985, Introduction: Conditions of Dalradian Metamorphism; Journal of the Geological Society, V. 142, Pt. 1, p. 1-5.

Harte, B. and Hudson, N. F. C., 1979; Pelite facies series and the temperatures and pressures of Dalradian metamorphism in E. Scotland; in the Caledonides of the British Isles - Reviewed, Geological Society of London, p. 323-337.

Henika, W. S., and P. A. Thayer, 1977, Geologic maps of the Blairs, Mount Herman Danville and Ringgold Quadrangles, Virginia; Virginia Division Mineral Resources Publication, no. 2, 45pp.

Hodges, K.V. and Spear, F. S., 1982, Geothermometry, geobarometry and the Al2SiO5 triple point at Mt. Moosilauke, New Hampshire; American Mineralogist, v. 67, p. 1118-1134.

Holdaway, M. J., 1971, Stability of andalusite and the aluminum silicate phase diagram; American Journal of Science, v. 271, p. 97-131.

Koons, P. O. and Thompson, A. B., 1985, Non-mafic rocks in the greenschist, blueschist and eclogite facies; Chemical Geology, v. 50,p. 3-30.

Kretz, R., 1983, Symbols for rock-forming minerals; American Mineralogist, v. 68, p. 277-279.

LeMaitre, R. W., 1981, GENMIX- A generalized petrological mixing model program; Computers and Geosciences, v. 7, p. 229-247.

Mohr, D. W., Barnett, R. L., and J. Michie, 1986, Chemical processes and migration of elements during retrogression of a staurolite-zone assemblage in western North Carolina; Contributions of Mineralogy and Petrology, v. 92, p. 400-411.

Newton, R. C. and Haselton, H. T., 1981, Thermodynamics of the garnet-plagioclase-Al2SiO5-Quartz geobarometer. In R.C. Newton, et al, Eds., Advances in Physical Geochemistry 1, p. 111-147, Springer-Verlag.

Odom, A. L., and G. S. Russell, 1975, The time of regional metamorphism of the Inner Piedmont, North Carolina and Smith River Allochthon: Inferences from whole-

rock ages; Geological Society of America Abstracts with Programs, vol. 7, no. 4, p. 522.

Orville, P. M., 1963, Alkali ion exchange between vapor and feldspar phases; American Journal of Science, v. 261, p. 201-237.

Pigage, K. C. and Greenwood, H. J., 1983; Internally consistant estimates of pressure and temperature: the staurolite problem; American Journal of Science, v. 283, p. 943-969.

Redden, J. A. 1963, Stratigraphy and metamorphism of the Altavista Area; in Geological Excursions in Southwestern Virginia; Eds. R. V. Dietrich; Virginia Polytechnic Institute Engineering Extension Service, Geology Guidebook No. 2, p77-99.

Richardson, A. W., Gilbert, M. C. and Bell, P. M., 1969, Experimental determination of kyanite-andalusite-sillimanite equilibria; the aluminum silicate triple point; American Journal of Science, v. 267, p. 259-272.

Rucklidge, J.C., 1971, Specifications of FORTRAN program SUPERRECAL; Deptartment of Geology, University of Toronto, Toronto, Ont.

Schreyer, W. and Seifert, F., 1969, Compatibility relations of the aluminum silicates in the systems MgO-Al2O3-SiO2-H_2O and K2O-MgO-Sl2O3-SiO2-H_2O at high pressures; American Journal of Science, V. 267, p. 371-388.

Selverstone, J., 1985, Petrologic constraints on Imbrication, Metamorphism and uplift in the SW Tauern Window, Eastern Alps; Tectonics, v. 4, no. 7,p. 687-704.

Solberg, T. N. and Speer, J. A., 1982, QALL, a 16-element analytical scheme for efficient petrologic work on an automated ARL-SEMQ: Application to mica reference samples; Microbeam Analysis - 1982, p. 422-426.

Spear, F. S., and Selverstone, J. 1983, Quantitative P-T paths from zoned minerals: Theory and Tectonic applications; Contributions of Mineralogy and Petrology, v. 83, p. 348-357.

Spear, F. S., Selverstone, J., Hickmott, Crowley, P. and Hodges, K. V., 1984, P-T paths from garnet zoning: A new technique for deciphering tectonic processes in crystalline terranes; Geology, v. 12, p. 87-90.

Thompson, A. B., 1976, Mineral reactions in pelitic rocks: I prediction of P-T-X (Fe-Mg) phase relations; American Journal of Science, v. 276, p. 401-424.

Thompson, J. B., Jr., 1957, The graphical analysis of mineral assemblages in pelitic schists; American Mineralogist, v. 42, p. 842-858.

Wehr, F. and Glover, L. III, 1985, Stratigraphy and Tectonics of the Virginia-North Carolina Blue Ridge: Evolution of a late Proterozoic- early Paleozoic hinge zone; Geological Society of America Bulletin, v. 96, p. 285-295.

Williams, H., Tectonic lithofacies map of the Appalachian orogen, Map 1, Memorial University of Newfoundland, St. Johns, 1978.

Wintsch, R. P., 1975, Solid-fluid equilibria in the system KAlSi3O8-NaAlSi3O8-Al2SiO5-SiO2-H_2O-HCl; Journal of Petrology, v. 16, p. 51-79.

Yardley, B. W. D. and Baktatzis, E., 1985, Retrogression of staurolite schists and the sources of infiltrating fluids during metamorphism; Contributions of Mineralogy and Petrology, v. 89, p. 59-68.

THE SMITH RIVER ALLOCHTHON: GEOLOGY AND REGIONAL CONTEXT

A. E. Gates and L. Glover III

ABSTRACT

Previous workers have proposed that the Smith River Allochthon is a large rootless thrust sheet in the Southwesten Virginia Piedmont that contains a Grenville age stratigraphy unrelated to the rest of the Southern Appalachians. The Ridgeway-Chatham Fault to the east and Bowens Creek Fault to the west of the allochthon were proposed to merge at depth and represent the basal decollement upon which the allochthon moved. Mapping in the Altavista area however, has established a stratigraphy common to both the Smith River allochthon type area and the western Virginia Piedmont and Blue Ridge. The Early Paleozoic, metasedimentary Evington Group is correlated with the Fork Mountain Formation of the Smith River Allochthon and the Late Precambrian, metasedimentary Lynchburg and metavolcanic Catoctin Formations are correlated with the lower and upper Basset Formation respectively. The Smith River allochthon therefore contains the same stratigraphy as the Blue Ridge upon which it was proposed to have been thrust.

The deformed terrane of the central and eastern Smith River Allochthon displays an inverted amphibolite grade metamorphism. The isoclinal folding and metamorphism result from nappe emplacement during the Taconic Orogeny. Most of the nappe however, has been eroded away. The upright stratigraphy and inverted metamorphism indicate that only the footwall of the nappe remains. The major movement on the Bowens Creek fault appears to have occurred during a ca. 350-300 Ma dextral transpressional

phase of deformation. The Bowens Creek Fault is proposed to be the northern extension of the Brevard Zone, which also exhibits late dextral transcurrent movement.

INTRODUCTION

The Smith River Allochthon comprises a large area in the southwest Virginia Piedmont and northwestern North Carolina Piedmont (Figure 37). On the basis of detailed mapping along the southern Virginia border (Figure 38) Conley and Henika (1970;1973) proposed that the terrane represented a westward thrusted rootless allochthon. The allochthon is bounded to the west by the Bowens Creek Fault which separates it from the Blue Ridge (Conley and Henika, 1970; 1973; Conley, 1979) and to the east by the Ridgeway-Chatham Fault which separates it from the Sauratown Mountains Anticlinorium (Conley and Towe 1968; Conley and Henika, 1973; Henika and Thayer, 1977) (Figure 38). The Sauratown Mountains are composed of Grenville basement overlain by Lynchburg Formation (Conley and Henika, 1973; Conley, 1979) which also, in part, comprise the Blue Ridge.

The Smith River Allochthon was considered to consist of rock units that are unrelatable to any others in the southern Appalachians. The Bassett Formation and overlying Fork Mountain Formation were proposed to be of Grenville age based on an erroneous 1020 Ma age on the Leatherwood Granite which intruded both units after the peak of metamorphism (Conley and Henika, 1973). The Bowens Creek Fault was therefore considered to be responsible for transporting the Grenville terrane of the allochthon onto the Late Precambrian to Early Paleozoic, Lynchburg Formation-Catoctin Formation-Evington Group sequence of the Blue Ridge (Conley and Henika, 1973).The Leatherwood Granite however was redated at 450 Ma (Rankin, 1975) and 462 Ma (Odom and Russell, 1975) using Rb/Sr whole rock methods and 511 Ma (E. Hund

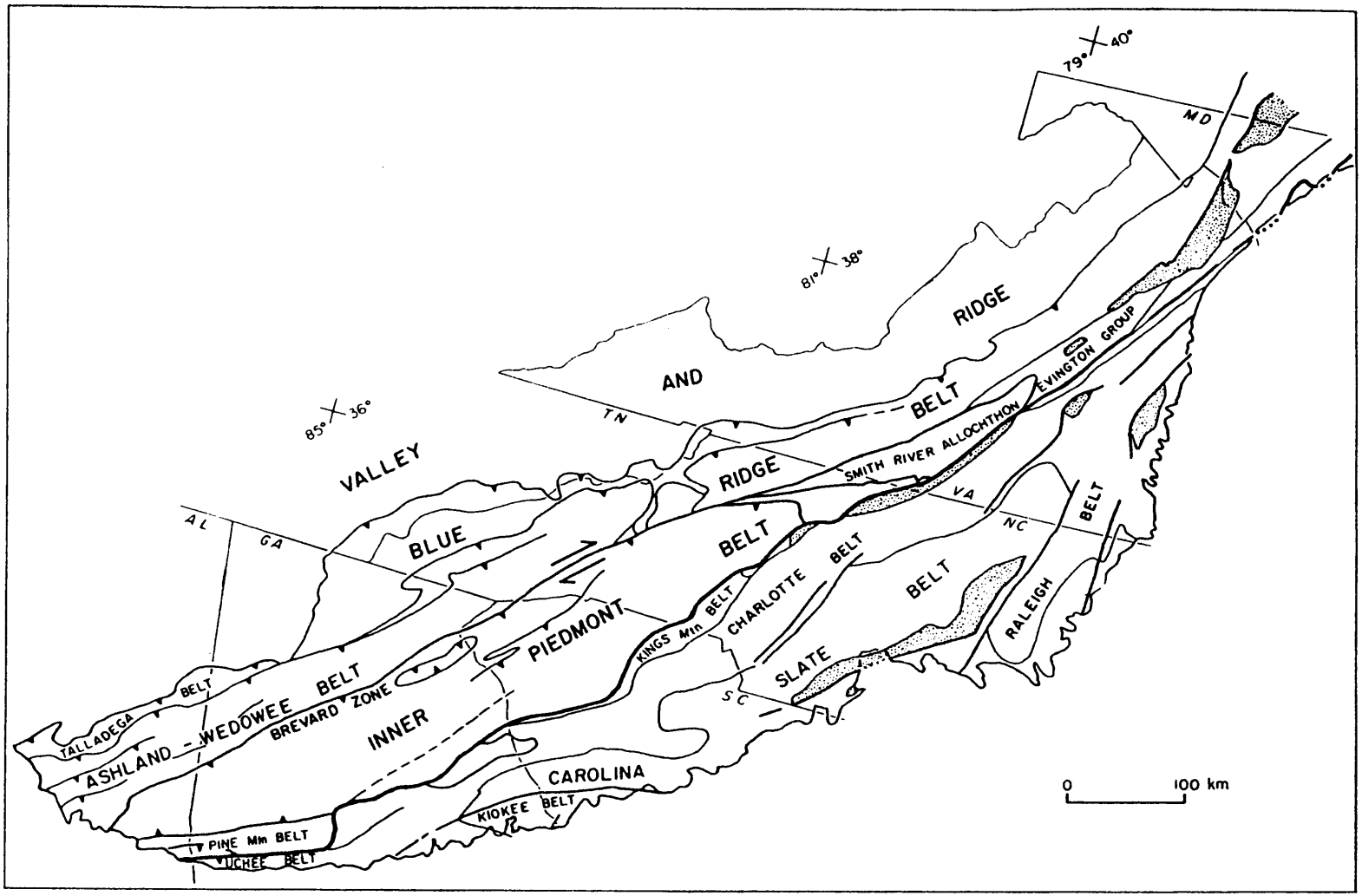

Figure 37. Tectonic map of the Southern Appalachians.

Figure 38. Geologic map of the Smith River Allochthon area, Southwest Virginia Piedmont (after Redden, 1963; Conley, 1978; 1981; Berquist, 1980; Marr, 1984; Gates et al., 1986).

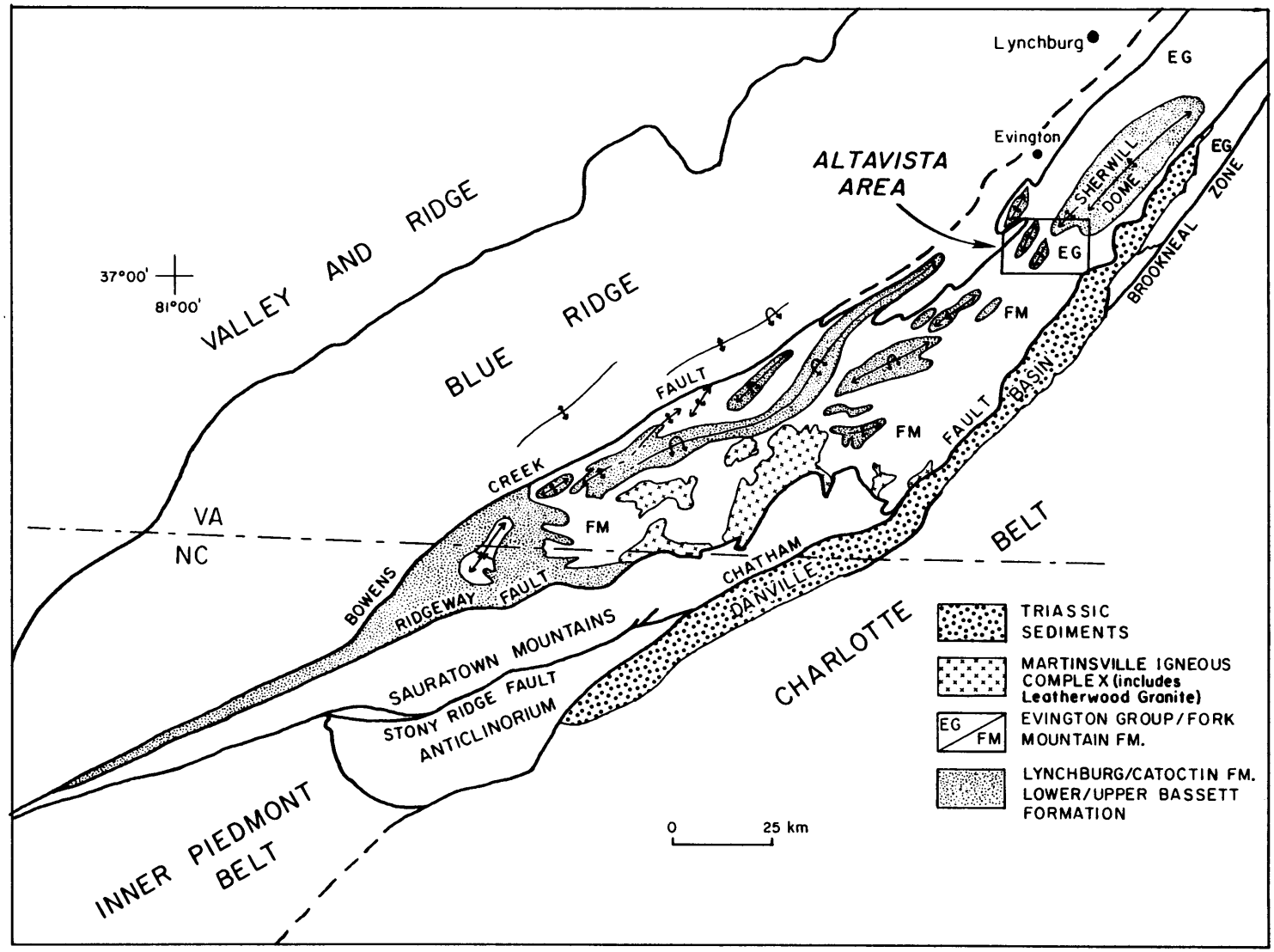
Lynchburg
EG
Evington
ALTAVISTA AREA
SHERWILL DOME
EG
EG
BROOKNEAL ZONE
37°00'
81°00'
VALLEY AND RIDGE
BLUE RIDGE
FM
FAULT
BASIN
FM
FAULT
CREEK
VA
NC
FM
BELT
BOWENS
RIDGEWAY FAULT
CHATHAM
DANVILLE
SAURATOWN MOUNTAINS
STONY RIDGE FAULT
ANTICLINORIUM
CHARLOTTE
INNER PIEDMONT BELT
0
25 km
TRIASSIC SEDIMENTS
MARTINSVILLE IGNEOUS COMPLEX (includes Leatherwood Granite)
EG
FM
EVINGTON GROUP/FORK MOUNTAIN FM.
LYNCHBURG/CATOCTIN FM.
LOWER/UPPER BASSETT FORMATION

and A. K. Sinha, personal communication, 1985) using U/Pb on zircon separates. This Paleozoic age casts doubt on the allochthon being a Grenville terrane but does not place constraints on its origin.

The central western Virginia Piedmont exhibits the same Lynchburg-Catoctin-Evington Group sequence as the entire eastern Blue Ridge of Virginia. The metasedimentary and metavolcanic units are of Late Precambrian to Early Paleozoic age and roughly correlatable to the rocks of the western Blue Ridge and lower Valley and Ridge section (Brown, 1958; 1970; Rankin, 1975; Evans, 1984; Wehr and Glover, 1985). The western Piedmont units were defined in Lynchburg and Evington, Virginia by Espenshade (1954) and Brown (1958) (Figure 38) and extended to the Altavista area through continuous field mappping. The northern extension of the proposed Smith River Allochthon of Conley (1979) however crosses that area (Figure 38). Through detailed mapping, stratigraphic, structural and metamorphic analysis of the Altavista area (Figure 38) which spans both the allochthon and part of the Blue Ridge to the west, this study attempts to place the Smith River Allochthon into the context of the western Virginia Piedmont and Southern Appalachians.

STRATIGRAPHY

The Altavista area is important in correlation of the stratigraphy of the western Piedmont and Blue Ridge with that of the Smith River Allochthon because it lies at the juncture of two well mapped areas. Altavista lies at the north end of an area of continuous detailed mapping (Redden, 1963; Price, et al. 1980; Berquist, 1980; Marr, 1984) that extends from the area in which the Smith River Allochthon was proposed (Conley and Towe, 1968; Conley and Henika, 1970; 1973). It also represents the southern end of a

large area of continuous mapping from the type local of both the Evington Group and the Lynchburg Formation units (Figure 38).

The Evington Group of Espenshade (1954) and Brown (1958) can be correlated with the Fork Mountain Formation of Conley and Henika (1970; 1973) because they are mapped directly into each other in Altavista (Figure 38) (Table 9). Along the western boundary of the Smith River Allochthon, anticlines and domes expose the Bassett Formation through the overlying Fork Mountain Formation. Similarly, the Lynchburg-Catoctin Formations are exposed in domes through the Evingtion Group both within and to the north of Altavista. The upper Bassett Formation is an amphibolite that contains preserved amygdules (Conley and Henika, 1973) and is reasonably correlated to the metavolcanic Catoctin Formation (Table 9). The Lower Bassett Formation is a biotite gneiss that is correlated to the metasedimentary Lynchburg Formation. The stratigraphy of the Smith River Allochthon is therefore the same as the Blue Ridge, Sauratown Mountain anticlinoruim and central western Virginia Piedmont.

The Altavista area (Figure 39) contains a typical stratigraphy for the Southwest Virginia Piedmont and eastern Blue Ridge. The domes in Altavista (Figure 39) are cored by Lynchburg and Catoctin Formation and surrounded by Evington Group lithologies. The rocks in the area are metamorphosed to at least upper greenschist facies and dominantly to upper amphibolite facies conditions. The metamorphism is assumed in the rock descriptions and lithologies are considered in terms of compositions and protoliths where demonstrable. Thicknesses given in the descriptions represent lithologic distribution and in most cases result from deformation. The estimated and measured thicknesses have no bearing on depositional thickness. Basic interpretations of the rocks in terms of protolith and environment of deposition follow each description.

TABLE 9: SMITH RIVER-ALTAVISTA AREA TIMING AND CORRELATION OF EVENTS

AGE	*SMITH RIVER AREA*	*ALTAVISTA*
350-300 Ma[1]	Retrogression on faults	M_2 Metamorphism
	Emplacement of allochthon on Ridgeway-Bowens Creek decollement	D_3 and D_4 dextral transpression and dome formation
440 Ma[2]	Regional cooling to 300°C	
462 Ma (Rb/Sr)[2] 511 Ma (U/Pb)[3]	Leatherwood Granite and contact metamorphism	
	Greenschist retrogression	M_1 Retrogression
Taconic[4]	Regional amphibolite metamorphism	M_1 Metamorphism and D_1, D_2 deformation and nappe emplacement
Ordovician(?)-Cambrian[5]	Fork Mountain Formation deposition	Evington Group deposition
Late Precambrian[6]	Upper Bassett Formation volcanism	Catoctin Formation volcanism
	Lower Bassett Formation deposition	Lynchburg Formation deposition
	Initiation of rifting	
	unconformity	

[1] Conley (1979) and Mose (pers. comm., 1986); [2] Odom and Russell (1975); [3] Hund and Sinha (pers. comm., 1985); [4] Glover et al (1983); [5] Brown (1970) and Evans (1984); [6] Brown (1970), Rankin (1975) and Wehr and Glover (1985).

Figure 39. Geologic Map of the Altavista Area.

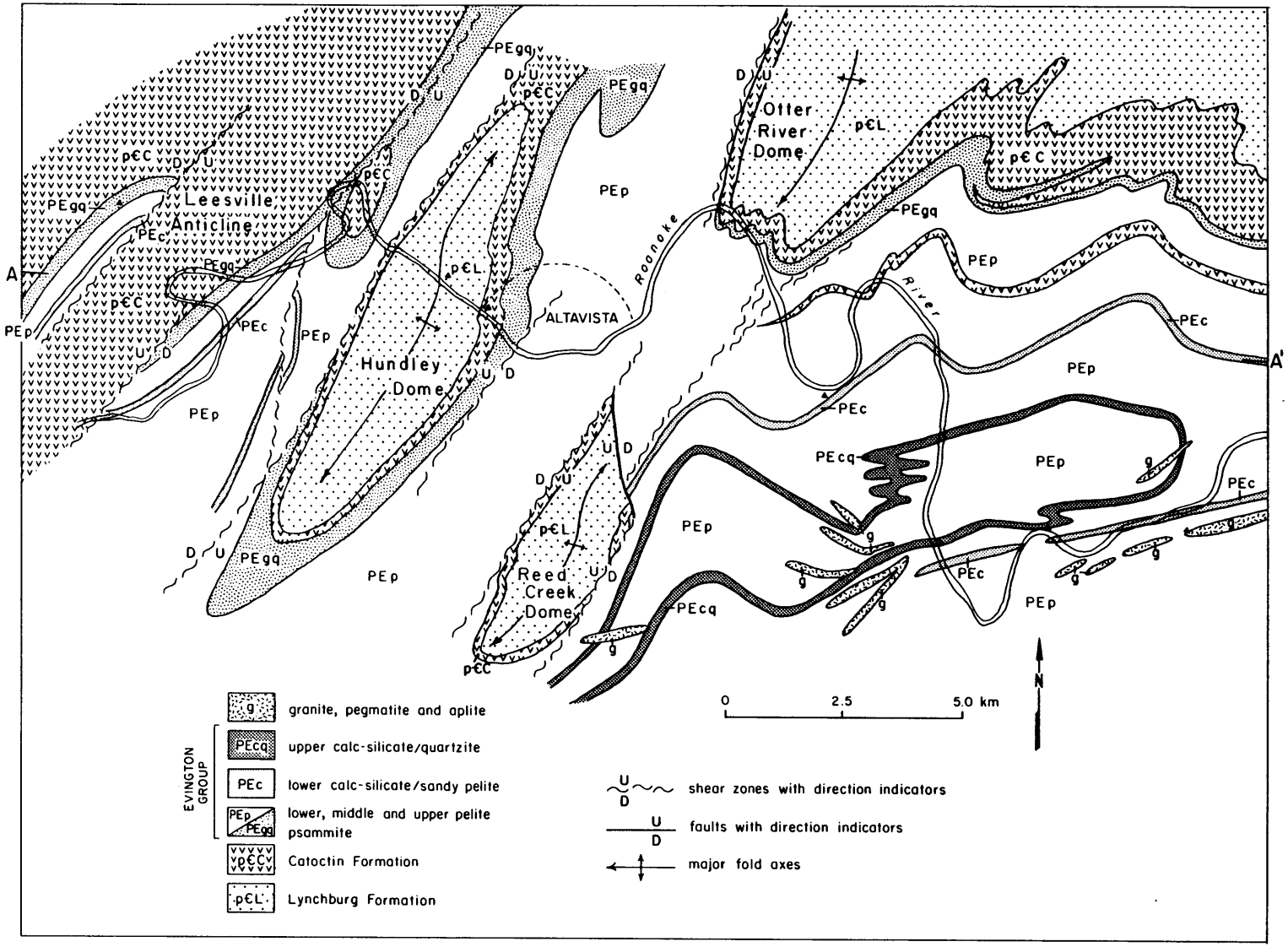
Leesville Anticline
Hundley Dome
Reed Creek Dome
Otter River Dome
ALTAVISTA
Roanoke River
A
A'
PEp
PEgq
PEc
PEcq
pCC
pCL
g
granite, pegmatite and aplite
upper calc-silicate/quartzite
lower calc-silicate/sandy pelite
lower, middle and upper pelite psammite
Catoctin Formation
Lynchburg Formation
EVINGTON GROUP
shear zones with direction indicators
faults with direction indicators
major fold axes
0
2.5
5.0 km
N

LYNCHBURG GROUP

The oldest unit exposed in the Altavista area is the Lynchburg Group (Figure 40) of late Precambrian age and whose type section is 50 km to the north (Brown, 1958; 1970; Espenshade, 1954). In Altavista, the Lynchburg Group is composed of very coarse- to medium-grained, terrigenous clastic sediments. The lowest portion of the Lynchburg exposed, occurs in the core of the Hundley dome. The coarse- to very coarse-, feldspathic to arkosic pebble conglomerate beds are discontinous, truncate the underlying strata and have abrupt basal contacts (Figure 41) (Appendix A). The 0.5 to 2 m thick conglomerate beds grade upward into coarse feldspathic sandstone. The very poorly sorted conglomerate contains quartz, blue quartz, and K-spar grains and granite and rip-up clasts of medium- to coarse-grained sandstone. The enclosing poorly to moderately well sorted feldspathic sandstone matrix contains metamorphic biotite and muscovite and is well foliated.

The upper portion of the Lynchburg Group is thinly to thickly layered, medium- to coarse-grained, feldspathic to quartz wacke with rare sedimentary structures. The moderately well to poorly sorted sandstone contains detrital quartz, rutilated quartz K-spar, zircon and plagioclase and metamorphic biotite and muscovite. In the upper portion there is a calc-silicate layer that consists of randomly oriented to slightly aligned diopside, K-spar, plagioclase, quartz and minor amphibole, epidote, titanite and apatite (Appendix A). The contacts with the sandstone were not observed. The top 50 m of the Lynchburg Group is composed of medium- to locally fine-grained graywacke to siltstone with upward fining beds from several centimeters to 0.5 m thick. The massive, medium-grained sandstone contains sections with thin micaceous laminations with 20 cm to 0.5 m spacing. The upper contact is abrupt in most areas but locally the sandstone is thinly interlayered with amphibolites of the Catoctin Formation.

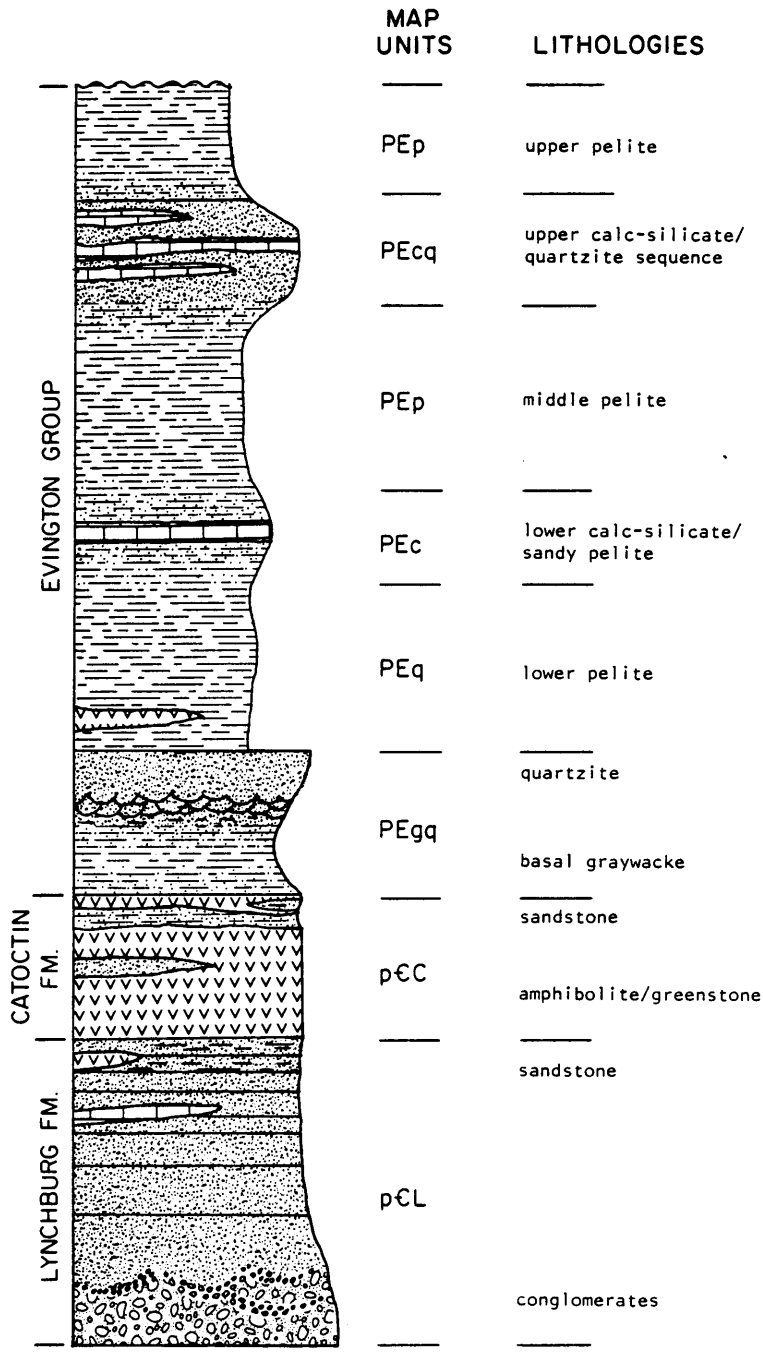

Figure 40. Stratigraphic Column for the Altavista area. Grainsize for upper Evington Group is interpretive because rock has undergone metamorphic recrystallization. Shales are schists to gneisses. Sandy sections contain more quartz and less aluminosilicates. Map symbols correspond to Figure 39, lithologies are described in text.

Figure 41. Conglomeratic channel deposit in lower Lynchburg Formation. Scale bar = 10 cm.

Figure 42. Trough cross-beds in upper graywacke/lower quartzite unit in lower Evington Group. Scale bar = 10 cm.

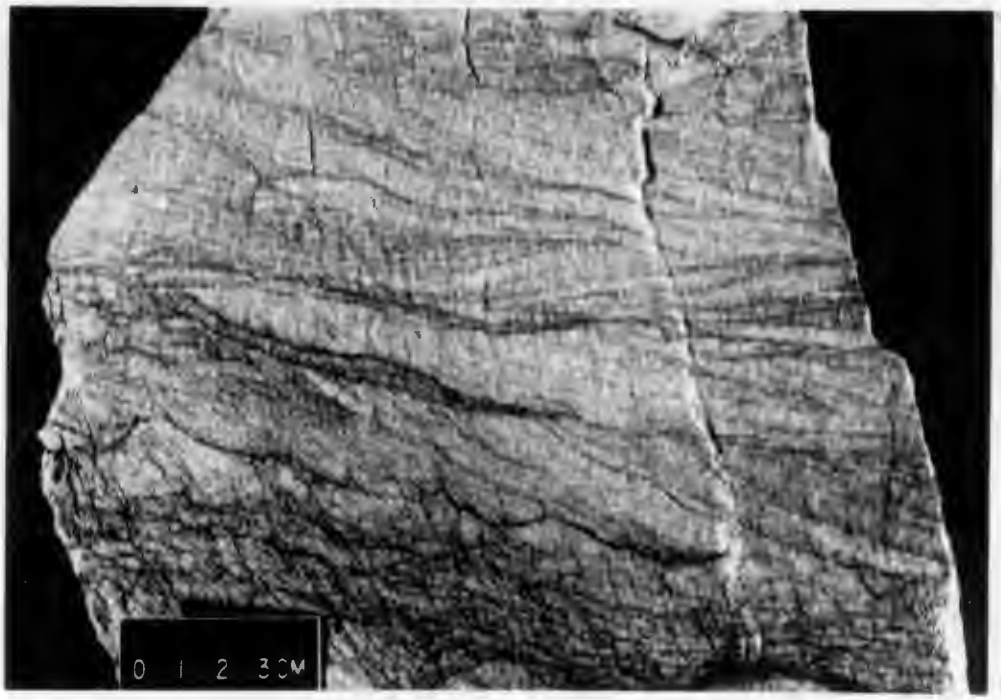
0 1 2 3CM

The thickness of the Lynchburg Group in the Altavista area cannot be accurately estimated because the lower contact is not observed.

Interpretation

The sandstones and conglomerates of the Lynchburg Group have been interpreted to be a rift basin fill, formed in the opening of the Iapetus Ocean basin (Brown, 1970; Rankin, 1975; Wehr and Glover, 1985). The lower discontinuous conglomerate beds in the Altavista area are channel deposits and indicate a very high energy environment. Wehr and Glover (1985) have shown that the coarse feldspathic wackes of the Lynchburg Formation are of deep water origin in central Virginia, in a basin that deepens to the south. They have also documented three separate fining upward sequences, an upper, middle and a lower formation. In Altavista, only one fining upward sequence is observable. Either only the upper Lynchburg is exposed or because the sediments exposed in Altavista may have filled a smaller separate basin from the main rift, there may have only been one fining up sequence developed. In the latter case, the coarse terrigenous clastics may rest unconformably on Grenville basement.

CATOCTIN FORMATION

Conformably overlying the Lynchburg Group in Altavista is the metavolcanic Catoctin Formation of late Precambrian age (Espenshade, 1954; Reed, 1955; Brown, 1958) (Figure 40). The Catoctin Formation is a greenstone, chlorite-epidote-albite schist with preserved epidote filled amygdules in the westernmost field area (Appendix A). Through the rest of the area however, it is an amphibolite consisting of hornblende,

andesine, titanite, magnetite and quartz with biotite locally developed. The meta-mafic volcanic is massive in the lower section, but is interlayered with 1 to 3 m thick, discontinuous quartz arenite layers and lenses in the middle of the section. The sandstone layers contain more pelitic material, and are thicker and more common in the upper section of the Catoctin Formation (Appendix A). The upper sandstone layers are interbedded with meta tuff. Amygdules are more common in the middle to upper section.

The 1-5 m thick metatuff layers are plagioclase-biotite-quartz gneisses with minor amounts of epidote, titanite, K-spar, muscovite and amphibole (Appendix A). The upper sandstone units are 0.5 to 15 m thick and commonly boudinaged. They consist of 70 to 85% quartz with plagioclase, biotite, muscovite, magnetite, titanite and zircon. Compositional layering of 1 cm - 0.5 m in the thicker sections, is expressed in mica content and grain size. There are also boudinaged quartz-epidote layers of 5 cm to 0.5 m thickness. Around the level of the quartz-epidote layers are thin pegmatitic tonalite veins or metamorphic segregations. The veins are discontinuous and are rimmed by pure hornblende schist. Near and within the veins are large (2-5 cm) clots of magnetite with bornite weathering surfaces. There are also magnetite rich zones in the sandstone and tuff near the contact with amphibolite.

The Catoctin Formation is highly deformed on the southeast and northwest limbs of the domes which precludes accurate thickness estimates. The thickness generally appears to increase to the north and to the east and west relative to the central map area but is highly variable.

Interpretation

The Catoctin Formation is generally regarded as a rift-generated metabasalt (Reed, 1963; Brown,1970; Rankin, 1975; Brown and Blackburn, 1976) as is the upper Bassett

Formation (Conley, 1981). The lower Catoctin Formation is massive in nature and lacks interlayered sediments and amygdules. The fairly coarse discontinuous sandstone interbeds of the middle section lack pelitic material and suggest a relatively high energy environment. The presence of amygdules indicates that the fluid pressure in the melt exceeded the confining pressure. Moore (1965) suggests that the vesiculation only occurs in water depths of 500 m or less. In the upper section, the Catoctin sandstones contain more pelitic material, indicating lower energy conditions.

EVINGTON GROUP

The Altavista area was partly mapped by Espenshade (1954), who defined the stratigraphy of the Evington Group in terms of the formations and proposed a sequence, but suggested that it might be inverted. The stratigraphy includes the basal Candler phyllite (pelite), Joshua schist (graphitic/calcareous), Arch marble, Pelier schist (sandy pelite), Mount Athos quartzite, and the Slippery Creek greenstone (Brown, 1958). Redden (1963) remapped part of the Altavista area in terms of the Evington Group formations and proposed that the stratigraphic sequence was inverted. In this study the Evington Group is described in terms of lithology and not the formation names because detailed mapping between Altavista and the Evington Group type area is incomplete, precluding detailed correlation.

Basal Graywacke.

The lowest unit in the Evington Group is gradational from the upper sandstones of the Catoctin Formation (Figure 40). The amphibolite layers between the sandstone

units are thinner and less common in the upper Catoctin section. The contact with the graywacke is therefore gradational and may not be everywhere time equivalent. The thickness of the graywacke unit is variable from approximately 50 to 250 m.

The basal graywacke is a massive biotite schist with muscovite, epidote, plagioclase, magnetite, zircon and K-spar and small wispy greenstone or amphibolite pods. In the upper sections of the unit to the west, layers are weakly, but normally graded in 0.5 to 1.5 m thick cycles. At the top of the graywacke unit, the graded cycles are 20 to 50 cm thick, well defined and contain 2 to 3 cm thick sets of trough cross-bedding (Figure 42) (Appendix A). The deformation precludes the documentation of source direction. To the east, the graywacke grades into a pelitic siltstone to fine graywacke that lacks sedimentary structures.

Quartzite

Conformably overlying the graywacke in the western Altavista area (Figure 39) is a quartz arenite (quartzite) consisting of 98% quartz with minor muscovite, biotite, zircon, epidote and rutile. In the west, the quartzite is massive and up to 100 m thick. It is more commonly 3 to 10 m thick however and erratic in distribution though generally coarser and thicker to the north. The quartzite grades eastward into a biotite metasandstone that is slightly coarser than the underlying graywacke/pelite.

Lower Pelite.

Conformably overlying the quartzite in west Altavista and biotite metasandstone in eastern Altavista is a highly aluminous pelite (Figure 40). The pelite exhibits middle

to upper amphibolite facies assemblages of sil + grt + bt to the east and st + grt + bt to the north and west. The rocks also contain muscovite, plagioclase, quartz, ilmenite and zircon. In the westernmost area, the rock is a fine silver phyllite with muscovite, biotite, chlorite, quartz and plagioclase. Some sections in the pelite are sandy (more quartz rich). The sil + grt + bt schists to gneisses are locally retrograded to chl + cld schists that contain relicts of the early high grade assemblage. The cld + chl assemblage also includes muscovite, magnetite, tourmaline and/or kyanite, garnet and staurolite (Appendix A).

The schist/gneiss contains migmatites and is intruded by fine-grained two mica, garnet, tourmaline granite, aplite and pegmatite dikes along the southern map area (Figure 39) (Appendix A). The intrusives are monzogranites (Streckheisen, 1973 classification) with granitic texture. The mafic phases include muscovite, biotite, garnet, tourmaline, epidote, and sillimanite locally, all of which crystallized early in the history. The feldspars and quartz crystallized late and in no apparent order. The granites appear both texturally and compositionally to have been minimum temperature melts.

Lower Calc-silicate/sandy pelite.

The lower pelite, grades upward into a less aluminous, more quartz rich pelitic schist (metasiltstone to sandstone) (Figure 40). To the west, above the sandy zone, normally graded, silty laminae are interlayered with graphitic pelite and graphitic calcareous schist (Appendix A). The silty to sandy layers consist of quartz, muscovite, chlorite and biotite. The graphitic layers are quartz, muscovite chlorite, biotite, graphite, magnetite, calcite and dolomite. To the east, the unit is a zoned calc-silcate to sandy pelite (Appendix A). The rocks are zoned in distinct bands dominated by micas, garnet, epidote, tremolite, and diopside-K-spar in the core. This indicates an original sequence

of laminated calcareous/pelitic lithologies. The pelite zone consists of sandy biotite schist.

The rocks enclosing the calc-silicate are sandier than those to the west. Fine grained sandstone is interlaminated to thinly interbedded with biotite schist. The schist contains garnet, muscovite and in the thicker sections, staurolite and sillimanite. Deformation has rendered graded bedding unreliable to unidentifiable. No cross bedding was recognized in this section. The thickness of the calc-silicate is difficult to determine but is approximately 5 to 15 m. The enclosing siltstone to sandstone is 40 to 80 m and thicker to the east.

Middle pelite.

The upper contact of the lower calc-silicate/sandy pelite is gradational into a pelitic schist to gneiss that is indistinquishable from the lower pelite (Figure 40). The middle pelite appears thicker than the lower section but again, deformation precludes even a rough estimate.

Upper Calcsilicate/Quartzite Sequence.

The middle pelite is sandy in its upper section and is gradational into a biotite schist sandstone (Figure 40). The biotite sandstone is sparsely interlayered with calc-silicate schist of amphibole, epidote, plagioclase, apatite and quartz. The sandstone also grades into a calcareous sandstone (quartzite) (Appendix A) of 70 to 75% quartz with amphibole, clinozoisite, epidote, garnet, plagioclase and minor mica. The associated quartzite is thick (100 m) in some areas but irregular and locally not developed. In un-

certain relation with the quartzite but apparently better developed where the quartzite is thinner, is a highly contorted calc-silicate schist/marble (Appendix A). In the most calcareous sections, the rock consists of 45 to 60% calcite and dolomite with thin spaced laminations of amphibole-diopside schist. In most areas however, it resembles the other zoned calc-silicate units with thinly zoned pelite to calc-silicate layers. The sandstone sequence is present on top of the calc-silicate as well.

The thickness of the calc-silicate/marble is highly variable. In most areas it is 10 to 15 m thick but at structural culminations in the eastern map area, it appears to be several hundred meters. The complicating factor in estimating thickness is the extremely complex folding (Figure 43). The thick sections in the culminations and thin sections on the limbs are likely the result of deformation rather than sedimentation. The thickness of the sandstone/calc-silicate sequence also appears variable but averages 75 to 200 m.

Upper Pelite.

The uppermost unit exposed in Altavista is also a pelitic schist to gneiss unit (Figure 40). The rock is indistinquishable from the other pelitic units though only a small amount is exposed.

Interpretation

The Evington Group has been proposed to be a deeper water equivalent of the Early Paleozoic Valley and Ridge shelf deposits (Brown, 1958; 1970; Evans, 1984). The Evingtion Group in Altavista is basically a pelitic sequence with sporadic occurrences

Figure 43. Disharmonic folds in upper calc-silicate unit of Evington Group. Marble layers weather out. Scale bar = 10 cm.

Figure 44. F_2 folds in conglomeratic layer in lower Lynchburg Formation. Folds "point" to higher competency layer. S_2 foliation fans but is dominantly axial planar. Scale bar = 10 cm.


S2

of sandstone and carbonate bearing lithologies. The basal graywacke unit contains graded beds and trough crossbeds and is finer grained and more pelitic than those in the middle of the Catoctin Formation. This graywacke unit is probably a fairly deep water unit, possibly even a turbidite deposit.

The overlying quartzite is coarse and clean and indicates high energy conditions, possibly also deposited as a turbidite. The lower pelite unit directly overlying the quartzite represents a drastic change in energy conditions. The protolith of the unit was apparently a highly aluminous mud on the basis of the metamorphic mineralogy. The source of coarse clastics was apparently cut off from the basin and muds were deposited under low energy conditions.

Slightly coarser material succeeds the mud in a highly graphitic-carbonate rich unit with thin silty laminae (calc-silicate/sandy pelite). The siltstones to fine sandstones are normally graded and appear to be very distal turbidite deposits. This unit probably represents the building out of the shelf into a starved basin dominated by carbonaceous mud. The calcareous material probably was eroded off of the carbonate shelf to the west because carbonate was not formed in deep water environments during the early Paleozoic (Read, 1985). Massive black carbonaceous mud in front of a carbonate shelf is a common association (Wilson, 1969) which may be the case in Altavista. The calc-silicate is overlain by the middle pelite which signals the return to more quiet water conditions. The thick shale (pelite) sequence is again interrupted by a sand/carbonate section. The upper carbonate is clearly better developed than the lower but generally appears to be of deep water origin. The thin carbonate layers are 2-3 cm thick with a smaller pelite component than the lower unit. The sandstone is composed of clear quartz with interstitial calcareous material.

STRUCTURE AND METAMORPHISM.

The Smith River allochthon is proposed to be a large sheet of amphibolite facies metamorphic rocks that was thrust over greenschist facies rocks of the Blue Ridge on a major decollement (Conley and Henika, 1970; 1973; Conley, 1979). Conley and Henika (1970; 1973) proposed that an early regional amphibolite grade metamorphism produced a staurolite-sillimanite assemblage in the Bassett and Fork Mountain Formations (Table 9). The rocks were then retrograded to greenschist facies conditions prior to the intrusion of the Martinsville Igneous complex (Table 9) (Figure 38). The igneous intrusions include the Late Cambrian or Middle Ordovician Leatherwood Granite (Rankin, 1975; Odom and Russell, 1975; E. Hund, personal communication, 1985) and the associated Rich Acres gabbro, norite and diorite (Conley and Henika, 1973). There was also a late phase of retrogression during the emplacement of the Smith River Allochthon (Conley and Henika, 1973; Conley, 1979) (Table 9).

A rigorous structural history has not been proposed for the Smith River Allochthon though several fold generations and major faults have been identified (Conley and Henika, 1970; 1973; Price et al., 1980; Berquist, 1980; Marr, 1984). Folding is proposed to have accompanied the regional amphibolite facies metamorphism (Conley and Henika, 1973) but the major deformation is associated with emplacement of the allochthon (Conley and Henika, 1970; 1973; Conley, 1979). The basal decollement on which thrusting of the allochthon is proposed to have occurred, is exposed on the western edge of the allochthon as the Bowens Creek Fault and on the east as the Ridgeway-Chatham Fault (Table 9, Figure 38). The movement on the decollement is proposed to have occurred between 356 and 300 Ma through Rb/Sr dating of sheared pegmatites on the Ridgeway fault and correltation of the Bowens Creek Fault with the Brevard Zone to the south (Conley, 1979) (Figure 37). The correlation of the stratigraphy across the Bowens Creek Fault however indicates that the fault did not

necessarily experience large scale movement. Minimum displacement on the Bowens Creek Fault according to the map and interpretation of Conley (1979) is approximately 35 km in the Smith River area (Figure 38).

The continuous detailed mapping from the type area of the Smith River Allochthon (Redden, 1963; Price et al., 1980; Berquist, 1980; Marr, 1984) (Figure 38) suggests that the Altavista area exhibits the same metamorphic and deformational features as the rest of the allochthon. Detailed analysis of the metamorphism and structural elements indicates that the Altavista area underwent four deformational events and two associated metamorphic events. The D_1 and D_2 events are closely related in time and space and related to the M_1 metamorphism (Table 9). The D_3 and D_4 events are also both spatially and temporally related and are spanned by the M_2 metamorphism (Table 9).

D_1

The elements of the D_1 event are largely overprinted and transposed by D_2 structural elements. The large recumbent isoclinal fold in the southeast Altavista map area (Figure 39) may be an F_1 structure because it appears to be folded by a nearly coaxial structure unrelated to D_3 and D_4. The shape however, may have been modified by F_2 folding which is isoclinal. The main evidence of F_1 and S_1 are isoclinally folded gneissic quartz segregations in the S_2 pervasive foliation. There are also rootless isoclines with preserved foliation in the hinge regions, oblique to S_2 (Appendix A). Cores of garnet and staurolite porphyroblasts contain aligned quartz and opaque inclusions that are oblique to the enclosing pervasive foliation. Some garnets exhibit helictic trails of inclusions which indicates that they have rotated.

D_2

The D_2 event imposed the strongest deformation on the Altavista area. The D_2 structures appear to increase in intensity towards the eastern portion of the map area (Figure 39). F_2 is characterized by isoclinal and recumbent folding that is best displayed in the pelitic gneisses and calc-silicate rocks (Figure 43) of the Evington Group. Small F_2 folds are also displayed in conglomeratic beds in the lower Lynchburg Group (Figure 44). Map scale folds are also isoclinal and apparently nearly coaxial to F_1 folds. The large recumbent isoclinal fold defined by the upper calc-silicate unit in the southeastern map area (Figure 39) is refolded by smaller isoclinal folds. Earlier structures may have also been tightened during this event.

The strongest structural element in the D_2 event is the S_2 pervasive foliation. S_2 is the best developed foliation in the Altavista area. It is defined by all micaceous and platy minerals in both the high grade an lower grade rocks. S_2 is axial planar to the F_2 structures and has transposed the S_1 foliation and minor F_1 structures into parallelism with it. The S_2 foliation is nearly parallel to the preserved bedding in the Lynchburg Group and sandy Evington Group rocks. This suggests that the S_2 foliation was horizontal prior to the passive rotation of the eastern area during Sherwill Dome formation (D_3 and D_4). To the south, away from the Sherwill dome and in the center of the Smith River Allochthon area, the S_2 foliation is sub-horizontal (Conley and Henika, 1973). Stereographic projections of poles to S_2 from rocks to the east of the Reed Creek and Otter River domes yields a tight concentration of points showing the 25 - 40° rotation to the south (Figure 45). The tightness of the concentration indicate that the S_2 is fairly uniform and parallel.

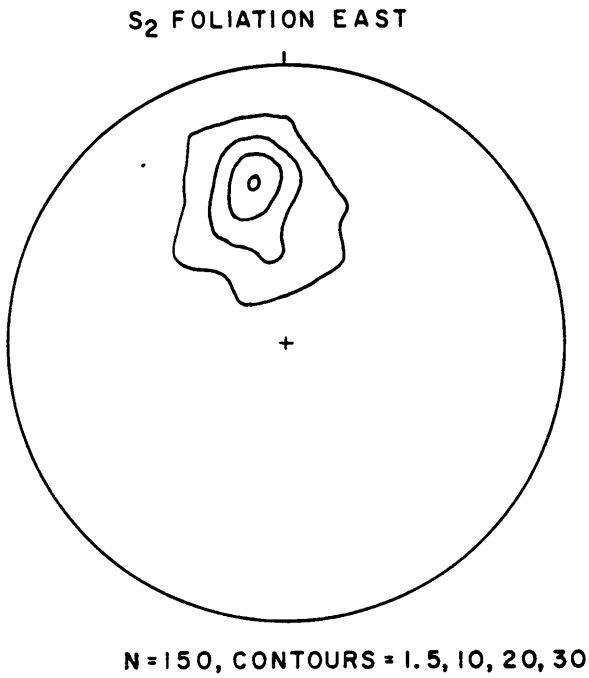

Figure 45. Stereographic Projection of poles to S_2 from eastern map area.

M_1

The M_1 metamorphism spans D_1 and D_2 showing a long and complex history. The M_1 peak metamorphism indicates a thermal gradient that decreased to the west and northwest (Gates and Speer, in prep.). The peak assemblage is bt + grt + sil and occurs in the southeastern map area (Appendix A). It is separated from the bt + grt + st assemblage to the nothwest and west by the sil-in, st-out isograd (Figure 38) (Gates and Speer, in prep) (Appendix A). Along the southern margin of the eastern map area, the pelitic gneisses are migmatitic and intruded by small garnet-tourmaline, two mica granite dikes (Figure 39) (Appendix A). The Catoctin Formation also shows the gradient in that it is an amphibolite through most of the Altavista area but is a greenstone in the westernmost portion. The greenstone, chl + ab + ep schist indicates greenschist facies conditions which is in contrast to the amphibolite facies conditions that prevailed throughout the rest of the field area (Figure 39). Garnet/biotite geothermometers also indicate an increase in temperature to the south and east (Gates and Speer, in prep).

Application of the grt + bt + pl + sil geobarometer (Newton and Haselton, 1981) to the rocks of appropriate assemblage indicates pressures of 5.5 to 6.2 kb at 615° C for peak metamorphic conditions (Gates and Speer, in prep). The same geobarometer applied to garnet and plagioclase cores, and assuming equilibrium of garnet cores with biotite, yields pressures of 6.3 to 6.6 kb at 585° C. The path of the P-T trajectory is therefore one of decreasing pressure and increasing temperature to peak conditions (Figure 46). Applying the data to the Gibbs-Duhem method (Figure 2 of Spear and Selverstone, 1983) yields a similar P-T trajectory (Gates and Speer, in prep.)

The S_1 foliation was apparently formed in the high pressure phase of metamorphism because the inclusions that are aligned oblique to S_2, correspond to the position in the zoned garnets where the geobarometer indicates higher pressure. The

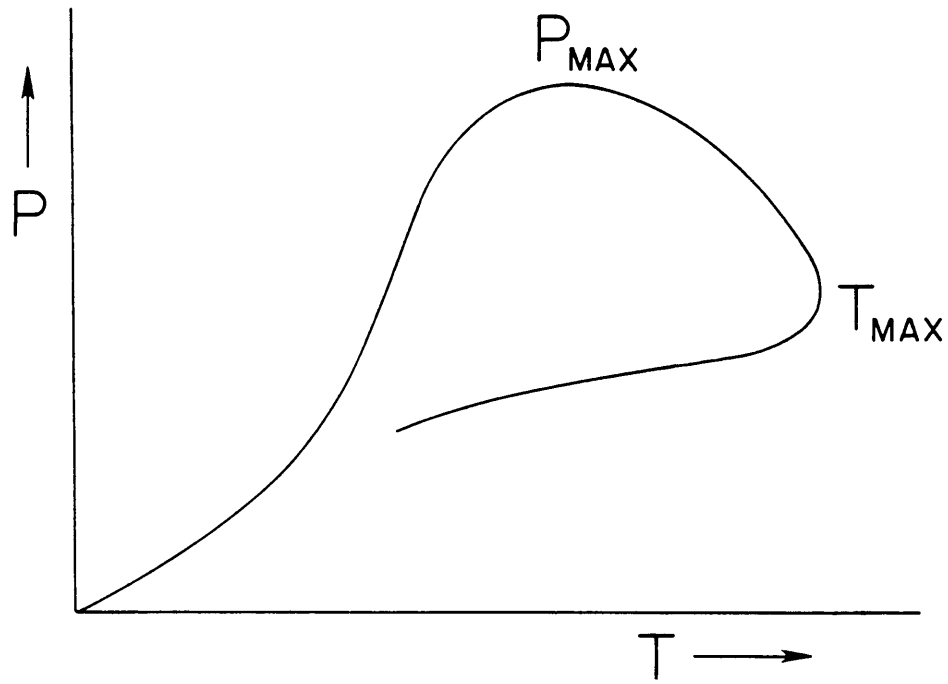

Figure 46. Schematic Pressure-Temperature loop for the Taconic Metamorphism in the Altavista area (from Gates and Speer, in prep).

high temperature, lower pressure garnet composition corresponds to S_2. The sillimanite and micas define the S_2 foliation in the high grade rocks.

The sil-prograde assemblages were retrograded through staurolite, chloritoid-staurolite, chloritoid-garnet, and chloritoid-kyanite assemblage conditions in discrete zones of hydration (Gates and Speer, in prep) (Appendix A). The retrogression was nearly isobaric and reasonably constrained by the position of the observed reactions in P-T space. Koons and Thompson (1985) assembled a P-T grid based on experimental data and projections that when applied to the rocks of the Altavista area indicates approximately 150° C of cooling in the retrogression. The st-retrograde rocks exhibit a strong S_2 foliation but the cld-bearing rocks are weakly foliatied to unfoliatied. Therefore, although the pressure was still high (5.0 to 6.0 kb by reactions) strain was minor during the later stages of the retrogression.

Interpretation

The inverted metamorphic gradient in an upright stratigraphy coupled with the geothermometry/geobarometry of zoned minerals indicates that the early D_1, D_2 and M_1 event reflects nappe emplacement (Table 9). The pressure-temperature path for the M_1 metamorphism (Figure 46) which shows regional metamorphism followed by a rapid pressure increase and later temperature increase before retrogression, is characteristic of a terrane onto which a nappe was emplaced (Spear et al., 1984). The exposed Altavista area is therefore the footwall of a nappe which explains the inverted gradient in upright rocks. The D_1 and D_2 deformational features increase in intensity towards the eastern map area (Figure 39) or the root zone of the nappe. The recumbent isoclinal folds (now reclined) and rootless isoclines in the gneisses indicate the kind of intense deformation associated with nappe emplacement.

D_3, D_4 and M_2

The D_3 and D_4 deformational and M_2 metamorphic events clearly postdate the D_1, D_2, and M_1 events (Table 9). The D_3 and D_4 events formed the domal structures and reverse faults (Figure 39). They also formed multiple crenulation (S_3 and S_4) and dextral shear cleavages that are well developed in Evington Group pelites on the limbs of the domes (Appendix A). The limbs of the domes also exhibit high angle, ductile reverse faults in which S_3 and S_4 cleavages are well developed and the lower Evington Group units are tectonically thinned.

D_3 and D_4 are apparently closely related in time and space and spanned by the M_2 greenschist facies retrogression. The M_2 minerals are best developed on the sheared limbs of the domes where there is intense cleavage development. In these areas, aligned chlorite and muscovite replace the M_1 minerals (especially cld, bt, grt and st).

Interpretation

The D_3, D_4 and M_2 events appear to be intimately related both in time and space. Because the effects are more intense in discrete zones that are concentrated and better developed in the western map area (Figure 39) where Conley (1979) has projected an extension of the Bowens Creek Fault, the event appears fault related. The dextral shear bands coupled with analysis of folding and crenulation cleavages, suggest that the the event reflects dextral transpression (Gates, in prep.). The domes are interpreted to be "positive flower" structures (Gates, in prep.). F_3 structures were formed with a north-

south orientation and then were apparently partially rotated in the transcurrent shearing. The F_4 structures trend northeast and have refolded the F_3 structures. The F_3 folds form the saddles in the northeast oriented F_4 structures (Figure 39) (Gates, in prep).

REGIONAL CORRELATION OF MAJOR STRUCTURES

The Bowens Creek Fault has been mapped by Marr (1984) into an area south of Altavista that was determined to be unfaulted by Redden (1963) (Figure 38). There are both reverse and strike-slip faults along the western side of the Altavista area into which the Bowens Creek Fault may extend (Figure 39). Because the Fork Mountain-Basset sequence correlates to the Evington Group-Catoctin-Lynchburg sequence however, the Bowens Creek Fault does not separate units of greatly varying age or grade. The Bowens Creek Fault to the south separates rocks exhibiting conditions of greenschist facies from those exhibiting amphibolite facies metamorphism. The change in metamorphic grade in Altavista however is continuous across the area and decreases to the west. Gates (in prep) suggests that the Bowens Creek Fault and associated domes formed in a late dextral transpressional event. The correlation of the Bowens Creek Fault with the Brevard Zone to the south (Figure 37) (Rankin et al.., 1972; Espenshade et al.., 1975; Rankin, 1975; Conley, 1979), further supports late dextral transcurrent movement because Bobyarchick (1984) has shown that late movement on the Brevard Zone is dextral in North Carolina.

Rb/Sr mineral and whole rock dating in the western Smith River Allochthon (Fullagar and Dietrich, 1976; D. Mose, personal communication, 1986) yield ages of approximately 360 to 275 Ma or Late Devonian to Carboniferous (Table 9). This age range correlates well with the 356 to 300 Ma age of movement on the northern Brevard Zone and proposed age of movement on the Bowens Creek Fault (Conley, 1979) (Table

9). Rb/Sr biotite-whole rock dating within the Smith River allochthon in the Fork Mountain gneiss yields ages of 440 ± 20 Ma (Odom and Russell, 1975) (Table 9). These are interpreted to be cooling ages of Taconic metamorphism (Glover et al., 1983) and apparently related to the M_1 metamorphism, D_1 and D_2 deformational events and nappe emplacement (Table 9). The transpressional event is related to D_3 and D_4 deformations which clearly post-date D_1, D_2 and the concurrent high grade metamorphism. The high grade metamorphism is therefore unrelated to the major movement on the Bowens Creek Fault. The late D_3 and D_4 events appear to have been part of the Carboniferous dextral strike-slip event proposed by Gates et al.. (1986) and exemplified in the Brookneal area, 15 km to the east (Figure 38). The Bowens Creek-Brevard system was active during this event and may have experienced both reverse and dextral transcurrent motion during the Late Paleozoic.

TECTONIC EVOLUTION

The Altavista area in the northern Smith River Allochthon area contains a typical and apparently uninterrupted Late Precambrian to Early Paleozoic sequence for the western Virginia Piedmont and Blue Ridge. Late Precambrian rifting produced rift grabens into which the Lynchburg and equivalent lower Bassett Formations were deposited (Brown, 1970; Rankin, 1975; Wehr and Glover, 1985) (Table 9). The coarse, clastic rocks are composed of terrigenous detritus derived from a Grenville basement source and deposited as turbidites in deep basins (Wehr and Glover, 1985). Late in the event, the rift-generated basalts of the Catoctin and equivalent upper Bassett Formations were extruded (Reed, 1963; Brown, 1970; Rankin, 1975; Glover and Wehr, 1985) (Table 9). Discrimination plots of immobile trace elements support continental

extrusion for the lavas (Conley, 1981; Blackburn and Brown, 1976) (see Appendix B for detailed tectonic evolution).

Interlayered with and apparently conformably overlying the Catoctin/upper Bassett Formation is the Evington Group and equivalent Fork Mountain Formation. The lower Evington Group consists of fine- to coarse-grained clastic metasedimentary rocks that include the basal graywacke and quartzite sequence in Altavista and sandy biotite schist of the Fork Mountain Formation. The position of this unit above the Catoctin Formation suggests that it may be in part equivalent to the Chilhowee Group of the Valley and Ridge Province. The Chillhowee Group is middle Cambrian in age (Simpson and Sundberg, in review). Brown (1970) suggests that the Candler Formation of the lowermost Evington Group may be the deep water equivalent of the Chillhowee Group. The upper, pelite-calc-silicate section of the Evington Group probably formed during the late Cambrian to Cambro-Ordovician carbonate buildup on the Valley and Ridge shelf. Evans (1984) proposed a unit by unit correlation in this section of the Evington Group in Central Virginia.

The southwestern Virginia Piedmont underwent a major deformational/metamorphic event during the Ordovician. The event is attributed to the Taconic Orogeny (Gates, 1981; Gates and Glover, 1983; Glover et al., 1983) and is characterized by west directed fold and thrust nappe emplacement. The nappe emplacement is recorded in a two phase deformational event that exhibits recumbent isoclinal folding and a subhorizontal pervasive foliation. The major foliation is S_2 and defined by all platy and prismatic minerals. The accompanying metamorphism also suggests nappe emplacement. An inverted thermal gradient is suggested by a bt + grt + sil assemblage of upper amphibolite facies (approximately 650° C by geothermometry) grading structurally and stratigraphically lower to upper greenschist facies conditions (Gates and Speer, in prep). Geobaromatric applications to zoned minerals indicate a transition from higher pressures to higher temperatures and lower pres-

sures (Gates and Speer, in prep) reflecting nappe emplacement followed by thermal equilibration.

These Taconic nappes however, were eroded away, exposing the footwall through most of the Smith River Allochthon area. The footwall of the nappe is characterized by an upright stratigraphy and an inverted metamorphic gradient. If there is any remnant hanging wall, it lies on the east side of the area mapped as the Smith River Allochthon area. The western bounding Bowens Creek Fault may have had some Taconic movement but Gates (in prep) has found that most of the deformation is clearly post-Taconic and transpressive. The Bowens Creek Fault also does not separate units of greatly differing age and therefore as suggested by Rankin et al. (1973), reverse movement is relatively minor.

CONCLUSIONS

Detailed structural and metamorphic (Gates and Speer, in prep) studies in the Altavista area suggests that the metamorphism in the Smith River Allochthon is the result of nappe emplacment. The Smith River Allochthon however is not such a nappe and is no more allochthonous than the Blue Ridge anticlinorium to the west. The stratigraphy, which includes a Late Precambrian through early Paleozoic succession is the same on both sides of the western bounding Bowens Creek Fault and appears complete. The stratigraphy is recognizable throughout the western Virginia Piedmont and is generally correlatable throughout the Southern Appalachians (review in Wehr and Glover, 1985). The late deformation in the Smith River Allochthon area is not the result of nappe emplacement but rather late Paleozoic dextral transpression.

REFERENCES

Berquist, C. R., 1980, Sandy Level Quadrangle: Its Geology and Regional Interpretation, in Price, V. Jr., Thayer, P. A., and Ronson, W. A., eds., Geol. Inv. of the Pied. and Triassic Rocks, Cent. N. Ca. and Va.; Carolina Geol. Soc. Field Trip Guidebook, P. I-1 - I-10.

Bland, A. E. and Blackburn, W. H., 1980, Geochemical studies on the Greenstones of the Atlantic Seaboard Volcanic Province, South-Central Appalachians; in Wones, D. R., ed., The Caledonides in the U. S. A., IGCP project 27: Caledonide Orogen, Vir. Poly. Inst. and State Univ., mem. no. 2, p. 263-270.

Brown, W. R., 1958, Geology and mineral resources of the Lynchburg quadrangle, Virginia; Va. Div. of Min. Res. Bull. 74, 99p.

Brown, W. R. 1970, Investigations of the sedimentary record in the Piedmont and Blue Ridge of Virginia; *in* Fisher,G. W., Pettijohn, F.J., Reed, J. C., and Weaver, K. N. eds. Studies of Appalachian geology; Central and Southern: New York, Wiley Interscience, p. 335-349.

Blackburn, W. H., and Brown, W. R., 1976, Petrochemical evidence relating the Catoctin volcanic series to late Precambrian continental separation; Geol. Soc. Am. Abst. w. Progs., v. 8, p. 136-137.

Conley, J. F., 1978, Geology of the Piedmont of Virginia, Interpretations and Problems; *in* Contrib. to Vir. Geol., Vir. Div. Min. Res., Pub. 7, p. 115-149.

Conley, J. F., and Henika, W. S., 1970, Geology of the Philpott Reservoir quadrangle, Virginia; Vir. Div. Min. Res. Rept. Inv. 22, 46pp.

Conley, J. F., and Henika,W. S., 1973, Geology of the Snow Creek, Martinsville East, Price and Spray Quadrangles, Virginia, Rep. Invest. Va. Div. Min. Res., no. 33, 71 pp..

Conley, J. F., Marr, J. D., Jr. and Berquist, C. R., Jr., 1981, Stratigraphic relationships between rocks of the Blue Ridge Anticlinorium and the Smith River Allochthon in the Southwestern Virginia Piedmont; Vir. Div. Min. Res., 13 ann. Vir. Geol. Field Conf., 34pp.

Espenshade, G. H., 1954, Geology and mineral Deposits of the James River-Roanoke River Manganese District, Virginia, U. S. Geol. Surv. Bull. 1008, 155p.

Evans, N. H., 1984, Latest Precambrian to Ordovician metamorphism and orogenesis in the Blue Ridge and western Piedmont, Virginia Appalachians; unpub. PhD dissertation, Virginia Polytechnic Institute and State University; p. 324.

Fullagar, P. D. and Butler, J. R., 1980, Radiometric dating in the Sauratown Mountains Area, North Carolina, in Price, S. Jr., Thayer, P. A., and Ronson, W. A., eds., Geol. Inv. of the Pied. and Triassic Rocks, Cent. N. Ca. and Va.; Carolina Geol. Soc, Field Trip Guidebook,p. II.1 - II.10.

Fullagar, P. D. and Dietrich, R. V., 1976, Rb-Sr isotopic study of the Lynchburg and probable correlative formations of the Blue Ridge and western Piedmont of Virginia and North Carolina; Am. Jour. Sci., v. 276, p. 347-365.

Gates, A. E., 1981, Geology of the western boundary of the Charlotte belt at Brookneal, Va., M. S. thesis, Va. Polytech. Inst.Blacksburg.

Gates, A. E., in prep, Transpressional Dome Formation in the Southwest Virginia Piedmont;

Gates, A. E., in prep, Prograde and Retrograde meatamorphism in Response to Nappe Emplacement, Southwest Virginia Piedmont;

Gates, A. E., Simpson, C., and Glover, L.,III, 1986, Appalachian Carboniferous dextral strike-slip faults: an example from Brookneal, Virginia; Tectonics, v. 5, no. 1, p. 119-133.

Glover, L., III, Speer, J. A., Russell, G. S. and Farrar, S.S., 1983, Ages of regional metamorphism and ductile deformation in the central and southern Appalachians, Lithos, v. 16, p. 223-245.

Glover, L., III, Costain, J. K., Coruh, C., Evans, N. H., Bollinger, G. A., Farrar, S. S. and Sibol, M. S., in prep, Seismicity, seismic reflection studies, gravity and geology of the Central Virginia seismic zone: Part IV, Tectonic History and current seismicity;

Henika, W. S., 1971, Geology of the Bassett quadrangle, Virginia; Vir. Div. Min. Res. Rept. Inv. 26, 43pp.

Henika, W. S. and Thayer, P. A., 1977, Geologic Maps of the Blairs, Mount Hermon, Danville and Ringgold quadrangles, Virginia; Vir. Div. Min. Res., Pub 2., 45pp.

Koons, P. O. and Thompson, A. B., 1985, Non-mafic rocks in the greenschist, blueschist and eclogite facies; Chemical Geology, v. 50,p. 3-30.

Marr, J. D., Jr., 1984, Geologic Map of the Pittsville and Chatham quadrangles, Virginia; Vir. Div. Min. Res., Pub. 49.

Moore, J. G., 1965, Petrology of Deep-Sea Basalt near Hawaii; Am. Jour. Sci., v. 263, p. 40-52.

Newton, R. C. and Haselton, H. T., 1981, Thermodynamics of the garnet-plagioclase-Al2SiO5-Quartz geobarometer; *in* R.C. Newton, et al., eds., Advances in Physical Geochemistry 1, p. 111-147, Springer-Verlag.

Odom, A. L., and G. S. Russell, 1975, The time of regional metamorphism of the Inner Piedmont, North Carolina and Smith River Allochthon: Inferences from whole-rock ages; Geol. Soc. Am. Abstrs. w. Progs., v. 7 no. 4, p. 522.

Price, V., Conley, J. F., Piepul, R. G., Robinson, G. R., Thayer, P A. and Henika, W. S., 1980, Geology of the Whitmell and Brosville quadrangles, Virginia; Vir. Div Min. Res., pub. 21.

Rankin, D. W., 1975, The continental margin of eastern North America in the southern Appalachians: The opening and closing of the proto-Atlantic Ocean; Am. Jour. Sci., v. 275-A, p. 298-336.

Read, J. F., 1985, Carbonate Platform Facies Models; Am. Assoc. Pet. Geol. Bull. v. 69, no. 1 p. 1-21.

Redden, J. A. 1963, Stratigraphy and metamorphism of the Altavista Area; in Geological Excursions in Southwestern Virginia; Eds. R. V. Dietrich; Vir. Polytech. Inst. Eng. Ext. Ser., Geol. Guidebook No. 2, p77-99.

Reed, J. C., Jr., 1964, Chemistry of Greenstone of the Catoctin Formation in the Blue Ridge of Central Virginia; U. S. Geol. Surv. Prof. Paper, 501-C, P. C69-C73.

Selverstone, J., 1985, Petrologic constraints on Imbrication, Metamorphism and uplift in the SW Tauern Window, Eastern Alps; Tectonics, v. 4, no. 7,p. 687-704.

Simpson, E. L., and Eriksson, K. A., 1985, Paleoenvironmental constraints provided by paleowave reconstructions: Early Cambrian Chilhowee Group drift stage sedimentation in the Central Appalachians; Geol. Soc. Am. Abst. w. Progs., v. 17, p. 718.

Simpson, E. L., and Sundberg, F. A., in review, Early Cambrian age for syn-rift deposits of the Chillhowee Group of Southestern Virginia; Geology.

Streckheisen, A. L., 1973, Plutonic rocks: Classification and nomenclature Recommended by the IUGS Subcommission of the Systematics of Igneous Rocks; Geotimes, v. 18, no. 10, P. 26-31.

Spear, F. S., and Selverstone, J. 1983, Quantitative P-T paths from zoned minerals: Theory and Tectonic applications; Contrib. Min. Pet., v. 83, p. 348-357.

Spear, F. S., Selverstone, J., Hickmott, Crowley, P. and Hodges, K. V., 1984, P-T paths from garnet zoning: A new technique for deciphering tectonic processes in crystalline terranes; Geology, v. 12, p. 87-90.

Wehr, F. and Glover, L. III, 1985, Stratigraphy and Tectonics of the Virginia-North Carolina Blue Ridge: Evolution of a late Proterozoic- early Paleozoic hinge zone; Geol. Soc. Am. Bull., v. 96, p. 285-295.

Williams, H., Tectonic lithofacies map of the Appalachian orogen, Map 1, Mem. Univ. of Newfoundland, St. Johns, 1978.

Wilson, J. L., 1969, Microfacies and sedimentary structures in "deeper water" lime mudstones; *in* Friedman, G. M. ed., Depositional Environments in Carbonate Rocks: Soc. Econ. Paleo. Miner. Spec. Pub., no. 14, p. 4-19.

APPENDIX A

FIELD LOCATIONS

1) AG4-266 Outcrop on face of hill over Roanoke River, center of Hundley Dome. Channel conglomerate deposits in the lower Lynchburg Formation also includes; granite clasts, sandstone rip-up clasts, graded beds.

1A) AG4-266 (next to 1) F_2 folds of conglomerate bed in coarse sandstone, axial planar S_2 foliation. Pointed versus rounded hinges show competency contrast.

2) AG4-241 Outcrop beside power station, behind field, Leesville Anticline. Preserved epidote filled amygdules in Catoctin Formation amphibolites. S2 foliation strong.

3) AG4-259 Quarry face along River, east side of Hundley dome. Quartzite layers in Catoctin Formation amphibolite.

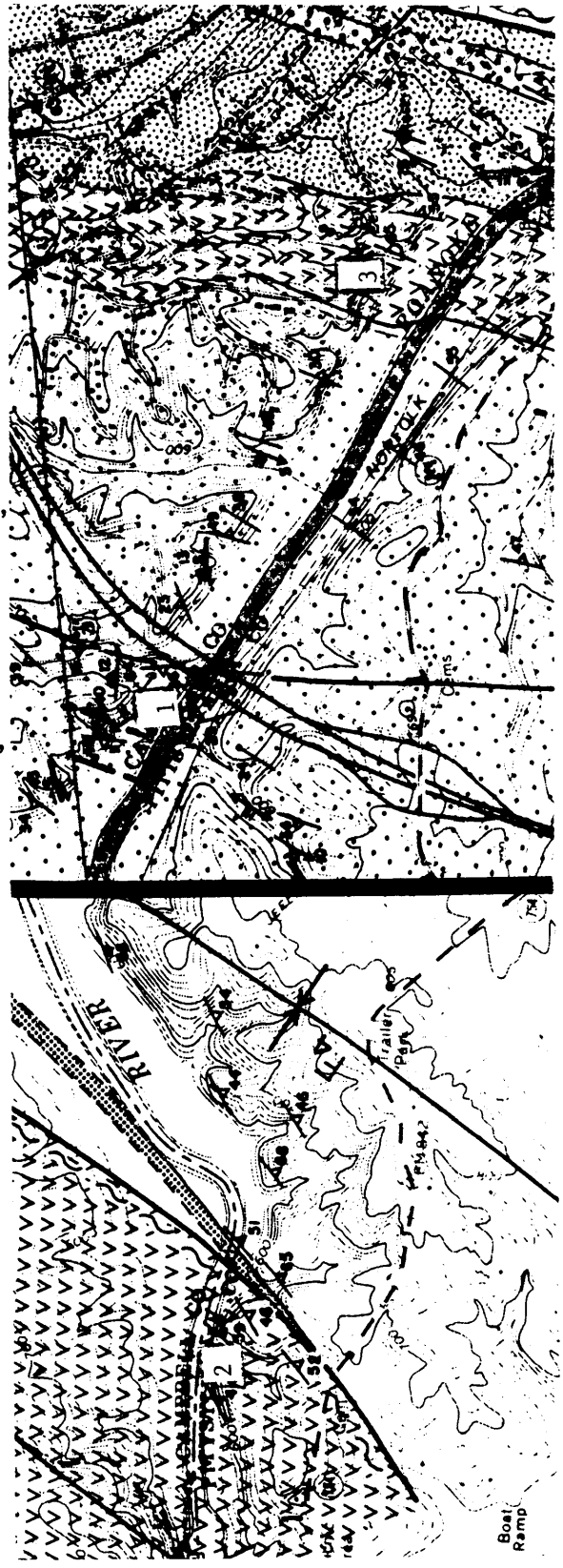

4) AG4-497, Rt. 699, 50 m east on Hills Creek. Felsic metatuff of upper Catoctin Formation, lineated L_3 and foliatied S_2.

5) AG5-1238 Quarry on Rt 43, base of Moon Mtn. Trough-crossbed ripples in Evington Group graywacke-quartzite contact. Grade upwards in 0.5 to 1 m beds. foliated by S_2 and lineated L_3 with small Folds.

6) AG4-159 Riverface southeast of Mansion. Chloritoid-Chlorite schist with Kyanite and staurolite. Kyanite deposit on hilltop 1-2 m thick.

7) AG4-179 (also AG4-2 to 6) On Roanoke River face at eastern map area (south of river). Migmatitic pelitic (bt + grt + sil) gneiss with small granite, pegmatite and aplite dikes. Rootless isoclines in migmatitic gneiss.

9) AG4-18 on Roanoke River (railroad tracks) path off of Rt 696 Brown Mountain. Disharmonic folds in

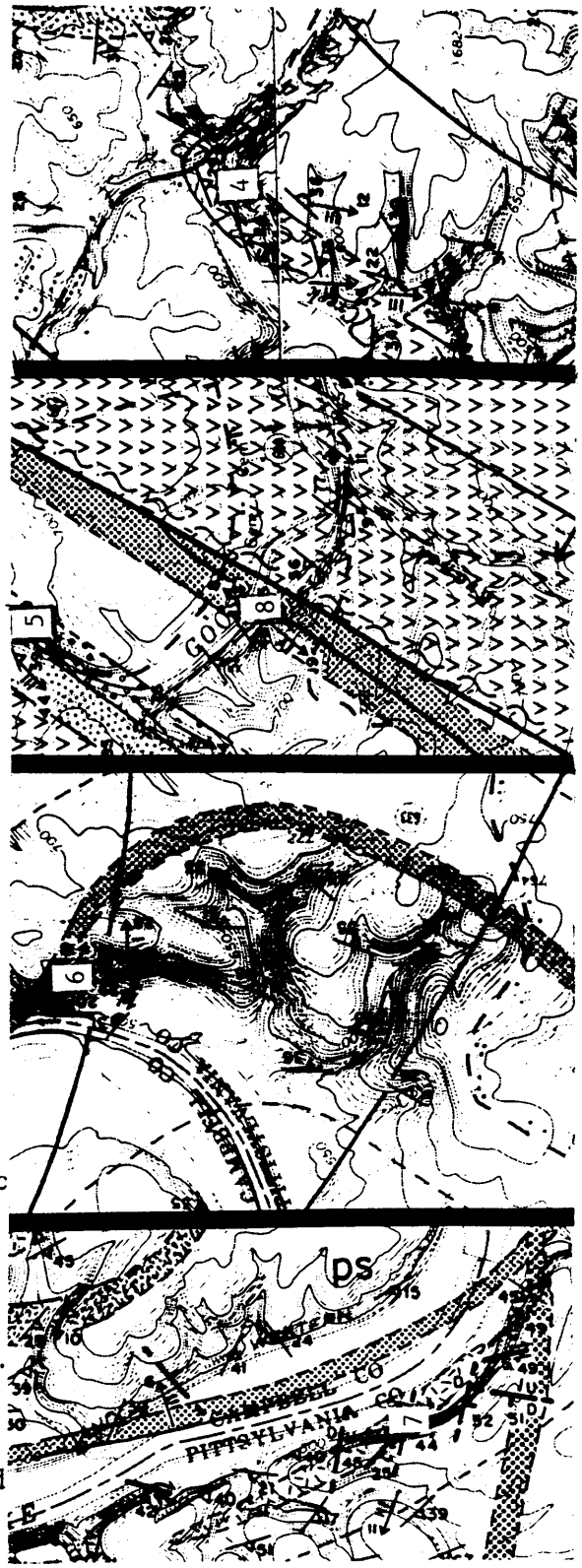

Evington Group Calc-silicate, thin laminations of pelite and calcareous material.

8) AG4-84 Railroad cut on Goose Creek. Thinly laminated calcareous/graphitic schist with thin normally graded siltstone laminations. Multiple crenulation cleavages; near reverse fault.

10) AG4-31 South of Taber and Rt. 696/Railroad tracks intersection, Brown Mountain. Thick, massive calcareous quartzite, weathered out.

11) AG5-887 (or AG5-718 of AG5-851) on Rt. 711 southeast of Scott Mtn. Staurolite porphyroblasts (to 3 cm) in bt + grt + st schist.

12) AG5-929 On Rt. 633 on Mill Creek (Perrows Pond). Dextral shear bands in Evington Group cld-chl-grt schist (retrograde).

13) AG4-42 Railroad tracks by Mansion Bridge. Multiple crenulation cleavages (S_2, S_3, S_4) in Evington Group Pelitic Schist. (Other locations AG4-51 by Minter Creek, AG4-66 at Roanoke River and Otter River, AG5-972 in Hurt).

APPENDIX B

The Regional Correlations and Plate Tectonic Implications of the Roanoke River Geology, Brookneal to Altavista, Virginia.

Introduction

The western Virginia Piedmont is a key area in constraining the Late Precambrian through Early Paleozoic history of the Appalachians because it exhibits the rift, drift and collisional phases in detail. The Piedmont also provides a link to the Blue Ridge and Valley and Ridge where response to orogenic events is mostly late and marginal. In correlating the Piedmont basin stratigraphy to the Valley and Ridge shelf, processes of both can be better understood. The western Roanoke River area (Altavista) in the southwestern Virginia Piedmont is important not only because it can constrain the timing of events in the Blue Ridge and Valley and Ridge but also because it links the greenschist facies central Virginia Piedmont with the middle to upper amphibolite facies southern Virginia Piedmont.

The stratigraphy of the western central Piedmont has been studied by several researchers (Espenshade, 1954; Brown, 1958; 1970; Evans, 1984; Patterson, in progress) and roughly correlated to the Blue Ridge and Valley and Ridge section. The southern Piedmont and Smith River Allochthon has been mapped in detail (Conley and Henika, 1970; 1973; Henika and Thayer, 1977; Marr, 1984; Berquist, 1980) in terms of structure, metamorphism and stratigraphy but has not been correlated to either the central Piedmont or the Blue Ridge and Valley and Ridge.

The eastern Roanoke River area (Brookneal) contains the suture between an eastern volcanic terrane (Charlotte Belt) and the western metasedimentary sequence of North American affinity. The suture has been studied in the central and northern Virginia Piedmont (Bland and Brown, 1977; Pavlides, 1978; Evans, 1984; Bland and Blackburn, 1980) and is proposed to be the Taconic Suture zone.

Correlation with the Valley and Ridge.

The Lynchburg and Catoctin equivalents and their stratigraphic positions have been documented on the western side of the Blue Ridge (see Wehr and Glover, 1984). The Evington Group has been proposed to be equivalent to portions of the Valley and Ridge section (Conley, 1978; Brown, 1958; 1970) but only Evans (1984) has attempted a unit by unit correlation. In the Altavista area, the Evington Group stratigraphy appears better constrained than in the other areas of study. The domes expose the Lynchburg and Catoctin units in various places throughout the area. The Lynchburg to Catoctin succession indicates a documented younging direction which coupled with position of Evington Group lithologies, suggests a stratigraphic order. In the westernmost map area, cross-beds and graded beds support the succession indicated in the rest of the area. Certainly however, the intense deformation and lack of outcrop precludes certainty in any stratigraphic sequence. The gradational nature of the Lower Evington-upper Catoctin contact and lack of constraints on time equivalence makes correlation of the lower Chillhowee-upper Catoctin Formation contact difficult. The shelf chronostratigraphy/sea level curve diagram of Read (in press), however makes rough correlations possible.

The lower Chillhowee Group in Virginia was deposited during a time of transgression. The lower quartzites of the Unicoi Formation are overlain by the more pelitic and finer grained Hampton and Murray Formations (Schwab, 1972). Similarly, coarse,

clean quartzite in the Catoctin was succeeded by graywacke in the lower Evington Group. On the shelf, sedimentological evidence suggests an ensuing regression to coarse sandstone of the Erwin Formation (Schwab, 1972). In Altavista, the graywacke is overlain by a coarse, clean quartzite, also suggesting a regression. The upper part of the graywacke exhibits fining up cycles and apparent unidirectional trough cross bedding, suggesting either distal shelf or deep water turbidite deposition.

The apparent eastward coarsening of the quartzite to the coarse sand-granule graywacke in Brookneal could be due to deep sea fan formation. The main channel could have been near Lynchburg or Evington, 30-50 km north and the fan spread laterally in the depositional lobes some distance to the east. A second possibity is that the coarse material was deposited adjacent to Lynchburg and Alleghanian dextral transcurrent faults (Gates, et al, 1986) slid the eastern block containing coarse material to the south and opposite the Altavista area. Eastward derivation for the unit is not possible however because there is no source for rutilated quartz and K-spar in the Charlotte Belt which bounds the Evington Group to the east (Gates, 1981).

The rapid energy decrease indicated by pelite overlying quartzite is then explained by two events on the Valley and Ridge shelf. The first is a rapid transgression at the Erwin-Shady dolomite boundary (Read, in press; Simpson, personal communication). This drowned the shelf and therefore prevented transport of coarse clastics across it. The second event was the formation of the Patterson-Shady carbonate bank which effectively cut off the shelf from the basin (Pfeil and Read, 1980). As the shelf built out in the middle Cambrian regression, carbonate and clastic detritus washed out into the basin, possibly as storm deposits. The thin calcareous graded beds to laminae of the lower calc-silicate unit were suggested to have had a slope lithofacies similar to the Shady dolomite (Pfeil and Read, 1980). In fact the Shady and lower Carbonate are very similar and may be facies equivalents. The shady built basinward during the Rome regression and could have formed the lower calc-silicate.

A carbonate bank was again built on the shelf after Rome deposition in a rapid, middle Cambrian transgression (Read, in press) (Figure 1). The Elbrook bank cut off the shelf from the basin and carbonaceous mud dominated in the Piedmont in the middle pelite. The Elbrook buildup is marked by a gentle transgression and the building out of the Conasauga shale. In late Cambrian time a rapid regression caused sand to build out on the shelf in the basal Copper Ridge (Read, in press). The incursion of sand on the Copper Ridge-Conococheaque platform happened several times with especially extensive development at the top of the sequence. The correlation breaks down in this sequence because the upper quartzite/calcareous unit of the Evington Group may be equivalent to all or some of the Copper Ridge sand/carbonate sequence. The calc-silicate and sandy layers are interlayered with pelites suggesting that it may represent a large part of the Copper Ridge but correlation of the thick sand sections is not resolvable.

A second possibility for the upper and lower calc-silicate/sandstone sequences is that they may be facies equivalents of the same unit. The sequence could have been duplicated through thrust faulting and then folded. The plastic nature of carbonates caused them to form a series of semi-continuous, contorted pods. Their map pattern is probably the least reliable of the units in the Altavista area.

Tectonic Synthesis of the Southwestern Piedmont

The geology of the Roanoke River traverse from Brookneal to Altavista displays a complete late Precambrian through early Paleozoic history for the western Virginia Piedmont. This history represents the opening and closing of the Iapetus Ocean basin. The cycle involves a rift stage followed by a drift stage and finally terminates in the Taconic collision. This Late Precambrian through early Paleozoic history is reflected throughout the Applachians, but is probably more applicable in timing of events to the southern Appalachians.

The late Precambrian rifting event is well documented in the Central and Southern Appalachians, in rift basins and rift generated plutonics and volcanics. The Crossnore Group of peralkaline granites intrude the basement rocks of the Blue Ridge (Rankin, 1975; Odom and Fullagar, 1984). Geochronologic studies of these rocks suggest that the rifting event occured between 690 and 570 Ma (Odom and Fullagar, 1984). Wehr and Glover (1985) suggest that this plutonic period also represents the period of normal faulting and rift sedimentation. The Lynchburg Group basin and correlative Ashe Formation and Ocoee Supergroup basins to the south (Rankin, 1975; Wehr and Glover, 1985) formed during this time. Feeder dikes to the overlying Catoctin Formation have been constrained in age to younger than 570 ± 15 Ma in northern Virginia by cross cutting relations with the Robertson River Granite (Mose and Nagel, 1984). Volcanic activity however, may have begun long before this in other areas. On the other hand this age implies that rifting continued into the lower Cambrian as suggested by Bond et al (1984).

Shelley fossils in the Hampton Formation and trace fossils in the Unicoi Formation indicate that the Chilhowee Group is early Cambrian (560-570 and younger) in age (Simpson and Sundberg, in press). The basal Unicoi Formation is composed of detritus from rifted basement blocks (Schwab, 1972) and the upper portion contains basalts (Rankin, 1967). The lower Chilhowee Group was deposited synchronously with the late Catoctin Formation.

The transition from rift to drift stage and passive margin development (Figure 2) probably did not take place until the middle of the early Cambrian (550 Ma) or later. Simpson and Eriksson (1986) suggest that the Hampton and Erwin Formations accumulated in shelf environments. These units probably correspond to the lower quartzite in the Evington Group. There is also a layer of amphibolite in the eastern Altavista area that postdates the quartzite. Immobile trace element discrimination plots indicate that

the Slippery Creek is a continental rift basalt (Blackburn and Brown, 1977) 1977). Rifting in the basin may have continued into the middle Cambrian.

On the Eastern side of the Evington Group Basin, the eastern volcanic rocks have been correlated with the Chopawamsic Formation of central and northern Virginia and to the rocks of the Charlotte Belt of the Carolinas (Gates, 1981; Glover et al, 1983). The Chopawamsic Formation has been dated at 570 to 540 Ma by zircons (Higgins, et al, 1977; Tilton et al, 1970). According to the chronostratigraphic diagram of Read (in press) and correlations made herein, the Evington Group and volcanic sequence are largely time equivalent. The two were therefore deposited on opposite sides of a basin (Figure 2). The Evington Group built eastward from the west and the volcaniclastic, graywacke aprons built in front of the volcanic arc (Pavlides, 1978; Gates, 1981). The source of the distal Evingtion Group pelites may have been from both the west and east. The Cambrian sediments therefore fined eastward on the west side of the basin and westward on the east side. The presence of dacitic volcanic rocks with the metabasalts and trace element discrimination plots (Bland and Blackburn, 1980) indicate that the volcanic sequence is part of an island arc. The coarse graywackes also indicate topographic relief in a shallow high energy environment.

The Evington basin was apparently rather wide because no dacitic or andesitic volcanic units are recognized in the Evingtion Group rocks and no ash deposits are present on the Valley and Ridge shelf (Glover et al, in prep). Simpson and Eriksson (1985) estimated that the minimum width of the upper Chilhowee basin was 150 to 350 km based on paleowave reconstructions. Other evidence to suggest a large ocean basin is the lack of carbonate rims on the volcanic arc when at the same time there was high production of carbonate on the western shelf (Glover et al, in prep).

The Evington Group was intensely deformed and metamorphosed prior to the intrusion of the Melrose. Detailed petrologic (Gates and Speer, in prep) and structural analysis indicates that this orogenic event was characterized by west directed fold and

possibly thrust nappe emplacement. P-T paths from zoned minerals can determine the tectonic history, especially in terranes characterized by nappe emplacement (Spear et al, 1984). Spear, et al (1984) have proposed an ideal P-T loop for such terranes. In their model, after undergiong regional metamorphism, rocks in the footwall of a nappe experience a high pressure phase (P max) in response to nappe emplacement. The thermal response of the footwall to the heat source on the hanging wall is slower. Thermal equilibration (T max) coincides with depressurization through erosion of the overlying strata. The retrograde path follows T max as the pile re-equilibrates to the uplift and removal of overlying strata. In the Altavista area, the zoned minerals record the progression from P max to T max and the retrograde path.

The P-T path indicated by the M1 metamorphism directly reflects the structural development and tectonics of the Altavista area. The Taconic D1 and D2 deformations are closely related and possibly a continuum of a single event or protracted event. The complexity and degree of deformation indicate that D1 and D2 were intense. The F1 and F2 folding events are isoclinal and recumbent and correspond to a high grade metamorphic event. The metamorphism indicates that temperatures were lower at lower levels in the stratigraphy and to the west. In the upper portions of the mapped stratigraphy, melting of pelitic rocks took place. The geothermal gradient was therefore inverted. The folding and metamorphism are the result of nappe emplacement. The high grade rocks form a continuous zone to Brookneal and the eastern volcanic rocks. The high grade rocks were thrust or folded westward by D1 and D2 over low grade rocks, some of which are still preserved in the western field area. Nappe emplacement caused the pressure to increase on the footwall which comprises most of Altavista. The F1 isoclinal recumbent fold in the southern part of the eastern area, marks the base of the hanging wall. The heat of the nappe then caused the reverse metamorphism by conduction or convection downward into the footwall. The root zone for the nappe is either

between Altavista and Brookneal (mainly beneath the Danville Basin) or under the volcanic rocks of Brookneal.

The direction of nappe emplacement, east over west, suggests the polarity of the subduction zone in collision. In the Himalayas, the Indian plate subducted beneath Asia. The high grade nappes that contain anatectic granitic dikes and plutons and exhibit inverted metamorphic isograds were emplaced southward or away from the suture zone on the subducting plate (Lefort, 1976).

In the southwestern Virginia Piedmont the age of the collision is constrained by the Melrose Granite in Brookneal and the associated Leatherwood Granite to the south. If the zircon ages of 511 Ma are not inherited, then the collision is required to have taken place in the middle to late Cambrian. If the Rb/Sr whole rock ages are correct, the collision was probably more likely Ordovician though still could have been late Cambrian. The early age is supported by the zircon ages from the Chopwamsic (540-570) though they may be inherited (Higgins et al, 1977). Nd/Sm ages of 490 Ma from the Baltimore mafic complex ion the correlative James Run volcanics (Wasserburg et al, 1981) support the younger age.

The two latest deformational events D3 and D4 and second metamorphic event M2, occurred late in the development of the area and are probably related to the late Acadian or Alleghanian orogenic event. The deformational events produced the northeast trending domal structures in the eastern map area and Sherwill Dome in the western map area. Associated with these structures are multiple crenulation and shear cleavages that overprint the earlier foliations. Metamorphism associatied with the event produces chlorite and muscovite overgrowths on the early minerals. The late event is of dextral transpression (Gates, in prep).

The age of the Melrose and mafic associate is the same as the Leatherwood Granite and Rich Acres associate (Odom and Russell, 1975; Rankin, 1975; Sinha, personal communication). Both associations have been described as cointrusive and both intrude

the Evington Group/Fork Mountain Formation. These Cambrian to Ordovician intrusives are related to a series of plutons that define a belt along the eastern contact of the Evingtion Group and western contact of the metavolcanic terrane (Gates, 1981; Sinha, personal communication).

REFERENCES

Berquist, C. R., 1980, Sandy Level Quadrangle: Its Geology and Regional Interpretation, in Price, V. Jr., Thayer, P. A., and Ronson, W. A., eds., Geol. Inv. of the Pied. and Triassic Rocks, Cent. N. Ca. and Va.; Carolina Geol. Soc. Field Trip Guidebook, P. I-1 - I-10.

Bland, A. E. and Blackburn, W. H., 1980, Geochemical studies on the Greenstones of the Atlantic Seaboard Volcanic Province, South-Central Appalachians; in Wones, D. R., ed., The Caledonides in the U. S. A., IGCP project 27: Caledonide Orogen, Vir. Poly. Inst. and State Univ., mem. no. 2, p. 263-270.

Bland, A. E. and Brown, W. R., 1977, Evington Group(?) of the Arvonia District: Rear Arc Sedimentation and Volcanism; Geol. Soc. Am. Abs. with Progs. v. 9., no. 2, p. 120.

Bond, G. C., Nickeson, P. A., and Kominz, A. A., 1984, Breakup of a super continent between 625 Ma and 555 Ma: New evidence and implications for continental histories; Earth Plan. Sci. Lett., v. 70, p. 325-345.

Brown, W. R., 1958, Geology and mineral resources of the Lynchburg quadrangle, Virginia; Va. Div. of Min. Res. Bull. 74, 99p.

Brown, W. R. 1970, Investigations of the sedimentary record in the Piedmont and Blue Ridge of Virginia; in Fisher,G. W., Pettijohn, F.J., Reed, J. C., and Weaver, K. N. eds. Studies of Appalachian geology; Central and Southern: New York, Wiley Interscience, p. 335-349.

Blackburn, W. H., and Brown, W. R., 1976, Petrochemical evidence relating the Catoctin volcanic series to late Precambrian continental separation; Geol. Soc, Am. Abst. with progs., v. 8, p. 136-137.

Conley, J. F., 1978, Geology of the Piedmont of Virginia, Interpretations and Problems; in Contrib. to Vir. Geol., Vir. Div. Min. Res., Pub. 7, p. 115-149.

Conley, J. F., and Henika, W. S., 1970, Geology of the Philpott Reservoir quadrangle, Virginia; Vir. Div. Min. Res. Rept. Inv. 22, 46pp.

Conley, J. F., and Henika, W. S., 1973, Geology of the Snow Creek, Martinsville East, Price and Spray Quadrangles, Virginia; Rep. Invest. Va. Div. Miner. Resour., no. 33, 71 pp..

Espenshade, G. H., 1954, Geology and mineral Deposits of the James River-Roanoke River Manganese District, Virginia, U. S. Geol. Surv. Bull. 1008, 155p.

Evans, N. H., 1984, Latest Precambrian to Ordovician metamorphism and orogenesis in the Blue Ridge and western Piedmont, Virginia Appalachians; unpub. PhD dissertation, Virginia Polytechnic Institute and State University; p. 324.

Gates, A. E., Geology of the western boundary of the Charlotte belt at Brookneal, Va., M. S. thesis, Va. Polytech. Inst.Blacksburg, 1981.

Gates, A. E., in prep, Prograde and Retrograde meatamorphism in Response to Nappe Emplacement, Southwest Virginia Piedmont;

Gates, A. E., C. Simpson, and L. Glover III, 1986, Appalachian Carboniferous dextral strike-slip faults: an example from Brookneal, Virginia; Tectonics, vol. 5 no. 1, p. 119-133.

Glover, L., III, Speer, J. A., Russell, G. S. and Farrar, S. S., 1983 Ages of regional metamorphism and ductile deformation in the central and southern Appalachians; Lithos, vol. 16, p. 223-245.

Glover, L., III, Costain, J. K., Coruh, C., Evans, N. H., Bollinger, G. A., Farrar, S. S. and Sibol, M. S., in prep, Seismicity, seismic reflection studies, gravity and geology of the Central Virginia seismic zone: Part IV, Tectonic History and current seismicity;

Henika, W. S. and Thayer, P. A., 1977, Geologic Maps of the Blairs, Mount Hermon, Danville and Ringgold quadrangles, Virginia; Vir. Div. Min. Res., Pub 2., 45pp.

Higgins, M. W., Sinha. A. K., Zartman, R. E. and Kirk, W. S., 1977, U-Pb Zircon dates from the central Appalachian Piedmont: A possible case of ingerited radiogenic lead; Geol. Soc. Am. Bull., vol. 88, p. 125-132.

LeFort, P., 1975, Himalayas: The collided range. Present knowledge of the continental arc; Am. Jour. Sci., v. 275-A, p. 1-44.

Marr, J. D., Jr., 1984, Geologic Map of the Pittsville and Chatham quadrangles, Virginia; Vir. Div. Min. Res., Pub. 49.

Mose, D. G. and Nagel,. S., 1984; Rb-Sr age for the Robertson River pluton in Virginia and its implication of the age of the Catoctin Formation; in Bartholomew, M. J., ed, The Grenville Event in the Appalachians and related topics: Geol. Soc, Am, Spec. paper 194, p. 255-261.

Newton, R. C. and Haselton, H. T., 1981, Thermodynamics of the garnet-plagioclase-Al2SiO5-Quartz geobarometer. In R.C. Newton, et al, Eds., Advances in Physical Geochemistry 1, p. 111-147, Springer-Verlag.

Odom, A. L., and G. S. Russell, 1975, The time of regional metamorphism of the Inner Piedmont, North Carolina and Smith River Allochthon: Inferences from whole-rock ages; Geol. Soc. Am. Abstrs. Progs., vol. 7, no. 4, p. 522.

Pavlides, L., 1978, Tectonic model for Northeast Virginia Piedmont; in Geol. Surv. Res.: U. S. Geol. Surv. Prof. Paper 1100, 51pp.

Pfeil, R. W. and Read, J. F., 1980; Cambrian carbonate platform marginal facies, Shady Dolomite, southwestern Virginia, U. S. A.; J. Sed. Pet. v. 50, p. 91-116.

Rankin, D. W., 1975, The continental margin of eastern North America in the southern Appalachians: The opening and closing of the proto-Atlantic Ocean; Am. J. Sci., v. 275-A, p. 298-336.

Read, J. F., in press, Evolution of Cambro-Ordovician passive margin, U. S. Appalachians; in Decade of North Am. Geol. Synth. Vol.: Appalachian-Ouachita.

Schwab, F. L., 1972, The Chilhowee Group and the late Precambrian-early Paleozoic sedimentary framework in the central and southern Appalachians; in Lessing, P. Hayhurst, R. O., Barlow, J. A. and Woodfork, L. D., eds., Appalachian structures: Origin, evolution, and potential for new exploration frontiers: Morgantown, West Virginia, West Virginia University and West Virginia Geologic and Economic Survey, p. 59-101.

Simpson, E. L., and Eriksson, K. A., 1985, Paleoenvironmental constraints provided by paleowave reconstructions: Early Cambrian Chilhowee Group drift stage sedimentation in the Central Appalachians; Geol. Soc, Am. Abst. W. Progs., v. 17, p. 718.

Simpson, E. L., and Sundberg, F. A., in review, Early Cambrian age for syn-rift deposits of the Chillhowee Group of Southestern Virginia; Geology.

Streckheisen, A. L., 1973, Plutonic rocks: Classification and nomenclature Recommended by the IUGS Subcommission of the Systematics of Igneous Rocks; Geotimes, v. 18, no. 10, P. 26-31.

Spear, F. S., Selverstone, J., Hickmott, Crowley, P. and Hodges, K. V., 1984, P-T paths from garnet zoning: A new technique for deciphering tectonic processes in crystalline terranes; Geology, v. 12, p. 87-90.

Tilton, G. W., Doe, B. R. and Hopson, C. A., 1970, Zircon age measurements in the Maryland Piedmont with special reference to Baltimore gneiss problems; in Gisher, G. W., Pettijohn, F. J., Reed, J. C. and Weaver, I. N., eds., Studies of Appalachian Geology, central and southern: New York Interscience Publishers, p. 429-437.

Wehr, F. and Glover, L. III, 1985, Stratigraphy and Tectonics of the Virginia-North Carolina Blue Ridge: Evolution of a late Proterozoic- early Paleozoic hinge zone. Geol. Soc. of Am. Bull., v. 96, p. 285-295.

APPENDIX C

Microprobe Analyses

MUSCOVITE ANALYSES (OH CALCULATED)

SUPER RECAL	9	10	11	12	13	14
SIO2	46.08	46.91	46.91	47.25	43.28	44.99
TIO2	0.70	0.47	1.18	0.38	0.13	0.57
A203	34.49	35.82	35.43	37.84	42.78	33.97
FEO	2.94	1.20	1.10	0.87	1.22	2.70
MNO	0.01	0.02	0.02	0.03	0.06	-0.03
MGO	0.72	0.58	0.55	0.48	0.18	0.62
CAO	0.01	0.01	0.01	0.03	0.11	-0.02
BAO	0.0	0.0	0.0	0.0	0.0	0.34
NA2O	0.83	0.95	1.37	1.74	0.81	1.11
K2O	9.78	9.47	8.77	8.39	7.76	9.00
F	0.0	0.0	0.0	0.0	0.0	0.03
CL	0.0	0.0	0.0	0.0	0.0	0.0
H2O	4.49	4.54	4.55	4.64	4.62	4.37
SUM	100.05	99.97	99.89	101.65	100.95	97.65
-O= F+CL	0.0	0.0	0.0	0.0	0.0	0.01
SUM	100.05	99.97	99.89	101.65	100.95	97.64

SI	6.152	*	6.190	*	6.182	*	6.096	*	5.614	*	6.146	*
AL	1.848	8.000	1.810	8.000	1.818	8.000	1.904	8.000	2.386	8.000	1.854	8.000
AL	3.577	*	3.760	*	3.684	*	3.849	*	4.154	*	3.615	*
TI	0.070	*	0.047	*	0.117	*	0.037	*	0.013	*	0.059	*
FE	0.328	*	0.132	*	0.121	*	0.094	*	0.132	*	0.308	*
MN	0.001	*	0.002	*	0.002	*	0.003	*	0.007	*	-0.003	*
MG	0.143	4.120	0.114	4.055	0.108	4.033	0.092	4.075	0.035	4.340	0.126	4.105
CA	0.001	*	0.001	*	0.001	*	0.004	*	0.015	*	-0.003	*
NA	0.215	*	0.243	*	0.350	*	0.435	*	0.204	*	0.294	*
K	1.665	*	1.594	*	1.474	*	1.381	*	1.284	*	1.568	*
BA	0.0	1.882	0.0	1.838	0.0	1.826	0.0	1.820	0.0	1.503	0.018	1.878
CL	0.0	*	0.0	*	0.0	*	0.0	*	0.0	*	0.0	*
F	0.0	*	0.0	*	0.0	*	0.0	*	0.0	*	0.013	*
H	4.000	4.000	4.000	4.000	4.000	4.000	4.000	4.000	4.000	4.000	3.987	4.000
O	24.000	*	24.000	*	24.000	*	24.000	*	24.000	*	24.000	*
	MUSC	88.51		86.70		80.75		75.86		85.43		84.34
	PARG	11.42		13.22		19.17		23.91		13.55		15.81
	MARG	0.08		0.08		0.08		0.23		1.02		-0.16
	F/M	2.299		1.180		1.143		1.052		3.992		2.416
	F/FM	0.697		0.541		0.533		0.513		0.800		0.707

9 188C AG4-59
10 364B AG4-3A
11 380M AG4-6
12 418X AG4-6
13 438Y AG5-505
14 AG5-523

SUPER RECAL — MUSCOVITE ANALYSES (OH CALCULATED)

	1	2	3	4	5	6	7	8
SIO2	46.74	45.36	46.64	46.14	45.64	46.50	45.88	45.66
TIO2	0.22	0.39	0.62	0.65	0.71	0.72	0.33	0.65
A203	36.58	36.10	34.21	34.65	34.57	34.42	35.74	34.42
FEO	1.71	1.93	2.59	2.96	2.82	2.27	1.90	2.20
MNO	-0.07	-0.04	-0.04	-0.06	-0.05	-0.03	-0.02	0.01
MGO	0.41	0.47	0.70	0.72	0.67	0.76	0.43	0.68
CAO	-0.01	-0.01	0.0	-0.02	-0.02	-0.01	-0.01	-0.02
BAO	0.0	0.33	0.46	0.39	0.36	0.39	0.36	0.40
NA20	1.60	1.43	1.06	1.26	0.91	1.32	1.71	1.25
K20	8.66	8.12	9.00	9.07	9.37	8.50	7.65	8.67
F	-0.04	0.02	0.08	0.06	0.04	0.09	-0.02	0.0
CL	0.0	0.0	0.0	0.0	0.0	0.0	0.0	0.0
H20	4.58	4.46	4.45	4.47	4.44	4.45	4.48	4.44
SUM	100.38	98.56	99.77	100.29	99.46	99.38	98.43	98.36
-O= F+CL	-0.02	0.01	0.03	0.03	0.02	0.04	-0.01	0.0
SUM	100.40	98.55	99.74	100.26	99.44	99.34	98.44	98.36

SI	6.140	*	6.080	*	6.220	*	6.142	*	6.129	*	6.202	*	6.143	*	6.166	*
AL	1.860	8.000	1.920	8.000	1.780	8.000	1.858	8.000	1.871	8.000	1.798	8.000	1.857	8.000	1.834	8.000
AL	3.802	*	3.782	*	3.597	*	3.578	*	3.599	*	3.612	*	3.782	*	3.644	*
TI	0.022	*	0.039	*	0.062	*	0.065	*	0.072	*	0.072	*	0.033	*	0.066	*
FE	0.188	*	0.216	*	0.289	*	0.330	*	0.317	*	0.253	*	0.213	*	0.248	*
MN	-0.008	*	-0.005	*	-0.005	*	-0.007	*	-0.006	*	-0.003	*	-0.002	*	0.001	*
MG	0.080	4.084	0.094	4.127	0.139	4.082	0.143	4.109	0.134	4.116	0.151	4.085	0.086	4.112	0.137	4.097
CA	-0.001	*	-0.001	*	0.0	*	-0.003	*	-0.003	*	-0.001	*	-0.001	*	-0.003	*
NA	0.407	*	0.372	*	0.274	*	0.325	*	0,237	*	0.341	*	0.444	*	0.327	*
K	1.451	*	1.388	*	1.531	*	1.540	*	1.605	*	1.446	*	1.307	*	1.493	*
BA	0.0	1.857	0.017	1.776	0.024	1.829	0.020	1.883	0.019	1.858	0.020	1.806	0.019	1.768	0.021	1.839
CL	0.0	*	0.0	*	0.0	*	0.0	*	0.0	*	0.0	*	0.0	*	0.0	*
F	-0.017	*	0.008	*	0.034	*	0.025	*	0.017	*	0.038	*	-0.008	*	0.0	*
H	4.017	4.000	3.992	4.000	3.966	4.000	3.975	4.000	3.983	4.000	3.962	4.000	4.008	4.000	4.000	4.000
O	24.000	*	24.000	*	24.000	*	24.000	*	24.000	*	24.000	*	24.000	*	24.000	*
	MUSC	78.13		78.95		84.82		82.69		87.27		80.97		74.70		82.15
	PARG	21.94		21.13		15.18		17.46		12.88		19.11		25.38		18.00
	MARG	-0.08		-0.08		0.0		-0.15		-0.16		-0.08		-0.08		-0.16
	F/M	2.243		2.256		2.044		2.259		2.319		1.653		2.453		1.824
	F/FM	0.692		0.693		0.671		0.693		0.699		0.623		0.710		0.646

1 77C AG4-225++
2 102+ AG4-159+
3 1173 AG4-159+
4 141C AG5-929
5 1754 AG5-929
6 245C AG4-2A
7 2615 AG4-268+
8 2665 AG4-268+

SUPER RECAL — FELDSPAR ANALYSES

	1	2	3	4	5
SIO2	55.06	55.74	55.40	55.74	55.06
TIO2	0.02	0.03	0.02	0.03	0.02
A203	29.93	29.96	29.94	29.96	29.93
FEO	0.05	0.13	0.09	0.13	0.05
MNO	0.02	0.03	0.02	0.03	0.02
MGO	0.04	0.0	0.02	0.04	0.0
CAO	10.69	10.30	10.49	10.69	10.30
BAO	0.0	0.0	0.0	0.0	0.0
NA2O	5.36	5.51	5.43	5.51	5.36
K2O	0.05	0.05	0.05	0.05	0.05
F	0.0	0.0	0.0	0.0	0.0
CL	0.0	0.0	0.0	0.0	0.0
SUM	101.22	101.75	101.48	102.18	100.79
-O= F+CL	0.0	0.0	0.0	0.0	0.0
SUM	101.22	101.75	101.48	102.18	100.79

SI	2.449	*	2.463	*	2.456	*	2.457	*	2.455	*
AL	1.569	*	1.560	*	1.564	*	1.556	*	1.573	*
TI	0.001	4.018	0.001	4.024	0.001	4.021	0.001	4.014	0.001	4.029
FE	0.002	*	0.005	*	0.003	*	0.005	*	0.002	*
MN	0.001	*	0.001	*	0.001	*	0.001	*	0.001	*
MG	0.003	*	0.0	*	0.001	*	0.003	*	0.0	*
CA	0.509	*	0.488	*	0.498	*	0.505	*	0.492	*
BA	0.0	*	0.0	*	0.0	*	0.0	*	0.0	*
NA	0.462	*	0.472	*	0.467	*	0.471	*	0.463	*
K	0.003	0.980	0.003	0.968	0.003	0.974	0.003	0.987	0.003	0.961
O	8.000	*	8.000	*	8.000	*	8.000	*	8.000	*
AN	52.28		50.66		51.47		51.59		51.35	
AB	47.43		49.04		48.24		48.12		48.35	
OR	0.29		0.29		0.29		0.29		0.30	
CN	0.0		0.0		0.0		0.0		0.0	
F/M	0.985		0.0		3.235		2.250		0.0	
F/FM	0.496		0.0		0.764		0.692		0.0	

1 171C AG4-59 RIM
2 179C AG4-59 RIM
3 AVERAGE
4 AVERAGE PLUS SIGMA
5 AVERAGE MINUS SIGMA

SUPER RECAL — FELDSPAR ANALYSES

	1	2	3	4	5
SIO2	60.43	60.08	60.25	60.43	60.08
TIO2	0.01	0.0	0.00	0.01	0.0
A203	25.12	26.36	25.74	26.36	25.12
FEO	0.13	0.07	0.10	0.13	0.07
MNO	-0.03	0.0	-0.02	-0.00	-0.03
MGO	0.05	0.0	0.02	0.05	0.0
CAO	6.96	7.60	7.28	7.60	6.96
BAO	0.0	0.0	0.0	0.0	0.0
NA2O	6.81	6.97	6.89	6.97	6.81
K2O	0.05	0.07	0.06	0.07	0.05
F	0.0	0.0	0.0	0.0	0.0
CL	0.0	0.0	0.0	0.0	0.0
SUM	99.53	101.15	100.34	101.62	99.06
-O= F+CL	0.0	0.0	0.0	0.0	0.0
SUM	99.53	101.15	100.34	101.62	99.06

SI	2.693	*	2.644	*	2.668	*	2.647	*	2.690	*
AL	1.319	*	1.367	*	1.343	*	1.361	*	1.325	*
TI	0.000	4.012	0.0	4.011	0.000	4.012	0.000	4.008	0.0	4.015
FE	0.005	*	0.003	*	0.004	*	0.005	*	0.003	*
MN	-0.001	*	0.0	*	-0.001	*	-0.000	*	-0.001	*
MG	0.003	*	0.0	*	0.002	*	0.003	*	0.0	*
CA	0.332	*	0.358	*	0.345	*	0.357	*	0.334	*
BA	0.0	*	0.0	*	0.0	*	0.0	*	0.0	*
NA	0.588	*	0.595	*	0.592	*	0.592	*	0.591	*
K	0.003	0.930	0.004	0.960	0.003	0.945	0.004	0.961	0.003	0.929
O	8.000	*	8.000	*	8.000	*	8.000	*	8.000	*
AN	35.98		37.45		36.73		37.45		35.98	
AB	63.71		62.14		62.91		62.14		63.71	
OR	0.31		0.41		0.36		0.41		0.31	
CN	0.0		0.0		0.0		0.0		0.0	
F/M	1.118		0.0		1.903		1.459		0.0	
F/FM	0.528		0.0		0.656		0.593		0.0	

1 4PL2 AG5-1066+
2 4PL3 AG5-1066+
3 AVERAGE
4 AVERAGE PLUS SIGMA
5 AVERAGE MINUS SIGMA

FELDSPAR ANALYSES

SUPER RECAL	1		2		3		4		5		6		7		8	
SIO2	58.53		61.68		65.68		62.04		63.86		58.54		59.42		63.04	
TIO2	0.0		0.01		-0.01		-0.01		0.02		0.05		0.02		0.02	
A203	27.77		26.08		20.44		22.74		22.56		29.00		27.49		25.00	
FEO	0.03		0.07		-0.06		-0.07		-0.04		0.04		0.07		0.05	
MNO	0.02		0.01		-0.07		-0.07		-0.01		0.0		0.03		0.03	
MGO	-0.03		0.02		-0.01		0.0		0.0		0.01		0.0		-0.01	
CAO	7.85		5.59		1.26		4.18		3.20		9.41		7.65		4.53	
BAO	0.0		0.0		-0.11		-0.08		-0.01		0.0		0.0		0.0	
NA20	7.04		7.86		10.48		8.81		8.54		5.77		7.01		8.60	
K20	0.05		0.07		-0.02		0.0		-0.02		0.08		0.06		0.04	
F	0.0		0.0		0.0		-0.02		-0.02		0.0		0.0		0.0	
CL	0.0		0.0		0.0		0.0		0.0		0.0		0.0		0.0	
SUM	101.26		101.39		97.58		97.54		98.10		102.90		101.75		101.30	
-O= F+CL	0.0		0.0		0.0		0.0		0.0		0.0		0.0		0.0	
SUM	101.26		101.39		97.58		97.54		98.10		102.90		101.75		101.30	
SI	2.581	*	2.693	*	2.938	*	2.802	*	2.850	*	2.542	*	2.603	*	2.747	*
AL	1.443	*	1.342	*	1.078	*	1.210	*	1.186	*	1.484	*	1.419	*	1.284	*
TI	0.0	4.024	0.000	4.035	-0.000	4.016	-0.000	4.012	0.001	4.037	0.002	4.028	0.001	4.023	0.001	4.032
FE	0.001	*	0.003	*	-0.002	*	-0.003	*	-0.001	*	0.001	*	0.003	*	0.002	*
MN	0.001	*	0.000	*	-0.003	*	-0.003	*	-0.000	*	0.0	*	0.001	*	0.001	*
MG	-0.002	*	0.001	*	-0.001	*	0.0	*	0.0	*	0.001	*	0.0	*	-0.001	*
CA	0.371	*	0.261	*	0.060	*	0.202	*	0.153	*	0.438	*	0.359	*	0.212	*
BA	0.0	*	0.0	*	-0.002	*	-0.001	*	-0.000	*	0.0	*	0.0	*	0.0	*
NA	0.602	*	0.665	*	0.909	*	0.772	*	0.739	*	0.486	*	0.595	*	0.727	*
K	0.003	0.975	0.004	0.935	-0.001	0.961	0.0	0.967	-0.001	0.889	0.004	0.930	0.003	0.962	0.002	0.943
O	8.000	*	8.000	*	8.000	*	8.000	*	8.000	*	8.000	*	8.000	*	8.000	*
AN	38.02		28.10		6.25		20.80		17.18		47.18		37.49		22.49	
AB	61.70		71.49		94.07		79.34		82.97		52.35		62.16		77.27	
OR	0.29		0.42		-0.12		0.0		-0.13		0.48		0.35		0.24	
CN	0.0		0.0		-0.20		-0.15		-0.02		0.0		0.0		0.0	
F/M	1.118		2.248		1.903		1.459		0.0		2.244		0.0		0.0	
F/FM	0.528		0.692		0.656		0.593		0.0		0.692		0.0		0.0	

SUPER RECAL	9	
SIO2	63.92	
TIO2	0.01	
A203	22.65	
FEO	-0.07	
MNO	-0.04	
MGO	0.0	
CAO	2.78	
BAO	0.29	
NA20	7.98	
K20	0.0	
F	-0.02	
CL	0.0	
SUM	97.52	
-O= F+CL	0.0	
SUM	97.52	
SI	2.863	*
AL	1.195	*
TI	0.000	4.059
FE	-0.003	*
MN	-0.002	*
MG	0.0	*
CA	0.133	*
BA	0.005	*
NA	0.693	*
K	0.0	0.827
O	8.000	*
AN	16.04	
AB	83.34	
OR	0.0	
CN	0.61	
F/M	1.118	
F/FM	0.528	

1 172C AG4-59 CORE
2 422Y AG5-505
3 47E AG4-225++ L
4 50E AG4-225++H
5 240B AG4-2A
6 346B AG4-3A
7 362B AG4-3A
8 388X AG4-6 AVG
9 2595 AG4-268+

SUPER RECAL — BIOTITE ANALYSES (H2O INPUTTED)

	1	2	3	4	5	6	7	8
SIO2	35.58	36.00	35.32	34.95	35.86	35.43	35.43	35.32
TIO2	1.42	1.63	1.59	1.43	1.45	1.46	1.46	1.70
A2O3	19.46	19.47	19.96	19.54	18.92	19.44	19.35	20.10
FEO	21.13	20.92	20.79	20.88	20.35	20.63	21.67	21.26
MNO	0.05	0.06	0.05	0.03	0.05	0.04	0.06	0.18
MGO	9.41	9.06	9.85	9.62	9.49	9.37	9.48	9.09
CAO	0.02	0.03	0.03	0.03	0.03	0.04	0.05	0.08
BAO	0.0	0.0	0.0	0.0	0.0	0.0	0.0	0.0
NA2O	0.19	0.24	0.26	0.21	0.23	0.23	0.25	0.20
K2O	8.65	8.92	8.87	8.96	8.70	8.78	8.61	8.88
F	0.0	0.0	0.0	0.0	0.0	0.0	0.0	0.0
CL	0.0	0.0	0.0	0.0	0.0	0.0	0.0	0.0
H2O	3.95	3.97	3.99	3.93	3.93	3.94	3.96	3.98
SUM	99.86	100.30	100.71	99.58	99.01	99.36	100.32	100.79
-O= F+CL	0.0	0.0	0.0	0.0	0.0	0.0	0.0	0.0
SUM	99.86	100.30	100.71	99.58	99.01	99.36	100.32	100.79

SI	5.393	*	5.430	*	5.308	*	5.326	*	5.465	*	5.392	*	5.362	*	5.317	*
AL	2.607	8.000	2.570	8.000	2.692	8.000	2.674	8.000	2.535	8.000	2.608	8.000	2.638	8.000	2.683	8.000
AL	0.869	*	0.890	*	0.843	*	0.835	*	0.863	*	0.879	*	0.813	*	0.882	*
TI	0.162	*	0.185	*	0.180	*	0.164	*	0.166	*	0.167	*	0.166	*	0.192	*
FE	2.678	*	2.639	*	2.613	*	2.661	*	2.594	*	2.626	*	2.743	*	2.676	*
MN	0.006	*	0.008	*	0.006	*	0.004	*	0.006	*	0.005	*	0.008	*	0.023	*
MG	2.126	5.841	2.037	5.758	2.207	5.849	2.185	5.849	2.156	5.785	2.126	5.802	2.139	5.869	2.039	5.813
CA	0.003	*	0.005	*	0.005	*	0.005	*	0.005	*	0.007	*	0.008	*	0.013	*
NA	0.056	*	0.070	*	0.076	*	0.062	*	0.068	*	0.068	*	0.073	*	0.058	*
K	1.672	*	1.716	*	1.700	*	1.742	*	1.691	*	1.704	*	1.662	*	1.705	*
BA	0.0	1.731	0.0	1.791	0.0	1.781	0.0	1.809	0.0	1.764	0.0	1.779	0.0	1.744	0.0	1.776
CL	0.0	*	0.0	*	0.0	*	0.0	*	0.0	*	0.0	*	0.0	*	0.0	*
F	0.0	*	0.0	*	0.0	*	0.0	*	0.0	*	0.0	*	0.0	*	0.0	*
H	3.994	3.994	3.994	3.994	4.000	4.000	3.995	3.995	3.995	3.995	4.000	4.000	3.998	3.998	3.997	3.997
O	24.000	*	24.000	*	24.000	*	24.000	*	24.000	*	24.000	*	24.000	*	24.000	*
MG		44.19		43.49		45.72		45.05		45.33		44.69		43.74		43.04
FE		55.81		56.51		54.28		54.95		54.67		55.31		56.26		56.96
F/M		1.263		1.299		1.187		1.220		1.206		1.238		1.286		1.324
F/FM		0.558		0.565		0.543		0.549		0.547		0.553		0.563		0.570
A* =		0.158		0.157		0.160		0.154		0.152		0.158		0.155		0.165
A =		-0.191		-0.220		-0.194		-0.215		-0.214		-0.207		-0.187		-0.197
M =		0.443		0.436		0.458		0.451		0.454		0.447		0.438		0.432

1 329 AG4-179 BT3
2 369 AG4-179 BT3
3 379 AG4-179 BT4
4 389 AG4-179 BT5
5 393 AG4-179 BT1
6 403 AG4-179 BT2
7 413 AG4-179 BT3
8 47B AG4-179 BT INCL

SUPER RECAL — BIOTITE ANALYSES (H2O INPUTTED)

	9	10	11	12	13	14	15	16
SIO2	35.73	34.68	35.71	35.33	35.90	36.19	35.13	35.50
TIO2	1.65	1.63	1.61	1.51	1.63	1.60	1.59	1.56
A2O3	20.55	20.29	20.02	20.19	20.59	20.16	20.31	19.89
FEO	20.51	21.42	21.61	21.32	21.02	21.46	21.59	21.10
MNO	0.06	0.05	0.06	0.06	0.06	0.07	0.05	0.06
MGO	9.48	9.61	9.44	9.21	9.39	9.33	9.55	9.43
CAO	0.03	0.03	0.03	0.04	0.03	0.04	0.02	0.04
BAO	0.0	0.0	0.0	0.0	0.0	0.0	0.0	0.0
NA2O	0.28	0.28	0.24	0.25	0.27	0.23	0.18	0.24
K2O	8.88	8.49	8.83	9.02	8.97	8.73	8.79	8.81
F	0.0	0.0	0.0	0.0	0.0	0.0	0.0	0.0
CL	0.0	0.0	0.0	0.0	0.0	0.0	0.0	0.0
H2O	4.02	3.97	4.01	3.98	4.04	4.04	3.78	3.97
SUM	101.19	100.45	101.56	100.91	101.90	101.85	100.99	100.59
-O= F+CL	0.0	0.0	0.0	0.0	0.0	0.0	0.0	0.0
SUM	101.19	100.45	101.56	100.91	101.90	101.85	100.99	100.59

SI	5.327	*	5.237	*	5.333	*	5.314	*	5.326	*	5.373	*	5.292	*	5.346	*
AL	2.673	8.000	2.763	8.000	2.667	8.000	2.686	8.000	2.674	8.000	2.627	8.000	2.708	8.000	2.654	8.000
AL	0.937	*	0.848	*	0.856	*	0.893	*	0.925	*	0.900	*	0.898	*	0.876	*
TI	0.185	*	0.185	*	0.181	*	0.171	*	0.182	*	0.179	*	0.180	*	0.176	*
FE	2.557	*	2.705	*	2.699	*	2.682	*	2.608	*	2.664	*	2.720	*	2.658	*
MN	0.008	*	0.006	*	0.008	*	0.008	*	0.008	*	0.009	*	0.006	*	0.008	*
MG	2.106	5.793	2.163	5.907	2.101	5.845	2.065	5.818	2.076	5.799	2.065	5.816	2.144	5.949	2.115	5.833
CA	0.005	*	0.005	*	0.005	*	0.006	*	0.005	*	0.006	*	0.003	*	0.006	*
NA	0.081	*	0.082	*	0.069	*	0.073	*	0.078	*	0.066	*	0.053	*	0.069	*
K	1.689	*	1.635	*	1.682	*	1.731	*	1.697	*	1.653	*	1.689	*	1.691	*
BA	0.0	1.774	0.0	1.722	0.0	1.756	0.0	1.810	0.0	1.780	0.0	1.726	0.0	1.745	0.0	1.766
CL	0.0	*	0.0	*	0.0	*	0.0	*	0.0	*	0.0	*	0.0	*	0.0	*
F	0.0	*	0.0	*	0.0	*	0.0	*	0.0	*	0.0	*	0.0	*	0.0	*
H	3.998	3.998	3.999	3.999	3.995	3.995	3.994	3.994	3.998	3.998	4.001	4.001	3.799	3.799	3.984	3.984
O	24.000	*	24.000	*	24.000	*	24.000	*	24.000	*	24.000	*	24.000	*	24.000	*
	MG	45.10		44.37		43.71		43.43		44.26		43.58		44.03		44.25
	FE	54.90		55.63		56.29		56.57		55.74		56.42		55.97		55.75
	F/M	1.217		1.254		1.288		1.303		1.260		1.295		1.271		1.260
	F/FM	0.549		0.556		0.563		0.566		0.557		0.564		0.560		0.558
	A* =	0.171		0.169		0.161		0.163		0.169		0.165		0.165		0.161
	A =	-0.185		-0.153		-0.189		-0.205		-0.190		-0.178		-0.177		-0.193
	M =	0.452		0.444		0.438		0.435		0.443		0.437		0.441		0.443

9	682	AG4-179 BT1	13	924 AG4-179 BT1
10	702	AG4-179 BT2	14	934 AG4-179 BT2
11	722	AG4-179 BT3	15	944 AG4-179 BT3
12	762	AG4-179 BT4	16	AVERAGE

SUPER RECAL BIOTITE ANALYSES (H2O INPUTTED)

	17		18	
SIO2	35.90		35.11	
TIO2	1.65		1.47	
A203	20.37		19.41	
FEO	21.51		20.70	
MNO	0.09		0.03	
MGO	9.62		9.23	
CAO	0.05		0.02	
BAO	0.0		0.0	
NA2O	0.27		0.21	
K2O	8.95		8.66	
F	0.0		0.0	
CL	0.0		0.0	
H2O	4.03		3.91	
SUM	102.43		98.74	
-O= F+CL	0.0		0.0	
SUM	102.43		98.74	

SI	5.314	*	5.380	*
AL	2.686	8.000	2.620	8.000
AL	0.866	*	0.886	*
TI	0.183	*	0.169	*
FE	2.662	*	2.653	*
MN	0.012	*	0.004	*
MG	2.123	5.846	2.108	5.819
CA	0.008	*	0.003	*
NA	0.076	*	0.061	*
K	1.689	*	1.693	*
BA	0.0	1.773	0.0	1.758
CL	0.0	*	0.0	*
F	0.0	*	0.0	*
H	3.976	3.976	3.992	3.992
O	24.000	*	24.000	*
MG		44.25		44.24
FE		55.75		55.76
F/M		1.260		1.260
F/FM		0.557		0.558
A* =		0.163		0.160
A =		-0.188		-0.198
M =		0.444		0.443

17 AVERAGE PLUS SIGMA

18 AVERAGE MINUS SIGMA

SUPER RECAL — BIOTITE ANALYSES (H2O INPUTTED)

	1	2	3	4	5	6	7	8
SIO2	36.53	36.33	36.15	36.02	36.36	35.92	35.97	36.18
TIO2	1.61	1.83	1.85	1.44	1.76	1.66	1.62	1.68
A203	19.59	20.14	20.40	20.47	20.21	20.96	20.85	20.37
FEO	18.66	18.38	18.30	18.72	18.30	18.61	18.46	18.49
MNO	0.20	0.19	0.16	0.17	0.17	0.25	0.22	0.19
MGO	10.60	11.03	11.15	11.23	10.76	11.19	11.33	11.04
CAO	0.04	0.04	0.02	0.06	0.03	0.05	0.08	0.05
BAO	0.0	0.0	0.0	0.0	0.0	0.0	0.0	0.0
NA20	0.28	0.27	0.33	0.30	0.32	0.28	0.32	0.30
K20	8.92	9.13	9.04	8.90	9.07	8.99	9.04	9.01
F	0.0	0.0	0.0	0.0	0.0	0.0	0.0	0.0
CL	0.0	0.0	0.0	0.0	0.0	0.0	0.0	0.0
H20	3.81	3.85	3.85	3.84	3.84	3.87	3.87	3.85
SUM	100.24	101.19	101.25	101.15	100.82	101.78	101.76	101.17
-0= F+CL	0.0	0.0	0.0	0.0	0.0	0.0	0.0	0.0
SUM	100.24	101.19	101.25	101.15	100.82	101.78	101.76	101.17

SI	5.466	*	5.383	*	5.350	*	5.344	*	5.402	*	5.295	*	5.302	*	5.363	*
AL	2.534	8.000	2.617	8.000	2.650	8.000	2.656	8.000	2.598	8.000	2.705	8.000	2.698	8.000	2.637	8.000
AL	0.919	*	0.900	*	0.908	*	0.922	*	0.941	*	0.935	*	0.923	*	0.921	*
TI	0.181	*	0.204	*	0.206	*	0.161	*	0.197	*	0.184	*	0.180	*	0.187	*
FE	2.335	*	2.278	*	2.265	*	2.322	*	2.274	*	2.294	*	2.275	*	2.292	*
MN	0.025	*	0.024	*	0.020	*	0.021	*	0.021	*	0.031	*	0.027	*	0.024	*
MG	2.364	5.825	2.436	5.841	2.460	5.858	2.483	5.910	2.383	5.816	2.458	5.903	2.489	5.895	2.439	5.864
CA	0.006	*	0.006	*	0.003	*	0.010	*	0.005	*	0.008	*	0.013	*	0.007	*
NA	0.081	*	0.078	*	0.095	*	0.086	*	0.092	*	0.080	*	0.091	*	0.086	*
K	1.702	*	1.726	*	1.706	*	1.684	*	1.719	*	1.690	*	1.700	*	1.704	*
BA	0.0	1.790	0.0	1.809	0.0	1.804	0.0	1.780	0.0	1.816	0.0	1.778	0.0	1.804	0.0	1.797
CL	0.0	*	0.0	*	0.0	*	0.0	*	0.0	*	0.0	*	0.0	*	0.0	*
F	0.0	*	0.0	*	0.0	*	0.0	*	0.0	*	0.0	*	0.0	*	0.0	*
H	3.803	3.803	3.806	3.806	3.801	3.801	3.800	3.800	3.806	3.806	3.805	3.805	3.805	3.805	3.804	3.804
O	24.000	*	24.000	*	24.000	*	24.000	*	24.000	*	24.000	*	24.000	*	24.000	*
	MG	50.04		51.42		51.84		51.44		50.94		51.39		51.94		51.29
	FE	49.96		48.58		48.16		48.56		49.06		48.61		48.06		48.71
	F/M	0.998		0.945		0.929		0.944		0.963		0.946		0.925		0.950
	F/FM	0.500		0.486		0.482		0.486		0.491		0.486		0.481		0.487
	A* =	0.157		0.160		0.164		0.165		0.163		0.170		0.168		0.164
	A =	-0.213		-0.214		-0.198		-0.181		-0.210		-0.177		-0.183		-0.196
	M =	0.503		0.517		0.521		0.517		0.512		0.517		0.522		0.516

1 128C AG4-59 2B1
2 142C AG4-59 2B5 W/MUS
3 160C AG4-59 3B1
4 161C AG4-59 3B4
5 164C AG4-59 3B5
6 183C AG4-59 4B1
7 191C AG4-59 4B7
8 AVERAGE

SUPER RECAL — BIOTITE ANALYSES (H2O INPUTTED)

	9		10	
SIO2	36.40		35.97	
TIO2	1.81		1.55	
A2O3	20.80		19.95	
FEO	18.65		18.33	
MNO	0.22		0.16	
MGO	11.29		10.79	
CAO	0.06		0.03	
BAO	0.0		0.0	
NA2O	0.32		0.28	
K2O	9.09		8.94	
F	0.0		0.0	
CL	0.0		0.0	
H2O	3.87		3.83	
SUM	102.52		99.82	
-O= F+CL	0.0		0.0	
SUM	102.52		99.82	
SI	5.327	*	5.400	*
AL	2.673	8.000	2.600	8.000
AL	0.914	*	0.929	*
TI	0.200	*	0.175	*
FE	2.283	*	2.301	*
MN	0.028	*	0.021	*
MG	2.462	5.886	2.415	5.841
CA	0.010	*	0.004	*
NA	0.091	*	0.081	*
K	1.697	*	1.711	*
BA	0.0	1.798	0.0	1.797
CL	0.0	*	0.0	*
F	0.0	*	0.0	*
H	3.775	3.775	3.834	3.834
O	24.000	*	24.000	*
MG	51.59		50.98	
FE	48.41		49.02	
F/M	0.938		0.961	
F/FM	0.484		0.490	
A* =	0.166		0.162	
A =	-0.188		-0.205	
M =	0.519		0.512	

9 AVERAGE PLUS SIGMA

10 AVERAGE MINUS SIGMA

SUPER RECAL — BIOTITE ANALYSES (H2O INPUTTED)

	1	2	3	4	5
SIO2	38.01	37.16	37.58	38.01	37.16
TIO2	1.74	1.70	1.72	1.74	1.70
A203	19.07	19.20	19.13	19.20	19.07
FEO	16.37	15.97	16.17	16.37	15.97
MNO	0.02	0.23	0.13	0.23	0.02
MGO	11.69	12.29	11.99	12.29	11.69
CAO	0.03	0.06	0.04	0.06	0.03
BAO	0.25	0.18	0.21	0.25	0.18
NA2O	0.23	0.26	0.25	0.26	0.23
K2O	8.87	8.84	8.85	8.87	8.84
F	0.59	0.94	0.76	0.94	0.59
CL	0.06	0.08	0.07	0.08	0.06
H2O	3.78	3.59	3.68	3.78	3.59
SUM	100.71	100.50	100.60	102.08	99.13
-O= F+CL	0.26	0.41	0.34	0.41	0.26
SUM	100.45	100.09	100.27	101.67	98.87

SI	5.593	*	5.497	*	5.545	*	5.528	*	5.563	*
AL	2.407	8.000	2.503	8.000	2.455	8.000	2.472	8.000	2.437	8.000
AL	0.900	*	0.843	*	0.872	*	0.818	*	0.927	*
TI	0.193	*	0.189	*	0.191	*	0.190	*	0.191	*
FE	2.015	*	1.976	*	1.995	*	1.991	*	1.999	*
MN	0.002	*	0.029	*	0.016	*	0.028	*	0.003	*
MG	2.564	5.674	2.710	5.746	2.637	5.710	2.664	5.692	2.608	5.729
CA	0.005	*	0.010	*	0.007	*	0.009	*	0.005	*
NA	0.066	*	0.075	*	0.070	*	0.073	*	0.067	*
K	1.665	*	1.668	*	1.666	*	1.645	*	1.688	*
BA	0.014	1.750	0.010	1.762	0.012	1.756	0.014	1.742	0.011	1.770
CL	0.015	*	0.020	*	0.018	*	0.020	*	0.015	*
F	0.275	*	0.440	*	0.357	*	0.432	*	0.279	*
H	3.711	4.000	3.542	4.002	3.627	4.001	3.667	4.119	3.585	3.880
O	24.000	*	24.000	*	24.000	*	24.000	*	24.000	*
	MG	55.97		57.48		56.73		56.88		56.58
	FE	44.03		42.52		43.27		43.12		43.42
	F/M	0.787		0.740		0.763		0.758		0.767
	F/FM	0.440		0.425		0.433		0.431		0.434
	A* =	0.152		0.152		0.152		0.150		0.154
	A =	-0.226		-0.215		-0.220		-0.215		-0.226
	M =	0.560		0.578		0.569		0.572		0.566

1 13B*AG4-3A B1B1
2 18B*B1B4
3 AVERAGE
4 AVERAGE PLUS SIGMA
5 AVERAGE MINUS SIGMA

SUPER RECAL — BIOTITE ANALYSES (H2O INPUTTED)

	1	2	3	4	5
SIO2	35.42	35.61	35.51	35.61	35.42
TIO2	1.55	1.39	1.47	1.55	1.39
A203	19.79	20.24	20.01	20.24	19.79
FEO	23.42	23.34	23.38	23.42	23.34
MNO	0.10	0.07	0.08	0.10	0.07
MGO	7.82	7.33	7.57	7.82	7.33
CAO	0.09	0.04	0.06	0.09	0.04
BAO	0.19	0.22	0.20	0.22	0.19
NA2O	0.34	0.24	0.29	0.34	0.24
K2O	8.54	8.77	8.65	8.77	8.54
F	0.19	0.14	0.16	0.19	0.14
CL	0.01	0.02	0.02	0.02	0.01
H2O	3.87	3.89	3.88	3.89	3.87
SUM	101.33	101.30	101.31	102.26	100.37
-O= F+CL	0.08	0.06	0.07	0.08	0.06
SUM	101.25	101.24	101.24	102.18	100.31

SI	5.358	*	5.383	*	5.370	*	5.339	*	5.402	*
AL	2.642	8.000	2.617	8.000	2.630	8.000	2.661	8.000	2.598	8.000
AL	0.886	*	0.988	*	0.937	*	0.915	*	0.959	*
TI	0.176	*	0.158	*	0.167	*	0.175	*	0.159	*
FE	2.963	*	2.950	*	2.957	*	2.937	*	2.977	*
MN	0.013	*	0.009	*	0.011	*	0.013	*	0.009	*
MG	1.763	5.801	1.651	5.757	1.707	5.779	1.748	5.787	1.666	5.770
CA	0.015	*	0.006	*	0.011	*	0.014	*	0.007	*
NA	0.100	*	0.070	*	0.085	*	0.099	*	0.071	*
K	1.648	*	1.691	*	1.669	*	1.677	*	1.661	*
BA	0.011	1.773	0.013	1.781	0.012	1.777	0.013	1.803	0.011	1.750
CL	0.003	*	0.005	*	0.004	*	0.005	*	0.003	*
F	0.091	*	0.067	*	0.079	*	0.090	*	0.068	*
H	3.905	3.999	3.923	3.995	3.914	3.997	3.891	3.986	3.937	4.007
O	24.000	*	24.000	*	24.000	*	24.000	*	24.000	*
	MG	37.21		35.82		36.52		37.21		35.82
	FE	62.79		64.18		63.48		62.79		64.18
	F/M	1.688		1.792		1.738		1.688		1.792
	F/FM	0.628		0.642		0.635		0.628		0.642
	A* =	0.166		0.172		0.169		0.169		0.170
	A =	-0.176		-0.190		-0.183		-0.184		-0.182
	M =	0.373		0.359		0.366		0.373		0.359

1 53Y*AG5-505
2 58Y*TRV
3 AVERAGE
4 AVERAGE PLUS SIGMA
5 AVERAGE MINUS SIGMA

SUPER RECAL — BIOTITE ANALYSES (H2O INPUTTED)

	1	2	3	4	5	6	7	8
SIO2	35.69	35.39	35.59	34.66	34.64	35.19	35.65	34.74
TIO2	1.71	1.78	1.78	1.94	2.08	1.86	1.99	1.72
A203	19.76	19.44	19.66	20.61	19.91	19.88	20.27	19.48
FEO	22.18	22.90	23.57	22.16	22.92	22.75	23.27	22.22
MNO	0.07	0.07	0.07	0.11	0.12	0.09	0.11	0.07
MGO	8.78	7.79	7.68	7.70	7.17	7.82	8.35	7.30
CAO	0.08	0.07	0.05	0.05	0.07	0.06	0.08	0.05
BAO	0.0	0.0	0.0	0.0	0.0	0.0	0.0	0.0
NA2O	0.30	0.25	0.26	0.30	0.25	0.27	0.30	0.25
K2O	8.93	8.92	8.81	8.87	8.74	8.85	8.93	8.78
F	0.0	0.0	0.0	0.0	0.0	0.0	0.0	0.0
CL	0.0	0.0	0.0	0.0	0.0	0.0	0.0	0.0
H2O	3.99	3.94	3.97	3.94	3.91	3.95	3.98	3.92
SUM	101.49	100.55	101.44	100.34	99.81	100.73	102.92	98.53
-O= F+CL	0.0	0.0	0.0	0.0	0.0	0.0	0.0	0.0
SUM	101.49	100.55	101.44	100.34	99.81	100.73	102.92	98.53

SI	5.355	*	5.382	*	5.372	*	5.267	*	5.312	*	5.338	*	5.299	*	5.379	*
AL	2.645	8.000	2.618	8.000	2.628	8.000	2.733	8.000	2.688	8.000	2.662	8.000	2.701	8.000	2.621	8.000
AL	0.848	*	0.866	*	0.869	*	0.958	*	0.910	*	0.890	*	0.849	*	0.932	*
TI	0.193	*	0.204	*	0.202	*	0.222	*	0.240	*	0.212	*	0.223	*	0.201	*
FE	2.783	*	2.913	*	2.975	*	2.816	*	2.939	*	2.885	*	2.893	*	2.877	*
MN	0.009	*	0.009	*	0.009	*	0.014	*	0.016	*	0.011	*	0.014	*	0.009	*
MG	1.963	5.796	1.766	5.758	1.728	5.783	1.744	5.754	1.639	5.744	1.769	5.767	1.850	5.829	1.684	5.703
CA	0.013	*	0.011	*	0.008	*	0.008	*	0.012	*	0.010	*	0.012	*	0.009	*
NA	0.087	*	0.074	*	0.076	*	0.088	*	0.074	*	0.080	*	0.085	*	0.075	*
K	1.709	*	1.730	*	1.696	*	1.719	*	1.709	*	1.713	*	1.692	*	1.734	*
BA	0.0	1.809	0.0	1.815	0.0	1.780	0.0	1.816	0.0	1.795	0.0	1.803	0.0	1.789	0.0	1.818
CL	0.0	*	0.0	*	0.0	*	0.0	*	0.0	*	0.0	*	0.0	*	0.0	*
F	0.0	*	0.0	*	0.0	*	0.0	*	0.0	*	0.0	*	0.0	*	0.0	*
H	3.993	3.993	3.997	3.997	3.997	3.997	3.994	3.994	4.000	4.000	3.996	3.996	3.944	3.944	4.051	4.051
O	24.000	*	24.000	*	24.000	*	24.000	*	24.000	*	24.000	*	24.000	*	24.000	*
	MG	41.29		37.67		36.67		38.13		35.68		37.91		38.89		36.86
	FE	58.71		62.33		63.33		61.87		64.32		62.09		61.11		63.14
	F/M	1.422		1.654		1.727		1.623		1.803		1.638		1.572		1.713
	F/FM	0.587		0.623		0.633		0.619		0.643		0.621		0.611		0.631
	A* =	0.158		0.158		0.161		0.178		0.171		0.165		0.164		0.166
	A =	-0.208		-0.223		-0.204		-0.192		-0.201		-0.205		-0.192		-0.221
	M =	0.414		0.377		0.367		0.382		0.358		0.380		0.390		0.369

1 AG5-1066+ 3BT4
2 2BT1
3 5BT1
4 5BT2
5 5BT3
6 AVERAGE
7 AVERAGE PLUS SIGMA
8 AVERAGE MINUS SIGMA

SUPER RECAL — BIOTITE ANALYSES (H2O INPUTTED)

	1	2	3	4	5	6	7	8
SIO2	34.81	39.37	35.70	34.73	35.57	36.04	37.75	34.32
TIO2	1.64	1.55	1.59	1.56	1.66	1.60	1.64	1.56
A2O3	20.15	19.22	19.76	18.49	19.49	19.42	19.98	18.86
FEO	20.37	18.55	21.83	23.16	21.57	21.10	22.65	19.54
MNO	-0.04	-0.03	0.0	-0.02	-0.02	-0.02	-0.01	-0.04
MGO	8.92	7.53	8.38	8.44	8.42	8.34	8.79	7.89
CAO	-0.01	-0.01	-0.01	0.01	0.0	-0.00	0.00	-0.01
BAO	-0.27	-0.34	0.05	-0.05	0.03	-0.12	0.04	-0.28
NA2O	0.23	0.17	0.08	0.06	0.27	0.16	0.24	0.08
K2O	8.41	8.43	8.84	8.25	8.71	8.53	8.74	8.31
F	0.29	0.31	0.34	0.22	0.34	0.30	0.34	0.26
CL	0.0	0.0	0.0	0.0	0.0	0.0	0.0	0.0
H2O	3.86	3.85	3.84	3.89	3.84	3.86	3.87	3.84
SUM	98.36	98.60	100.40	98.74	99.88	99.20	104.05	94.34
-O= F+CL	0.12	0.13	0.14	0.09	0.14	0.13	0.14	0.11
SUM	98.24	98.47	100.26	98.65	99.74	99.07	103.91	94.23

SI	5.327	*	5.887	*	5.404	*	5.375	*	5.408	*	5.482	*	5.503	*	5.460	*
AL	2.673	8.000	2.113	8.000	2.596	8.000	2.625	8.000	2.592	8.000	2.518	8.000	2.497	8.000	2.540	8.000
AL	0.961	*	1.274	*	0.929	*	0.747	*	0.900	*	0.964	*	0.935	*	0.996	*
TI	0.189	*	0.174	*	0.181	*	0.182	*	0.190	*	0.183	*	0.180	*	0.186	*
FE	2.607	*	2.320	*	2.763	*	2.998	*	2.743	*	2.684	*	2.761	*	2.600	*
MN	-0.005	*	-0.004	*	0.0	*	-0.003	*	-0.003	*	-0.003	*	-0.001	*	-0.005	*
MG	2.035	5.787	1.678	5.442	1.891	5.764	1.947	5.871	1.908	5.738	1.891	5.719	1.909	5.785	1.870	5.647
CA	-0.002	*	-0.002	*	-0.002	*	0.002	*	0.0	*	-0.001	*	0.001	*	-0.002	*
NA	0.068	*	0.049	*	0.023	*	0.018	*	0.080	*	0.048	*	0.069	*	0.025	*
K	1.642	*	1.608	*	1.707	*	1.629	*	1.689	*	1.655	*	1.626	*	1.687	*
BA	-0.016	1.692	-0.020	1.636	0.003	1.732	-0.003	1.645	0.002	1.771	-0.007	1.695	0.002	1.698	-0.017	1.692
CL	0.0	*	0.0	*	0.0	*	0.0	*	0.0	*	0.0	*	0.0	*	0.0	*
F	0.140	*	0.147	*	0.163	*	0.108	*	0.163	*	0.144	*	0.159	*	0.129	*
H	3.941	4.081	3.840	3.987	3.878	4.040	4.016	4.124	3.895	4.058	3.913	4.058	3.768	3.927	4.072	4.201
O	24.000	*	24.000	*	24.000	*	24.000	*	24.000	*	24.000	*	24.000	*	24.000	*
	MG	43.88		42.02		40.62		39.40		41.05		41.36		40.89		41.88
	FE	56.12		57.98		59.38		60.60		58.95		58.64		59.11		58.12
	F/M	1.279		1.380		1.462		1.538		1.436		1.418		1.445		1.388
	F/FM	0.561		0.580		0.594		0.606		0.589		0.586		0.591		0.581
	A* =	0.177		0.182		0.163		0.150		0.162		0.166		0.162		0.171
	A =	-0.162		-0.219		-0.207		-0.181		-0.204		-0.193		-0.183		-0.205
	M =	0.438		0.420		0.406		0.394		0.410		0.413		0.409		0.418

1 232 AG4-217 RIM
2 24B CORE
3 372 W/GT
4 382 W/GT
5 392 W/BT
6 AVERAGE
7 AVERAGE PLUS SIGMA
8 AVERAGE MINUS SIGMA

SUPER RECAL — BIOTITE ANALYSES (H2O INPUTTED)

	1	2	3	4	5	6	7	8
SIO2	35.01	35.21	34.54	34.70	34.21	34.85	34.56	34.54
TIO2	1.68	1.50	1.90	1.73	1.76	1.41	1.47	1.71
A203	19.38	19.07	18.75	18.60	18.88	18.82	18.46	19.39
FEO	20.47	20.44	21.06	21.34	22.19	20.39	21.26	20.52
MNO	0.02	-0.04	-0.01	0.02	0.0	0.02	0.0	-0.02
MGO	8.34	8.64	8.35	8.65	8.58	8.23	8.27	8.70
CAO	0.01	0.0	0.01	0.0	0.02	-0.01	-0.02	0.0
BAO	-0.03	-0.07	0.06	0.03	-0.01	0.0	0.02	0.07
NA20	0.09	0.14	0.08	0.12	0.06	0.19	0.09	0.07
K20	8.60	8.52	8.45	8.19	8.26	8.60	8.68	8.54
F	0.29	0.42	0.29	0.42	0.26	0.36	0.31	0.32
CL	0.0	0.0	0.0	0.0	0.0	0.0	0.0	0.0
H20	3.86	3.80	3.86	3.79	3.87	3.82	3.85	3.84
SUM	97.72	97.63	97.34	97.59	98.08	96.68	96.95	97.68
-O= F+CL	0.12	0.18	0.12	0.18	0.11	0.15	0.13	0.13
SUM	97.60	97.45	97.22	97.41	97.97	96.53	96.82	97.55

SI	5.411	*	5.444	*	5.384	*	5.397	*	5.316	*	5.452	*	5.420	*	5.351	*
AL	2.589	8.000	2.556	8.000	2.616	8.000	2.603	8.000	2.684	8.000	2.548	8.000	2.580	8.000	2.649	8.000
AL	0.940	*	0.919	*	0.827	*	0.806	*	0.772	*	0.922	*	0.832	*	0.891	*
TI	0.195	*	0.174	*	0.223	*	0.202	*	0.206	*	0.166	*	0.173	*	0.199	*
FE	2.646	*	2.643	*	2.745	*	2.776	*	2.883	*	2.668	*	2.789	*	2.659	*
MN	0.003	*	-0.005	*	-0.001	*	0.003	*	0.0	*	0.003	*	0.0	*	-0.003	*
MG	1.921	5.705	1.991	5.722	1.940	5.734	2.005	5.792	1.987	5.848	1.919	5.677	1.933	5.727	2.009	5.756
CA	0.002	*	0.0	*	0.002	*	0.0	*	0.003	*	-0.002	*	-0.003	*	0.0	*
NA	0.027	*	0.042	*	0.024	*	0.036	*	0.018	*	0.058	*	0.027	*	0.021	*
K	1.695	*	1.680	*	1.680	*	1.625	*	1.637	*	1.716	*	1.736	*	1.688	*
BA	-0.002	1.722	-0.004	1.718	0.004	1.709	0.002	1.663	-0.001	1.658	0.0	1.772	0.001	1.762	0.004	1.713
CL	0.0	*	0.0	*	0.0	*	0.0	*	0.0	*	0.0	*	0.0	*	0.0	*
F	0.142	*	0.205	*	0.143	*	0.207	*	0.128	*	0.178	*	0.154	*	0.157	*
H	3.980	4.121	3.920	4.125	4.013	4.156	3.932	4.139	4.011	4.139	3.987	4.165	4.028	4.182	3.969	4.126
O	24.000	*	24.000	*	24.000	*	24.000	*	24.000	*	24.000	*	24.000	*	24.000	*
	MG	42.04		43.02		41.42		41.92		40.80		41.82		40.94		43.07
	FE	57.96		56.98		58.58		58.08		59.20		58.18		59.06		56.93
	F/M	1.378		1.325		1.414		1.386		1.451		1.391		1.442		1.322
	F/FM	0.580		0.570		0.586		0.581		0.592		0.582		0.591		0.569
	A* =	0.167		0.162		0.158		0.157		0.157		0.160		0.151		0.166
	A =	-0.205		-0.203		-0.205		-0.181		-0.175		-0.224		-0.235		-0.195
	M =	0.421		0.430		0.414		0.419		0.408		0.418		0.409		0.430

1 42A AG4-225++ B1
2 43A B2
3 45B B1
4 52B W/ST
5 53B B3
6 64C B1
7 65C B2
8 67C B4

SUPER RECAL

BIOTITE ANALYSES (H2O INPUTTED)

	9	10	11	12	13	14	15
SIO2	35.15	34.73	35.48	35.16	34.84	35.19	34.50
TIO2	1.62	1.85	1.54	1.74	1.66	1.81	1.51
A203	18.80	18.86	19.35	19.64	19.00	19.35	18.65
FEO	21.16	21.94	20.54	20.37	20.97	21.57	20.37
MNO	-0.05	0.0	-0.01	0.0	-0.01	0.02	-0.03
MGO	8.71	8.92	8.98	8.87	8.60	8.85	8.36
CAO	0.0	0.0	0.0	0.01	0.00	0.01	-0.01
BAO	0.04	0.04	0.04	0.02	0.02	0.06	-0.02
NA20	0.08	0.06	0.25	0.19	0.12	0.18	0.06
K20	8.55	8.07	8.47	8.67	8.47	8.65	8.28
F	0.16	0.34	0.31	0.33	0.32	0.38	0.25
CL	0.0	0.0	0.0	0.0	0.0	0.0	0.0
H20	3.92	3.84	3.85	3.84	3.84	3.88	3.81
SUM	98.14	98.65	98.80	98.84	97.84	99.94	95.74
-O= F+CL	0.07	0.14	0.13	0.14	0.13	0.16	0.11
SUM	98.07	98.51	98.67	98.70	97.71	99.78	95.63

SI	5.425	*	5.350	*	5.422	*	5.375	*	5.396	*	5.352	*	5.441	*
AL	2.575	8.000	2.650	8.000	2.578	8.000	2.625	8.000	2.604	8.000	2.648	8.000	2.559	8.000
AL	0.845	*	0.773	*	0.907	*	0.913	*	0.863	*	0.819	*	0.908	*
TI	0.188	*	0.214	*	0.177	*	0.200	*	0.193	*	0.207	*	0.179	*
FE	2.731	*	2.826	*	2.625	*	2.604	*	2.716	*	2.743	*	2.688	*
MN	-0.007	*	0.0	*	-0.001	*	0.0	*	-0.001	*	0.002	*	-0.004	*
MG	2.004	5.761	2.048	5.862	2.046	5.754	2.021	5.739	1.986	5.757	2.006	5.776	1.965	5.736
CA	0.0	*	0.0	*	0.0	*	0.002	*	0.000	*	0.002	*	-0.001	*
NA	0.024	*	0.018	*	0.074	*	0.056	*	0.036	*	0.052	*	0.018	*
K	1.683	*	1.586	*	1.651	*	1.691	*	1.672	*	1.678	*	1.666	*
BA	0.002	1.710	0.002	1.606	0.002	1.728	0.001	1.750	0.001	1.709	0.003	1.736	-0.001	1.681
CL	0.0	*	0.0	*	0.0	*	0.0	*	0.0	*	0.0	*	0.0	*
F	0.078	*	0.166	*	0.150	*	0.160	*	0.155	*	0.185	*	0.125	*
H	4.036	4.114	3.946	4.112	3.925	4.075	3.916	4.076	3.972	4.127	3.933	4.118	4.012	4.137
O	24.000	*	24.000	*	24.000	*	24.000	*	24.000	*	24.000	*	24.000	*
	MG	42.38		42.02		43.81		43.70		42.24		42.21		42.27
	FE	57.62		57.98		56.19		56.30		57.76		57.79		57.73
	F/M	1.360		1.380		1.283		1.289		1.367		1.369		1.366
	F/FM	0.576		0.580		0.562		0.563		0.578		0.578		0.577
	A* =	0.155		0.159		0.164		0.166		0.160		0.159		0.162
	A =	-0.208		-0.158		-0.187		-0.199		-0.197		-0.198		-0.197
	M =	0.423		0.420		0.438		0.437		0.422		0.422		0.422

9 71C B6
10 78D B1
11 85E W/ST
12 91F B1

13 AVERAGE
14 AVERAGE PLUS SIGMA
15 AVERAGE MINUS SIGMA

SUPER RECAL — BIOTITE ANALYSES (H2O INPUTTED)

	1	2	3	4	5	6
SIO2	34.81	34.71	34.98	34.83	34.94	34.72
TIO2	1.63	1.83	1.68	1.71	1.80	1.63
A203	19.29	19.35	19.20	19.28	19.34	19.22
FEO	20.33	21.42	21.53	21.09	21.63	20.55
MNO	0.06	0.06	0.11	0.08	0.10	0.05
MGO	8.89	8.54	8.89	8.77	8.94	8.61
CAO	0.02	0.03	-0.02	0.01	0.03	-0.01
BAO	0.29	0.39	0.26	0.31	0.37	0.26
NA2O	0.24	0.22	0.19	0.22	0.24	0.20
K2O	8.35	8.08	8.68	8.37	8.62	8.12
F	0.26	0.22	0.24	0.24	0.26	0.22
CL	0.0	0.0	0.0	0.0	0.0	0.0
H2O	3.87	3.89	3.88	3.88	3.89	3.87
SUM	98.04	98.74	99.62	98.80	100.16	97.44
-O= F+CL	0.11	0.09	0.10	0.10	0.11	0.09
SUM	97.93	98.65	99.52	98.70	100.05	97.35

SI	5.373	*	5.342	*	5.350	*	5.355	*	5.322	*	5.388	*
AL	2.627	8.000	2.658	8.000	2.650	8.000	2.645	8.000	2.678	8.000	2.612	8.000
AL	0.881	*	0.850	*	0.811	*	0.847	*	0.794	*	0.902	*
TI	0.189	*	0.212	*	0.193	*	0.198	*	0.206	*	0.190	*
FE	2.624	*	2.757	*	2.754	*	2.712	*	2.756	*	2.667	*
MN	0.008	*	0.008	*	0.014	*	0.010	*	0.013	*	0.007	*
MG	2.045	5.747	1.959	5.786	2.027	5.799	2.010	5.777	2.029	5.798	1.991	5.757
CA	0.003	*	0.005	*	-0.003	*	0.002	*	0.005	*	-0.002	*
NA	0.072	*	0.066	*	0.056	*	0.065	*	0.070	*	0.059	*
K	1.644	*	1.586	*	1.693	*	1.641	*	1.674	*	1.608	*
BA	0.018	1.736	0.024	1.680	0.016	1.762	0.019	1.726	0.022	1.771	0.016	1.681
CL	0.0	*	0.0	*	0.0	*	0.0	*	0.0	*	0.0	*
F	0.127	*	0.107	*	0.116	*	0.117	*	0.123	*	0.110	*
H	3.985	4.111	3.993	4.100	3.959	4.075	3.979	4.096	3.950	4.074	4.008	4.118
O	24.000	*	24.000	*	24.000	*	24.000	*	24.000	*	24.000	*
	MG	43.73		41.47		42.27		42.48		42.29		42.68
	FE	56.27		58.53		57.73		57.52		57.71		57.32
	F/M	1.287		1.411		1.366		1.354		1.364		1.343
	F/FM	0.563		0.585		0.577		0.575		0.577		0.573
	A* =	0.166		0.169		0.156		0.164		0.158		0.170
	A =	-0.180		-0.153		-0.204		-0.179		-0.193		-0.164
	M =	0.438		0.415		0.424		0.426		0.424		0.427

1 2173 AG5-523 W/GT
2 2244 B1
3 2254 B2
4 AVERAGE
5 AVERAGE PLUS SIGMA
6 AVERAGE MINUS SIGMA

SUPER RECAL — BIOTITE ANALYSES (H2O INPUTTED)

	1	2	3	4	5	6
SIO2	37.00	36.87	37.21	37.03	37.17	36.89
TIO2	1.32	1.30	1.30	1.31	1.32	1.30
A203	18.43	18.80	19.30	18.84	19.20	18.49
FEO	13.95	14.06	14.07	14.03	14.08	13.97
MNO	0.11	0.08	0.08	0.09	0.10	0.08
MGO	13.98	14.25	13.99	14.07	14.20	13.95
CAO	-0.01	-0.02	-0.02	-0.02	-0.01	-0.02
BAO	0.08	0.37	0.38	0.28	0.42	0.14
NA2O	0.23	0.19	0.28	0.23	0.27	0.20
K2O	8.73	8.64	8.76	8.71	8.76	8.66
F	0.59	0.59	0.54	0.57	0.60	0.55
CL	0.0	0.0	0.0	0.0	0.0	0.0
H2O	3.72	3.72	3.75	3.73	3.74	3.72
SUM	98.13	98.85	99.64	98.87	99.84	97.90
-O= F+CL	0.25	0.25	0.23	0.24	0.25	0.23
SUM	97.88	98.60	99.41	98.63	99.59	97.67

SI	5.539	*	5.491	*	5.494	*	5.508	*	5.482	*	5.534	*
AL	2.461	8.000	2.509	8.000	2.506	8.000	2.492	8.000	2.518	8.000	2.466	8.000
AL	0.790	*	0.790	*	0.852	*	0.811	*	0.819	*	0.803	*
TI	0.149	*	0.146	*	0.144	*	0.146	*	0.146	*	0.146	*
FE	1.746	*	1.751	*	1.737	*	1.745	*	1.737	*	1.753	*
MN	0.014	*	0.010	*	0.010	*	0.011	*	0.013	*	0.010	*
MG	3.119	5.818	3.163	5.859	3.079	5.823	3.120	5.833	3.121	5.836	3.119	5.831
CA	-0.002	*	-0.003	*	-0.003	*	-0.003	*	-0.002	*	-0.003	*
NA	0.067	*	0.055	*	0.080	*	0.067	*	0.077	*	0.057	*
K	1.667	*	1.641	*	1.650	*	1.653	*	1.648	*	1.657	*
BA	0.005	1.737	0.022	1.714	0.022	1.749	0.016	1.733	0.024	1.748	0.008	1.719
CL	0.0	*	0.0	*	0.0	*	0.0	*	0.0	*	0.0	*
F	0.279	*	0.278	*	0.252	*	0.270	*	0.278	*	0.261	*
H	3.715	3.994	3.695	3.973	3.694	3.946	3.701	3.971	3.684	3.962	3.719	3.980
O	24.000	*	24.000	*	24.000	*	24.000	*	24.000	*	24.000	*
	MG	63.92		64.23		63.79		63.99		64.08		63.89
	FE	36.08		35.76		36.21		36.01		35.92		36.11
	F/M	0.564		0.557		0.568		0.563		0.561		0.565
	F/FM	0.361		0.358		0.362		0.360		0.359		0.361
	A* =	0.140		0.144		0.151		0.145		0.148		0.142
	A =	-0.219		-0.198		-0.198		-0.205		-0.198		-0.212
	M =	0.641		0.644		0.639		0.641		0.642		0.640

1 2635 AG5-268+ BT1
2 2645 BT2
3 2655 BT3
4 AVERAGE
5 AVERAGE PLUS SIGMA
6 AVERAGE MINUS SIGMA

BIOTITE ANALYSES (H2O INPUTTED)

SUPER RECAL	1	2	3	4	5	6	7
SIO2	37.00	36.87	37.43	37.44	37.18	37.44	36.93
TIO2	1.51	1.38	1.39	1.52	1.45	1.52	1.38
A2O3	18.74	18.81	19.19	19.52	19.07	19.38	18.75
FEO	13.30	12.61	13.53	13.14	13.14	13.48	12.81
MNO	0.08	0.09	0.09	0.10	0.09	0.10	0.08
MGO	13.49	14.19	14.18	14.20	14.01	14.32	13.71
CAO	0.0	0.0	0.01	-0.03	-0.00	0.01	-0.02
BAO	0.30	0.08	0.15	0.32	0.21	0.31	0.11
NA2O	0.24	0.26	0.29	0.26	0.26	0.28	0.24
K2O	8.67	8.43	8.72	8.61	8.61	8.72	8.50
F	0.32	0.16	0.39	0.20	0.27	0.36	0.18
CL	0.0	0.0	0.0	0.0	0.0	0.0	0.0
H2O	3.85	3.92	3.82	3.91	3.88	3.92	3.83
SUM	97.50	96.80	99.19	99.19	98.17	99.83	96.51
-O= F+CL	0.13	0.07	0.16	0.08	0.11	0.15	0.07
SUM	97.37	96.73	99.03	99.11	98.06	99.68	96.44

SI	5.552	*	5.536	*	5.522	*	5.509	*	5.530	*	5.488	*	5.572	*
AL	2.448	8.000	2.464	8.000	2.478	8.000	2.491	8.000	2.470	8.000	2.512	8.000	2.428	8.000
AL	0.866	*	0.864	*	0.858	*	0.893	*	0.870	*	0.836	*	0.906	*
TI	0.170	*	0.156	*	0.154	*	0.168	*	0.162	*	0.167	*	0.157	*
FE	1.669	*	1.583	*	1.669	*	1.617	*	1.635	*	1.653	*	1.616	*
MN	0.010	*	0.011	*	0.011	*	0.012	*	0.011	*	0.012	*	0.011	*
MG	3.017	5.733	3.176	5.791	3.118	5.811	3.114	5.805	3.106	5.785	3.128	5.796	3.084	5.774
CA	0.0	*	0.0	*	0.002	*	-0.005	*	-0.001	*	0.002	*	-0.003	*
NA	0.070	*	0.076	*	0.083	*	0.074	*	0.076	*	0.080	*	0.072	*
K	1.659	*	1.614	*	1.641	*	1.616	*	1.633	*	1.630	*	1.635	*
BA	0.018	1.747	0.005	1.695	0.009	1.734	0.018	1.704	0.012	1.720	0.018	1.729	0.007	1.710
CL	0.0	*	0.0	*	0.0	*	0.0	*	0.0	*	0.0	*	0.0	*
F	0.152	*	0.076	*	0.182	*	0.093	*	0.126	*	0.167	*	0.084	*
H	3.854	4.006	3.926	4.002	3.759	3.941	3.838	3.931	3.844	3.970	3.830	3.997	3.858	3.942
O	24.000	*	24.000	*	24.000	*	24.000	*	24.000	*	24.000	*	24.000	*
	MG	64.24		66.57		64.98		65.65		65.36		65.26		65.47
	FE	35.76		33.43		35.02		34.35		34.64		34.74		34.53
	F/M	0.557		0.502		0.539		0.523		0.530		0.532		0.527
	F/FM	0.358		0.334		0.350		0.343		0.346		0.347		0.345
	A* =	0.150		0.153		0.150		0.158		0.153		0.152		0.153
	A =	-0.216		-0.189		-0.199		-0.183		-0.196		-0.192		-0.201
	M =	0.644		0.667		0.651		0.658		0.655		0.654		0.656

1 236B AG4-2A BT1
2 237B W/GT
3 241B W/PL
4 242C W/GT

5 AVERAGE
6 AVERAGE PLUS SIGMA
7 AVERAGE MINUS SIGMA

SUPER RECAL	1
SIO2	37.72
TIO2	1.31
A2O3	19.32
FEO	16.94
MNO	0.07
MGO	12.87
CAO	0.02
BAO	0.18
NA2O	0.33
K2O	8.49
F	0.86
CL	0.07
H2O	3.69
SUM	101.87
-O= F+CL	0.38
SUM	101.49

SI	5.502	*	
AL	2.498	8.000	
AL	0.823	*	
TI	0.144	*	
FE	2.066	*	
MN	0.009	*	
MG	2.798	5.840	
CA	0.003	*	
NA	0.093	*	
K	1.580	*	
BA	0.010	1.686	
CL	0.017	*	
F	0.397	*	
H	3.591	4.005	
O	24.000	*	
	MG	57.42	
	FE	42.58	
	F/M	0.742	
	F/FM	0.426	
	A* =	0.152	
	A =	-0.171	
	M =	0.575	

1 35X*AG4-6 W/GT

SUPER RECAL — GARNET ANALYSES

	1	2	3	4	5	6
SIO2	38.17	37.84	38.23	38.08	38.25	37.91
TIO2	0.14	0.17	0.13	0.15	0.16	0.13
A203	20.88	20.54	20.93	20.78	20.96	20.61
FEO	29.39	28.03	28.38	28.60	29.18	28.02
MNO	7.59	8.76	9.51	8.62	9.41	7.83
MGO	3.09	2.79	3.11	3.00	3.14	2.85
CAO	3.40	2.87	2.43	2.90	3.30	2.50
BAO	0.0	0.0	0.0	0.0	0.0	0.0
NA2O	0.01	0.03	0.02	0.02	0.03	0.01
K2O	0.04	0.03	0.02	0.03	0.04	0.02
F	0.0	0.0	0.0	0.0	0.0	0.0
CL	0.0	0.0	0.0	0.0	0.0	0.0
SUM	102.71	101.06	102.76	102.18	104.46	99.89
-O= F+CL	0.0	0.0	0.0	0.0	0.0	0.0
SUM	102.71	101.06	102.76	102.18	104.46	99.89

SI	2.998	*	3.019	*	3.004	*	3.007	*	2.972	*	3.043	*
TI	0.008	*	0.010	*	0.008	*	0.009	*	0.010	*	0.008	*
AL	0.0	3.007	0.0	3.029	0.0	3.012	0.0	3.016	0.018	3.000	0.0	3.051
AL	1.933	*	1.931	*	1.938	*	1.934	*	1.900	*	1.950	*
FE	0.067	2.000	0.069	2.000	0.062	2.000	0.066	2.000	0.100	2.000	0.050	2.000
FE	1.864	*	1.802	*	1.803	*	1.823	*	1.796	*	1.831	*
MG	0.362	*	0.332	*	0.364	*	0.353	*	0.364	*	0.341	*
MN	0.505	*	0.592	*	0.633	*	0.577	*	0.619	*	0.532	*
CA	0.286	*	0.245	*	0.205	*	0.245	*	0.274	*	0.215	*
NA	0.002	*	0.005	*	0.003	*	0.003	*	0.004	*	0.002	*
K	0.004	3.022	0.003	2.978	0.002	3.009	0.003	3.003	0.004	3.062	0.002	2.924
O	12.000	*	12.000	*	12.000	*	12.000	*	12.000	*	12.000	*
	AL	62.61		61.53		60.81		61.66		60.12		63.34
	PY	11.73		10.92		11.88		11.51		11.54		11.48
	SP	16.38		19.48		20.64		18.82		19.64		17.93
	GR	9.28		8.07		6.67		8.01		8.70		7.25
	F/M	6.547		7.214		6.687		6.802		6.636		6.930
	F/FM	0.867		0.878		0.870		0.872		0.869		0.874
	A* =	0.296		0.305		0.303		0.301		0.298		0.305
	A =	0.295		0.304		0.302		0.300		0.297		0.304
	M =	0.158		0.151		0.163		0.157		0.161		0.153

1 151R AG4-59
2 152R AG4-59
3 153R AG4-59

4 AVERAGE
5 AVERAGE PLUS SIGMA
6 AVERAGE MINUS SIGMA

SUPER RECAL — GARNET ANALYSES

	1	2	3	4	5
SIO2	38.30	39.55	38.93	39.55	38.30
TIO2	0.13	0.15	0.14	0.15	0.13
A203	21.35	21.51	21.43	21.51	21.35
FEO	30.57	30.36	30.46	30.57	30.36
MNO	5.54	5.57	5.55	5.57	5.54
MGO	3.02	3.00	3.01	3.02	3.00
CAO	3.81	3.77	3.79	3.81	3.77
BAO	0.0	0.0	0.0	0.0	0.0
NA2O	0.04	0.03	0.03	0.04	0.03
K2O	0.03	0.03	0.03	0.03	0.03
F	0.0	0.0	0.0	0.0	0.0
CL	0.0	0.0	0.0	0.0	0.0
SUM	102.79	103.97	103.38	104.25	102.51
-O= F+CL	0.0	0.0	0.0	0.0	0.0
SUM	102.79	103.97	103.38	104.25	102.51

SI	2.995	*	3.042	*	3.019	*	3.037	*	3.000	*
TI	0.008	*	0.009	*	0.008	*	0.009	*	0.008	*
AL	0.0	3.003	0.0	3.050	0.0	3.027	0.0	3.045	0.0	3.008
AL	1.967	*	1.949	*	1.958	*	1.946	*	1.971	*
FE	0.033	2.000	0.051	2.000	0.042	2.000	0.054	2.000	0.029	2.000
FE	1.967	*	1.902	*	1.934	*	1.909	*	1.960	*
MG	0.352	*	0.344	*	0.348	*	0.346	*	0.350	*
MN	0.367	*	0.363	*	0.365	*	0.362	*	0.368	*
CA	0.319	*	0.311	*	0.315	*	0.313	*	0.316	*
NA	0.006	*	0.004	*	0.005	*	0.006	*	0.005	*
K	0.003	3.014	0.003	2.927	0.003	2.970	0.003	2.939	0.003	3.002
O	12.000	*	12.000	*	12.000	*	12.000	*	12.000	*
	AL	65.82		65.75		65.78		65.78		65.79
	PY	11.59		11.58		11.58		11.58		11.59
	SP	12.08		12.22		12.15		12.14		12.16
	GR	10.51		10.46		10.48		10.50		10.47
	F/M	6.630		6.586		6.608		6.572		6.644
	F/FM	0.869		0.868		0.869		0.868		0.869
	A* =	0.295		0.298		0.296		0.296		0.296
	A =	0.294		0.297		0.296		0.296		0.295
	M =	0.150		0.150		0.150		0.150		0.150

1 169C AG4-59 CORE
2 116C AG4-59 CORE
3 AVERAGE
4 AVERAGE PLUS SIGMA
5 AVERAGE MINUS SIGMA

SUPER RECAL — GARNET ANALYSES

	1	2	3	4	5
SIO2	38.16	38.32	38.24	38.32	38.16
TIO2	0.11	0.09	0.10	0.11	0.09
A203	20.74	21.07	20.90	21.07	20.74
FEO	33.89	33.91	33.90	33.91	33.89
MNO	4.89	4.85	4.87	4.89	4.85
MGO	2.19	2.14	2.16	2.19	2.14
CAO	1.97	1.97	1.97	1.97	1.97
BAO	0.0	0.0	0.0	0.0	0.0
NA2O	0.04	0.08	0.06	0.08	0.04
K2O	0.03	0.04	0.03	0.04	0.03
F	0.0	0.0	0.0	0.0	0.0
CL	0.0	0.0	0.0	0.0	0.0
SUM	102.02	102.47	102.24	102.58	101.91
-O= F+CL	0.0	0.0	0.0	0.0	0.0
SUM	102.02	102.47	102.24	102.58	101.91

SI	3.031	*	3.027	*	3.029	*	3.024	*	3.034	*
TI	0.007	*	0.005	*	0.006	*	0.007	*	0.005	*
AL	0.0	3.038	0.0	3.033	0.0	3.035	0.0	3.031	0.0	3.039
AL	1.941	*	1.961	*	1.951	*	1.960	*	1.943	*
FE	0.059	2.000	0.039	2.000	0.049	2.000	0.040	2.000	0.057	2.000
FE	2.192	*	2.202	*	2.197	*	2.198	*	2.196	*
MG	0.259	*	0.252	*	0.256	*	0.258	*	0.254	*
MN	0.329	*	0.325	*	0.327	*	0.327	*	0.327	*
CA	0.168	*	0.167	*	0.167	*	0.167	*	0.168	*
NA	0.006	*	0.012	*	0.009	*	0.012	*	0.006	*
K	0.003	2.958	0.004	2.961	0.004	2.959	0.004	2.965	0.003	2.954
O	12.000	*	12.000	*	12.000	*	12.000	*	12.000	*
	AL	74.86		75.09		74.98		74.87		75.08
	PY	8.62		8.45		8.53		8.62		8.45
	SP	10.94		10.88		10.91		10.94		10.88
	GR	5.58		5.59		5.58		5.57		5.59
	F/M	9.725		10.025		9.873		9.800		9.949
	F/FM	0.907		0.909		0.908		0.907		0.909
	A* =	0.279		0.282		0.280		0.282		0.279
	A =	0.278		0.281		0.280		0.281		0.278
	M =	0.103		0.101		0.102		0.103		0.101

1 3GC1 AG5-1066+
2 6GC2 AG5-1066+
3 AVERAGE
4 AVERAGE PLUS SIGMA
5 AVERAGE MINUS SIGMA

SUPER RECAL — GARNET ANALYSES

	1	2	3	4	5	6	7
SIO2	37.65	37.50	37.41	37.61	37.54	37.64	37.45
TIO2	0.11	0.15	0.13	0.13	0.13	0.14	0.12
A203	21.39	21.57	21.45	21.26	21.42	21.53	21.31
FEO	36.21	35.59	35.99	34.41	35.55	36.24	34.86
MNO	2.68	2.92	2.83	2.93	2.84	2.94	2.74
MGO	2.51	2.62	2.33	2.59	2.51	2.63	2.40
CAO	0.53	0.76	0.56	1.35	0.80	1.13	0.47
BAO	0.03	-0.08	-0.02	-0.06	-0.03	0.01	-0.07
NA20	0.0	0.03	0.01	0.01	0.01	0.02	0.00
K20	-0.02	-0.01	-0.01	-0.02	-0.02	-0.01	-0.02
F	-0.02	0.02	0.05	-0.01	0.01	0.04	-0.02
CL	0.0	0.0	0.0	0.0	0.0	0.0	0.0
SUM	101.06	101.13	100.70	100.27	100.79	102.26	99.32
-O= F+CL	0.0	0.0	0.0	0.0	0.0	0.0	0.0
SUM	101.06	101.13	100.70	100.27	100.79	102.26	99.32

SI	3.010	*	2.993	*	3.001	*	3.018	*	3.005	*	2.980	*	3.031	*
TI	0.007	*	0.009	*	0.008	*	0.008	*	0.008	*	0.009	*	0.007	*
AL	0.0	3.017	0.0	3.002	0.0	3.009	0.0	3.026	0.0	3.013	0.011	3.000	0.0	3.038
AL	2.015	*	2.028	*	2.028	*	2.010	*	2.020	*	1.997	*	2.032	*
FE	0.0	2.015	0.0	2.028	0.0	2.028	0.0	2.010	0.0	2.020	0.003	2.000	0.0	2.032
FE	2.421	*	2.375	*	2.414	*	2.309	*	2.380	*	2.397	*	2.359	*
MG	0.299	*	0.312	*	0.279	*	0.310	*	0.300	*	0.310	*	0.290	*
MN	0.181	*	0.197	*	0.192	*	0.199	*	0.193	*	0.197	*	0.188	*
CA	0.045	*	0.065	*	0.048	*	0.116	*	0.069	*	0.096	*	0.041	*
NA	0.0	*	0.005	*	0.002	*	0.002	*	0.002	*	0.004	*	0.000	*
K	-0.002	2.945	-0.001	2.953	-0.001	2.934	-0.002	2.933	-0.002	2.941	-0.001	3.003	-0.002	2.876
O	12.000	*	12.000	*	12.000	*	12.000	*	12.000	*	12.000	*	12.000	*
	AL	82.15		80.54		82.31		78.70		80.93		79.92		81.99
	PY	10.15		10.57		9.50		10.56		10.19		10.32		10.06
	SP	6.16		6.69		6.55		6.79		6.55		6.57		6.53
	GR	1.54		2.20		1.64		3.96		2.33		3.19		1.42
	F/M	8.701		8.255		9.357		8.097		8.581		8.374		8.798
	F/FM	0.897		0.892		0.903		0.890		0.896		0.893		0.898
	A* =	0.271		0.274		0.274		0.278		0.274		0.271		0.277
	A =	0.271		0.274		0.274		0.278		0.274		0.271		0.278
	M =	0.110		0.116		0.103		0.118		0.112		0.114		0.109

1 402 AG4-225++
2 41A 225++
3 95G 225++
4 96G 225++

5 AVERAGE
6 AVERAGE PLUS SIGMA
7 AVERAGE MINUS SIGMA

SUPER RECAL — GARNET ANALYSES

	1	2	3	4	5	6	7
SIO2	37.99	38.52	37.86	37.88	38.06	38.33	37.79
TIO2	0.15	0.16	0.14	0.17	0.15	0.17	0.14
A2O3	21.27	21.45	20.64	20.74	21.02	21.37	20.68
FEO	36.89	36.72	36.51	36.41	36.63	36.82	36.45
MNO	0.65	0.61	0.59	0.79	0.66	0.74	0.58
MGO	2.31	2.34	2.26	2.40	2.33	2.38	2.28
CAO	3.38	3.54	2.63	3.28	3.21	3.55	2.86
BAO	0.0	0.0	0.0	0.0	0.0	0.0	0.0
NA2O	0.03	0.06	0.06	0.02	0.04	0.06	0.02
K2O	0.03	0.04	0.03	0.03	0.03	0.04	0.03
F	0.0	0.0	0.0	0.0	0.0	0.0	0.0
CL	0.0	0.0	0.0	0.0	0.0	0.0	0.0
SUM	102.70	103.44	100.72	101.72	102.14	103.45	100.84
-O= F+CL	0.0	0.0	0.0	0.0	0.0	0.0	0.0
SUM	102.70	103.44	100.72	101.72	102.14	103.45	100.84

SI	2.993	*	3.006	*	3.034	*	3.012	*	3.011	*	2.996	*	3.027	*
TI	0.009	*	0.009	*	0.008	*	0.010	*	0.009	*	0.010	*	0.009	*
AL	0.0	3.002	0.0	3.015	0.0	3.043	0.0	3.022	0.0	3.020	0.0	3.005	0.0	3.035
AL	1.974	*	1.972	*	1.949	*	1.943	*	1.960	*	1.968	*	1.952	*
FE	0.026	2.000	0.028	2.000	0.051	2.000	0.057	2.000	0.040	2.000	0.032	2.000	0.048	2.000
FE	2.405	*	2.368	*	2.397	*	2.364	*	2.383	*	2.374	*	2.393	*
MG	0.271	*	0.272	*	0.270	*	0.284	*	0.274	*	0.277	*	0.272	*
MN	0.043	*	0.040	*	0.040	*	0.053	*	0.044	*	0.049	*	0.039	*
CA	0.285	*	0.296	*	0.226	*	0.279	*	0.272	*	0.298	*	0.246	*
NA	0.005	*	0.009	*	0.009	*	0.003	*	0.007	*	0.009	*	0.004	*
K	0.003	3.012	0.004	2.990	0.003	2.945	0.003	2.987	0.003	2.984	0.004	3.011	0.003	2.956
O	12.000	*	12.000	*	12.000	*	12.000	*	12.000	*	12.000	*	12.000	*
AL	80.20		79.75		82.04		79.69		80.41		79.42		81.43	
PY	8.95		9.06		9.05		9.36		9.11		9.14		9.07	
SP	1.43		1.34		1.34		1.75		1.47		1.61		1.32	
GR	9.41		9.85		7.57		9.20		9.02		9.82		8.19	
F/M	9.026		8.850		9.025		8.499		8.846		8.747		8.949	
F/FM	0.900		0.898		0.900		0.895		0.898		0.897		0.899	
A* =	0.267		0.269		0.264		0.264		0.266		0.268		0.264	
A =	0.267		0.269		0.263		0.263		0.265		0.267		0.264	
M =	0.100		0.102		0.099		0.105		0.102		0.103		0.100	

1 97 AG4-179
2 127 AG4-179
3 199 AG4-179
4 553 AG4-179

5 AVERAGE
6 AVERAGE PLUS SIGMA
7 AVERAGE MINUS SIGMA

SUPER RECAL — GARNET ANALYSES

	1	2	3	4	5	6	7	8	9
SIO2	38.06	37.23	37.35	37.84	37.02	37.70	37.53	37.90	37.17
TIO2	0.12	0.12	0.11	0.12	0.12	0.18	0.13	0.15	0.10
A203	21.33	21.26	20.91	21.04	21.14	21.46	21.19	21.37	21.01
FEO	33.19	32.71	32.46	33.05	32.46	32.84	32.79	33.06	32.51
MNO	6.51	6.41	6.33	6.16	6.37	5.75	6.25	6.50	6.01
MGO	2.13	2.31	2.35	2.03	2.19	2.38	2.23	2.36	2.11
CAO	1.16	1.47	1.16	1.50	1.52	1.58	1.40	1.57	1.23
BAO	0.20	0.0	0.22	0.01	0.28	0.19	0.15	0.26	0.04
NA2O	-0.01	-0.04	-0.02	-0.05	-0.02	0.01	-0.02	-0.00	-0.04
K2O	-0.02	-0.02	-0.02	-0.02	-0.02	-0.01	-0.02	-0.01	-0.02
F	0.04	0.05	-0.01	0.01	0.08	0.07	0.04	0.07	0.01
CL	0.0	0.0	0.0	0.0	0.0	0.0	0.0	0.0	0.0
SUM	102.47	101.45	100.63	101.67	100.78	101.89	101.48	102.90	100.07
-O= F+CL	0.0	0.0	0.0	0.0	0.0	0.0	0.0	0.0	0.0
SUM	102.47	101.45	100.63	101.67	100.78	101.89	101.48	102.90	100.07

SI	3.010	*	2.977	*	3.007	*	3.017	*	2.979	*	2.990	*	2.997	*	2.987	*	3.007	*
TI	0.007	*	0.007	*	0.007	*	0.007	*	0.007	*	0.011	*	0.008	*	0.009	*	0.006	*
AL	0.0	3.017	0.016	3.000	0.0	3.014	0.0	3.024	0.014	3.000	0.0	3.001	0.0	3.004	0.004	3.000	0.0	3.014
AL	1.988	*	1.988	*	1.984	*	1.977	*	1.991	*	2.006	*	1.994	*	1.980	*	2.003	*
FE	0.012	2.000	0.012	2.000	0.016	2.000	0.023	2.000	0.009	2.000	0.0	2.006	0.006	2.000	0.020	2.000	0.0	2.003
FE	2.183	*	2.175	*	2.169	*	2.180	*	2.175	*	2.178	*	2.183	*	2.159	*	2.199	*
MG	0.251	*	0.275	*	0.282	*	0.241	*	0.263	*	0.281	*	0.266	*	0.277	*	0.254	*
MN	0.436	*	0.434	*	0.432	*	0.416	*	0.434	*	0.386	*	0.423	*	0.434	*	0.412	*
CA	0.098	*	0.126	*	0.100	*	0.128	*	0.131	*	0.134	*	0.120	*	0.133	*	0.106	*
NA	-0.002	*	-0.006	*	-0.003	*	-0.008	*	-0.003	*	0.002	*	-0.003	*	-0.000	*	-0.006	*
K	-0.002	2.964	-0.002	3.002	-0.002	2.978	-0.002	2.956	-0.002	2.998	-0.001	2.981	-0.002	2.986	-0.001	3.001	-0.002	2.963
O	12.000	*	12.000	*	12.000	*	12.000	*	12.000	*	12.000	*	12.000	*	12.000	*	12.000	*
	AL	73.65		72.36		72.87		73.73		72.52		73.09		73.04		72.09		74.02
	PY	8.42		9.11		9.40		8.07		8.72		9.44		8.86		9.16		8.55
	SP	14.63		14.36		14.39		13.92		14.41		12.96		14.11		14.36		13.85
	GR	3.30		4.17		3.34		4.29		4.35		4.51		3.99		4.39		3.58
	F/M	10.430		9.477		9.223		10.763		9.934		9.115		9.811		9.365		10.282
	F/FM	0.913		0.905		0.902		0.915		0.909		0.901		0.908		0.904		0.911
	A* =	0.289		0.289		0.287		0.288		0.291		0.290		0.289		0.288		0.290
	A =	0.290		0.290		0.287		0.289		0.291		0.290		0.289		0.288		0.291
	M =	0.103		0.112		0.114		0.099		0.107		0.114		0.108		0.113		0.104

1 2045 AG5-523
2 2051 AG5-523
3 2112 AG5-523
4 2143 AG5-523
5 2224 AG5-523
6 2234 AG5-523
7 AVERAGE
8 AVERAGE PLUS SIGMA
9 AVERAGE MINUS SIGMA

SUPER RECAL — GARNET ANALYSES

	1	2	3	4	5
SIO2	38.76	38.46	38.61	38.76	38.46
TIO2	0.12	0.13	0.13	0.13	0.12
A203	21.53	20.71	21.12	21.53	20.71
FEO	25.04	25.46	25.25	25.46	25.04
MNO	9.67	9.67	9.67	9.67	9.67
MGO	3.58	3.67	3.63	3.67	3.58
CAO	2.01	2.07	2.04	2.07	2.01
BAO	0.21	0.09	0.15	0.21	0.09
NA20	-0.02	0.0	-0.01	-0.00	-0.02
K20	-0.02	0.0	-0.01	-0.00	-0.02
F	-0.01	0.09	0.04	0.09	-0.01
CL	0.0	0.0	0.0	0.0	0.0
SUM	100.67	100.17	100.42	101.29	99.55
-O= F+CL	0.0	0.0	0.0	0.0	0.0
SUM	100.67	100.17	100.42	101.29	99.55

SI	3.053	*	3.055	*	3.054	*	3.038	*	3.071	*
TI	0.007	*	0.008	*	0.007	*	0.008	*	0.007	*
AL	0.0	3.060	0.0	3.063	0.0	3.062	0.0	3.046	0.0	3.078
AL	1.998	*	1.939	*	1.969	*	1.989	*	1.949	*
FE	0.002	2.000	0.061	2.000	0.031	2.000	0.011	2.000	0.051	2.000
FE	1.648	*	1.630	*	1.639	*	1.657	*	1.621	*
MG	0.420	*	0.435	*	0.427	*	0.429	*	0.426	*
MN	0.645	*	0.651	*	0.648	*	0.642	*	0.654	*
CA	0.170	*	0.176	*	0.173	*	0.174	*	0.172	*
NA	-0.003	*	0.0	*	-0.002	*	-0.000	*	-0.003	*
K	-0.002	2.878	0.0	2.892	-0.001	2.885	-0.000	2.902	-0.002	2.867
O	12.000	*	12.000	*	12.000	*	12.000	*	12.000	*

AL	57.18	57.28	57.23	57.28	57.18
PY	14.57	14.72	14.64	14.72	14.57
SP	22.37	22.04	22.20	22.04	22.37
GR	5.88	5.97	5.92	5.97	5.88
F/M	5.456	5.249	5.351	5.363	5.339
F/FM	0.845	0.840	0.843	0.843	0.842
A* =	0.326	0.313	0.320	0.322	0.317
A =	0.326	0.313	0.320	0.322	0.318
M =	0.203	0.204	0.204	0.204	0.203

1 238B AG4-2A
2 243C AG4-2A
3 AVERAGE
4 AVERAGE PLUS SIGMA
5 AVERAGE MINUS SIGMA

SUPER RECAL — GARNET ANALYSES

	1	2	3	4
SIO2	38.04	37.73	37.13	37.99
TIO2	0.12	0.15	0.19	0.15
A203	21.00	21.19	21.14	21.21
FEO	36.14	34.49	33.75	33.17
MNO	0.22	2.67	0.95	2.01
MGO	2.29	2.71	2.96	3.27
CAO	3.21	2.40	4.88	3.45
BAO	-0.41	0.0	0.0	0.0
NA20	0.0	0.04	0.08	0.03
K20	-0.01	0.03	0.06	0.03
F	0.06	0.0	0.0	0.0
CL	0.0	0.0	0.0	0.0
SUM	101.01	101.41	101.14	101.31
-O= F+CL	0.0	0.0	0.0	0.0
SUM	101.01	101.41	101.14	101.31

SI	3.028	*	3.000	*	2.956	*	3.004	*
TI	0.007	*	0.009	*	0.011	*	0.009	*
AL	0.0	3.035	0.0	3.009	0.032	3.000	0.0	3.013
AL	1.970	*	1.985	*	1.951	*	1.976	*
FE	0.030	2.000	0.015	2.000	0.049	2.000	0.024	2.000
FE	2.376	*	2.279	*	2.199	*	2.169	*
MG	0.272	*	0.321	*	0.351	*	0.385	*
MN	0.015	*	0.180	*	0.064	*	0.135	*
CA	0.274	*	0.204	*	0.416	*	0.292	*
NA	0.0	*	0.006	*	0.012	*	0.005	*
K	-0.001	2.935	0.003	2.993	0.006	3.049	0.003	2.989
O	12.000	*	12.000	*	12.000	*	12.000	*

AL	81.11	76.48	72.99	72.98
PY	9.16	10.71	11.41	12.82
SP	0.50	6.00	2.08	4.48
GR	9.23	6.82	13.52	9.72
F/M	8.799	7.655	6.441	5.979
F/FM	0.898	0.884	0.866	0.857
A* =	0.269	0.275	0.276	0.277
A =	0.269	0.274	0.274	0.276
M =	0.101	0.123	0.135	0.149

1 19G AG4-217
2 235Y AG5-505
3 193B AG4-3A
4 397X AG4-6

SUPER RECAL — GARNET ANALYSES

	1	2	3	4	5	6	7
SI02	37.46	37.83	38.55	38.13	37.99	38.39	37.59
TI02	0.14	0.15	0.15	0.14	0.14	0.15	0.14
A203	21.09	20.91	21.09	20.98	21.02	21.09	20.94
FEO	23.44	22.05	21.68	22.63	22.45	23.11	21.79
MNO	14.73	14.77	14.96	14.88	14.83	14.93	14.74
MGO	2.82	2.90	2.87	3.04	2.91	2.99	2.83
CAO	0.63	1.10	1.87	1.14	1.18	1.63	0.74
BAO	0.09	0.19	0.16	-0.02	0.10	0.19	0.02
NA20	0.01	0.02	0.0	-0.04	-0.00	0.02	-0.03
K20	-0.03	-0.03	-0.03	-0.03	-0.03	-0.03	-0.03
F	0.07	0.05	0.10	0.09	0.08	0.10	0.06
CL	0.0	0.0	0.0	0.0	0.0	0.0	0.0
SUM	100.29	99.70	101.14	100.87	100.50	102.28	98.72
-0= F+CL	0.0	0.0	0.0	0.0	0.0	0.0	0.0
SUM	100.29	99.70	101.14	100.87	100.50	102.28	98.72

SI	3.007	*	3.039	*	3.047	*	3.032	*	3.031	*	3.018	*	3.044	*
TI	0.008	*	0.009	*	0.009	*	0.008	*	0.009	*	0.009	*	0.009	*
AL	0.0	3.016	0.0	3.048	0.0	3.056	0.0	3.040	0.0	3.040	0.0	3.027	0.0	3.053
AL	1.995	*	1.979	*	1.964	*	1.966	*	1.976	*	1.954	*	1.998	*
FE	0.005	2.000	0.021	2.000	0.036	2.000	0.034	2.000	0.024	2.000	0.046	2.000	0.002	2.000
FE	1.569	*	1.460	*	1.397	*	1.470	*	1.474	*	1.474	*	1.474	*
MG	0.337	*	0.347	*	0.338	*	0.360	*	0.346	*	0.350	*	0.341	*
MN	1.002	*	1.005	*	1.001	*	1.002	*	1.002	*	0.994	*	1.011	*
CA	0.054	*	0.095	*	0.158	*	0.097	*	0.101	*	0.137	*	0.064	*
NA	0.002	*	0.003	*	0.0	*	-0.006	*	-0.000	*	0.003	*	-0.004	*
K	-0.003	2.960	-0.003	2.907	-0.003	2.892	-0.003	2.920	-0.003	2.920	-0.003	2.955	-0.003	2.883
O	12.000	*	12.000	*	12.000	*	12.000	*	12.000	*	12.000	*	12.000	*
	AL	53.04		50.59		48.89		50.76		50.82		50.64		51.01
	PY	11.37		11.86		11.54		12.15		11.73		11.67		11.79
	SP	33.76		34.32		34.17		33.81		34.01		33.12		34.97
	GR	1.83		3.23		5.40		3.28		3.44		4.57		2.22
	F/M	7.617		7.101		7.094		6.863		7.162		7.045		7.286
	F/FM	0.884		0.877		0.876		0.873		0.877		0.876		0.879
	A* =	0.343		0.352		0.357		0.346		0.349		0.344		0.355
	A =	0.344		0.352		0.358		0.346		0.350		0.344		0.356
	M =	0.177		0.190		0.191		0.193		0.188		0.187		0.188

1 2505 AG5-268+
2 2516 AG5-268+
3 2526 AG5-286+
4 2536 AG5-268+

5 AVERAGE
6 AVERAGE PLUS SIGMA
7 AVERAGE MINUS SIGMA

SUPER RECAL — GARNET ANALYSES

	1	2	3	4	5	6	7	8
SIO2	37.91	38.27	38.18	38.72	37.44	37.78	37.90	37.84
TIO2	0.16	0.13	0.14	0.10	0.13	0.12	0.22	0.12
A203	21.21	21.19	20.82	21.13	20.79	21.22	21.10	21.09
FEO	24.65	24.68	25.25	24.29	32.91	32.90	32.92	32.25
MNO	12.81	12.70	12.71	13.68	6.89	6.35	6.04	7.20
MGO	3.72	3.72	3.62	3.16	1.73	1.77	1.73	2.31
CAO	1.02	0.97	1.12	1.14	2.49	2.49	2.63	1.78
BAO	0.07	0.0	-0.01	0.15	0.0	0.0	0.0	0.0
NA20	0.0	0.01	-0.02	0.0	0.03	0.04	0.06	0.10
K20	-0.01	-0.01	-0.02	-0.02	0.03	0.04	0.03	0.03
F	0.01	0.10	0.05	0.02	0.0	0.0	0.0	0.0
CL	0.0	0.0	0.0	0.0	0.0	0.0	0.0	0.0
SUM	101.47	101.66	101.80	102.40	102.44	102.71	102.63	102.72
-O= F+CL	0.0	0.0	0.0	0.0	0.0	0.0	0.0	0.0
SUM	101.47	101.66	101.80	102.40	102.44	102.71	102.63	102.72

SI	2.999	*	3.014	*	3.016	*	3.037	*	2.985	*	2.992	*	3.001	*	2.994	*
TI	0.010	*	0.008	*	0.008	*	0.006	*	0.008	*	0.007	*	0.013	*	0.007	*
AL	0.0	3.009	0.0	3.022	0.0	3.024	0.0	3.043	0.007	3.000	0.001	3.000	0.0	3.014	0.0	3.001
AL	1.977	*	1.967	*	1.938	*	1.953	*	1.947	*	1.979	*	1.969	*	1.966	*
FE	0.023	2.000	0.033	2.000	0.062	2.000	0.047	2.000	0.053	2.000	0.021	2.000	0.031	2.000	0.034	2.000
FE	1.608	*	1.593	*	1.606	*	1.547	*	2.141	*	2.158	*	2.148	*	2.100	*
MG	0.439	*	0.437	*	0.426	*	0.369	*	0.206	*	0.209	*	0.204	*	0.272	*
MN	0.858	*	0.847	*	0.850	*	0.922	*	0.465	*	0.426	*	0.405	*	0.482	*
CA	0.086	*	0.082	*	0.095	*	0.096	*	0.213	*	0.211	*	0.223	*	0.151	*
NA	0.0	*	0.002	*	-0.003	*	0.0	*	0.005	*	0.006	*	0.009	*	0.015	*
K	-0.001	2.991	-0.001	2.959	-0.002	2.972	-0.002	2.932	0.003	3.033	0.004	3.015	0.003	2.993	0.003	3.024
O	12.000	*	12.000	*	12.000	*	12.000	*	12.000	*	12.000	*	12.000	*	12.000	*
	AL	54.10		54.34		54.88		53.45		71.29		72.03		72.37		70.20
	PY	14.55		14.60		14.02		12.39		6.68		6.91		6.78		8.96
	SP	28.48		28.32		27.98		30.94		15.12		14.08		13.45		15.87
	GR	2.87		2.74		3.12		3.21		6.91		6.98		7.41		4.96
	F/M	5.623		5.586		5.763		6.682		12.678		12.369		12.507		9.480
	F/FM	0.849		0.848		0.852		0.870		0.927		0.925		0.926		0.905
	A* =	0.323		0.323		0.317		0.332		0.289		0.293		0.292		0.290
	A =	0.324		0.323		0.317		0.333		0.288		0.292		0.291		0.289
	M =	0.212		0.212		0.204		0.188		0.086		0.087		0.086		0.113

1 130A AG5-929
2 131A AG5-929
3 132A AG5-929
4 134B AG5-929
5 894C AG4-179 CORE
6 904C AG4-179 CORE
7 1055 AG4-179 CORE
8 884C AG4-179 RIM

SUPER RECAL — GARNET ANALYSES

	9	10	11	12	13	14	15
SIO2	37.83	37.82	38.05	37.64	38.68	37.71	37.74
TIO2	0.11	0.13	0.18	0.18	0.14	0.17	0.14
A203	21.23	20.99	21.01	21.22	21.27	20.53	21.12
FEO	34.34	34.13	29.53	33.42	33.12	33.88	31.74
MNO	5.84	5.55	7.09	6.18	6.50	6.57	10.43
MGO	2.27	2.06	2.80	2.68	2.61	1.87	1.92
CAO	1.69	2.03	3.92	1.61	1.43	1.02	0.54
BAO	0.0	0.0	0.0	0.0	0.0	0.0	0.0
NA20	0.05	0.05	0.01	0.06	0.06	0.05	0.06
K20	0.04	0.03	0.03	0.03	0.05	0.03	0.03
F	0.0	0.0	0.0	0.0	0.0	0.0	0.0
CL	0.0	0.0	0.0	0.0	0.0	0.0	0.0
SUM	103.40	102.79	102.62	103.02	103.86	101.83	103.72
-O= F+CL	0.0	0.0	0.0	0.0	0.0	0.0	0.0
SUM	103.40	102.79	102.62	103.02	103.86	101.83	103.72

SI	2.981	*	2.996	*	2.992	*	2.971	*	3.016	*	3.020	*	2.981	*
TI	0.007	*	0.008	*	0.011	*	0.011	*	0.008	*	0.010	*	0.008	*
AL	0.013	3.000	0.0	3.003	0.0	3.002	0.019	3.000	0.0	3.024	0.0	3.031	0.011	3.000
AL	1.958	*	1.959	*	1.947	*	1.955	*	1.954	*	1.938	*	1.955	*
FE	0.042	2.000	0.041	2.000	0.053	2.000	0.045	2.000	0.046	2.000	0.062	2.000	0.045	2.000
FE	2.221	*	2.220	*	1.888	*	2.160	*	2.114	*	2.207	*	2.051	*
MG	0.267	*	0.243	*	0.328	*	0.315	*	0.303	*	0.223	*	0.226	*
MN	0.390	*	0.372	*	0.472	*	0.413	*	0.429	*	0.446	*	0.698	*
CA	0.143	*	0.172	*	0.330	*	0.136	*	0.119	*	0.088	*	0.046	*
NA	0.008	*	0.008	*	0.002	*	0.009	*	0.009	*	0.008	*	0.009	*
K	0.004	3.032	0.003	3.018	0.003	3.023	0.003	3.037	0.005	2.980	0.003	2.974	0.003	3.033
O	12.000	*	12.000	*	12.000	*	12.000	*	12.000	*	12.000	*	12.000	*
	AL	73.90		74.16		63.20		71.84		71.71		75.00		68.38
	PY	8.71		7.98		10.68		10.27		10.07		7.38		7.37
	SP	12.73		12.21		15.37		13.46		14.25		14.73		22.76
	GR	4.66		5.65		10.75		4.43		3.97		2.89		1.49
	F/M	9.794		10.659		7.193		8.163		8.385		11.883		12.162
	F/FM	0.907		0.914		0.878		0.891		0.893		0.922		0.924
	A* =	0.280		0.281		0.300		0.281		0.284		0.280		0.297
	A =	0.279		0.280		0.299		0.280		0.283		0.279		0.296
	M =	0.105		0.097		0.145		0.125		0.123		0.090		0.097

9 1105 AG4-179 RIM
10 1095 AG4-179 RIM
11 135M AG4-59 MID
12 272B AG4-3A CORE
13 202 AG4-3A MID
14 375 AG4-6 MID
15 372 AG4-6 CORE

SUPER RECAL — STAUROLITE ANALYSES (OH) CALCULATED

	9	10	11	12	13	14	15	16
SIO2	27.97	28.29	28.56	28.42	28.08	28.14	28.45	27.83
TIO2	0.52	0.54	0.57	0.55	0.53	0.54	0.61	0.47
A2O3	53.74	53.38	53.84	53.70	53.96	53.97	54.34	53.61
FEO	13.95	13.72	13.70	13.65	13.71	13.63	13.83	13.43
MNO	0.05	0.11	0.05	0.06	0.09	0.09	0.11	0.06
MGO	1.45	1.46	1.44	1.41	1.48	1.36	1.45	1.26
CAO	-0.03	-0.01	-0.01	-0.02	-0.03	-0.02	-0.01	-0.02
BAO	-0.07	-0.09	-0.12	-0.12	-0.01	-0.08	-0.05	-0.12
NA2O	-0.03	-0.03	-0.05	-0.05	-0.02	-0.03	-0.02	-0.05
K2O	-0.04	-0.04	-0.03	-0.04	-0.03	-0.03	-0.03	-0.04
F	-0.07	-0.02	-0.03	0.10	0.06	0.01	0.06	-0.04
CL	0.0	0.0	0.0	0.0	0.0	0.0	0.0	0.0
H2O	2.39	2.37	2.39	2.32	2.34	2.36	2.36	2.36
SUM	99.83	99.68	100.31	99.98	100.16	99.93	101.12	98.75
-O= F+CL	-0.03	-0.01	-0.01	0.04	0.03	0.00	0.03	-0.02
SUM	99.86	99.69	100.32	99.94	100.13	99.93	101.09	98.77

SI	7.103	*	7.184	*	7.198	*	7.182	*	7.099	*	7.122	*	7.122	*	7.122	*
TI	0.099	*	0.103	*	0.108	*	0.105	*	0.101	*	0.103	*	0.114	*	0.091	*
AL	16.081	*	15.974	*	15.989	*	15.991	*	16.075	*	16.099	*	16.031	*	16.168	*
FE	2.963	*	2.914	*	2.888	*	2.885	*	2.899	*	2.886	*	2.896	*	2.875	*
MN	0.011	*	0.024	*	0.011	*	0.013	*	0.019	*	0.019	*	0.024	*	0.014	*
MG	0.549	*	0.553	*	0.541	*	0.531	*	0.558	*	0.511	*	0.543	*	0.479	*
BA	-0.007	*	-0.009	*	-0.012	*	-0.012	*	-0.001	*	-0.008	*	-0.004	*	-0.012	*
CA	-0.008	*	-0.003	*	-0.003	*	-0.005	*	-0.008	*	-0.004	*	-0.002	*	-0.006	*
K	-0.013	*	-0.013	*	-0.010	*	-0.013	*	-0.010	*	-0.011	*	-0.009	*	-0.013	*
NA	-0.015	26.763	-0.015	26.712	-0.024	26.686	-0.024	26.651	-0.010	26.721	-0.017	26.699	-0.010	26.705	-0.025	26.694
F	-0.056	*	-0.016	*	-0.024	*	0.080	*	0.048	*	0.008	*	0.051	*	-0.036	*
CL	0.0	0.0	0.0	0.0	0.0	0.0	0.0	0.0	0.0	0.0	0.0	0.0	0.0	0.0	0.0	0.0
H	4.056	4.000	4.016	4.000	4.024	4.000	3.920	4.000	3.952	4.000	3.992	4.000	3.949	4.000	4.036	4.000
O	44.000	*	44.000	*	44.000	*	44.000	*	44.000	*	44.000	*	44.000	*	44.000	*
	FEMN	84.42		84.17		84.27		84.51		83.95		85.03		84.33		85.77
	MG	15.58		15.83		15.73		15.49		16.05		14.97		15.67		14.23
	F/M	5.418		5.315		5.358		5.456		5.232		5.680		5.380		6.029
	F/FM	0.844		0.842		0.843		0.845		0.840		0.850		0.843		0.858
	A* =	0.696		0.698		0.700		0.701		0.699		0.703		0.700		0.707
	A =	0.697		0.698		0.700		0.701		0.700		0.704		0.700		0.707
	M =	0.156		0.159		0.158		0.155		0.161		0.151		0.158		0.143

9 80D AG4-225++
10 83E AG4-225++
11 87E AG4-225++
12 89F AG4-225++
13 90F AG4-225++
14 AVERAGE
15 AVERAGE PLUS SIGMA
16 AVERAGE MINUS SIGMA

SUPER RECAL — STAUROLITE ANALYSES (OH) CALCULATED

	1	2	3	4	5
SIO2	27.76	28.21	27.99	28.21	27.76
TIO2	0.48	0.50	0.49	0.50	0.48
A203	52.97	53.60	53.29	53.60	52.97
FEO	13.75	13.62	13.68	13.75	13.62
MNO	-0.04	-0.05	-0.04	-0.04	-0.05
MGO	1.25	1.26	1.26	1.26	1.25
CAO	-0.02	-0.01	-0.02	-0.01	-0.02
BAO	-0.38	-0.46	-0.42	-0.38	-0.46
NA2O	-0.02	-0.03	-0.02	-0.02	-0.03
K2O	-0.04	-0.03	-0.03	-0.03	-0.04
F	0.02	-0.04	-0.01	0.02	-0.04
CL	0.0	0.0	0.0	0.0	0.0
H2O	2.32	2.37	2.34	2.35	2.34
SUM	98.05	98.94	98.49	99.21	97.78
-O= F+CL	0.01	-0.02	-0.00	0.01	-0.02
SUM	98.04	98.96	98.50	99.20	97.80

SI	7.151	*	7.186	*	7.169	*	7.175	*	7.162	*
TI	0.093	*	0.096	*	0.094	*	0.096	*	0.093	*
AL	16.079	*	16.090	*	16.084	*	16.065	*	16.104	*
FE	2.962	*	2.902	*	2.932	*	2.925	*	2.939	*
MN	-0.009	*	-0.011	*	-0.010	*	-0.009	*	-0.011	*
MG	0.480	*	0.478	*	0.479	*	0.478	*	0.481	*
BA	-0.038	*	-0.046	*	-0.042	*	-0.038	*	-0.047	*
CA	-0.006	*	-0.003	*	-0.004	*	-0.003	*	-0.006	*
K	-0.013	*	-0.010	*	-0.011	*	-0.010	*	-0.013	*
NA	-0.010	26.689	-0.015	26.668	-0.012	26.678	-0.010	26.670	-0.015	26.687
F	0.016	*	-0.032	*	-0.008	*	0.016	*	-0.033	*
CL	0.0	0.0	0.0	0.0	0.0	0.0	0.0	0.0	0.0	0.0
H	3.984	4.000	4.032	4.000	4.008	4.000	3.984	4.000	4.033	4.000
O	44.000	*	44.000	*	44.000	*	44.000	*	44.000	*
	FEMN	86.02		85.80		85.91		85.93		85.90
	MG	13.98		14.20		14.09		14.07		14.10
	F/M	6.154		6.042		6.098		6.105		6.091
	F/FM	0.860		0.858		0.859		0.859		0.859
	A* =	0.700		0.704		0.702		0.703		0.702
	A =	0.701		0.705		0.703		0.703		0.702
	M =	0.139		0.142		0.140		0.140		0.141

1 25S AG4-217
2 26S AG4-217
3 AVERAGE
4 AVERAGE PLUS SIGMA
5 AVERAGE MINUS SIGMA

SUPER RECAL — STAUROLITE ANALYSES (OH) CALCULATED

	1	2	3	4	5	6
SIO2	29.64	28.66	28.72	29.01	29.46	28.56
TIO2	0.24	0.44	0.39	0.36	0.44	0.27
A203	54.91	55.19	55.06	55.05	55.17	54.94
FEO	10.28	10.62	10.65	10.52	10.68	10.35
MNO	0.70	0.77	0.69	0.72	0.76	0.68
MGO	1.17	1.14	1.22	1.18	1.21	1.14
CAO	-0.01	-0.01	-0.02	-0.01	-0.01	-0.02
BAO	0.06	-0.02	-0.08	-0.01	0.04	-0.07
NA2O	0.04	0.0	0.02	0.02	0.04	0.00
K2O	-0.04	-0.04	-0.04	-0.04	-0.04	-0.04
F	-0.01	0.03	0.03	0.02	0.04	-0.00
CL	0.0	0.0	0.0	0.0	0.0	0.0
H2O	2.40	2.36	2.36	2.37	2.39	2.36
SUM	99.38	99.14	99.00	99.17	100.17	98.18
-O= F+CL	-0.00	0.01	0.01	0.01	0.01	-0.00
SUM	99.38	99.13	98.99	99.17	100.15	98.18

SI	7.424	*	7.216	*	7.237	*	7.293	*	7.339	*	7.246	*
TI	0.045	*	0.083	*	0.074	*	0.067	*	0.083	*	0.052	*
AL	16.207	*	16.375	*	16.349	*	16.310	*	16.197	*	16.426	*
FE	2.153	*	2.236	*	2.244	*	2.211	*	2.226	*	2.196	*
MN	0.149	*	0.164	*	0.147	*	0.153	*	0.159	*	0.147	*
MG	0.437	*	0.428	*	0.458	*	0.441	*	0.449	*	0.433	*
BA	0.006	*	-0.002	*	-0.008	*	-0.001	*	0.004	*	-0.007	*
CA	-0.003	*	-0.003	*	-0.005	*	-0.004	*	-0.002	*	-0.005	*
K	-0.013	*	-0.013	*	-0.013	*	-0.013	*	-0.013	*	-0.013	*
NA	0.019	26.425	0.0	26.486	0.010	26.493	0.010	26.468	0.018	26.460	0.002	26.476
F	-0.008	*	0.024	*	0.024	*	0.013	*	0.028	*	-0.002	*
CL	0.0	0.0	0.0	0.0	0.0	0.0	0.0	0.0	0.0	0.0	0.0	0.0
H	4.008	4.000	3.976	4.000	3.976	4.000	3.987	4.000	3.972	4.000	4.002	4.000
O	44.000	*	44.000	*	44.000	*	44.000	*	44.000	*	44.000	*
	FEMN	84.05		84.87		83.92		84.28		84.15		84.42
	MG	15.95		15.13		16.08		15.72		15.85		15.58
	F/M	5.270		5.611		5.219		5.362		5.311		5.417
	F/FM	0.841		0.849		0.839		0.843		0.842		0.844
	A* =	0.758		0.755		0.752		0.755		0.752		0.758
	A =	0.758		0.755		0.752		0.755		0.752		0.758
	M =	0.169		0.161		0.170		0.166		0.168		0.165

1 1072 AG4-159+
2 1082 AG4-159+
3 1224 AG4-159+
4 AVERAGE
5 AVERAGE PLUS SIGMA
6 AVERAGE MINUS SIGMA

SUPER RECAL — STAUROLITE ANALYSES (OH) CALCULATED

	1	2	3	4	5	6	7	8
SIO2	28.37	27.94	28.41	28.02	28.33	27.31	27.94	28.14
TIO2	0.54	0.46	0.36	0.55	0.61	0.62	0.60	0.57
A203	53.50	54.04	54.64	54.00	54.62	54.07	54.32	53.85
FEO	13.55	13.29	13.57	13.43	13.26	13.80	13.86	13.75
MNO	0.11	0.07	0.07	0.09	0.13	0.09	0.10	0.11
MGO	1.22	1.28	1.25	1.34	1.23	1.44	1.21	1.41
CAO	-0.01	-0.01	-0.02	-0.01	-0.01	-0.01	-0.02	-0.01
BAO	-0.09	-0.02	-0.09	-0.08	-0.15	-0.06	-0.11	-0.07
NA20	-0.05	-0.04	-0.05	-0.05	-0.01	-0.01	-0.04	-0.02
K20	-0.03	-0.03	-0.04	-0.03	-0.04	-0.03	-0.03	-0.03
F	-0.03	0.12	-0.01	0.05	-0.02	-0.02	-0.03	0.03
CL	0.0	0.0	0.0	0.0	0.0	0.0	0.0	0.0
H20	2.37	2.30	2.39	2.34	2.39	2.36	2.38	2.35
SUM	99.45	99.40	100.48	99.65	100.34	99.56	100.18	100.08
-O= F+CL	-0.01	0.05	-0.00	0.02	-0.01	-0.01	-0.01	0.01
SUM	99.46	99.35	100.48	99.63	100.35	99.57	100.20	100.07

		*		*		*		*		*		*		*		*
SI	7.211	*	7.098	*	7.141	*	7.106	*	7.123	*	6.959	*	7.063	*	7.119	*
TI	0.103	*	0.088	*	0.068	*	0.105	*	0.115	*	0.119	*	0.114	*	0.108	*
AL	16.025	*	16.178	*	16.183	*	16.136	*	16.182	*	16.235	*	16.182	*	16.053	*
FE	2.880	*	2.824	*	2.852	*	2.848	*	2.788	*	2.941	*	2.930	*	2.909	*
MN	0.024	*	0.015	*	0.015	*	0.019	*	0.028	*	0.019	*	0.021	*	0.024	*
MG	0.462	*	0.485	*	0.468	*	0.506	*	0.461	*	0.547	*	0.456	*	0.532	*
BA	-0.009	*	-0.002	*	-0.009	*	-0.008	*	-0.015	*	-0.006	*	-0.011	*	-0.007	*
CA	-0.003	*	-0.003	*	-0.005	*	-0.003	*	-0.003	*	-0.003	*	-0.005	*	-0.003	*
K	-0.010	*	-0.010	*	-0.013	*	-0.010	*	-0.013	*	-0.010	*	-0.010	*	-0.010	*
NA	-0.025	26.659	-0.020	26.653	-0.024	26.676	-0.025	26.676	-0.005	26.661	-0.005	26.797	-0.020	26.721	-0.010	26.716
F	-0.024	*	0.096	*	-0.008	*	0.040	*	-0.016	*	-0.016	*	-0.024	*	0.024	*
CL	0.0	0.0	0.0	0.0	0.0	0.0	0.0	0.0	0.0	0.0	0.0	0.0	0.0	0.0	0.0	0.0
H	4.024	4.000	3.904	4.000	4.008	4.000	3.960	4.000	4.016	4.000	4.016	4.000	4.024	4.000	3.976	4.000
O	44.000	*	44.000	*	44.000	*	44.000	*	44.000	*	44.000	*	44.000	*	44.000	*
	FEMN	86.27		85.42		85.96		84.99		85.93		84.41		86.62		84.65
	MG	13.73		14.58		14.04		15.01		14.07		15.59		13.38		15.35
	F/M	6.283		5.857		6.123		5.661		6.109		5.412		6.474		5.516
	F/FM	0.863		0.854		0.860		0.850		0.859		0.844		0.866		0.847
	A* =	0.706		0.710		0.709		0.706		0.714		0.700		0.705		0.700
	A =	0.706		0.710		0.710		0.707		0.714		0.700		0.705		0.700
	M =	0.138		0.147		0.141		0.151		0.142		0.157		0.135		0.155

1 59B AG4-225++
2 60B AG4-225++
3 61B AG4-225++
4 62B AG4-225++
5 69C AG4-225++
6 74C AG4-225++
7 76C AG4-225++
8 79D AG4-225++

SUPER RECAL — STAUROLITE ANALYSES (OH) CALCULATED

	1	2	3	4	5
SIO2	28.74	28.24	28.49	28.74	28.24
TIO2	0.29	0.34	0.31	0.34	0.29
A203	54.17	53.58	53.88	54.17	53.58
FEO	9.85	10.82	10.33	10.82	9.85
MNO	0.40	0.32	0.36	0.40	0.32
MGO	0.85	0.93	0.89	0.93	0.85
CAO	-0.03	-0.01	-0.02	-0.01	-0.03
BAO	0.08	0.05	0.06	0.08	0.05
NA2O	0.12	0.06	0.09	0.12	0.06
K2O	-0.04	-0.03	-0.03	-0.03	-0.04
F	0.01	0.04	0.02	0.04	0.01
CL	0.0	0.0	0.0	0.0	0.0
H2O	2.33	2.30	2.31	2.33	2.30
SUM	96.77	96.64	96.70	97.93	95.48
-O= F+CL	0.00	0.02	0.01	0.02	0.00
SUM	96.77	96.62	96.69	97.91	95.47

SI	7.376	*	7.297	*	7.337	*	7.328	*	7.346	*
TI	0.056	*	0.066	*	0.061	*	0.065	*	0.057	*
AL	16.383	*	16.314	*	16.348	*	16.275	*	16.423	*
FE	2.114	*	2.338	*	2.226	*	2.307	*	2.143	*
MN	0.087	*	0.070	*	0.079	*	0.086	*	0.071	*
MG	0.325	*	0.358	*	0.342	*	0.353	*	0.330	*
BA	0.008	*	0.005	*	0.007	*	0.008	*	0.005	*
CA	-0.008	*	-0.003	*	-0.006	*	-0.003	*	-0.008	*
K	-0.013	*	-0.010	*	-0.011	*	-0.010	*	-0.013	*
NA	0.060	26.387	0.030	26.465	0.045	26.426	0.059	26.470	0.030	26.382
F	0.008	*	0.033	*	0.020	*	0.032	*	0.008	*
CL	0.0	0.0	0.0	0.0	0.0	0.0	0.0	0.0	0.0	0.0
H	3.992	4.000	3.967	4.000	3.980	4.000	3.968	4.000	3.992	4.000
O	44.000	*	44.000	*	44.000	*	44.000	*	44.000	*
	FEMN	87.13		87.05		87.09		87.13		87.04
	MG	12.87		12.95		12.91		12.87		12.96
	F/M	6.769		6.723		6.745		6.772		6.716
	F/FM	0.871		0.871		0.871		0.871		0.870
	A* =	0.771		0.752		0.761		0.754		0.769
	A =	0.771		0.752		0.761		0.754		0.769
	M =	0.133		0.133		0.133		0.133		0.133

1 189F AG4-34
2 202B AG4-34
3 AVERAGE
4 AVERAGE PLUS SIGMA
5 AVERAGE MINUS SIGMA

SUPER RECAL — STAUROLITE ANALYSES (OH) CALCULATED

	1	2	3	4	5	6
SIO2	28.20	29.34	28.64	28.73	29.20	28.26
TIO2	0.39	0.19	0.12	0.23	0.35	0.12
A203	53.04	51.64	52.57	52.42	53.00	51.83
FEO	14.92	14.28	14.50	14.57	14.83	14.30
MNO	0.22	0.21	0.15	0.19	0.22	0.16
MGO	1.50	1.55	1.60	1.55	1.59	1.51
CAO	0.0	-0.01	-0.02	-0.01	-0.00	-0.02
BAO	0.26	0.10	0.0	0.12	0.23	0.01
NA2O	-0.03	-0.01	-0.01	-0.02	-0.01	-0.03
K2O	-0.02	-0.03	-0.04	-0.03	-0.02	-0.04
F	0.03	-0.01	0.01	0.01	0.03	-0.01
CL	0.0	0.0	0.0	0.0	0.0	0.0
H2O	2.35	2.35	2.35	2.35	2.38	2.32
SUM	100.86	99.60	99.87	100.11	101.79	98.43
-O= F+CL	0.01	-0.00	0.00	0.00	0.01	-0.00
SUM	100.85	99.61	99.86	100.11	101.78	98.43

SI	7.144	*	7.482	*	7.290	*	7.305	*	7.312	*	7.298	*
TI	0.074	*	0.036	*	0.023	*	0.045	*	0.065	*	0.023	*
AL	15.835	*	15.519	*	15.767	*	15.707	*	15.641	*	15.775	*
FE	3.161	*	3.046	*	3.086	*	3.098	*	3.107	*	3.089	*
MN	0.047	*	0.045	*	0.032	*	0.042	*	0.048	*	0.036	*
MG	0.566	*	0.589	*	0.607	*	0.588	*	0.594	*	0.581	*
BA	0.026	*	0.010	*	0.0	*	0.012	*	0.022	*	0.001	*
CA	0.0	*	-0.003	*	-0.005	*	-0.003	*	-0.000	*	-0.005	*
K	-0.006	*	-0.010	*	-0.013	*	-0.010	*	-0.007	*	-0.013	*
NA	-0.015	26.833	-0.005	26.710	-0.005	26.782	-0.008	26.775	-0.004	26.778	-0.013	26.773
F	0.024	*	-0.008	*	0.008	*	0.008	*	0.021	*	-0.005	*
CL	0.0	0.0	0.0	0.0	0.0	0.0	0.0	0.0	0.0	0.0	0.0	0.0
H	3.976	4.000	4.008	4.000	3.992	4.000	3.992	4.000	3.979	4.000	4.005	4.000
O	44.000	*	44.000	*	44.000	*	44.000	*	44.000	*	44.000	*
	FEMN	84.99		83.99		83.71		84.24		84.16		84.32
	MG	15.01		16.01		16.29		15.76		15.84		15.68
	F/M	5.664		5.246		5.138		5.344		5.311		5.378
	F/FM	0.850		0.840		0.837		0.842		0.842		0.843
	A* =	0.680		0.681		0.681		0.681		0.679		0.683
	A =	0.680		0.681		0.682		0.681		0.679		0.683
	M =	0.152		0.162		0.164		0.159		0.160		0.158

1 2071 AG5-523
2 2183 AG5-523
3 2214 AG5-523
4 AVERAGE
5 AVERAGE PLUS SIGMA
6 AVERAGE MINUS SIGMA

SUPER RECAL — STAUROLITE ANALYSES (OH) CALCULATED

	1	2	3	4	5
SIO2	30.92	28.45	29.68	30.92	28.45
TIO2	0.47	0.42	0.44	0.47	0.42
A203	50.54	53.17	51.85	53.17	50.54
FEO	12.31	12.90	12.60	12.90	12.31
MNO	0.48	0.36	0.42	0.48	0.36
MGO	2.26	2.35	2.31	2.35	2.26
CAO	-0.02	-0.01	-0.02	-0.01	-0.02
BAO	0.18	0.16	0.17	0.18	0.16
NA2O	-0.01	-0.05	-0.03	-0.01	-0.05
K2O	-0.05	-0.04	-0.04	-0.04	-0.05
F	-0.04	-0.01	-0.02	-0.01	-0.04
CL	0.0	0.0	0.0	0.0	0.0
H2O	2.39	2.37	2.38	2.45	2.31
SUM	99.43	100.07	99.75	102.85	96.65
-O= F+CL	-0.02	-0.00	-0.01	-0.00	-0.02
SUM	99.44	100.08	99.76	102.85	96.67

		*		*		*		*		*
SI	7.827	*	7.194	*	7.510	*	7.583	*	7.433	*
TI	0.089	*	0.080	*	0.085	*	0.087	*	0.083	*
AL	15.075	*	15.842	*	15.459	*	15.365	*	15.559	*
FE	2.606	*	2.728	*	2.667	*	2.646	*	2.690	*
MN	0.103	*	0.077	*	0.090	*	0.100	*	0.080	*
MG	0.853	*	0.886	*	0.869	*	0.859	*	0.880	*
BA	0.018	*	0.016	*	0.017	*	0.017	*	0.016	*
CA	-0.005	*	-0.003	*	-0.004	*	-0.003	*	-0.006	*
K	-0.016	*	-0.013	*	-0.015	*	-0.013	*	-0.017	*
NA	-0.005	26.544	-0.025	26.782	-0.015	26.663	-0.005	26.636	-0.025	26.692
F	-0.032	*	-0.008	*	-0.020	*	-0.008	*	-0.033	*
CL	0.0	0.0	0.0	0.0	0.0	0.0	0.0	0.0	0.0	0.0
H	4.032	4.000	4.008	4.000	4.020	4.000	4.008	4.000	4.033	4.000
O	44.000	*	44.000	*	44.000	*	44.000	*	44.000	*
	FEMN	76.06		76.00		76.03		76.17		75.88
	MG	23.94		24.00		23.97		23.83		24.12
	F/M	3.177		3.167		3.172		3.196		3.147
	F/FM	0.761		0.760		0.760		0.762		0.759
	A* =	0.686		0.687		0.686		0.687		0.686
	A =	0.686		0.687		0.687		0.687		0.686
	M =	0.247		0.245		0.246		0.245		0.247

1 235B AG4-2A
2 2556 AG4-2A
3 AVERAGE
4 AVERAGE PLUS SIGMA
5 AVERAGE MINUS SIGMA

SUPER RECAL — STAUROLITE ANALYSES (OH) CALCULATED

	1	2	3	4
SIO2	28.34	28.34	28.34	28.34
TIO2	0.32	0.32	0.32	0.32
A203	53.61	53.61	53.61	53.61
FEO	12.61	12.61	12.61	12.61
MNO	0.27	0.27	0.27	0.27
MGO	2.28	2.28	2.28	2.28
CAO	-0.02	-0.02	-0.02	-0.02
BAO	0.03	0.03	0.03	0.03
NA2O	-0.02	-0.02	-0.02	-0.02
K2O	-0.05	-0.05	-0.05	-0.05
F	-0.07	-0.07	-0.07	-0.07
CL	0.0	0.0	0.0	0.0
H2O	2.40	2.40	2.40	2.40
SUM	99.70	99.70	99.70	99.70
-O= F+CL	-0.03	-0.03	-0.03	-0.03
SUM	99.73	99.73	99.73	99.73

		*		*		*		*
SI	7.172	*	7.172	*	7.172	*	7.172	*
TI	0.061	*	0.061	*	0.061	*	0.061	*
AL	15.988	*	15.988	*	15.988	*	15.988	*
FE	2.669	*	2.669	*	2.669	*	2.669	*
MN	0.058	*	0.058	*	0.058	*	0.058	*
MG	0.860	*	0.860	*	0.860	*	0.860	*
BA	0.003	*	0.003	*	0.003	*	0.003	*
CA	-0.005	*	-0.005	*	-0.005	*	-0.005	*
K	-0.016	*	-0.016	*	-0.016	*	-0.016	*
NA	-0.010	26.779	-0.010	26.779	-0.010	26.779	-0.010	26.779
F	-0.056	*	-0.056	*	-0.056	*	-0.056	*
CL	0.0	0.0	0.0	0.0	0.0	0.0	0.0	0.0
H	4.056	4.000	4.056	4.000	4.056	4.000	4.056	4.000
O	44.000	*	44.000	*	44.000	*	44.000	*
	FEMN	76.02		76.02		76.02		76.02
	MG	23.98		23.98		23.98		23.98
	F/M	3.170		3.170		3.170		3.170
	F/FM	0.760		0.760		0.760		0.760
	A* =	0.694		0.694		0.694		0.694
	A =	0.694		0.694		0.694		0.694
	M =	0.244		0.244		0.244		0.244

1 2625 AG4-268+
2 AVERAGE
3 AVERAGE PLUS SIGMA
4 AVERAGE MINUS SIGMA

SUPER RECAL STAUROLITE ANALYSES (OH) CALCULATED

	1	2	3	4	5	6	7	8
SIO2	27.15	27.44	28.51	28.67	28.12	28.45	29.05	28.05
TIO2	0.62	0.66	0.60	0.61	0.64	0.67	0.83	0.62
A203	53.29	54.47	54.66	54.32	54.07	52.48	53.06	53.38
FEO	12.96	13.07	13.09	12.75	12.62	13.02	13.21	13.05
MNO	0.58	0.63	0.55	0.61	0.58	0.57	0.66	0.58
MGO	1.18	1.18	1.18	1.23	1.16	1.19	1.28	1.28
CAO	0.06	0.04	0.04	0.02	0.10	0.04	0.09	0.05
BAO	0.0	0.0	0.0	0.0	0.0	0.0	0.0	0.0
NA20	0.04	0.06	0.06	0.07	0.01	0.09	0.05	0.10
K20	0.01	0.02	0.01	0.01	0.02	0.01	0.02	0.01
F	0.0	0.0	0.0	0.0	0.0	0.0	0.0	0.0
CL	0.0	0.0	0.0	0.0	0.0	0.0	0.0	0.0
H20	2.32	2.36	2.39	2.39	2.36	2.34	2.38	2.35
SUM	98.21	99.93	101.09	100.68	99.68	98.86	100.63	99.47
-O= F+CL	0.0	0.0	0.0	0.0	0.0	0.0	0.0	0.0
SUM	98.21	99.93	101.09	100.68	99.68	98.86	100.63	99.47

SI	7.010	*	6.963	*	7.134	*	7.193	*	7.127	*	7.287	*	7.313	*	7.145	*
TI	0.120	*	0.126	*	0.113	*	0.115	*	0.122	*	0.129	*	0.157	*	0.119	*
AL	16.215	*	16.287	*	16.117	*	16.058	*	16.149	*	15.839	*	15.740	*	16.022	*
FE	2.799	*	2.773	*	2.739	*	2.675	*	2.675	*	2.789	*	2.781	*	2.780	*
MN	0.127	*	0.135	*	0.117	*	0.130	*	0.125	*	0.124	*	0.141	*	0.125	*
MG	0.454	*	0.446	*	0.440	*	0.460	*	0.438	*	0.454	*	0.480	*	0.486	*
BA	0.0	*	0.0	*	0.0	*	0.0	*	0.0	*	0.0	*	0.0	*	0.0	*
CA	0.017	*	0.011	*	0.011	*	0.005	*	0.027	*	0.011	*	0.024	*	0.014	*
K	0.003	*	0.006	*	0.003	*	0.003	*	0.006	*	0.003	*	0.006	*	0.003	*
NA	0.020	26.765	0.030	26.777	0.029	26.702	0.034	26.673	0.005	26.674	0.045	26.680	0.024	26.667	0.049	26.743
F	0.0	*	0.0	*	0.0	*	0.0	*	0.0	*	0.0	*	0.0	*	0.0	*
CL	0.0	0.0	0.0	0.0	0.0	0.0	0.0	0.0	0.0	0.0	0.0	0.0	0.0	0.0	0.0	0.0
H	4.000	4.000	4.000	4.000	4.000	4.000	4.000	4.000	4.000	4.000	4.000	4.000	4.000	4.000	4.000	4.000
O	44.000	*	44.000	*	44.000	*	44.000	*	44.000	*	44.000	*	44.000	*	44.000	*
	FEMN	86.56		86.70		86.65		85.91		86.46		86.51		85.88		85.67
	MG	13.44		13.30		13.35		14.09		13.54		13.49		14.12		14.33
	F/M	6.442		6.518		6.489		6.098		6.388		6.411		6.083		5.978
	F/FM	0.866		0.867		0.866		0.859		0.865		0.865		0.859		0.857
	A* =	0.714		0.717		0.717		0.719		0.722		0.709		0.707		0.710
	A =	0.714		0.716		0.717		0.719		0.722		0.709		0.707		0.710
	M =	0.140		0.139		0.138		0.147		0.141		0.140		0.147		0.149

1 AG5-1195 1ST1
2 AG5-1195 1ST2
3 AG5-1195 1ST3
4 AG5-1195 3ST1
5 AG5-1195 3ST2
6 AG5-1195 3STC
7 AG5-1195 BSTC
8 AG5-1195 BSTCLR

SUPER RECAL — STAUROLITE ANALYSES (OH) CALCULATED

	9	10	11	12
SIO2	28.30	28.19	28.75	27.63
TIO2	0.60	0.65	0.72	0.58
A203	53.39	53.68	54.37	52.99
FEO	13.03	12.98	13.15	12.81
MNO	0.60	0.60	0.63	0.56
MGO	1.27	1.22	1.26	1.17
CAO	0.03	0.05	0.08	0.03
BAO	0.0	0.0	0.0	0.0
MA2O	0.07	0.06	0.09	0.04
K2O	0.01	0.01	0.02	0.01
F	0.0	0.0	0.0	0.0
CL	0.0	0.0	0.0	0.0
H2O	2.36	2.36	2.40	2.32
SUM	99.66	99.80	101.46	98.14
-O= F+CL	0.0	0.0	0.0	0.0
SUM	99.66	99.80	101.46	98.14

SI	7.190	*		7.152	*		7.175	*		7.127	*	
TI	0.115	*		0.124	*		0.135	*		0.113	*	
AL	15.984	*		16.045	*		15.988	*		16.105	*	
FE	2.769	*		2.753	*		2.744	*		2.762	*	
MN	0.129	*		0.128	*		0.133	*		0.123	*	
MG	0.481	*		0.460	*		0.470	*		0.450	*	
BA	0.0	*		0.0	*		0.0	*		0.0	*	
CA	0.008	*		0.014	*		0.021	*		0.007	*	
K	0.003	*		0.004	*		0.006	*		0.003	*	
NA	0.034	26.713		0.030	26.710		0.042	26.712		0.018	26.709	
F	0.0	*		0.0	*		0.0	*		0.0	*	
CL	0.0	0.0		0.0	0.0		0.0	0.0		0.0	0.0	
H	4.000	4.000		4.000	4.000		4.000	4.000		4.000	4.000	
O	44.000	*		44.000	*		44.000	*		44.000	*	
	FEMN	85.77			86.23			85.97			86.51	
	MG	14.23			13.77			14.03			13.49	
	F/M	6.025			6.263			6.126			6.411	
	F/FM	0.858			0.862			0.860			0.865	
	A* =	0.711			0.714			0.713			0.715	
	A =	0.711			0.714			0.713			0.715	
	M =	0.148			0.143			0.146			0.140	

9 AG5-1195 CSTC
10 AVERAGE
11 AVERAGE PLUS SIGMA
12 AVERAGE MINUS SIGMA

SUPER RECAL — STAUROLITE ANALYSES (OH) CALCULATED

	1	2	3	4	5	6	7	8
SIO2	29.54	29.73	30.11	29.29	28.96	28.98	28.95	29.67
TIO2	0.53	0.56	0.50	0.47	0.55	0.28	0.32	0.10
A203	52.19	52.39	51.94	52.32	52.51	52.84	53.48	52.74
FEO	14.04	13.80	13.61	13.83	14.05	13.93	13.60	13.78
MNO	0.06	0.05	0.06	0.08	0.04	0.06	0.07	0.12
MGO	0.17	0.13	0.13	0.16	0.09	0.07	0.07	0.06
CAO	1.81	1.83	1.80	1.88	1.84	1.98	1.96	2.03
BAO	0.01	0.02	0.01	0.02	0.01	0.05	0.0	0.01
NA20	0.05	0.03	0.04	-0.04	0.02	-0.02	0.06	0.01
K20	0.03	0.02	0.02	-0.02	0.01	0.02	0.01	0.0
F	0.08	0.12	0.27	0.02	0.01	0.01	0.02	0.02
CL	0.0	0.03	0.0	0.06	0.15	0.03	0.10	0.08
H20	2.33	2.31	2.25	2.34	2.32	2.35	2.34	2.35
SUM	100.84	101.02	100.74	100.41	100.56	100.58	100.98	100.97
-O= F+CL	0.03	0.06	0.11	0.02	0.04	0.01	0.03	0.03
SUM	100.81	100.97	100.62	100.39	100.52	100.57	100.95	100.94

SI	7.459	*	7.480	*	7.579	*	7.423	*	7.342	*	7.341	*	7.291	*	7.473	*
TI	0.101	*	0.106	*	0.095	*	0.090	*	0.105	*	0.053	*	0.061	*	0.019	*
AL	15.528	*	15.532	*	15.407	*	15.625	*	15.688	*	15.774	*	15.872	*	15.654	*
FE	2.965	*	2.904	*	2.865	*	2.931	*	2.979	*	2.951	*	2.864	*	2.903	*
MN	0.013	*	0.011	*	0.013	*	0.017	*	0.009	*	0.013	*	0.015	*	0.026	*
MG	0.064	*	0.049	*	0.049	*	0.060	*	0.034	*	0.026	*	0.026	*	0.023	*
BA	0.001	*	0.002	*	0.001	*	0.002	*	0.001	*	0.005	*	0.0	*	0.001	*
CA	0.490	*	0.493	*	0.485	*	0.510	*	0.500	*	0.537	*	0.529	*	0.548	*
K	0.010	*	0.006	*	0.006	*	-0.006	*	0.003	*	0.006	*	0.003	*	0.0	*
NA	0.024	26.654	0.015	26.597	0.020	26.520	-0.020	26.633	0.010	26.671	-0.010	26.698	0.029	26.691	0.005	26.650
F	0.064	*	0.095	*	0.215	*	0.016	*	0.008	*	0.008	*	0.016	*	0.016	*
CL	0.0	0.0	0.013	0.0	0.0	0.0	0.026	0.0	0.064	0.0	0.013	0.0	0.043	0.0	0.034	0.0
H	3.936	4.000	3.892	4.000	3.785	4.000	3.958	4.000	3.928	4.000	3.979	4.000	3.941	4.000	3.950	4.000
O	44.000	*	44.000	*	44.000	*	44.000	*	44.000	*	44.000	*	44.000	*	44.000	*
	FEMN	97.90		98.35		98.33		97.99		98.87		99.12		99.10		99.24
	MG	2.10		1.65		1.67		2.01		1.13		0.88		0.90		0.76
	F/M	46.539		59.779		59.002		48.782		87.843		112.141		109.577		129.997
	F/FM	0.979		0.984		0.983		0.980		0.989		0.991		0.991		0.992
	A* =	0.719		0.725		0.726		0.723		0.722		0.726		0.733		0.728
	A =	0.719		0.724		0.725		0.723		0.722		0.726		0.733		0.728
	M =	0.021		0.017		0.017		0.020		0.011		0.009		0.009		0.008

1 10B AG4-3A 1S6
2 11B AG4-3A
3 12B AG4-3A
4 14B AG4-3A 1S7
5 16B AG4-3A W/BT
6 25B AG4-3A CORE
7 26B AG4-3A RIM
8 27B AG4-3A W/GT

SUPER RECAL — STAUROLITE ANALYSES (OH) CALCULATED

	9	10	11	12	13
SIO2	29.88	28.95	29.41	29.82	28.99
TIO2	0.43	0.41	0.41	0.55	0.28
A203	51.69	52.89	52.50	52.99	52.01
FEO	13.80	13.92	13.84	13.98	13.69
MNO	0.05	0.02	0.06	0.09	0.04
MGO	0.15	0.13	0.12	0.15	0.08
CAO	1.98	2.02	1.91	2.00	1.83
BAO	0.03	0.02	0.02	0.03	0.00
NA2O	0.01	0.02	0.02	0.05	-0.01
K2O	0.03	0.03	0.01	0.03	0.00
F	0.01	0.02	0.06	0.14	-0.02
CL	0.05	0.05	0.05	0.10	0.01
H2O	2.35	2.35	2.33	2.31	2.35
SUM	100.46	100.83	100.74	102.24	99.24
-O= F+CL	0.02	0.02	0.04	0.08	-0.01
SUM	100.44	100.81	100.70	102.16	99.24

	9		10		11		12		13	
SI	7.568	*	7.317	*	7.427	*	7.425	*	7.430	*
TI	0.082	*	0.078	*	0.079	*	0.103	*	0.053	*
AL	15.427	*	15.752	*	15.626	*	15.547	*	15.707	*
FE	2.923	*	2.942	*	2.923	*	2.912	*	2.934	*
MN	0.011	*	0.004	*	0.013	*	0.018	*	0.008	*
MG	0.057	*	0.049	*	0.044	*	0.057	*	0.030	*
BA	0.003	*	0.002	*	0.002	*	0.003	*	0.000	*
CA	0.537	*	0.547	*	0.518	*	0.533	*	0.502	*
K	0.010	*	0.010	*	0.005	*	0.010	*	0.000	*
NA	0.005	26.621	0.010	26.711	0.009	26.644	0.023	26.631	-0.005	26.658
F	0.008	*	0.016	*	0.046	*	0.108	*	-0.017	*
CL	0.021	0.0	0.021	0.0	0.024	0.0	0.042	0.0	0.005	0.0
H	3.971	4.000	3.963	4.000	3.930	4.000	3.851	4.000	4.012	4.000
O	44.000	*	44.000	*	44.000	*	44.000	*	44.000	*
	FEMN	98.11		98.37		98.53		98.08		99.00
	MG	1.89		1.63		1.47		1.92		1.00
	F/M	51.808		60.166		67.222		51.175		99.064
	F/FM	0.981		0.984		0.985		0.981		0.990
	A* =	0.721		0.725		0.725		0.724		0.726
	A =	0.721		0.724		0.725		0.723		0.726
	M =	0.019		0.016		0.015		0.019		0.010

9 28B AG4-3A
10 29B AG4-3A
11 AVERAGE
12 AVERAGE PLUS SIGMA
13 AVERAGE MINUS SIGMA

SUPER RECAL — STAUROLITE ANALYSES (OH) CALCULATED

	1	2	3	4	5	6
SIO2	29.26	28.62	29.53	29.14	29.52	28.76
TIO2	0.19	0.36	0.13	0.23	0.32	0.13
A203	53.07	53.48	52.93	53.16	53.39	52.93
FEO	13.59	12.60	13.25	13.15	13.56	12.74
MNO	0.09	0.09	0.13	0.10	0.12	0.08
MGO	0.06	0.23	0.16	0.15	0.22	0.08
CAO	2.09	1.91	2.16	2.05	2.16	1.95
BAO	0.0	0.03	0.02	0.02	0.03	0.00
NA2O	0.04	0.05	0.0	0.03	0.05	0.01
K2O	0.0	0.06	-0.02	0.01	0.05	-0.02
F	0.01	0.03	0.01	0.02	0.03	0.01
CL	0.33	0.42	0.05	0.27	0.42	0.11
H2O	2.29	2.24	2.36	2.29	2.28	2.31
SUM	101.02	100.12	100.71	100.61	102.15	99.08
-O= F+CL	0.08	0.11	0.02	0.07	0.11	0.03
SUM	100.94	100.01	100.69	100.55	102.04	99.05

	1		2		3		4		5		6	
SI	7.370	*	7.248	*	7.443	*	7.354	*	7.357	*	7.350	*
TI	0.036	*	0.069	*	0.025	*	0.043	*	0.061	*	0.025	*
AL	15.751	*	15.959	*	15.720	*	15.810	*	15.682	*	15.941	*
FE	2.863	*	2.668	*	2.793	*	2.775	*	2.826	*	2.722	*
MN	0.019	*	0.019	*	0.028	*	0.022	*	0.026	*	0.018	*
MG	0.023	*	0.087	*	0.060	*	0.056	*	0.082	*	0.031	*
BA	0.0	*	0.003	*	0.002	*	0.002	*	0.003	*	0.000	*
CA	0.564	*	0.518	*	0.583	*	0.555	*	0.576	*	0.533	*
K	0.0	*	0.019	*	-0.006	*	0.004	*	0.015	*	-0.007	*
NA	0.020	26.645	0.025	26.615	0.0	26.647	0.015	26.636	0.025	26.653	0.004	26.618
F	0.008	*	0.024	*	0.008	*	0.013	*	0.021	*	0.006	*
CL	0.141	0.0	0.180	0.0	0.021	0.0	0.114	0.0	0.179	0.0	0.047	0.0
H	3.851	4.000	3.796	4.000	3.971	4.000	3.873	4.000	3.800	4.000	3.947	4.000
O	44.000	*	44.000	*	44.000	*	44.000	*	44.000	*	44.000	*
	FEMN	99.22		96.87		97.91		98.02		97.22		98.90
	MG	0.78		3.13		2.09		1.98		2.78		1.10
	F/M	127.936		30.960		46.926		49.567		34.929		89.656
	F/FM	0.992		0.969		0.979		0.980		0.972		0.989
	A* =	0.732		0.743		0.734		0.736		0.729		0.743
	A =	0.732		0.743		0.734		0.736		0.729		0.744
	M =	0.008		0.032		0.021		0.020		0.028		0.011

1 32X AG4-6 S1
2 33X AG4-6 S2
3 39X AG4-6
4 AVERAGE
5 AVERAGE PLUS SIGMA
6 AVERAGE MINUS SIGMA

SUPER RECAL — STAUROLITE ANALYSES (OH) CALCULATED

	1	2	3	4	5	6	7	8
SIO2	28.04	28.70	28.35	28.21	28.66	28.39	28.65	28.14
TIO2	0.61	0.68	0.60	0.57	0.63	0.62	0.65	0.58
A203	52.90	52.96	53.04	52.45	52.02	52.67	53.06	52.29
FEO	14.92	15.30	14.68	15.42	15.33	15.13	15.41	14.85
MNO	0.13	0.14	0.13	0.14	0.16	0.14	0.15	0.13
MGO	0.27	0.24	0.35	0.20	0.19	0.25	0.31	0.19
CAO	1.27	1.27	1.24	1.33	1.38	1.30	1.35	1.25
BAO	0.01	0.02	0.02	0.01	0.01	0.01	0.02	0.01
NA2O	0.03	0.02	0.06	0.05	0.05	0.04	0.06	0.03
K2O	0.0	0.02	-0.01	0.0	0.0	0.00	0.01	-0.01
F	0.01	0.01	0.02	0.01	0.02	0.01	0.02	0.01
CL	0.02	0.02	0.02	0.02	0.10	0.04	0.07	0.00
H2O	2.34	2.37	2.35	2.34	2.32	2.34	2.36	2.33
SUM	100.55	101.75	100.85	100.75	100.87	100.95	102.11	99.80
-O= F+CL	0.01	0.01	0.01	0.01	0.03	0.01	0.02	0.00
SUM	100.54	101.74	100.84	100.74	100.84	100.94	102.09	99.79

		*		*		*		*		*		*		*		*
SI	7.140		7.228		7.184		7.188		7.289		7.206		7.197		7.215	
TI	0.117		0.129		0.114		0.109		0.120		0.118		0.124		0.112	
AL	15.872		15.717		15.839		15.748		15.591		15.753		15.708		15.799	
FE	3.177		3.222		3.111		3.286		3.261		3.211		3.238		3.184	
MN	0.028		0.030		0.028		0.030		0.034		0.030		0.032		0.028	
MG	0.102		0.090		0.132		0.076		0.072		0.095		0.115		0.074	
BA	0.001		0.002		0.002		0.001		0.001		0.001		0.002		0.001	
CA	0.346		0.343		0.337		0.363		0.376		0.353		0.363		0.343	
K	0.0		0.006		-0.003		0.0		0.0		0.001		0.004		-0.003	
NA	0.015	26.798	0.010	26.777	0.029	26.774	0.025	26.825	0.025	26.769	0.021	26.789	0.028	26.811	0.014	26.766
F	0.008		0.008		0.016		0.008		0.016		0.011		0.015		0.007	
CL	0.009	0.0	0.009	0.0	0.009	0.0	0.009	0.0	0.043	0.0	0.015	0.0	0.029	0.0	0.002	0.0
H	3.983	4.000	3.983	4.000	3.975	4.000	3.983	4.000	3.941	4.000	3.973	4.000	3.956	4.000	3.991	4.000
O	44.000	*	44.000	*	44.000	*	44.000	*	44.000	*	44.000	*	44.000	*	44.000	*
	FEMN	96.90		97.30		95.96		97.76		97.86		97.17		96.60		97.76
	MG	3.10		2.70		4.04		2.24		2.14		2.83		3.40		2.24
	F/M	31.278		36.100		23.744		43.657		45.748		34.274		28.391		43.683
	F/FM	0.969		0.973		0.960		0.978		0.979		0.972		0.966		0.978
	A* =	0.708		0.703		0.710		0.701		0.701		0.704		0.701		0.708
	A =	0.708		0.703		0.710		0.701		0.701		0.704		0.701		0.708
	M =	0.031		0.027		0.041		0.023		0.022		0.029		0.034		0.023

1 50Y AG5-505 TRV
2 51Y AG5-505
3 55Y AG5-505
4 59Y AG5-505
5 60Y AG5-505
6 AVERAGE
7 AVERAGE PLUS SIGMA
8 AVERAGE MINUS SIGMA

SUPER RECAL — CHLORITE ANALYSES

	1	2	3	4	5
SIO2	24.07	23.64	23.85	24.07	23.64
TIO2	0.19	0.15	0.17	0.19	0.15
A203	23.24	22.79	23.01	23.24	22.79
FEO	28.58	28.58	28.58	28.58	28.58
MNO	0.07	0.07	0.07	0.07	0.07
MGO	11.75	11.16	11.45	11.75	11.16
CAO	0.0	0.0	0.0	0.0	0.0
BAO	-0.13	-0.03	-0.08	-0.03	-0.13
NA20	-0.03	-0.02	-0.02	-0.02	-0.03
K20	-0.03	0.01	-0.01	0.01	-0.03
F	0.09	0.08	0.08	0.09	0.08
CL	0.0	0.0	0.0	0.0	0.0
H20	11.16	10.95	11.05	11.17	10.94
SUM	98.96	97.38	98.17	99.12	97.22
-O= F+CL	0.04	0.03	0.04	0.04	0.03
SUM	98.92	97.35	98.13	99.08	97.19

SI	2.572	*	2.576	*	2.574	*	2.570	*	2.577	*
AL	1.428	4.000	1.424	4.000	1.426	4.000	1.430	4.000	1.423	4.000
AL	1.498	*	1.501	*	1.499	*	1.494	*	1.505	*
TI	0.015	*	0.012	*	0.014	*	0.015	*	0.012	*
FE	2.554	*	2.604	*	2.579	*	2.552	*	2.606	*
MN	0.006	*	0.006	*	0.006	*	0.006	*	0.006	*
MG	1.871	*	1.812	*	1.842	*	1.870	*	1.813	*
CA	0.0	*	0.0	*	0.0	*	0.0	*	0.0	*
NA	-0.006	*	-0.004	*	-0.005	*	-0.004	*	-0.006	*
K	-0.004	*	0.001	*	-0.001	*	0.001	*	-0.004	*
BA	-0.005	5.928	-0.001	5.932	-0.003	5.930	-0.001	5.934	-0.006	5.926
CL	0.0	*	0.0	*	0.0	*	0.0	*	0.0	*
F	0.030	*	0.028	*	0.029	*	0.030	*	0.028	*
H	7.970	8.000	7.972	8.000	7.971	8.000	7.970	8.000	7.972	8.000
O	18.000	*	18.000	*	18.000	*	18.000	*	18.000	*
	MG	42.23		40.98		41.61		42.23		40.98
	FE	57.63		58.88		58.25		57.63		58.88
	MN	0.14		0.15		0.14		0.14		0.15
	F/M	1.368		1.440		1.403		1.368		1.440
	F/FM	0.578		0.590		0.584		0.578		0.590
	A* =	0.249		0.249		0.249		0.248		0.249
	A =	0.249		0.249		0.249		0.248		0.250
	M =	0.423		0.410		0.417		0.423		0.410

1 93F AG4-225 C1
2 94F AG4-225 C2
3 AVERAGE
4 AVERAGE PLUS SIGMA
5 AVERAGE MINUS SIGMA

SUPER RECAL — CHLORITE ANALYSES

	1	2	3	4	5
SIO2	24.70	25.03	24.86	25.03	24.70
TIO2	0.08	0.15	0.11	0.15	0.08
A203	24.08	23.19	23.63	24.08	23.19
FEO	21.70	20.72	21.21	21.70	20.72
MNO	0.43	0.36	0.39	0.43	0.36
MGO	15.68	16.30	15.99	16.30	15.68
CAO	-0.01	0.0	-0.00	0.0	-0.01
BAO	-0.03	0.02	-0.00	0.02	-0.03
NA20	0.01	-0.02	-0.00	0.01	-0.02
K20	-0.03	0.0	-0.02	-0.00	-0.03
F	0.18	0.12	0.15	0.18	0.12
CL	0.0	0.0	0.0	0.0	0.0
H20	11.38	11.34	11.36	11.53	11.20
SUM	98.17	97.21	97.69	99.43	95.96
-O= F+CL	0.08	0.05	0.06	0.08	0.05
SUM	98.09	97.16	97.63	99.35	95.90

SI	2.576	*	2.627	*	2.601	*	2.577	*	2.627	*
AL	1.424	4.000	1.373	4.000	1.399	4.000	1.423	4.000	1.373	4.000
AL	1.536	*	1.495	*	1.515	*	1.499	*	1.532	*
TI	0.006	*	0.012	*	0.009	*	0.012	*	0.006	*
FE	1.893	*	1.819	*	1.856	*	1.868	*	1.843	*
MN	0.038	*	0.032	*	0.035	*	0.038	*	0.032	*
MG	2.438	*	2.550	*	2.493	*	2.501	*	2.485	*
CA	-0.001	*	0.0	*	-0.001	*	0.0	*	-0.001	*
NA	0.002	*	-0.004	*	-0.001	*	0.002	*	-0.004	*
K	-0.004	*	0.0	*	-0.002	*	-0.000	*	-0.004	*
BA	-0.001	5.906	0.001	5.904	-0.000	5.905	0.001	5.921	-0.001	5.888
CL	0.0	*	0.0	*	0.0	*	0.0	*	0.0	*
F	0.059	*	0.040	*	0.050	*	0.059	*	0.040	*
H	7.941	8.000	7.960	8.000	7.950	8.000	7.941	8.000	7.960	8.000
O	18.000	*	18.000	*	18.000	*	18.000	*	18.000	*
	MG	55.80		57.95		56.87		56.76		57.00
	FE	43.33		41.33		42.33		42.39		42.26
	MN	0.87		0.73		0.80		0.85		0.74
	F/M	0.792		0.726		0.758		0.762		0.754
	F/FM	0.442		0.421		0.431		0.432		0.430
	A* =	0.255		0.247		0.251		0.251		0.252
	A =	0.255		0.247		0.251		0.251		0.252
	M =	0.563		0.584		0.573		0.572		0.574

1 1163 AG4-159+ C1
2 1203 AG4-159+ C2
3 AVERAGE
4 AVERAGE PLUS SIGMA
5 AVERAGE MINUS SIGMA

SUPER RECAL — CHLORITE ANALYSES

	1	2	3	4	5	6	7
SIO2	25.07	24.40	25.49	25.27	25.06	25.47	24.65
TIO2	0.08	0.09	0.09	0.08	0.08	0.09	0.08
A203	22.87	22.37	23.18	23.21	22.91	23.25	22.57
FEO	21.00	21.12	20.77	21.28	21.04	21.23	20.86
MNO	0.20	0.23	0.13	0.20	0.19	0.23	0.15
MGO	16.70	16.38	17.25	16.49	16.71	17.04	16.37
CAO	0.0	-0.02	-0.01	-0.01	-0.01	-0.00	-0.02
BAO	-0.08	-0.03	-0.08	0.10	-0.02	0.05	-0.10
NA2O	-0.02	-0.02	-0.05	-0.03	-0.03	-0.02	-0.04
K2O	-0.03	-0.03	-0.03	-0.03	-0.03	-0.03	-0.03
F	0.06	0.09	0.12	0.11	0.09	0.12	0.07
CL	0.0	0.0	0.0	0.0	0.0	0.0	0.0
H2O	11.38	11.14	11.51	11.44	11.37	11.54	11.19
SUM	97.23	95.72	98.37	98.11	97.36	98.95	95.76
-O= F+CL	0.03	0.04	0.05	0.05	0.04	0.05	0.03
SUM	97.20	95.69	98.32	98.06	97.32	98.90	95.73

SI	2.632	*	2.611	*	2.636	*	2.632	*	2.628	*	2.628	*	2.628	*
AL	1.368	4.000	1.389	4.000	1.364	4.000	1.368	4.000	1.372	4.000	1.372	4.000	1.372	4.000
AL	1.461	*	1.432	*	1.461	*	1.481	*	1.459	*	1.454	*	1.464	*
TI	0.006	*	0.007	*	0.007	*	0.006	*	0.007	*	0.007	*	0.006	*
FE	1.844	*	1.890	*	1.796	*	1.854	*	1.846	*	1.832	*	1.860	*
MN	0.018	*	0.021	*	0.011	*	0.018	*	0.017	*	0.020	*	0.014	*
MG	2.613	*	2.613	*	2.659	*	2.560	*	2.611	*	2.621	*	2.602	*
CA	0.0	*	-0.002	*	-0.001	*	-0.001	*	-0.001	*	-0.000	*	-0.002	*
NA	-0.004	*	-0.004	*	-0.010	*	-0.006	*	-0.006	*	-0.004	*	-0.009	*
K	-0.004	*	-0.004	*	-0.004	*	-0.004	*	-0.004	*	-0.004	*	-0.004	*
BA	-0.003	5.931	-0.001	5.951	-0.003	5.916	0.004	5.912	-0.001	5.927	0.002	5.928	-0.004	5.927
CL	0.0	*	0.0	*	0.0	*	0.0	*	0.0	*	0.0	*	0.0	*
F	0.020	*	0.030	*	0.039	*	0.036	*	0.032	*	0.038	*	0.024	*
H	7.980	8.000	7.970	8.000	7.961	8.000	7.964	8.000	7.968	8.000	7.962	8.000	7.976	8.000
O	18.000	*	18.000	*	18.000	*	18.000	*	18.000	*	18.000	*	18.000	*
	MG	58.40		57.76		59.53		57.77		58.37		58.60		58.13
	FE	41.20		41.78		40.22		41.83		41.25		40.96		41.56
	MN	0.40		0.46		0.25		0.40		0.38		0.44		0.31
	F/M	0.712		0.731		0.680		0.731		0.713		0.707		0.720
	F/FM	0.416		0.422		0.405		0.422		0.416		0.414		0.419
	A* =	0.241		0.239		0.241		0.244		0.241		0.241		0.241
	A =	0.242		0.239		0.242		0.245		0.242		0.242		0.242
	M =	0.586		0.580		0.597		0.580		0.586		0.589		0.583

1 139B AG5-929 C1
2 140B AG5-929 C2
3 147C AG5-929 CD3
4 148C AG5-929 C2

5 AVERAGE
6 AVERAGE PLUS SIGMA
7 AVERAGE MINUS SIGMA

SUPER RECAL — CHLORITE ANALYSES

	1	2	3	4	5	6	7	8
SIO2	25.11	25.03	24.85	24.65	24.26	24.78	25.08	24.48
TIO2	0.17	0.73	0.10	0.19	0.13	0.26	0.50	0.03
A203	22.60	22.88	22.66	22.51	22.67	22.66	22.79	22.54
FEO	24.94	25.53	24.80	25.37	25.54	25.24	25.54	24.93
MNO	0.15	0.11	0.19	0.18	0.19	0.16	0.19	0.13
MGO	13.86	13.44	13.54	12.97	13.52	13.47	13.75	13.18
CAO	0.01	0.0	0.01	-0.01	-0.01	0.0	0.01	-0.01
BAO	0.08	0.04	0.09	0.07	0.04	0.06	0.08	0.04
NA20	-0.04	-0.05	-0.04	-0.03	-0.04	-0.04	-0.03	-0.05
K20	0.04	0.03	0.05	0.15	-0.03	0.05	0.11	-0.01
F	0.08	0.07	0.16	0.06	0.15	0.10	0.15	0.06
CL	0.0	0.0	0.0	0.0	0.0	0.0	0.0	0.0
H20	11.27	11.36	11.14	11.11	11.09	11.19	11.34	11.05
SUM	98.27	99.17	97.55	97.22	97.51	97.94	99.51	96.37
-O= F+CL	0.03	0.03	0.07	0.03	0.06	0.04	0.06	0.03
SUM	98.24	99.14	97.48	97.20	97.45	97.90	99.45	96.35

SI	2.658	*	2.631	*	2.650	*	2.649	*	2.600	*	2.638	*	2.630	*	2.646	*
AL	1.342	4.000	1.369	4.000	1.350	4.000	1.351	4.000	1.400	4.000	1.362	4.000	1.370	4.000	1.354	4.000
AL	1.478	*	1.465	*	1.497	*	1.500	*	1.462	*	1.480	*	1.445	*	1.517	*
TI	0.014	*	0.058	*	0.008	*	0.015	*	0.010	*	0.021	*	0.039	*	0.002	*
FE	2.208	*	2.244	*	2.212	*	2.280	*	2.289	*	2.246	*	2.239	*	2.254	*
MN	0.013	*	0.010	*	0.017	*	0.016	*	0.017	*	0.015	*	0.017	*	0.012	*
MG	2.187	*	2.106	*	2.152	*	2.078	*	2.159	*	2.136	*	2.149	*	2.124	*
CA	0.001	*	0.0	*	0.001	*	-0.001	*	-0.001	*	0.0	*	0.001	*	-0.001	*
NA	-0.008	*	-0.010	*	-0.008	*	-0.006	*	-0.008	*	-0.008	*	-0.007	*	-0.010	*
K	0.005	*	0.004	*	0.007	*	0.021	*	-0.004	*	0.007	*	0.014	*	-0.001	*
BA	0.003	5.902	0.002	5.878	0.004	5.889	0.003	5.906	0.002	5.926	0.003	5.900	0.003	5.901	0.002	5.899
CL	0.0	*	0.0	*	0.0	*	0.0	*	0.0	*	0.0	*	0.0	*	0.0	*
F	0.027	*	0.023	*	0.054	*	0.020	*	0.051	*	0.035	*	0.048	*	0.021	*
H	7.973	8.000	7.977	8.000	7.946	8.000	7.980	8.000	7.949	8.000	7.965	8.000	7.952	8.000	7.979	8.000
O	18.000	*	18.000	*	18.000	*	18.000	*	18.000	*	18.000	*	18.000	*	18.000	*
	MG	49.61		48.30		49.12		47.50		48.36		48.58		48.78		48.38
	FE	50.09		51.48		50.48		52.13		51.26		51.08		50.83		51.34
	MN	0.31		0.22		0.39		0.37		0.39		0.34		0.39		0.28
	F/M	1.016		1.070		1.036		1.105		1.068		1.058		1.050		1.067
	F/FM	0.504		0.517		0.509		0.525		0.516		0.514		0.512		0.516
	A* =	0.243		0.245		0.246		0.245		0.244		0.244		0.242		0.247
	A =	0.242		0.245		0.245		0.242		0.244		0.244		0.240		0.247
	M =	0.498		0.484		0.493		0.477		0.485		0.487		0.490		0.485

1 1682 AG4-78 C1
2 1692 AG4-78 C2 MID
3 1712 AG4-78 C3 CORE
4 1733 AG4-78 C1
5 1826 AG4-78 C1 NEAR QTZ
6 AVERAGE
7 AVERAGE PLUS SIGMA
8 AVERAGE MINUS SIGMA

SUPER RECAL — CHLORITE ANALYSES

	1	2	3	4	5	6	7
SIO2	23.72	24.11	27.57	24.88	25.07	26.57	23.57
TIO2	0.13	0.15	0.25	0.20	0.18	0.23	0.14
A203	23.31	23.09	23.98	22.12	23.12	23.79	22.46
FEO	29.03	29.09	25.30	28.48	27.97	29.54	26.41
MNO	0.29	0.26	0.26	0.30	0.28	0.30	0.26
MGO	11.53	10.89	9.89	11.55	10.96	11.64	10.29
CAO	0.0	0.01	0.0	0.01	0.00	0.01	-0.00
BAO	0.15	0.04	0.16	0.07	0.10	0.16	0.05
NA20	-0.03	-0.04	0.12	-0.04	0.00	0.07	-0.07
K20	-0.03	-0.03	1.28	0.16	0.34	0.89	-0.20
F	0.0	0.05	0.06	0.02	0.03	0.06	0.01
CL	0.0	0.0	0.0	0.0	0.0	0.0	0.0
H20	11.18	11.10	11.53	11.17	11.24	11.83	10.65
SUM	99.28	98.72	100.40	98.92	99.33	105.08	93.57
-O= F+CL	0.0	0.02	0.03	0.01	0.01	0.02	0.00
SUM	99.28	98.70	100.37	98.91	99.31	105.06	93.57

SI	2.543	*	2.594	*	2.856	*	2.667	*	2.667	*	2.683	*	2.649	*
AL	1.457	4.000	1.406	4.000	1.144	4.000	1.333	4.000	1.333	4.000	1.317	4.000	1.351	4.000
AL	1.488	*	1.522	*	1.784	*	1.462	*	1.566	*	1.514	*	1.624	*
TI	0.010	*	0.012	*	0.019	*	0.016	*	0.015	*	0.017	*	0.011	*
FE	2.603	*	2.618	*	2.192	*	2.553	*	2.489	*	2.494	*	2.483	*
MN	0.026	*	0.024	*	0.023	*	0.027	*	0.025	*	0.025	*	0.025	*
MG	1.843	*	1.747	*	1.527	*	1.846	*	1.739	*	1.752	*	1.724	*
CA	0.0	*	0.001	*	0.0	*	0.001	*	0.001	*	0.001	*	-0.000	*
NA	-0.006	*	-0.008	*	0.024	*	-0.008	*	0.001	*	0.014	*	-0.014	*
K	-0.004	*	-0.004	*	0.169	*	0.022	*	0.047	*	0.115	*	-0.029	*
BA	0.006	5.967	0.002	5.913	0.006	5.745	0.003	5.921	0.004	5.885	0.006	5.938	0.002	5.827
CL	0.0	*	0.0	*	0.0	*	0.0	*	0.0	*	0.0	*	0.0	*
F	0.0	*	0.017	*	0.020	*	0.007	*	0.011	*	0.018	*	0.003	*
H	8.000	8.000	7.983	8.000	7.980	8.000	7.993	8.000	7.989	8.000	7.982	8.000	7.997	8.000
O	18.000	*	18.000	*	18.000	*	18.000	*	18.000	*	18.000	*	18.000	*
MG	41.20		39.80		40.81		41.70		40.89		41.01		40.74	
FE	58.21		59.66		58.58		57.69		58.53		58.39		58.67	
MN	0.59		0.54		0.61		0.62		0.59		0.59		0.58	
F/M	1.427		1.512		1.450		1.398		1.446		1.438		1.455	
F/FM	0.588		0.602		0.592		0.583		0.591		0.590		0.593	
A* =	0.249		0.251		0.271		0.240		0.252		0.242		0.263	
A =	0.250		0.252		0.246		0.237		0.246		0.227		0.267	
M =	0.414		0.400		0.411		0.420		0.411		0.413		0.410	

1 190E AG4-34 C1 CORE
2 192E AG4-34 CD1 WITH CLD
3 195D AG4-34 C1 WITH CLD
4 203B AG4-34 C1 WITH MUS
5 AVERAGE
6 AVERAGE PLUS SIGMA
7 AVERAGE MINUS SIGMA

SUPER RECAL — CHLORITE ANALYSES

	1	2	3	4	5
SIO2	25.91	25.51	25.71	25.91	25.51
TIO2	0.07	0.06	0.06	0.07	0.06
A203	24.18	23.60	23.89	24.18	23.60
FEO	16.18	16.41	16.29	16.41	16.18
MNO	0.08	0.15	0.11	0.15	0.08
MGO	19.85	20.14	19.99	20.14	19.85
CAO	-0.02	-0.01	-0.02	-0.01	-0.02
BAO	0.06	0.07	0.06	0.07	0.06
NA2O	-0.02	-0.04	-0.03	-0.02	-0.04
K2O	0.07	-0.04	0.01	0.07	-0.04
F	0.13	0.04	0.08	0.13	0.04
CL	0.0	0.0	0.0	0.0	0.0
H2O	11.74	11.68	11.71	11.80	11.62
SUM	98.23	97.57	97.90	98.90	96.90
-O= F+CL	0.05	0.02	0.04	0.05	0.02
SUM	98.18	97.55	97.86	98.85	96.88

SI	2.627	*	2.612	*	2.619	*	2.613	*	2.626	*
AL	1.373	4.000	1.388	4.000	1.381	4.000	1.387	4.000	1.374	4.000
AL	1.515	*	1.460	*	1.488	*	1.487	*	1.488	*
TI	0.005	*	0.005	*	0.005	*	0.005	*	0.005	*
FE	1.372	*	1.405	*	1.388	*	1.384	*	1.393	*
MN	0.007	*	0.013	*	0.010	*	0.013	*	0.007	*
MG	2.999	*	3.074	*	3.036	*	3.028	*	3.045	*
CA	-0.002	*	-0.001	*	-0.002	*	-0.001	*	-0.002	*
NA	-0.004	*	-0.008	*	-0.006	*	-0.004	*	-0.008	*
K	0.009	*	-0.005	*	0.002	*	0.009	*	-0.005	*
BA	0.002	5.904	0.003	5.945	0.003	5.924	0.003	5.925	0.002	5.924
CL	0.0	*	0.0	*	0.0	*	0.0	*	0.0	*
F	0.042	*	0.013	*	0.027	*	0.041	*	0.013	*
H	7.958	8.000	7.987	8.000	7.973	8.000	7.959	8.000	7.987	8.000
O	18.000	*	18.000	*	18.000	*	18.000	*	18.000	*
	MG	68.51		68.43		68.47		68.43		68.51
	FE	31.33		31.28		31.31		31.28		31.33
	MN	0.16		0.29		0.22		0.29		0.16
	F/M	0.460		0.461		0.461		0.461		0.460
	F/FM	0.315		0.316		0.315		0.316		0.315
	A* =	0.248		0.242		0.245		0.245		0.244
	A =	0.247		0.242		0.244		0.244		0.245
	M =	0.686		0.686		0.686		0.686		0.686

1 2546 AG5-268+ C1 WITH GT
2 2566 AG5-268+ C2 WITH ST
3 AVERAGE
4 AVERAGE PLUS SIGMA
5 AVERAGE MINUS SIGMA

SUPER RECAL — CHLORITE ANALYSES

	1	2	3	4	5	6	7
SIO2	24.57	24.92	25.63	25.61	25.18	25.64	24.73
TIO2	0.08	0.10	0.29	0.32	0.20	0.31	0.09
A2O3	23.59	23.50	22.08	22.93	23.02	23.63	22.42
FEO	27.27	27.12	26.56	26.14	26.77	27.22	26.32
MNO	0.42	0.30	0.35	0.39	0.36	0.41	0.32
MGO	12.79	13.38	13.84	13.84	13.46	13.89	13.03
CAO	0.04	0.06	0.07	0.04	0.05	0.07	0.04
BAO	0.0	0.0	0.0	0.0	0.0	0.0	0.0
NA2O	-0.01	0.01	0.04	0.02	0.01	0.03	-0.00
K2O	0.02	0.03	0.25	0.24	0.13	0.25	0.02
F	0.0	0.0	0.0	0.0	0.0	0.0	0.0
CL	0.0	0.0	0.0	0.0	0.0	0.0	0.0
H2O	11.40	11.51	11.48	11.58	11.49	11.78	11.21
SUM	100.17	100.93	100.59	101.11	100.70	103.22	98.19
-O= F+CL	0.0	0.0	0.0	0.0	0.0	0.0	0.0
SUM	100.17	100.93	100.59	101.11	100.70	103.22	98.19

SI	2.582	*	2.594	*	2.675	*	2.650	*	2.625	*	2.609	*	2.643	*
AL	1.418	4.000	1.406	4.000	1.325	4.000	1.350	4.000	1.375	4.000	1.391	4.000	1.357	4.000
AL	1.502	*	1.476	*	1.390	*	1.447	*	1.454	*	1.441	*	1.467	*
TI	0.006	*	0.008	*	0.023	*	0.025	*	0.015	*	0.023	*	0.007	*
FE	2.396	*	2.361	*	2.318	*	2.262	*	2.334	*	2.317	*	2.352	*
MN	0.037	*	0.026	*	0.031	*	0.034	*	0.032	*	0.035	*	0.029	*
MG	2.003	*	2.076	*	2.153	*	2.135	*	2.092	*	2.107	*	2.076	*
CA	0.005	*	0.007	*	0.008	*	0.004	*	0.006	*	0.007	*	0.005	*
NA	-0.002	*	0.002	*	0.008	*	0.004	*	0.003	*	0.007	*	-0.001	*
K	0.003	*	0.004	*	0.033	*	0.032	*	0.018	*	0.032	*	0.003	*
BA	0.0	5.950	0.0	5.959	0.0	5.964	0.0	5.943	0.0	5.954	0.0	5.969	0.0	5.938
CL	0.0	*	0.0	*	0.0	*	0.0	*	0.0	*	0.0	*	0.0	*
F	0.0	*	0.0	*	0.0	*	0.0	*	0.0	*	0.0	*	0.0	*
H	8.000	8.000	8.000	8.000	8.000	8.000	8.000	8.000	8.000	8.000	8.000	8.000	8.000	8.000
O	18.000	*	18.000	*	18.000	*	18.000	*	18.000	*	18.000	*	18.000	*
MG	45.15		46.51		47.82		48.18		46.92		47.26		46.57	
FE	54.01		52.90		51.49		51.05		52.36		51.95		52.78	
MN	0.84		0.59		0.69		0.77		0.72		0.79		0.65	
F/M	1.215		1.150		1.091		1.076		1.131		1.116		1.147	
F/FM	0.549		0.535		0.522		0.518		0.531		0.527		0.534	
A* =	0.249		0.245		0.231		0.239		0.241		0.240		0.242	
A =	0.249		0.244		0.226		0.235		0.239		0.236		0.241	
M =	0.455		0.468		0.482		0.486		0.473		0.476		0.469	

1 AG5-1195 2CL2
2 AG5-1195 3CL1
3 AG5-1195 BCL1
4 AG5-1195 BCL3

5 AVERAGE
6 AVERAGE PLUS SIGMA
7 AVERAGE MINUS SIGMA

SUPER RECAL — CHLORITE ANALYSES

	1	2	3	4	5	6	7
SIO2	23.94	24.26	25.02	25.52	24.68	25.31	24.06
TIO2	0.22	0.25	0.13	0.48	0.27	0.40	0.14
A203	23.59	22.54	23.55	23.04	23.18	23.61	22.75
FEO	29.04	28.85	27.54	28.07	28.38	28.98	27.77
MNO	0.25	0.26	0.23	0.21	0.24	0.26	0.22
MGO	10.94	10.40	10.45	10.57	10.59	10.80	10.38
CAO	0.09	0.11	0.05	0.12	0.09	0.12	0.07
BAO	0.0	0.0	0.0	0.0	0.0	0.0	0.0
NA2O	0.08	0.13	0.12	0.09	0.10	0.13	0.08
K2O	0.07	0.09	0.53	0.19	0.22	0.40	0.04
F	0.0	0.0	0.0	0.0	0.0	0.0	0.0
CL	0.0	0.0	0.0	0.0	0.0	0.0	0.0
H2O	11.21	11.03	11.23	11.32	11.20	11.47	10.92
SUM	99.43	97.92	98.85	99.61	98.95	101.47	96.43
-O= F+CL	0.0	0.0	0.0	0.0	0.0	0.0	0.0
SUM	99.43	97.92	98.85	99.61	98.95	101.47	96.43

SI	2.560	*	2.635	*	2.670	*	2.702	*	2.642	*	2.644	*	2.640	*
AL	1.440	4.000	1.365	4.000	1.330	4.000	1.298	4.000	1.358	4.000	1.356	4.000	1.360	4.000
AL	1.532	*	1.520	*	1.632	*	1.576	*	1.565	*	1.550	*	1.581	*
TI	0.018	*	0.020	*	0.010	*	0.038	*	0.022	*	0.031	*	0.012	*
FE	2.597	*	2.620	*	2.458	*	2.485	*	2.540	*	2.532	*	2.548	*
MN	0.023	*	0.024	*	0.021	*	0.019	*	0.022	*	0.023	*	0.020	*
MG	1.743	*	1.684	*	1.662	*	1.668	*	1.689	*	1.682	*	1.697	*
CA	0.010	*	0.013	*	0.006	*	0.014	*	0.011	*	0.013	*	0.008	*
NA	0.017	*	0.027	*	0.025	*	0.018	*	0.022	*	0.025	*	0.018	*
K	0.010	*	0.012	*	0.072	*	0.026	*	0.030	*	0.054	*	0.005	*
BA	0.0	5.948	0.0	5.921	0.0	5.886	0.0	5.844	0.0	5.899	0.0	5.910	0.0	5.888
CL	0.0	*	0.0	*	0.0	*	0.0	*	0.0	*	0.0	*	0.0	*
F	0.0	*	0.0	*	0.0	*	0.0	*	0.0	*	0.0	*	0.0	*
H	8.000	8.000	8.000	8.000	8.000	8.000	8.000	8.000	8.000	8.000	8.000	8.000	8.000	8.000
O	18.000	*	18.000	*	18.000	*	18.000	*	18.000	*	18.000	*	18.000	*
	MG	39.96		38.90		40.14		39.98		39.74		39.70		39.79
	FE	59.52		60.55		59.36		59.57		59.75		59.76		59.74
	MN	0.52		0.55		0.50		0.45		0.51		0.54		0.48
	F/M	1.502		1.571		1.491		1.501		1.516		1.519		1.513
	F/FM	0.600		0.611		0.599		0.600		0.603		0.603		0.602
	A* =	0.254		0.250		0.260		0.255		0.255		0.253		0.257
	A =	0.253		0.249		0.250		0.252		0.251		0.246		0.256
	M =	0.402		0.391		0.403		0.402		0.399		0.399		0.400

1 AG5-388 UCHL1
2 AG5-388 UCL4
3 AG5-388 XCL2
4 AG5-388 XCL4

5 AVERAGE
6 AVERAGE PLUS SIGMA
7 AVERAGE MINUS SIGMA

SUPER RECAL — CHLORITOID ANALYSES

	1	2	3	4	5	6	7	8
SIO2	26.77	24.72	24.33	24.98	24.85	24.95	25.06	25.09
TIO2	0.07	0.06	0.06	0.06	0.08	0.06	0.06	0.06
A2O3	40.83	40.27	39.77	41.05	41.16	40.56	41.03	40.67
FEO	20.35	22.78	23.12	21.90	22.04	22.58	21.98	22.11
MNO	1.61	2.04	1.94	1.92	1.70	1.78	1.88	1.84
MGO	2.63	3.05	3.03	2.98	3.09	3.05	3.07	2.99
CAO	0.02	-0.01	-0.02	-0.01	0.0	-0.01	-0.01	-0.01
NA2O	0.0	-0.06	0.04	-0.05	0.0	-0.01	0.01	-0.01
K2O	0.41	-0.02	-0.03	-0.04	-0.03	-0.03	-0.05	0.03
F	0.66	-0.03	-0.02	-0.03	-0.02	-0.03	-0.02	0.07
H2O	7.10	7.30	7.23	7.35	7.35	7.33	7.36	7.29
SUM	100.45	100.10	99.45	100.11	100.22	100.23	100.37	100.13
-O= F	0.28	-0.01	-0.01	-0.01	-0.01	-0.01	-0.01	0.03
SUM	100.17	100.12	99.46	100.12	100.23	100.25	100.38	100.10

SI	2.149	*	2.033	*	2.020	*	2.041	*	2.028	*	2.043	*	2.042	*	2.051	*
AL	0.0	2.149	0.0	2.033	0.0	2.020	0.0	2.041	0.0	2.028	0.0	2.043	0.0	2.042	0.0	2.051
AL	3.863	*	3.902	*	3.891	*	3.952	*	3.959	*	3.913	*	3.940	*	3.917	*
TI	0.004	*	0.004	*	0.004	*	0.004	*	0.005	*	0.004	*	0.004	*	0.004	*
FE	0.133	4.000	0.094	4.000	0.105	4.000	0.044	4.000	0.036	4.000	0.083	4.000	0.056	4.000	0.079	4.000
FE	1.233	*	1.472	*	1.500	*	1.452	*	1.468	*	1.463	*	1.442	*	1.432	*
MN	0.109	*	0.142	*	0.136	*	0.133	*	0.118	*	0.123	*	0.130	*	0.127	*
MG	0.315	*	0.374	*	0.375	*	0.363	*	0.376	*	0.372	*	0.373	*	0.364	*
CA	0.002	*	-0.001	*	-0.002	*	-0.001	*	0.0	*	-0.001	*	-0.001	*	-0.001	*
NA	0.0	*	-0.010	*	0.006	*	-0.008	*	0.0	*	-0.002	*	0.002	*	-0.002	*
K	0.042	1.701	-0.002	1.976	-0.003	2.013	-0.004	1.935	-0.003	1.958	-0.003	1.953	-0.005	1.940	0.003	1.924
F	0.168	*	-0.008	*	-0.005	*	-0.008	*	-0.005	*	-0.008	*	-0.005	*	0.019	*
H	3.832	4.000	4.008	4.000	4.005	4.000	4.008	4.000	4.005	4.000	4.008	4.000	4.005	4.000	3.981	4.000
O	14.000	*	14.000	*	14.000	*	14.000	*	14.000	*	14.000	*	14.000	*	14.000	*
MG		17.58		17.95		17.71		18.22		18.82		18.23		18.64		18.17
FE		76.31		75.23		75.84		75.11		75.30		75.72		74.87		75.48
MN		6.11		6.82		6.45		6.67		5.88		6.05		6.49		6.36
F/M		4.266		4.319		4.364		4.367		4.218		4.263		4.215		4.287
F/FM		0.810		0.812		0.814		0.814		0.808		0.810		0.808		0.811
A* =		0.532		0.502		0.496		0.516		0.513		0.505		0.513		0.511
A =		0.526		0.502		0.496		0.516		0.513		0.506		0.514		0.510
M =		0.187		0.193		0.189		0.195		0.200		0.194		0.199		0.194

1 991 AG4-159+ CD
2 1032 AG4-159+ CD1 RIM
3 1062 AG4-159+ CD2
4 1112 AG4-159+ W/KY
5 1193 AG4-159+
6 1234 AG4-159+ CD1 W/KY
7 1254 AG4-159+ CD2 CORE
8 AVERAGE

SUPER RECAL CHLORITOID ANALYSES

	9	10
SIO2	25.81	24.37
TIO2	0.07	0.06
A203	41.13	40.20
FEO	22.94	21.27
MNO	1.98	1.70
MGO	3.13	2.84
CAO	0.01	-0.02
NA20	0.02	-0.04
K20	0.19	-0.13
F	0.31	-0.17
H20	7.35	7.23
SUM	102.94	97.32
-O= F	0.13	-0.07
SUM	102.81	97.39

SI	2.056	*	2.046	*
AL	0.0	2.056	0.0	2.046
AL	3.861	*	3.976	*
TI	0.004	*	0.004	*
FE	0.135	4.000	0.020	4.000
FE	1.394	*	1.473	*
MN	0.133	*	0.121	*
MG	0.372	*	0.355	*
CA	0.001	*	-0.002	*
NA	0.003	*	-0.007	*
K	0.019	1.922	-0.013	1.927
F	0.079	*	-0.044	*
H	3.921	4.000	4.044	4.000
O	14.000	*	14.000	*
	MG	18.30		18.02
	FE	75.14		75.84
	MN	6.56		6.14
	F/M	4.103		4.490
	F/FM	0.804		0.818
	A* =	0.503		0.519
	A =	0.500		0.521
	M =	0.196		0.192

9 AVERAGE PLUS SIGMA

10 AVERAGE MINUS SIGMA

SUPER RECAL — CHLORITOID ANALYSES

	1	2	3	4	5	6	7	8
SIO2	24.62	24.76	25.30	24.30	26.25	24.92	25.63	25.00
TIO2	0.05	0.25	0.05	0.07	0.06	0.04	0.06	0.06
A203	40.29	40.19	41.41	40.61	40.96	40.77	40.54	41.06
FEO	23.43	22.77	21.82	22.69	19.72	22.52	22.19	21.25
MNO	0.92	0.87	0.89	0.89	0.77	0.96	1.02	0.88
MGO	3.29	3.39	3.43	3.33	2.87	3.35	3.03	2.99
CAO	-0.02	-0.01	0.01	0.0	1.04	0.02	0.08	0.07
NA20	0.07	-0.08	0.07	-0.05	-0.05	0.02	0.06	-0.05
K20	-0.02	-0.04	0.0	-0.01	0.27	-0.02	0.08	0.05
F	-0.03	-0.03	-0.02	-0.02	0.0	-0.03	0.14	-0.01
H20	7.30	7.29	7.40	7.26	7.37	7.34	7.28	7.28
SUM	99.90	99.36	100.36	99.07	99.26	99.89	100.11	98.58
-0= F	-0.01	-0.01	-0.01	-0.01	0.0	-0.01	0.06	-0.00
SUM	99.91	99.37	100.37	99.07	99.26	99.90	100.05	98.58

SI	2.026	*	2.040	*	2.051	*	2.009	*	2.133	*	2.040	*	2.087	*	2.059	*
AL	0.0	2.026	0.0	2.040	0.0	2.051	0.0	2.009	0.0	2.133	0.0	2.040	0.0	2.087	0.0	2.059
AL	3.907	*	3.902	*	3.955	*	3.957	*	3.922	*	3.932	*	3.889	*	3.985	*
TI	0.003	*	0.015	*	0.003	*	0.004	*	0.004	*	0.002	*	0.004	*	0.004	*
FE	0.090	4.000	0.082	4.000	0.042	4.000	0.039	4.000	0.074	4.000	0.065	4.000	0.107	4.000	0.012	4.000
FE	1.523	*	1.487	*	1.437	*	1.531	*	1.266	*	1.476	*	1.404	*	1.452	*
MN	0.064	*	0.061	*	0.061	*	0.062	*	0.053	*	0.067	*	0.070	*	0.061	*
MG	0.404	*	0.416	*	0.414	*	0.410	*	0.348	*	0.409	*	0.368	*	0.367	*
CA	-0.002	*	-0.001	*	0.001	*	0.0	*	0.091	*	0.002	*	0.007	*	0.006	*
NA	0.011	*	-0.013	*	0.011	*	-0.008	*	-0.008	*	0.003	*	0.009	*	-0.008	*
K	-0.002	1.998	-0.004	1.946	0.0	1.924	-0.001	1.994	0.028	1.777	-0.002	1.954	0.008	1.867	0.005	1.884
F	-0.008	*	-0.008	*	-0.005	*	-0.005	*	0.0	*	-0.008	*	0.036	*	-0.003	*
H	4.008	4.000	4.008	4.000	4.005	4.000	4.005	4.000	4.000	4.000	4.008	4.000	3.964	4.000	4.003	4.000
O	14.000	*	14.000	*	14.000	*	14.000	*	14.000	*	14.000	*	14.000	*	14.000	*
	MG	19.40		20.35		21.20		20.10		19.97		20.27		18.87		19.40
	FE	77.52		76.68		75.67		76.85		76.99		76.43		77.52		77.36
	MN	3.08		2.97		3.13		3.05		3.04		3.30		3.61		3.24
	F/M	3.932		3.717		3.615		3.881		3.794		3.775		4.010		4.123
	F/FM	0.797		0.788		0.783		0.795		0.791		0.791		0.800		0.805
	A* =	0.492		0.496		0.511		0.500		0.536		0.502		0.508		0.521
	A =	0.493		0.496		0.511		0.500		0.532		0.502		0.507		0.520
	M =	0.200		0.210		0.219		0.207		0.206		0.210		0.196		0.200

1 133A AG5-929 CD2
2 143C AG5-929 CD1
3 144C AG5-929 CD2
4 149C AG5-929 CD3
5 152D AG5-929 W/MT
6 153C AG5-929 DC2
7 158F AG5-929 CD1 ZONED
8 159F AG5-929 CD2 ZONED

SUPER RECAL — CHLORITOID ANALYSES

	9	10	11
SIO2	25.10	25.68	24.52
TIO2	0.08	0.14	0.02
A203	40.73	41.11	40.35
FEO	22.05	23.12	20.98
MNO	0.90	0.97	0.83
MGO	3.21	3.41	3.01
CAO	0.15	0.49	-0.19
NA2O	-0.00	0.06	-0.06
K2O	0.04	0.13	-0.06
F	0.00	0.05	-0.05
H2O	7.31	7.47	7.16
SUM	99.57	102.63	96.50
-O= F	0.00	0.02	-0.02
SUM	99.57	102.61	96.52

SI	2.056	*	2.051	*	2.061	*
AL	0.0	2.056	0.0	2.051	0.0	2.061
AL	3.931	*	3.869	*	3.997	*
TI	0.005	*	0.009	*	0.001	*
FE	0.064	4.000	0.122	4.000	0.002	4.000
FE	1.447	*	1.422	*	1.472	*
MN	0.062	*	0.065	*	0.059	*
MG	0.392	*	0.406	*	0.377	*
CA	0.013	*	0.042	*	-0.017	*
NA	-0.000	*	0.009	*	-0.010	*
K	0.004	1.918	0.014	1.958	-0.006	1.876
F	0.000	*	0.014	*	-0.014	*
H	4.000	4.000	3.986	4.000	4.014	4.000
O	14.000	*	14.000	*	14.000	*
	MG	19.95		20.14		19.74
	FE	76.87		76.62		77.16
	MN	3.18		3.25		3.10
	F/M	3.850		3.665		4.060
	F/FM	0.794		0.786		0.802
	A* =	0.508		0.497		0.519
	A =	0.507		0.495		0.520
	M =	0.206		0.208		0.204

9 AVERAGE
10 AVERAGE PLUS SIGMA
11 AVERAGE MINUS SIGMA

SUPER RECAL — CHLORITOID ANALYSES

	1	2	3	4	5	6	7	8
SIO2	24.75	24.72	24.34	24.09	24.83	24.71	24.82	24.71
TIO2	0.06	0.12	0.04	0.05	0.08	0.08	0.07	0.08
A203	40.25	39.89	41.19	40.96	40.53	41.56	40.63	41.09
FEO	24.79	24.75	24.27	24.28	24.78	24.40	24.55	24.73
MNO	0.83	0.71	0.75	0.71	0.72	0.82	0.83	0.76
MGO	2.25	2.29	2.38	2.30	2.30	2.18	2.10	2.24
CAO	-0.01	-0.01	-0.01	-0.01	-0.02	-0.01	-0.02	-0.01
NA20	0.25	0.26	0.13	0.21	0.17	0.31	0.04	0.10
K20	-0.04	-0.02	0.0	-0.05	-0.01	-0.04	-0.03	-0.01
F	-0.02	-0.03	-0.02	-0.03	-0.03	-0.03	-0.02	-0.03
H20	7.29	7.26	7.31	7.26	7.32	7.39	7.30	7.35
SUM	100.40	99.94	100.38	99.77	100.67	101.37	100.27	101.01
-O= F	-0.01	-0.01	-0.01	-0.01	-0.01	-0.01	-0.01	-0.01
SUM	100.40	99.95	100.39	99.78	100.68	101.38	100.27	101.02

SI	2.038	*	2.045	*	1.999	*	1.992	*	2.037	*	2.009	*	2.041	*	2.019	*
AL	0.0	2.038	0.0	2.045	0.001	2.000	0.008	2.000	0.0	2.037	0.0	2.009	0.0	2.041	0.0	2.019
AL	3.906	*	3.889	*	3.984	*	3.983	*	3.918	*	3.982	*	3.937	*	3.956	*
TI	0.004	*	0.007	*	0.002	*	0.003	*	0.005	*	0.005	*	0.004	*	0.005	*
FE	0.091	4.000	0.104	4.000	0.013	4.000	0.014	4.000	0.078	4.000	0.013	4.000	0.058	4.000	0.040	4.000
FE	1.617	*	1.609	*	1.654	*	1.665	*	1.622	*	1.646	*	1.630	*	1.650	*
MN	0.058	*	0.050	*	0.052	*	0.050	*	0.050	*	0.056	*	0.058	*	0.053	*
MG	0.276	*	0.282	*	0.291	*	0.283	*	0.281	*	0.264	*	0.257	*	0.273	*
CA	-0.001	*	-0.001	*	-0.001	*	-0.001	*	-0.002	*	-0.001	*	-0.002	*	-0.001	*
NA	0.040	*	0.042	*	0.021	*	0.034	*	0.027	*	0.049	*	0.006	*	0.016	*
K	-0.004	1.986	-0.002	1.980	0.0	2.017	-0.005	2.026	-0.001	1.978	-0.004	2.010	-0.003	1.947	-0.001	1.989
F	-0.005	*	-0.008	*	-0.005	*	-0.008	*	-0.008	*	-0.008	*	-0.005	*	-0.008	*
H	4.005	4.000	4.008	4.000	4.005	4.000	4.008	4.000	4.008	4.000	4.008	4.000	4.005	4.000	4.008	4.000
O	14.000	*	14.000	*	14.000	*	14.000	*	14.000	*	14.000	*	14.000	*	14.000	*
MG		13.53		13.81		14.49		14.09		13.84		13.34		12.85		13.54
FE		83.63		83.75		82.91		83.44		83.69		83.80		84.27		83.85
MN		2.84		2.43		2.60		2.47		2.46		2.85		2.89		2.61
F/M		6.064		5.873		5.855		6.049		5.947		6.443		6.557		6.242
F/FM		0.858		0.855		0.854		0.858		0.856		0.866		0.868		0.862
A* =		0.496		0.494		0.504		0.505		0.497		0.509		0.503		0.502
A =		0.497		0.494		0.504		0.505		0.497		0.509		0.504		0.502
M =		0.139		0.142		0.149		0.144		0.142		0.137		0.132		0.139

1 184G AG4-34 CD1 RIM
2 185G AG4-34 CD2 CORE
3 187F AG4-34 RIM
4 188F AG4-34 CD1
5 193C AG4-34 RIM
6 194D AG4-34 CORE
7 198C AG4-34 CD1
8 199C AG4-34 S2

SUPER RECAL — CHLORITOID ANALYSES

	9	10	11	12	13
SIO2	24.22	24.49	24.57	24.82	24.32
TIO2	0.07	0.06	0.07	0.09	0.05
A203	40.38	40.54	40.70	41.17	40.23
FEO	24.63	24.42	24.56	24.75	24.37
MNO	0.89	0.79	0.78	0.84	0.72
MGO	2.17	2.17	2.24	2.32	2.16
CAO	-0.01	-0.01	-0.01	-0.01	-0.02
NA20	0.07	0.14	0.17	0.25	0.08
K20	-0.05	0.01	-0.02	-0.00	-0.04
F	-0.02	-0.02	-0.02	-0.02	-0.03
H20	7.23	7.26	7.30	7.38	7.21
SUM	99.58	99.85	100.32	101.60	99.05
-O= F	-0.01	-0.01	-0.01	-0.01	-0.01
SUM	99.59	99.86	100.33	101.61	99.06

SI	2.011	*	2.024	*	2.021	*	2.017	*	2.026	*
AL	0.0	2.011	0.0	2.024	0.0	2.021	0.0	2.017	0.0	2.026
AL	3.951	*	3.949	*	3.946	*	3.943	*	3.950	*
TI	0.004	*	0.004	*	0.004	*	0.006	*	0.003	*
FE	0.045	4.000	0.048	4.000	0.049	4.000	0.051	4.000	0.047	4.000
FE	1.665	*	1.640	*	1.641	*	1.631	*	1.650	*
MN	0.063	*	0.055	*	0.054	*	0.058	*	0.051	*
MG	0.269	*	0.267	*	0.274	*	0.281	*	0.268	*
CA	-0.001	*	-0.001	*	-0.001	*	-0.001	*	-0.001	*
NA	0.011	*	0.022	*	0.027	*	0.040	*	0.014	*
K	-0.005	2.002	0.001	1.986	-0.003	1.993	-0.000	2.008	-0.005	1.977
F	-0.005	*	-0.005	*	-0.007	*	-0.005	*	-0.008	*
H	4.005	4.000	4.005	4.000	4.007	4.000	4.005	4.000	4.008	4.000
O	14.000	*	14.000	*	14.000	*	14.000	*	14.000	*
	MG	13.16		13.30		13.60		13.89		13.29
	FE	83.78		83.95		83.71		83.25		84.18
	MN	3.07		2.75		2.70		2.86		2.53
	F/M	6.435		6.343		6.176		6.018		6.346
	F/FM	0.865		0.864		0.861		0.858		0.864
	A* =	0.500		0.502		0.501		0.501		0.501
	A =	0.501		0.502		0.502		0.501		0.502
	M =	0.136		0.137		0.140		0.143		0.136

9 2008 AG4-34 CD2
10 201B AG4-34
11 AVERAGE
12 AVERAGE PLUS SIGMA
13 AVERAGE MINUS SIGMA

SUPER RECAL — CHLORITOID ANALYSES

	1	2	3	4	5	6	7	8
SIO2	24.69	25.26	25.58	25.11	24.63	25.05	25.41	24.70
TIO2	0.07	0.07	0.06	0.22	0.18	0.12	0.19	0.05
A2O3	40.61	39.35	40.71	39.47	40.32	40.09	40.66	39.52
FEO	23.69	23.52	22.50	23.70	23.39	23.36	23.81	22.91
MNO	1.05	1.07	1.07	1.15	1.20	1.11	1.17	1.05
MGO	2.32	2.34	2.20	2.17	2.16	2.24	2.31	2.16
CAO	0.38	0.32	0.63	0.20	0.19	0.34	0.50	0.18
NA2O	0.0	0.0	0.0	0.0	0.0	0.0	0.0	0.0
K2O	0.12	0.16	0.37	0.16	0.13	0.19	0.28	0.10
F	0.01	0.03	0.02	0.14	0.14	0.07	0.13	0.01
H2O	7.28	7.21	7.34	7.16	7.17	7.23	7.33	7.13
SUM	100.22	99.33	100.48	99.48	99.51	99.80	101.79	97.82
-O= F	0.00	0.01	0.01	0.06	0.06	0.03	0.05	0.00
SUM	100.22	99.32	100.47	99.42	99.45	99.77	101.74	97.81

SI	2.030	*	2.094	*	2.086	*	2.079	*	2.037	*	2.065	*	2.057	*	2.074	*
AL	0.0	2.030	0.0	2.094	0.0	2.086	0.0	2.079	0.0	2.037	0.0	2.065	0.0	2.057	0.0	2.074
AL	3.935	*	3.844	*	3.911	*	3.852	*	3.929	*	3.894	*	3.878	*	3.911	*
TI	0.004	*	0.004	*	0.004	*	0.014	*	0.011	*	0.007	*	0.011	*	0.003	*
FE	0.061	4.000	0.152	4.000	0.085	4.000	0.135	4.000	0.060	4.000	0.098	4.000	0.110	4.000	0.086	4.000
FE	1.568	*	1.479	*	1.449	*	1.507	*	1.557	*	1.512	*	1.501	*	1.523	*
MN	0.073	*	0.075	*	0.074	*	0.081	*	0.084	*	0.077	*	0.080	*	0.075	*
MG	0.284	*	0.289	*	0.267	*	0.268	*	0.266	*	0.275	*	0.279	*	0.271	*
CA	0.033	*	0.028	*	0.055	*	0.018	*	0.017	*	0.030	*	0.044	*	0.017	*
NA	0.0	*	0.0	*	0.0	*	0.0	*	0.0	*	0.0	*	0.0	*	0.0	*
K	0.013	1.971	0.017	1.888	0.038	1.884	0.017	1.890	0.014	1.938	0.020	1.914	0.029	1.933	0.010	1.895
F	0.003	*	0.008	*	0.005	*	0.037	*	0.037	*	0.018	*	0.033	*	0.002	*
H	3.997	4.000	3.992	4.000	3.995	4.000	3.963	4.000	3.963	4.000	3.982	4.000	3.967	4.000	3.998	4.000
O	14.000	*	14.000	*	14.000	*	14.000	*	14.000	*	14.000	*	14.000	*	14.000	*
MG	14.31		14.49		14.26		13.46		13.53		14.01		14.17		13.84	
FE	82.01		81.74		81.80		82.49		82.20		82.05		81.77		82.33	
MN	3.68		3.77		3.94		4.05		4.27		3.94		4.05		3.82	
F/M	5.771		5.374		5.697		5.926		6.165		5.780		5.661		5.906	
F/FM	0.852		0.843		0.851		0.856		0.860		0.852		0.850		0.855	
A* =	0.506		0.499		0.518		0.501		0.510		0.507		0.505		0.509	
A =	0.505		0.497		0.513		0.499		0.508		0.504		0.501		0.508	
M =	0.149		0.151		0.148		0.140		0.141		0.146		0.148		0.144	

1 AG5-1195 1CD1
2 1CD2
3 2CD2
4 BCD1
5 BCD2
6 AVERAGE
7 AVERAGE PLUS SIGMA
8 AVERAGE MINUS SIGMA

SUPER RECAL — CHLORITOID ANALYSES

	1	2	3	4	5	6	7	8
SIO2	32.39	24.20	28.77	27.19	26.00	27.71	30.49	24.93
TIO2	1.02	0.12	0.08	2.15	1.04	0.88	1.64	0.12
A203	36.33	36.23	37.47	37.63	38.83	37.30	38.25	36.34
FEO	20.24	22.90	20.35	24.03	24.34	22.37	24.13	20.61
MNO	0.46	0.51	0.53	0.53	0.66	0.54	0.60	0.47
MGO	1.35	1.65	1.55	1.63	1.64	1.56	1.68	1.45
CAO	0.07	0.11	0.17	0.05	0.03	0.09	0.14	0.04
NA2O	0.0	0.0	0.0	0.0	0.0	0.0	0.0	0.0
K2O	0.24	0.21	0.26	0.16	0.08	0.19	0.25	0.13
F	1.37	0.42	0.90	0.68	0.38	0.75	1.11	0.39
H2O	6.85	6.54	6.77	7.03	7.09	6.86	7.20	6.52
SUM	100.32	92.89	96.85	101.08	100.09	98.25	105.49	91.00
-O= F	0.58	0.18	0.38	0.29	0.16	0.32	0.47	0.16
SUM	99.75	92.71	96.47	100.80	99.93	97.93	105.03	90.84

SI	2.552	*	2.142	*	2.373	*	2.199	*	2.133	*	2.284	*	2.340	*	2.219	*
AL	0.0	2.552	0.0	2.142	0.0	2.373	0.0	2.199	0.0	2.133	0.0	2.284	0.0	2.340	0.0	2.219
AL	3.374	*	3.778	*	3.642	*	3.587	*	3.754	*	3.623	*	3.460	*	3.811	*
TI	0.060	*	0.008	*	0.005	*	0.131	*	0.064	*	0.055	*	0.095	*	0.008	*
FE	0.566	4.000	0.214	4.000	0.353	4.000	0.283	4.000	0.182	4.000	0.323	4.000	0.445	4.000	0.181	4.000
FE	0.768	*	1.481	*	1.051	*	1.343	*	1.488	*	1.219	*	1.104	*	1.353	*
MN	0.031	*	0.038	*	0.037	*	0.036	*	0.046	*	0.038	*	0.039	*	0.036	*
MG	0.159	*	0.218	*	0.191	*	0.197	*	0.201	*	0.192	*	0.192	*	0.193	*
CA	0.006	*	0.010	*	0.015	*	0.004	*	0.003	*	0.008	*	0.011	*	0.003	*
NA	0.0	*	0.0	*	0.0	*	0.0	*	0.0	*	0.0	*	0.0	*	0.0	*
K	0.024	0.987	0.024	1.771	0.027	1.321	0.017	1.597	0.008	1.746	0.020	1.477	0.025	1.371	0.014	1.599
F	0.341	*	0.118	*	0.235	*	0.174	*	0.099	*	0.196	*	0.270	*	0.109	*
H	3.659	4.000	3.882	4.000	3.765	4.000	3.826	4.000	3.901	4.000	3.804	4.000	3.730	4.000	3.891	4.000
O	14.000	*	14.000	*	14.000	*	14.000	*	14.000	*	14.000	*	14.000	*	14.000	*
MG	10.41		11.16		11.68		10.57		10.46		10.84		10.77		10.93	
FE	87.57		86.88		86.05		87.47		87.14		87.04		87.02		87.06	
MN	2.02		1.96		2.27		1.95		2.39		2.12		2.21		2.02	
F/M	5.037		6.980		5.711		7.019		7.649		6.541		5.959		7.214	
F/FM	0.834		0.875		0.851		0.875		0.884		0.867		0.856		0.878	
A* =	0.529		0.495		0.531		0.495		0.500		0.510		0.497		0.524	
A =	0.525		0.492		0.528		0.493		0.499		0.507		0.493		0.522	
M =	0.106		0.114		0.120		0.108		0.107		0.111		0.110		0.112	

1 AG4-388VCD6
2 WCD2
3 WCD3
4 XCD1
5 XCD2
6 AVERAGE
7 AVERAGE PLUS SIGMA
8 AVERAGE MINUS SIGMA

SUPER RECAL — APATITE ANALYSES (OH INPUTTED)

	1	2	3	4	5	6
SIO2	0.10	0.06	0.08	0.08	0.10	0.06
TIO2	0.06	0.04	0.01	0.04	0.06	0.02
A203	0.25	0.05	0.12	0.14	0.22	0.06
FEO	0.23	0.27	0.40	0.30	0.37	0.23
MNO	0.09	0.08	0.09	0.09	0.09	0.08
MGO	0.06	0.05	0.05	0.05	0.06	0.05
CAO	54.76	54.65	54.36	54.59	54.76	54.42
BAO	0.04	0.06	0.01	0.04	0.06	0.02
NIO	0.14	0.16	0.20	0.17	0.19	0.14
F	3.07	3.49	3.10	3.22	3.41	3.03
CL	0.02	0.01	0.02	0.02	0.02	0.01
P205	39.91	40.64	40.80	40.45	40.84	40.06
ZNO	0.59	0.73	0.64	0.65	0.71	0.60
H20	0.46	0.29	0.47	0.41	0.49	0.32
SUM	98.64	99.49	99.32	99.15	100.08	98.22
-O= F+CL	1.30	1.47	1.31	1.36	1.44	1.28
SUM	97.34	98.02	98.01	97.79	98.64	96.94

SI	0.009	*	0.005	*	0.007	*	0.007	*	0.008	*	0.006	*
P	2.928	2.937	2.953	2.958	2.961	2.968	2.947	2.954	2.943	2.951	2.952	2.957
FE	0.017	*	0.019	*	0.029	*	0.022	*	0.027	*	0.017	*
MN	0.007	*	0.006	*	0.007	*	0.006	*	0.007	*	0.006	*
CA	5.084	*	5.025	*	4.993	*	5.034	*	4.994	*	5.075	*
B-T	0.0	5.108	0.0	5.050	0.0	5.028	0.0	5.062	0.0	5.027	13.000	5.097
CL	0.003	*	0.001	*	0.003	*	0.002	*	0.003	*	0.002	*
F	0.841	*	0.947	*	0.840	*	0.876	*	0.918	*	0.834	*
H	0.266	1.110	0.166	1.115	0.269	1.112	0.233	1.112	0.278	1.199	0.188	1.024
O	0.0	*	0.0	*	0.0	*	0.0	*	0.0	*	0.0	*

1 62Y
2 63Y
3 64Y
4 AVERAGE
5 AVERAGE PLUS SIGMA
6 AVERAGE MINUS SIGMA

SUPER RECAL — TOURMALINE ANALYSES (OH CALCULATED & B203 INPUTTED)

	1	2	3	4	5
SIO2	36.12	36.59	36.35	36.59	36.12
TIO2	0.46	0.40	0.43	0.46	0.40
A203	31.91	32.31	32.11	32.31	31.91
FEO	7.85	7.58	7.72	7.85	7.58
MNO	0.0	-0.07	-0.03	-0.00	-0.07
MGO	6.36	5.94	6.15	6.36	5.94
CAO	0.58	0.58	0.58	0.58	0.58
BAO	0.01	0.05	0.03	0.05	0.01
NA20	1.90	1.48	1.69	1.90	1.48
K20	-0.02	-0.03	-0.02	-0.02	-0.03
F	0.07	0.21	0.14	0.21	0.07
CL	0.0	0.0	0.0	0.0	0.0
B203	10.50	10.53	10.51	10.53	10.50
H20	3.58	3.52	3.55	3.55	3.55
SUM	99.31	99.04	99.18	100.32	98.03
-O= F+CL	0.03	0.09	0.06	0.09	0.03
SUM	99.28	98.95	99.12	100.23	98.00

SI	5.981	5.981	6.040	6.040	6.010	6.010	5.992	5.992	6.029	6.029
B	3.001	3.001	3.000	3.000	3.001	3.001	2.976	2.976	3.025	3.025
AL	6.226	*	6.285	*	6.256	*	6.235	*	6.277	*
FE	1.087	*	1.046	*	1.067	*	1.075	*	1.058	*
TI	0.057	*	0.050	*	0.053	*	0.057	*	0.050	*
MG	1.570	*	1.462	*	1.515	*	1.552	*	1.478	*
MN	0.0	*	-0.010	*	-0.005	*	-0.000	*	-0.010	*
CA	0.103	*	0.103	*	0.103	*	0.102	*	0.104	*
NA	0.610	*	0.474	*	0.542	*	0.603	*	0.479	*
K	-0.004	9.648	-0.006	9.403	-0.005	9.525	-0.004	9.620	-0.006	9.429
F	0.037	*	0.110	*	0.073	*	0.109	*	0.037	*
CL	0.0	0.0	0.0	0.0	0.0	0.0	0.0	0.0	0.0	0.0
H	3.963	4.000	3.890	4.000	3.927	4.000	3.891	4.000	3.963	4.000
O	31.000	*	31.000	*	31.000	*	31.000	*	31.000	*
	F/M	0.693		0.709		0.701		0.693		0.709
	F/FM	0.409		0.415		0.412		0.409		0.415

1 154E AG5-929
2 155E 929
3 AVERAGE
4 AVERAGE PLUS SIGMA
5 AVERAGE MINUS SIGMA

SUPER RECAL

TOURMALINE ANALYSES (OH CALCULATED & B203 INPUTTED)

	1	2	3	4	5	6	7	8
SI02	36.18	36.35	36.46	36.41	36.38	36.36	36.45	36.26
TI02	0.39	0.36	0.39	0.33	0.35	0.36	0.39	0.34
A203	31.45	31.90	31.97	31.72	31.30	31.67	31.93	31.41
FEO	8.49	7.97	8.42	8.64	8.27	8.36	8.59	8.13
MNO	0.03	-0.02	0.01	0.02	0.02	0.01	0.03	-0.01
MGO	6.13	5.93	5.97	6.02	5.92	5.99	6.07	5.92
CAO	0.73	0.69	0.70	0.61	0.74	0.69	0.74	0.65
BAO	0.07	0.24	0.0	0.01	0.21	0.11	0.21	0.01
NA20	1.59	1.66	1.57	1.59	1.60	1.60	1.63	1.57
K20	-0.02	0.24	-0.02	-0.03	-0.02	0.03	0.14	-0.08
F	0.21	0.20	0.20	0.14	0.35	0.22	0.29	0.15
CL	0.0	0.0	0.0	0.0	0.0	0.0	0.0	0.0
B203	10.46	10.50	10.54	10.50	10.45	10.49	10.52	10.46
H20	3.50	3.52	3.53	3.55	3.42	3.50	3.50	3.51
SUM	99.14	99.30	99.74	99.50	98.78	99.29	100.27	98.32
-O= F+CL	0.09	0.08	0.08	0.06	0.15	0.09	0.12	0.06
SUM	99.05	99.21	99.66	99.44	98.64	99.20	100.14	98.26

SI	6.011	6.011	6.019	6.019	6.013	6.013	6.027	6.027	6.052	6.052	6.024	6.024	5.994	5.994	6.055	6.055
B	3.000	3.000	3.001	3.001	3.000	3.000	3.000	3.000	3.001	3.001	3.000	3.000	2.987	2.987	3.014	3.014
AL	6.157	*	6.224	*	6.213	*	6.187	*	6.136	*	6.183	*	6.186	*	6.181	*
FE	1.180	*	1.104	*	1.161	*	1.196	*	1.151	*	1.158	*	1.181	*	1.135	*
TI	0.049	*	0.045	*	0.048	*	0.041	*	0.044	*	0.045	*	0.048	*	0.043	*
MG	1.518	*	1.464	*	1.467	*	1.485	*	1.468	*	1.480	*	1.488	*	1.473	*
MN	0.004	*	-0.003	*	0.001	*	0.003	*	0.003	*	0.002	*	0.004	*	-0.001	*
CA	0.130	*	0.122	*	0.124	*	0.108	*	0.132	*	0.123	*	0.130	*	0.116	*
NA	0.512	*	0.533	*	0.502	*	0.510	*	0.516	*	0.515	*	0.521	*	0.509	*
K	-0.004	9.546	0.051	9.540	-0.004	9.513	-0.006	9.524	-0.004	9.444	0.006	9.513	0.028	9.586	-0.016	9.439
F	0.110	*	0.105	*	0.104	*	0.073	*	0.184	*	0.115	*	0.151	*	0.079	*
CL	0.0	0.0	0.0	0.0	0.0	0.0	0.0	0.0	0.0	0.0	0.0	0.0	0.0	0.0	0.0	0.0
H	3.890	4.000	3.895	4.000	3.896	4.000	3.927	4.000	3.816	4.000	3.885	4.000	3.849	4.000	3.921	4.000
O	31.000	*	31.000	*	31.000	*	31.000	*	31.000	*	31.000	*	31.000	*	31.000	*
	F/M	0.780		0.752		0.792		0.807		0.786		0.783		0.796		0.770
	F/FM	0.438		0.429		0.442		0.447		0.440		0.439		0.443		0.435

1 1611 AG4-78
2 1631 AG4-78
3 1651 AG4-78
4 1764 AG4-78
5 1774 AG4-78
6 AVERAGE
7 AVERAGE PLUS SIGMA
8 AVERAGE MINUS SIGMA

SUPER RECAL — TOURMALINE ANALYSES (OH CALCULATED & B2O3 INPUTTED)

	1	2	3	4	5	6	7	8
SIO2	36.19	35.91	36.33	36.13	35.87	35.45	36.00	36.78
TIO2	0.41	0.61	0.52	0.41	0.44	0.36	0.44	0.28
A2O3	31.33	31.34	31.49	32.03	31.00	31.18	31.30	31.85
FEO	8.39	8.49	7.94	7.38	7.61	7.71	7.96	7.75
MNO	0.01	0.02	0.06	0.06	0.06	0.03	0.08	0.04
MGO	6.78	6.60	7.09	7.42	7.27	6.89	6.67	6.99
CAO	0.96	0.82	0.90	0.80	0.80	0.76	0.81	0.74
BAO	0.0	0.0	0.0	0.0	0.0	0.0	0.0	0.0
NA2O	1.93	1.76	1.84	1.94	1.95	2.13	2.00	1.70
K2O	0.03	0.04	0.03	0.03	0.05	0.08	0.04	0.03
F	0.0	0.0	0.0	0.0	0.0	0.0	0.0	0.0
CL	0.0	0.0	0.0	0.0	0.0	0.0	0.0	0.0
B2O3	10.53	10.48	10.58	10.61	10.45	10.38	10.47	10.62
H2O	3.63	3.61	3.65	3.66	3.60	3.58	3.61	3.66
SUM	100.19	99.68	100.43	100.47	99.10	98.55	99.38	100.44
-O= F+CL	0.0	0.0	0.0	0.0	0.0	0.0	0.0	0.0
SUM	100.19	99.68	100.43	100.47	99.10	98.55	99.38	100.44

SI	5.973	5.973	5.956	5.956	5.968	5.968	5.919	5.919	5.968	5.968	5.938	5.938	5.979	5.979	6.020	6.020
B	3.000	3.000	3.000	3.000	3.000	3.000	3.000	3.000	3.001	3.001	3.001	3.001	3.001	3.001	3.000	3.000
AL	6.093	*	6.125	*	6.095	*	6.183	*	6.078	*	6.155	*	6.126	*	6.143	*
FE	1.158	*	1.178	*	1.091	*	1.011	*	1.059	*	1.080	*	1.106	*	1.061	*
TI	0.051	*	0.076	*	0.064	*	0.051	*	0.055	*	0.045	*	0.055	*	0.034	*
MG	1.668	*	1.632	*	1.736	*	1.812	*	1.803	*	1.720	*	1.651	*	1.705	*
MN	0.001	*	0.003	*	0.008	*	0.008	*	0.008	*	0.004	*	0.011	*	0.006	*
CA	0.170	*	0.146	*	0.158	*	0.140	*	0.143	*	0.136	*	0.144	*	0.130	*
NA	0.618	*	0.566	*	0.586	*	0.616	*	0.629	*	0.692	*	0.644	*	0.539	*
K	0.006	9.765	0.008	9.733	0.006	9.745	0.006	9.828	0.011	9.785	0.017	9.850	0.008	9.745	0.006	9.624
F	0.0	*	0.0	*	0.0	*	0.0	*	0.0	*	0.0	*	0.0	*	0.0	*
CL	0.0	0.0	0.0	0.0	0.0	0.0	0.0	0.0	0.0	0.0	0.0	0.0	0.0	0.0	0.0	0.0
H	4.000	4.000	4.000	4.000	4.000	4.000	4.000	4.000	4.000	4.000	4.000	4.000	4.000	4.000	4.000	4.000
O	31.000	*	31.000	*	31.000	*	31.000	*	31.000	*	31.000	*	31.000	*	31.000	*
F/M	0.695		0.723		0.633		0.563		0.592		0.630		0.676		0.625	
F/FM	0.410		0.420		0.388		0.360		0.372		0.387		0.403		0.385	

1 AG5-1153+ LTR2
2 LTR3
3 MTRC
4 MTRO
5 MTRO2
6 MTRO3
7 MTRR
8 MTR3

SUPER RECAL — TOURMALINE ANALYSES (OH CALCULATED & B203 INPUTTED)

	9	10	11	12	13	14	15	16
SI02	35.97	36.18	35.16	35.91	37.45	36.10	36.64	35.56
TI02	0.42	0.40	0.35	0.39	0.56	0.43	0.52	0.34
A203	31.63	31.04	32.01	31.61	31.03	31.45	31.79	31.11
FEO	8.70	8.46	8.41	8.35	8.47	8.12	8.53	7.72
MNO	0.03	0.04	0.04	0.05	0.05	0.04	0.06	0.03
MGO	6.50	6.48	6.40	6.50	6.65	6.79	7.10	6.48
CAO	0.85	0.84	0.80	0.95	0.86	0.84	0.90	0.77
BAO	0.0	0.0	0.0	0.0	0.0	0.0	0.0	0.0
NA20	1.97	1.89	1.79	1.91	1.86	1.90	2.01	1.79
K20	0.02	0.02	0.02	0.14	0.02	0.04	0.07	0.01
F	0.0	0.0	0.0	0.0	0.0	0.0	0.0	0.0
CL	0.0	0.0	0.0	0.0	0.0	0.0	0.0	0.0
B203	10.52	10.46	10.40	10.50	10.67	10.51	10.60	10.43
H20	3.63	3.60	3.59	3.62	3.68	3.62	3.69	3.56
SUM	100.24	99.41	98.97	99.93	101.30	99.85	101.90	97.80
-O= F+CL	0.0	0.0	0.0	0.0	0.0	0.0	0.0	0.0
SUM	100.24	99.41	98.97	99.93	101.30	99.85	101.90	97.80

SI	5.942	5.942	6.015	6.015	5.874	5.874	5.945	5.945	6.101	6.101	5.969	5.969	5.956	5.956	5.984	5.984
B	2.999	2.999	3.001	3.001	2.999	2.999	3.001	3.001	3.000	3.000	3.000	3.000	2.973	2.973	3.029	3.029
AL	6.157	*	6.081	*	6.302	*	6.167	*	5.957	*	6.127	*	6.089	*	6.167	*
FE	1.202	*	1.176	*	1.175	*	1.156	*	1.154	*	1.123	*	1.159	*	1.087	*
TI	0.052	*	0.050	*	0.044	*	0.049	*	0.069	*	0.053	*	0.063	*	0.044	*
MG	1.600	*	1.606	*	1.594	*	1.604	*	1.615	*	1.673	*	1.720	*	1.624	*
MN	0.004	*	0.006	*	0.006	*	0.007	*	0.007	*	0.006	*	0.009	*	0.004	*
CA	0.150	*	0.150	*	0.143	*	0.169	*	0.150	*	0.148	*	0.157	*	0.140	*
NA	0.631	*	0.609	*	0.580	*	0.613	*	0.587	*	0.608	*	0.632	*	0.584	*
K	0.004	9.801	0.004	9.681	0.004	9.847	0.030	9.794	0.004	9.543	0.009	9.749	0.015	9.843	0.002	9.652
F	0.0	*	0.0	*	0.0	*	0.0	*	0.0	*	0.0	*	0.0	*	0.0	*
CL	0.0	0.0	0.0	0.0	0.0	0.0	0.0	0.0	0.0	0.0	0.0	0.0	0.0	0.0	0.0	0.0
H	4.000	4.000	4.000	4.000	4.000	4.000	4.000	4.000	4.000	4.000	4.000	4.000	4.000	4.000	4.000	4.000
O	31.000	*	31.000	*	31.000	*	31.000	*	31.000	*	31.000	*	31.000	*	31.000	*
	F/M	0.754		0.736		0.741		0.725		0.719		0.675		0.679		0.671
	F/FM	0.430		0.424		0.426		0.420		0.418		0.403		0.404		0.402

9 MTRR4
10 MTRC2
11 MTRC3
12 MTRO
13 NTRC
14 AVERAGE
15 AVERAGE PLUS SIGMA
16 AVERAGE MINUS SIGMA

The vita has been removed from the scanned document